APPENDIX A

Previous Studies of Laboratory Aging of Compacted Specimens and Loose Mixtures

Introduction

The issue of oxidative aging of asphalt binder has been recognized and studied for almost a century. Hubbard and Reeve (1913) published the first results of a study that examined the effects of a year of outdoor weathering on the physical (e.g., weight, hardness, etc.) and chemical (i.e., solubility) properties of paving grade asphalt cements. Subsequent studies confirmed their basic finding that oxidation, and not volatilization alone, is responsible for changes in asphalt properties that occur due to exposure (Thurston and Knowles 1936, Van Oort 1956, Corbett and Merz 1975). Significant research also has been conducted to investigate the chemical aspects of the aging process, and excellent reviews of these studies can be found in the literature (Wright 1965, Lee and Huang 1973, Jemison et al. 1992, Petersen 2009). In some of these studies, researchers conducted sophisticated experiments and proposed conceptual, empirical and/or analytical models to explain the aging phenomenon of asphalt binder (Lunsford 1994, Liu et al. 1996, Petersen and Harnsberger 1998, Glover et al. 2008). Although a significant amount of effort has been placed on understanding the aging process of asphalt binder, relatively little work has been put forth to develop laboratory aging procedures for producing aged mixture specimens for performance testing. In addition, very little effort has been made to validate the laboratory aging methods with field measurements. Furthermore, the existing laboratory aging methods do not allow for consideration of different climates, depths, etc., which are known to impact aging significantly. A review of the pertinent literature that can be used to develop a more comprehensive method of producing aged specimens for performance testing is provided in the following sections.

Overview of Methods for Aging Asphalt Mixtures in the Laboratory

Several asphalt mixture laboratory aging procedures have been tried. These procedures can be broadly classified based on (a) state of material during aging (compacted specimen vs. loose mix) and (b) pressure level (oven aging vs. pressurized aging). Thus, the discussion of the laboratory aging of asphalt mixtures will focus on these two factors.

Compacted Specimen Aging vs. Loose Mixture Aging

Compacted Specimen Aging

Aging compacted samples is helpful for characterizing the performance of asphalt mixtures throughout the service life of the pavement. The standard method used to assess the long-term aging of asphalt mixtures in the United States is AASHTO R30 (2002). In this method, compacted asphalt mixture specimens are subjected to short-term aging at 135°C for four hours. Then, the short-term aged mixture is compacted. The compacted specimen is cored or

sawn to the required dimensions and then placed in a forced draft oven for long-term aging. The long-term aging simulation is performed at 85°C ± 3°C for 120 ± 0.5 hours to represent five to ten years of aging in the field. Potential limitations associated with this aging method can be summarized as follows (Harrigan 2007):

- Although the mean air temperature in the United States varies with geographic region, AASHTO R30 specifies only one aging temperature and duration to represent the long-term aging spectra.
- The aging time range recommended by this standard is too wide for design purposes, and simulation of aging at any time beyond ten years is not possible.
- The standard does not consider the effect of air void content, which is speculated to have a significant effect on oxidative aging.

As part of a SHRP project, studies were performed on the short-term and long-term aging of asphalt mixtures in the laboratory (Bell 1989, Bell et al. 1994). The outcome of these studies was standardized as AASHTO R30 for the long-term aging of compacted asphalt specimens in the laboratory. Bell et al. (1994) conducted different experiments on compacted specimens during SHRP-A-390 project. They proposed oven aging of loose mixtures at 135°C for four hours to simulate short-term aging during the mixing, storage and placement processes that take place in actual construction practice. In order to simulate long-term aging, Bell et al. conditioned asphalt specimens in the oven for different lengths of time. They conducted performance tests on laboratory long-term aged specimens and corresponding field cores. Based on the results of these trials, their recommendation for the long-term aging of compacted specimens was to age specimens at 85°C for 2, 4, and 8 days in the oven. A detailed discussion of the SHRP project laboratory aging trials is presented later in this document.

Brown and Scholz (2000) conducted a laboratory aging study that was similar to the Bell et al. study (1994) in that Brown and Scholz aged compacted specimens in an oven. Short-term and long-term aged specimens were evaluated based on the stiffness measurements of the compacted mixture specimens. The Brown and Scholz study results indicate that short-term aging of loose mix specimens at 135°C significantly increases the stiffness of the mixture by 9% to 24% per hour of aging. They speculated that for continuously-graded mixtures, oven aging at 135°C for two hours is representative of the aging during the mixing, storage and transport that occur during actual construction. Brown and Scholz compared the stiffness modulus ratios for laboratory-aged specimens and field cores and concluded that five days of aging compacted samples at 85°C in the oven gives reasonable results for long-term aging in the United Kingdom. They also found that four days of aging compacted samples at 85°C in the oven represents 15 years of aging in the field for mixtures in the United States (Brown and Scholz 2000).

Several other aging procedures for compacted mixture specimens have been proposed in the literature. A summary of these methods is provided in Table A-1. It can be seen that the procedures vary with respect to temperature and duration, and most of the studies do not include field validation, which would provide an estimate of the level of field aging that the procedure simulates.

Table A-1. Accelerated laboratory aging procedures developed for compacted asphalt specimens

Aging Procedure	Temperature (°C)	Duration	Aging Equipment	Major Findings
AAMAS (Von Quintus et al. 1992)	2 days at 60 + 5 days at 107 in Oven, 60 in PA	7 days in Oven , 5 and 10 days in PA	Oven, PA	• Oven aging causes more severe aging in compacted specimens comparing to pressure oxygen aging.
TRL (Nicholls 2006)	60	48 hours	Oven	• Simulates 397 days of aging in the field.
EMPA (Van den Bergh 2011)	110-120	16 hours	Oven	• The method can simulate 20 years of aging in the field
AASHTO R30-02 (Bell et al. 1994)	85	5 days	Oven	• This method can cause 5 to 10 years of aging in compacted specimens.
Nottingham University SATS (Collop et al. 2004)	85	65 hours	Air-drafted oven (saturated, 2.1 MPa)	
Hachiya et al. (2003)	60	20 days	Oven	• This method efficiently simulates the field aging. • The top 5-mm of the compacted mix experiences the most severe aging and aging effect decreases through the depth.
Tia et al. (1988)	60	90 days	Oven with and without UV radiation	
Liverpool University	60	21 days	Oven	• Simulates 18 month of aging in the field
Mugler (1970)	163	5 hours	Oven	
Hveem et al. (1963)	60	1000 hours	Oven	
Martin et al. (2003)	3 days at 70 + 4 days at 80	7 days	PAV	

Several problems associated with the laboratory aging of compacted specimens have been cited in the literature. Slump can occur during the long-term oven aging (LTOA) of compacted asphalt specimens, leading to a change in air void distribution (Reed 2010). Performance results confounded by air void or volume changes are not reliable. To minimize slump, NCHRP 9-23 (2005) suggests wrapping specimens in a wire mesh held in place by three steel clamps to preserve the specimen integrity. However, even with the wire mesh, slump may occur. Another problem associated with the aging of compacted specimens is the development of an aging gradient through the specimen thickness. The NCHRP 9-23 project (2005)

demonstrated that LTOA leads to both a radial and vertical age gradient in mixture specimens. RILEM-206-ATB indicates that changes in the size and shape of compacted samples during the aging process affect the final results and their variability (Partl et al. 2013). Therefore, selecting an appropriate sample size may help to eliminate the problems associated with the aging gradient in the mixture specimen.

A recent aging study conducted by North Carolina State University (NCSU) and the Western Research Institute (WRI) clearly demonstrates the problems associated with aging compacted specimens for performance testing. NCSU prepared and aged compacted specimens according to AASHTO R30, and the WRI evaluated the extent of aging at the surface and interior of the compacted specimens using a micro-extraction method. Prior to compaction, loose mix was short-term aged in a forced draft oven at 135°C for four hours. The long-term aging was performed in a forced draft oven at 85°C. The effects of the short- and long-term laboratory aging were measured by first splitting open a short-term aged specimen and an 8-day long-term aged specimen and removing small samples of mastic from the edge and center of the open face of each core. Asphalt from the small mastic samples was recovered and evaluated using infrared (IR) spectrometry. Figure A-1 shows the extraction locations and moduli values estimated from different locations at different aging levels.

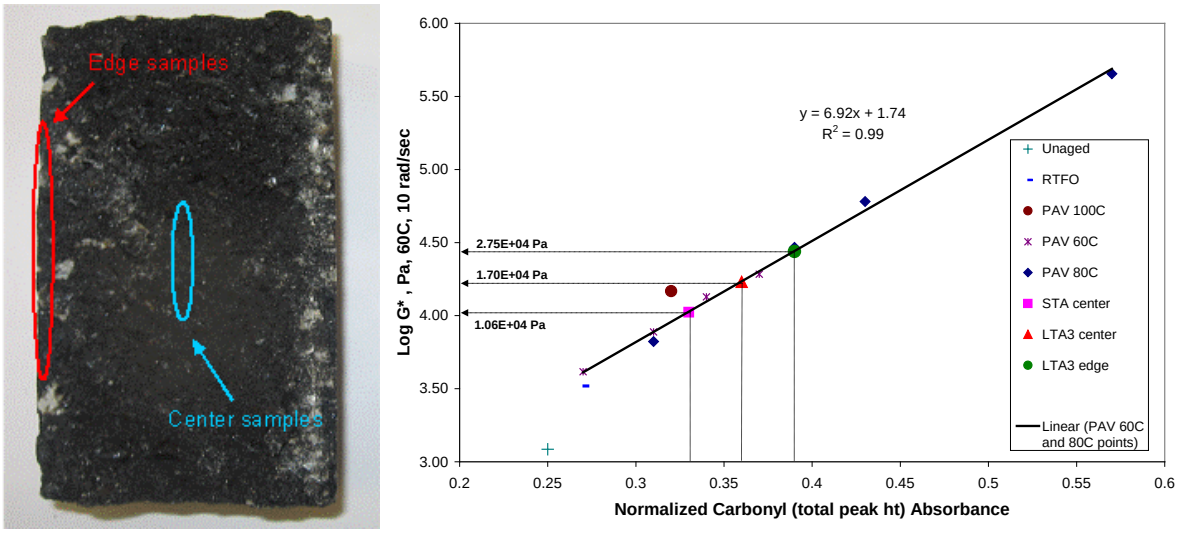

Figure A-1. (a) Split core face showing locations of extraction and (b) estimated modulus values based on carbonyl content at different locations and for long-term oven-aged versus short-term oven-aged specimens.

The IR spectra showed an increase in carbonyl at the center of the 8-day aged specimen compared to the center of the short-term aged specimen, which suggests that significant aging occurred during the 8-day oven aging period. Also, a carbonyl gradient from the center to the edge in the 8-day aged specimen was apparent. The observed differences in carbonyl content were further quantified by estimating the dynamic shear modulus, |G*| (at 10 rad/s and at 60°C). The asphalt at the center of the short-term aged specimen had a dynamic shear modulus value of 10.6 kPa. The dynamic shear modulus values at the center and edge of the long-term aged specimen were 17.0 kPa and 27.5 kPa, respectively. The dynamic shear modulus value of the pressurized aging vessel (PAV) -aged asphalt that was used to prepare the compacted specimens

was 14.7 kPa, which is somewhat lower than the dynamic shear modulus value at the center of the long-term aged specimen, thereby suggesting that the 8-day oven aging effect is more severe than that of the standard PAV test.

The aging gradient observed from the aged specimens using the AASHTO R30 method makes it difficult for the general approach to be used for conditioning specimens for performance testing. The performance properties measured from the aged specimens will be the 'average' properties of the materials that have a binder modulus value difference of almost a factor of two.

Loose Mixture Aging

Although less common than aging compacted specimens, the laboratory aging of loose (uncompacted) asphalt mixtures also has been tried. Some studies recommend aging loose mixtures in the laboratory to simulate the aging of asphalt pavements instead of aging compacted specimens (Mollenhauer and Mouillet 2011, Van den Bergh 2011). The primary advantages of loose mixture aging over compacted specimen aging are: (1) air and heat can easily circulate inside the loose asphalt mixture, which allows for uniform aging throughout the mix; (2) problems associated with the loss of compacted specimen integrity (e.g., slump) during laboratory aging may be reduced; and (3) the rate of oxidation may increase due to a larger area of the binder surface being exposed to oxygen. However, difficulties associated with the compaction of aged loose mixtures remains a major concern.

A review of studies that consider loose mixture aging is provided herein. The majority of the procedures proposed for loose mix aging utilize forced draft ovens at constant temperatures. However, a few procedures also consider using the binder PAV. It should be noted that the goal of a significant portion of the laboratory aging studies conducted on loose mixtures is to prepare reclaimed asphalt pavement (RAP) materials rather than to investigate compaction and subsequent performance testing. The compaction of aged materials is unnecessary for the preparation of RAP materials and, hence, any difficulty associated with highly aged loose mixtures is not a problem.

Von Quintus (1988) aged loose mixture specimens at 135°C in a forced draft oven for 8, 16, 24, and 36 hours to simulate long-term field oxidation. Von Quintus then conducted penetration and viscosity tests on the extracted and recovered asphalt binders. The results were promising, indicating similar short-term aging levels between the laboratory-aged materials and field samples taken from batching plants. However, the laboratory-aged materials exhibited considerable variability. Based on these results, Von Quintus recommended short-term aging of loose mixtures at 135°C in a forced draft oven for four hours before compaction. He also performed a study on the long-term aging of compacted asphalt mixtures in both an oven and in a pressurized oxidation vessel. The long-term aging procedures will be explained under the Pressure Aging section in this document.

Van den Bergh (2009) conducted an experimental program for aging loose mixtures in the laboratory with the goal of replicating RAP material. In this study, several mixtures were short-term aged in an air-ventilated oven at 130°C for three hours and then long-term aged at 90°C for extended times. Binder aging was evaluated by determining the increase in the ring and ball (R&B) softening point, the dynamic shear modulus, and the carbonyl and sulfoxide indices. For the carbonyl and sulfoxide indices, a plateau was reached after seven days of long-term oven aging, but the rheological properties did not reach such a plateau after seven days. Then, these results were compared with the ones for binders extracted from seven- to ten-year-old pavement

sections (Van den Bergh 2011). Based on this comparison, two procedures for producing RAP materials using a standard forced draft oven in the laboratory were recommended, as follows:

- Short-term aging at 130°C for 3 hours following long-term aging at 90°C for 168 hours (7 days).
- Short-term aging at 134°C for 4 hours following long-term aging at 85°C for 168 hours.

Because the goal of the Van den Bergh study was to produce RAP material, the compaction of the aged loose mixtures was not attempted.

Mollenhauer and Mouillet (2011) also conducted a study on the aging of loose mixtures to produce RAP materials. The properties of the binders extracted from laboratory-aged mixtures were compared with the properties of binders extracted from 11- to 12-year-old sections. The results suggest that aging asphalt loose mixtures in the PAV at 90°C with a pressure level of 2.1 MPa for 20 hours gives a comparable aging level with the oven aging of loose mixtures at 85°C for nine days. These researchers concluded that the aging time can be significantly reduced by using oxygen pressure. A summary of the comparison of the properties of the recovered binders for each aging method is shown in Table A-2. Mollenhauer and Mouillet (2011) also reported that aging at a low temperature (i.e., 60°C) is safer for mixtures that contain polymer-modified asphalt binder and produces less scattered results.

Table A-2. Properties of the binders extracted and recovered after different aging methods (after Mollenhauer and Mouillet 2011)

Binder property	Aging method (temperature)	Pure binder (-1)	After mixing (0)	LTA 1 day (1)	LTA 3 days (3)	LTA 6 days (6)	LTA 9 days (9)	LTA 14 days (14)
Penetration (25 °C) [1/10 mm]	BRRC (60 °C)	36	28	28	27	-	26	23
	RILEM (85 °C)		28	-	25	23	20	-
	UV (60 °C)		27	-	-	-	-	22
	PAV (90 °C)		28	20	-	-	-	-
	PAV (100 °C)		25	-	-	2	-	-
Softening temp. $T_{R\&B}$ [°C]	BRRC (60 °C)	62	67,2	67,4	68,0	-	68,6	69,4
	RILEM (85 °C)		68,6	-	70,8	72,4	73,6	-
	UV (60 °C)		68,8	-	-	-	-	73,8
	PAV (90 °C)		66,8	72,4	-	-	-	-
	PAV (100 °C)		68,6	-	-	122	-	-

Partl et al. (2013) conducted a study (RILEM 206-ATB) with the goal of reproducing RAP via the laboratory oven aging of loose mixture specimens. Asphalt mixtures from the same component materials were produced in nine laboratories and a batching plant. A comprehensive study was performed on the binders recovered from long-term aged plant-produced and laboratory-produced mixtures. The laboratory-produced mixtures first were short-term aged for four hours at 135°C and compared with the plant-produced mixtures. The penetration and R&B softening point results obtained from the laboratory-aged mixtures showed a strong correlation with those from the plant-produced mixtures, but the plant-produced mixtures had higher dynamic shear modulus values and lower phase angles than the short-term aged laboratory-produced mixtures. The long-term aging process consisted of conditioning both the plant-

produced and short-term laboratory-produced loose mixtures in the oven for 1, 2, 5, 7, and 9 days at 85°C.

The results of the Partl et al. (2013) study suggest that binder oxidation continues up to nine days of conditioning, but that the rate of oxidation decreases with an increase in the duration of the conditioning. Another significant finding is that performing extraction and recovery immediately following the laboratory aging process is important, because the binders that were extracted and recovered after a considerable amount of time were stiffer than those recovered immediately after aging. The Partl study also found that these laboratory aging procedures produce reasonable repeatability and reproducibility. The authors concluded that loose mixture aging in the laboratory to produce RAP material is an appropriate approach. Partl et al. (2013) cautioned, "However, with such a method, directly determining the mixture characteristics afterwards is not possible." Despite this comprehensive study of long-term aging of loose mixtures in the laboratory, the research team did not validate using field measurements.

Reed (2010) compared laboratory-aged loose mixtures to compacted specimens produced with crumb rubber-modified asphalt. Both the loose and compacted mixture samples were conditioned at 85°C for 5 and 14 days. Loose mixture aging was conducted in pans with sample heights ranging from 50 mm to 100 mm. The samples were agitated daily. Following aging, the loose mixtures were compacted and cored for testing. A significantly higher number of gyrations and higher shear stress levels were required to compact the aged loose mix comparing to the short-term aged loose mix, suggesting that aged loose material is stiffer than aged core materials. However, Reed also found that the dynamic modulus values of the compacted specimens following loose mix aging decreased with aging time, which is counter-intuitive. Reed (2010) concluded that the apparent reduction in the dynamic modulus values with an increase in aging time was caused by a lack of cohesion between the aggregate particles in the specimens that were compacted following loose mixture aging. He hypothesized that this outcome was influenced by the uniform aging of the asphalt around each aggregate particle in the laboratory-aged loose mix, as opposed to the field- and laboratory-aged compacted specimens that exhibit an aging gradient throughout the binder film (Figure A-2). Reed also reported significant changes in air void content despite the negligible dimensional changes during the long-term aging of the compacted specimens.

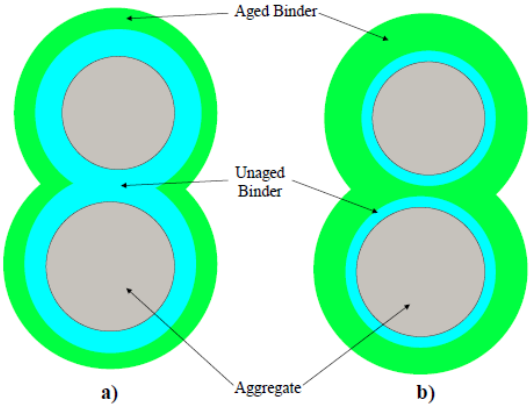

Figure A-2. Schematic of binder film on aggregate particles: (a) core and (b) loose mix (after Reed 2010).

A summary of loose mix aging procedures is presented in Table A-3. It should be noted that most of the studies on loose mixture aging were conducted by European researchers.

Table A-3. Accelerated laboratory aging procedures developed for loose mixtures

Aging Procedure	Short-term Aging		Long-term Aging		Aging Equipment	Major Findings
	Temp. (°C)	Duration	Temp. (°C)	Duration		
Van Gooswilligen (1989)	-	-	160	16 hours	Loose hot mix in sealed tin in oven	
Shell (Read and Whiteoak 2003)	Mixing Temp.	2 h	80	7 days	Oven	
LCPC (Such et al. 1997)	135	4 h	100	24 h	Oven	
RILEM TG5 (De la Roche et al. 2009)	135	4 h	85	7-9 days	Oven	• After 9 days of aging of loose mix at 85°C, a plateau region starts for oxidation of mix. • Laboratory aging of loose mix an appropriate way to produce RAP material. • Due to issues associated to compaction of aged loose mix, performance of mixture cannot directly be determined. • A more homogenous aged mix obtained from aging of loose mix.
BRRC (Belgian Road Research Center) (Piérard and Vanelstraete 2009)	135	1.5 h	60	14 days	Oven	• Due to low temperature used for aging of loose mixes, the polymer degradation is not a concern. • Less scattered results for aging are obtained comparing to methods which use higher temperatures.
Re-Road (Mollenhauer	135	4 h	90	20 h	PAV	• Oxygen pressure can be used to increase the aging time significantly.

and Mouillet 2011)						• Low temperatures (i. e., 60°C) should be used for mixes containing modified binders. • Due to limited capacity of the PAV, small amount of asphalt mixtures can be aged at once.
Van den Bergh (2011)	135,130	4 h, 3 h	85, 90	7 days	Oven	• The method can simulate 7-10 years of aging in the field.

Based on the results found in the literature, loose mixture aging appears to be advantageous over compacted specimen aging due to the homogeneity and efficiency of aging. However, for performance testing purposes, the aged loose mix must be compacted to the specified requirements. Previous studies of the long-term aging of loose mixtures indicate that more effort may be required to compact long-term aged loose mixtures than un-aged/short-term aged loose mixtures (Reed 2010). Very high compaction forces may cause degradation in the aggregate structure and change the mixture properties (Gatchalian et al. 2006).

To avoid problems associated with compacting aged loose mixes, it has been recommended that specimens should be compacted at equiviscous temperatures based on the viscosity of the short-term aged mix (Bell 1994). This method requires obtaining the viscosity of the binder in the short-term aged and long-term aged loose mixtures to determine the temperatures required for an equivalent binder viscosity for two different aging levels. It is expected that very high (approximately 370°F) temperatures will be required for the long-term aged material to obtain the same viscosity as the reference short-term aged material.

The use of a warm mix additive that can allow the mixing and compaction temperature to be reduced may offer an alternative to increasing the compaction temperature. Aspha-min® zeolite is a product that can reduce the production temperature by as much as 20 percent without affecting mixture performance. Zeolite contains 21 percent water by mass that is released in the temperature range of 85°C to 182°C (185°F-360°F). A study conducted by the National Center for Asphalt Technology (NCAT) shows that adding 0.3 percent zeolite improves the compactability of the mixture at temperatures as low as 88°C (190°F) without changing resilient modulus and rutting resistance of the compacted specimen. This product was also used in a mix containing 20 percent RAP and reduced the production and compaction temperature by 19°C (35°F) while offering the same in-place density and performance. During the study, it was noted that an average 0.65 percent reduction in air void content occurred when zeolite was used in the asphalt mix production (Hurley and Prowell 2005).

West et al. (2010) conducted a study as part of the NCHRP 9-39 project to introduce a procedure that can determine appropriate mixing and compaction temperatures for asphalt mixtures that contain both modified and unmodified asphalt binders. Three candidate methods were evaluated in the laboratory:

1. Candidate Method A is designed to determine the equiviscosity temperature at high shear rates, as recommended by Yildirim et al. (2000). This method is based on the fact that most modified asphalt binders exhibit shear thinning behavior. To determine the equiviscosity temperature required for compaction, the viscosity was measured in

a rotational viscometer at shear rates ranging from 0.1 s^{-1} to 93 s^{-1} and at temperatures ranging from135°C to 165°C. The viscosity rate was fitted to the Cross-William model, and extrapolation then was used to estimate the temperatures at which the viscosity at a shear rate of 500 s^{-1} is equal to 0.17 ± 0.02 Pa/s (for mixing) and 0.28 ± 0.03 Pa/s (for compaction) (Yildirim et al. 2000).

2. Candidate Method B also is based on the equiviscosity concept but differs from Candidate Method A in that the viscosity is measured using a dynamic shear rheometer (DSR) rather than the rotational viscometer. This approach is based on the method developed by Reinke (2003). The approach uses the viscosity data measured by a DSR with 25-mm parallel plate geometry and a 500-micron gap. The viscosities of the binders are measured in constant shear mode over a range of shear stress levels at temperatures ranging from 76°C to 94°C. Steady-state viscosity of the modified binders was observed at shear rates as high as 500 s^{-1}. The viscosity results at 500 Pa shear were extrapolated to 180°C using a log viscosity versus log temperature chart. The temperature that corresponded to a viscosity of 0.17 ± 0.002 Pa.s was selected for mixing, as in Method A. However, Reinke recommended determining the temperature for compaction based on the temperature that corresponded to a viscosity of 0.35 ± 0.03 Pa.s (Reinke 2003).
3. Candidate Method C consists of the so-called Casola method (Casola 2008). The Casola method is based on an equiphase angle concept rather than on equiviscosity. In this method, a DSR with 25-mm parallel plate geometry and 1-mm gap is used. Frequency sweep testing with frequencies ranging from 0.001 rad/s to 100 rad/s was used to generate a phase angle versus frequency mastercurve at a reference temperature of 80°C. “The binder’s transition point from viscous behavior to viscoelastic behavior was represented by the Phase Angle of 86°. The frequency corresponding to this transition point was correlated to the temperatures where binders provide good aggregate coating during mixing and lubrication during compaction” (Casola 2008).

The NCAT study incorporated laboratory testing to assess the three candidate methods. The emissions potential and binder degradation at high temperatures using modified and unmodified binders was evaluated. The study also assessed aggregate coating, workability, compactability, and properties of the compacted asphalt mixtures at low temperatures.

Method A resulted in mix temperatures above 177°C for all the mixtures that contained modified asphalt binders; these temperatures are considered to be too high in the asphalt paving industry. On the other hand, the results obtained from the high shear rate viscosity method were very similar to the ones obtained from the traditional equiviscous method that applied a Brookfield rotational viscometer at a shear rate as low as 6.8 s-1 (AASHTO T 316). These results suggest that no improvements to the current procedure are resulted from Method A. Table A-4 shows some typical results of the measurements performed in this study.

Table A-4. Comparison between the mixing and compaction temperatures for the high shear rate viscosity method and traditional equiviscous method (after West et al. 2010)

Binder ID	True Grade	Mixing Temperature °F (°C)		Compaction Temperature °F (°C)	
		Equiviscous Method	High Shear Rate Viscosity	Equiviscous Method	High Shear Rate Viscosity
M	**85.5 -19.5**	**372 (189)**	**363 (184)**	**343 (173)**	**336 (169)**
N	**84.3 -25.5**	**433 (223)**	**433 (223)**	**401 (205)**	**401 (205)**
G	**82.5 -24.2**	**379 (193)**	**372 (189)**	**352 (178)**	**349 (176)**
H	**78.3 -26.1**	**365 (185)**	**363 (184)**	**338 (170)**	**338 (170)**
C	**75.1 -38.7**	**388 (198)**	**385 (196)**	**355 (179)**	**352 (178)**
I	71.8 -29.2	333 (167)	333 (167)	311 (155)	311 (155)
B	**69.3 -37.3**	**354 (179)**	**352 (178)**	**325 (163)**	**325 (163)**
F	67.8 -21.3	320 (160)	318 (159)	298 (148)	297 (147)
O	65.6 -29.7	318 (159)	318 (159)	293 (145)	297 (147)
K	65.3 -13.0	295 (146)	295 (146)	271 (132)	275 (135)
J	64.3 -20.7	295 (146)	295 (146)	275 (135)	273 (134)
E	60.9 -33.1	293 (145)	293 (145)	273 (134)	297 (147)
D	60.3 -31.7	295 (146)	297 (147)	275 (135)	279 (137)

Method B resulted in lower mixing and compaction temperatures compared to the traditional equiviscosity method for both the modified and unmodified binders. These results also demonstrate that the temperature difference between Methods A and B is greater for the modified binders than the unmodified binders, thereby confirming their shear thinning behavior (see Table A-5).

Table A-5. Comparison between the mixing and compaction temperatures for the steady shear flow viscosity method and traditional equiviscous method (after West et al. 2010)

Binder ID	True Grade	Mixing Temperature °F (°C)		Compaction Temperature °F (°C)	
		Equiviscous Method	Steady Shear Flow Viscosity	Equiviscous Method	Steady Shear Flow Viscosity
M	**85.5 -19.5**	**372 (189)**	**296 (147)**	**343 (173)**	**275 (135)**
N	**84.3 -25.5**	**433 (223)**	**337 (169)**	**401 (205)**	**311 (155)**
G	**82.5 -24.2**	**379 (193)**	**340 (171)**	**352 (178)**	**312 (156)**
H	**78.3 -26.1**	**365 (185)**	**333 (167)**	**338 (170)**	**304 (151)**
C	**75.1 -38.7**	**388 (198)**	**320 (160)**	**355 (179)**	**291 (144)**
I	71.8 -29.2	333 (167)	316 (158)	311 (155)	289 (143)
B	**69.3 -37.3**	**354 (179)**	**325 (163)**	**325 (163)**	**295 (146)**
F	67.8 -21.3	320 (160)	309 (154)	298 (148)	281 (138)
O	65.6 -29.7	318 (159)	309 (154)	293 (145)	280 (138)
K	65.3 -13.0	295 (146)	280 (138)	271 (132)	257 (125)
J	64.3 -20.7	295 (146)	289 (143)	275 (135)	263 (128)
E	60.9 -33.1	293 (145)	293 (145)	273 (134)	269 (132)
D	60.3 -31.7	295 (146)	289 (143)	275 (135)	262 (128)

Method C yielded lower mixing and compaction temperatures than the equiviscosity method for the modified binders. However, for the unmodified binders, in some cases Method C resulted in lower temperatures and in some cases higher temperatures than the equiviscosity method (see Table A-6).

Table A-6. Comparison between the mixing and compaction temperatures for the phase angle method and traditional equiviscous method (after West et al. 2010)

Binder ID	True Grade	Freq. at δ =86° T=80°C	Mixing Temp. °F (°C)		Compaction Temp. °F (°C)	
			Equiviscous Method	Phase Angle Method	Equiviscous Method	Phase Angle Method
M	**85.5 -19.5**	**0.07**	**372 (189)**	**337 (169)**	**343 (173)**	**310 (154)**
N	**84.3 -25.5**	**0.03**	**433 (223)**	**341 (172)**	**401 (205)**	**313 (156)**
G	**82.5 -24.2**	**0.03**	**379 (193)**	**341 (172)**	**352 (178)**	**313 (156)**
H	**78.3 -26.1**	**0.22**	**365 (185)**	**332 (167)**	**338 (170)**	**305 (152)**
C	**75.1 -38.7**	**0.21**	**388 (198)**	**332 (167)**	**355 (179)**	**306 (152)**
I	71.8 -29.2	2.98	333 (167)	320 (160)	311 (155)	296 (147)
B	69.3 -37.3	1.10	354 (179)	325 (163)	325 (163)	300 (149)
F	67.8 -21.3	75.00	320 (160)	307 (153)	298 (148)	285 (141)
O	65.6 -29.7	21.12	318 (159)	312 (156)	293 (145)	289 (143)
K	65.3 -13.0	800	295 (146)	297 (147)	271 (132)	277 (136)
J	64.3 -20.7	580	295 (146)	298 (148)	275 (135)	278 (137)
E	60.9 -33.1	37.85	293 (145)	309 (154)	273 (134)	287 (142)
D	60.3 -31.7	122.56	295 (146)	305 (152)	275 (135)	283 (139)

The NCAT study concluded that both Methods B and C provide a reasonable way to determine the temperatures for mixing and compacting mixtures, and that both candidate methods are applicable to both unmodified and modified asphalts.

Oven Aging vs. Pressure Aging

Two general types of aging procedures have been used to age asphalt mixtures in a laboratory setting: long-term oven aging and pressurized aging. Each type of procedure has associated advantages and disadvantages that are discussed in this report. In addition, the operating parameters for each type of procedure differ among researchers and, hence, these parameters are reviewed in the following sections.

Oven Aging

Long-term oven aging (LTOA) is the most common method that is used to simulate oxidative aging of asphalt mixtures in the laboratory. As discussed, the current standard procedure, AASHTO R30, consists of conditioning compacted asphalt concrete specimens in an oven at 85°C for five days. However, other oven aging procedures have been tried and are cited in the literature. Although they are somewhat similar in terms of methodology, the LTOA

procedures differ in terms of temperature and duration (e.g., Bell et al. 1994, Houston et al. 2005, Reed 2010).

The SHRP project conducted an extensive evaluation of long-term aging procedures for asphalt mixtures (Bell 1989, Bell et al. 1994). LTOA was conducted at both 85°C and 100°C. The results for LTOA at 100°C were similar to those at 85°C, but the same level of hardening was achieved in less time. It was reported that the modulus measurements for most of the laboratory-aged specimens that were subjected to eight days of aging at 85°C and four days at 100°C were comparable. However, greater specimen-to-specimen variability was observed at 100°C and, therefore, the research team suggested that 85°C is preferable. Based on the field validation, Bell et al. (1994) recommended the LTOA of compacted specimens at 85°C for 2, 4, and 8 days to simulate long-term aging. The resilient modulus values for the laboratory- and field-aged cores were compared to determine the extent of aging that the laboratory procedures simulated. The resilient modulus test results demonstrated good agreement between the oxidation levels of the asphalt mixtures that were aged in the field for 14 to 19 years and the mixtures that were laboratory aged for 4 to 8 days (Bell 1994). However, Bell cautioned that in some cases, the LTOA method leads to less aging than that observed in the field. In addition, it was reported that due to some undefined factors (e.g., traffic and moisture-induced cracks) no correlation could be made between the measured modulus values of the field cores and the corresponding laboratory-aged samples. Also, no comparison was made between the binder properties of the laboratory- and field-aged mixtures.

According to Petersen (1989), aging can develop at higher temperatures for a longer time and to a higher level than at lower temperatures. Therefore, Petersen concluded that at higher temperatures, the plateau region for the aging index is reached after a longer time and at higher levels compared to lower aging temperatures (Figure A-3). Bell (1989) conducted a study on the possible effects of different aging methods. He speculated that very high temperatures can cause severe aging in asphalt mixtures and may exceed the field aging level (Figure A-3), which is important for evaluating oven aging methods (Bell 1989).

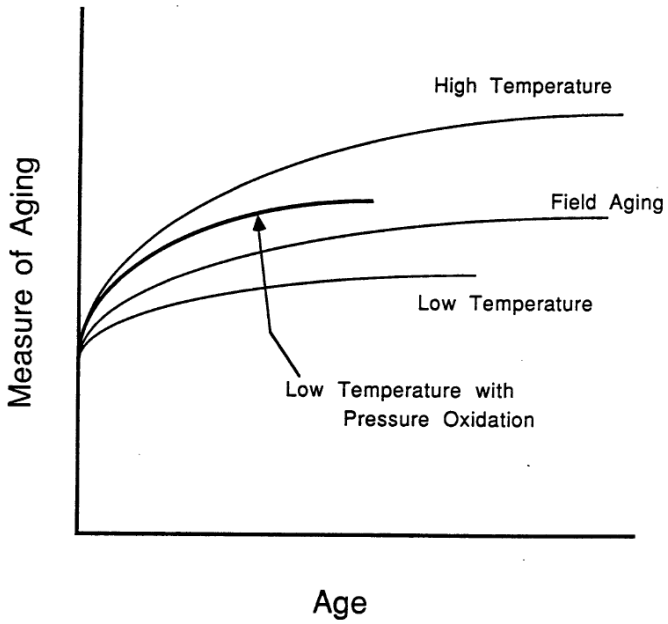

Figure A-3. Possible interactive effects of temperature and pressure oxidation on aging (after Bell 1989).

As discussed, increasing the temperature of LTOA conditioning expedites aging significantly. Based on the Re-Road study conducted for producing RAP mixtures in the laboratory, conditioning loose mixture at 85°C for nine days was found to cause more severe aging than conditioning at 60°C for 14 days (the BRRC aging method), but with more scattered results (Mollenhauer and Mouillet, 2011). In addition, applying elevated temperatures as high as 100°C can expedite the aging process, but such high temperatures may cause degradation of the binders and may damage the compacted specimens (Partl et al. 2013, Mollenhauer and Mouillet 2011, Bell and Sosnovske 1994, Bell et al. 1994). Therefore, numerous aging studies recommend 85°C for aging either loose or compacted asphalt mixtures, although they may suggest different aging durations. (Tables 1 and 2 provide summaries of the oven aging procedures found in the literature).

The summaries of compacted and loose mixture aging trials presented in Tables 1 and 2 demonstrate that LTOA requires considerable time to produce oxidation levels that correspond to field conditions near the end of a pavement's service life, thus providing the motivation to conduct trials of pressure aging to expedite the oxidation process. Despite the advantages offered by oven aging of availability, easier function, and higher capacity compared to a pressurized system, ovens differ with respect to their mechanisms of air drafting (Partl et al. 2013). This oven variability may impact the aging process of asphalt mixtures and, therefore, may contribute to a lack of repeatability between laboratories. On the other hand, PAVs are standardized equipment, thereby reducing problems associated with instrument variability.

Pressure Aging

As an alternative to the oven aging, pressure and forced air can be used to increase the rate of oxidation in asphalt mixture specimens. Pressure aging asphalt mixtures has been tried by several researchers for both compacted and loose mixture specimens.

Kumar and Goetz (1977) aged compacted specimens at 60°C using 'pulled air' at a constant water-head of 0.5 mm for durations varying between one and ten days. Figure A-4 depicts the apparatus used in the Kumar study. Kumar evaluated the aged specimens using a nondestructive compressive test with creep loading at 21°C ± 2°C. The slope and intercept of the creep curve (creep deformation versus loading time) were used to indicate the oxidation progress. No comparisons were made between laboratory and field aging; however, the Kumar study results indicate that this method does not induce significant aging in the asphalt specimens within a reasonable period of time (i.e., 10 days). The Kumar study reports that specimen integrity was maintained during the aging procedure and recommends that oxygen be tried instead of air to increase the rate of oxidation in the test.

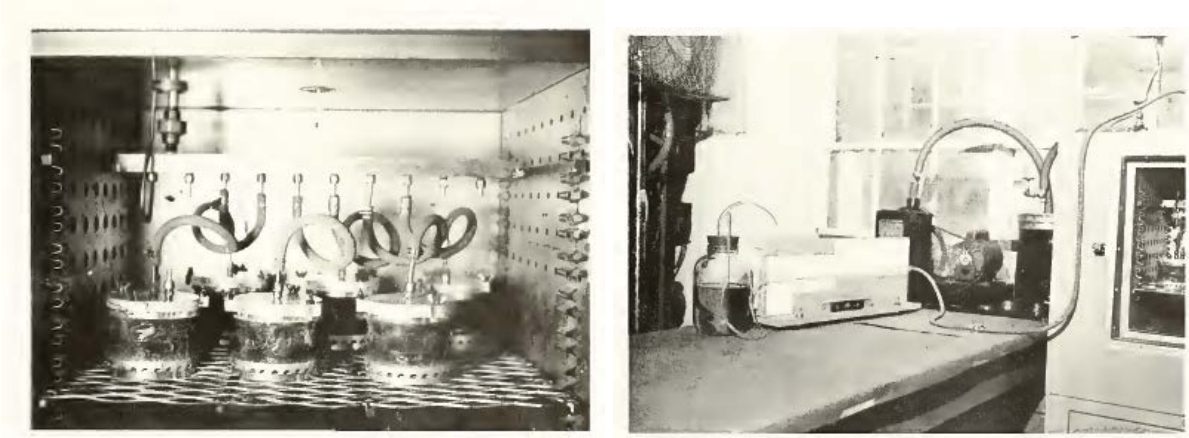

Figure A-4. Kumar pressure aging procedure (after Kumar and Goetz1977).

Von Quintus et al. (1988) performed a study on LTOA and long-term pressure aging of compacted asphalt mixture specimens. The study consisted of LTOA compacted specimens at 60°C for two days following five days of conditioning at 107°C. Pressure aging was conducted at 60°C at 100 psi (690 kPa) for durations of five and ten days. Following aging, the indirect tensile strength of the aged specimens was measured and it was found that the oven-aged specimens had higher indirect tensile strength levels and lower failure strain levels than the pressure-aged samples. The authors attributed this finding to a higher aging level for the oven-aged specimens than for the pressure-aged samples. In addition, penetration and viscosity tests on the extracted and recovered binders demonstrated more severe aging in the LTOA procedure than from the pressure aging procedure. Hence, Von Quintas et al. (1988) recommended oven aging over pressure aging but also advised that a more comprehensive study and evaluation of pressure aging should be conducted.

In a similar study, Kim et al. (1986) applied pressure to laboratory-aged compacted asphalt mixture samples. Specimens were compacted to different levels of the original sample (i. e., 88%, 94%, and 100%) to study the effect of air void content on the extent of oxidation. Specimens were subjected to oxygen pressure at 100 psi (690 kPa) and at 60°C for 0, 1, 2, 3, and 5 days. The resilient modulus values and fatigue life data obtained from diametral testing were

measured following the aging process. Modulus ratios (i.e., the modulus value of the aged mixture divided by the modulus value of the un-aged mixture) were compared for specimens aged for the various durations. The Kim et al. findings showed that the modulus ratios increased overall with aging, and the rate of increase was higher for the less compacted samples. Figure A-5 depicts an example of measured modulus ratios for two different compaction levels. Interestingly, the modulus ratio decreases at the early aging levels. The authors attributed this outcome to the loss of cohesion in the specimens at 60°C, suggesting the potential loss of specimen integrity during the laboratory aging procedure. Figure A-6 indicates that the fatigue life also increases with the aging level of the specimens.

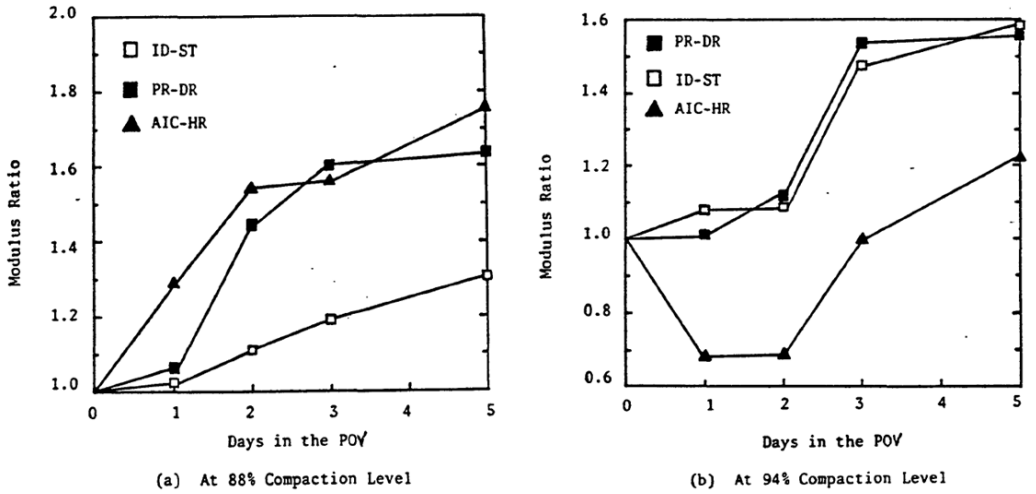

Figure A-5. Aging modulus ratios for different compaction levels and three mixture types (after Kim et al. 1986).

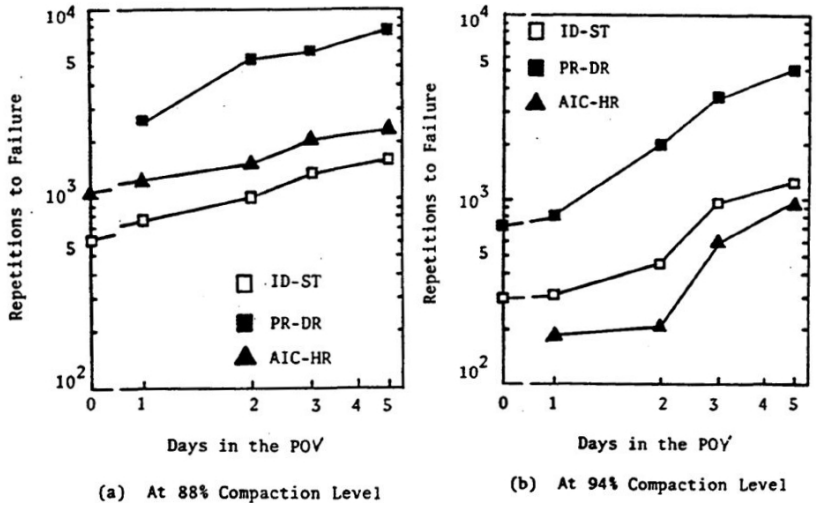

Figure A-6. Fatigue life data for different compaction levels and three mixture types (after Kim et al. 1986).

Bell et al. (1994) evaluated several pressure aging systems as part of the SHRP project. They first tried 'pressure oxidation' of compacted specimens using several pressure/temperature combinations in a pressurized vessel. Compacted samples were exposed to air or oxygen for 0, 2, or 7 days at pressures of 690 kPa or 2070 kPa and at 25°C or 60°C. The results revealed an unexpected trend in the modulus of the pressure-oxidized specimens (e.g., see Figure A-7). With an increase in the level of oxidation (air or oxygen pressure), the modulus value decreases. The authors attributed this finding to the destructive effect of relieving the pressure at the end of the test.

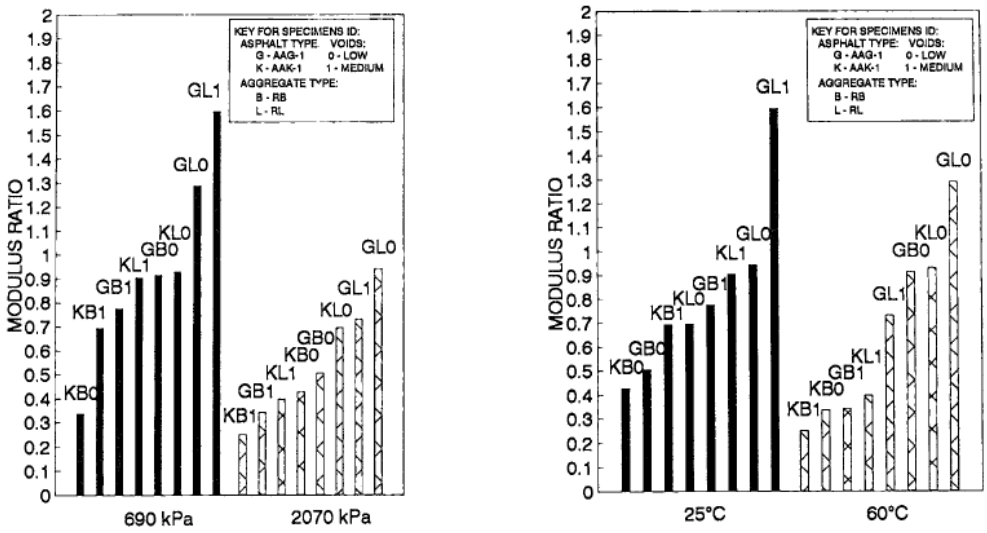

Figure A-7. Effect of oxygen pressure and temperature on modulus ratio using the pressure oxidation method.

This outcome prompted Bell et al. (1994) to switch to a different pressure oxidation procedure in which oxygen was passed through the asphalt specimens using a triaxial cell set-up and using a much lower pressure level than was used in previous trials. Although specimen integrity problems were reported for the pressure vessel tests, no further trials (with lower pressures or solutions for preserving the specimen during pressure release) were conducted to improve the test method, so Bell et al. switched the procedure from the pressure vessel set-up to the triaxial set-up depicted in Figure A-8. The aging procedure included a flow rate of 0.11 m3/hour (equivalent to roughly 50 psi (345 kPa)) at temperatures of both 25°C and 60°C for 1, 3, and 7 days. The resilient modulus was measured throughout conditioning in order to track the age hardening of the material. The authors concluded that the triaxial cell set-up appears "viable for realistic long-term oxidative aging, particularly since the mixture is 'supported' by a confining pressure throughout the aging process. It is also much safer than the pressure-oxidation approach, since the required pressure is much lower" (Bell et al. 1994). However, in comparing the modulus ratios for triaxial and LTOA, the latter method causes more severe aging in the compacted specimens. Note that these conclusions all were drawn from mixture test results. No tests were conducted on extracted binders, so the actual levels of oxidation achieved are unknown.

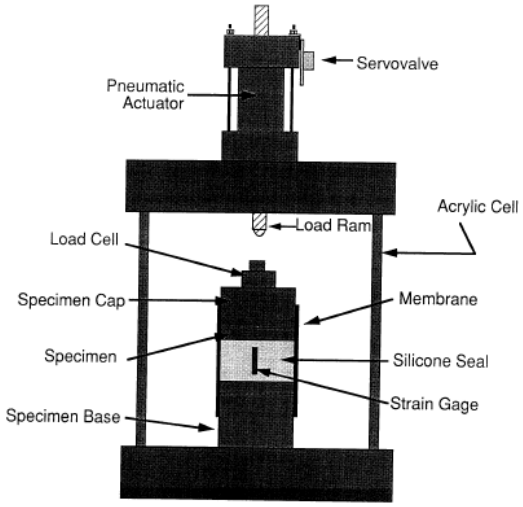

Figure A-8. SHRP triaxial aging procedure (after Bell et al. 1994).

Table A-7 presents the resilient modulus results for different test sections in the Bell et al. study (1994). The data indicate very severe effects of LTOA on the stiffness of the specimens, indicating that a high level of aging has occurred.

Table A-7. Summary of long-term oven aging data (after Bell et al. 1994)

SAMPLE ID	ACTUAL VOIDS (%)	MODULUS (MPa)		MODULUS RATIO
		BEFORE AGING	AFTER AGING	
GLLL00O	7.38	1718	2029	1.18
GLLL10O	7.99	2346	6403	2.73
GLLL20O	7.42	2767	10674	3.86
GLLL01O	7.91	2422	2532	1.05
GLLL11O	7.87	2001	5969	2.98
GLLL21O	7.54	2270	10950	4.82
GLML01O	10.00	1615	2401	1.49
GLML11O	9.30	1656	4685	2.83
GLML21O	10.00	1780	7838	4.40
KLLL00O	6.69	2036	2263	1.11
KLLL10O	7.55	2125	3498	1.65
KLLL20O	7.23	2450	10992	4.49
KLML00O	9.20	1366	1656	1.21
KLML10O	9.50	1277	4340	3.40
KLML20O	9.10	1435	8867	6.18

Bell et al. (1994) concluded that the triaxial pressure test method provides reasonable aging results (modulus ratios). They also speculated that the aging level may be increased if 85°C is used instead of 60°C. The results of the SHRP-A-383 project are presented in Table A-8.

Table A-8. Summary of triaxial (oxygen) aging data (after Bell et al. 1994)

SAMPLE ID	AGING CONDITION		ACTUAL VOIDS (%)	MODULUS (MPa)		MODULUS RATIO
	PERIOD (day)	TEMP. (°C)		BEFORE AGING	AFTER AGING	
KLLL00TO	0	25	4.9	2670	2670	1.00
KLLL10TO	1	25	5.0	2870	3450	1.20
KLLL20TO	3	25	5.3	3374	3795	1.12
KLML01TO	0	60	7.3	2808	2808	1.00
KLML11TO	1	60	7.0	2843	2732	0.96
KLML21TO	3	60	7.9	2318	2967	1.28
KLML31TO	7	60	7.4	2187	3298	1.51
GLLL01TO	0	60	6.3	2905	2905	1.00
GLLL11TO	1	60	5.5	3153	3788	1.20
GLLL21TO	3	60	6.1	3174	4092	1.29
GLML00TO	0	25	7.1	2912	2912	1.00
GLML10TO	1	25	8.3	2125	2691	1.27
GLML20TO	3	25	8.1	2788	3360	1.21
GLML31TO	7	60	7.8	3091	5154	1.67
KBLL01TO	0	60	5.3	2305	2305	1.00
KBLL11TO	1	60	5.2	2415	3209	1.33
KBLL21TO	3	60	4.8	2332	3450	1.48
KBML00TO	0	25	7.8	1994	1994	1.00
KBML10TO	1	25	6.6	1932	1842	0.95
KBML20TO	3	25	7.4	2036	2208	1.08
KBML31TO	7	60	6.7	1960	3422	1.75

Korsgaard et al. (1996) aged compacted specimens in a standard binder PAV and found that mixture aging for 72 hours at 100°C and at 2.07 MPa leads to the same level of aging of extracted binders as standard PAV aging of binders. No problems associated with specimen integrity loss upon pressure release were noted.

Khalid and Walsh (2002) developed an accelerated pressure oven procedure for simulating the long-term aging of porous asphalt mixtures. This procedure forces air through compacted specimens at a rate of 3 L/min at 60°C. A rubber membrane is placed on the specimens to maintain air flow throughout the sample and minimize peripheral localization (Figure A-9). This procedure is able to simulate aging to the same extent that AASHTO R30 specifications can simulate aging, although due to the low temperature used, a longer aging time (up to 25 days) was required for the Khalid and Walsh study than for the AASHTO guidelines.

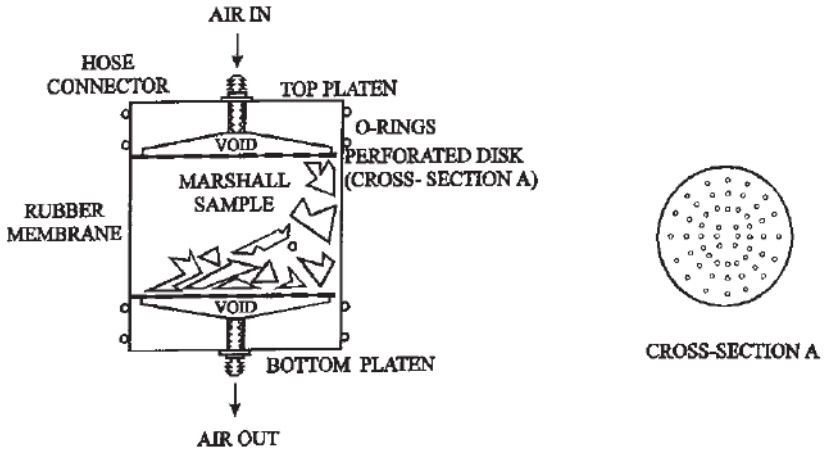

Figure A-9. Khalid and Walsh pressure aging system (after Khalid and Walsh 2002).

The combined effect of oxidation and water conditioning on an asphalt mixture's performance was evaluated in a study conducted at the University of Nottingham (Airey 2003). Compacted specimens were exposed to moisture and 2.1 Mpa oxygen pressure at 85°C for 65 hours. As shown in Figure A-10, the moisture conditioning was provided from condensed water dripping onto the specimen. The results showed similar rheological properties ($|G^*|$ and δ) for recovered asphalt binders from both field- and laboratory-conditioned samples (Airey 2003). Nevertheless, the performance of the laboratory-conditioned mixture specimens differed from that of the field cores. It was speculated that the difference in performance of the two mixture types was caused mainly by water damage during aging. The destructive effect of water not only has an adverse effect on adhesion but also on the cohesion of the asphalt binder/asphalt mastic in the mixture (Hagos 2008, Airey 2003). Figure A-10 shows the test set-up developed by Airey (2003) to determine the effects of both pressure oxidation and moisture on the performance of asphalt mixtures.

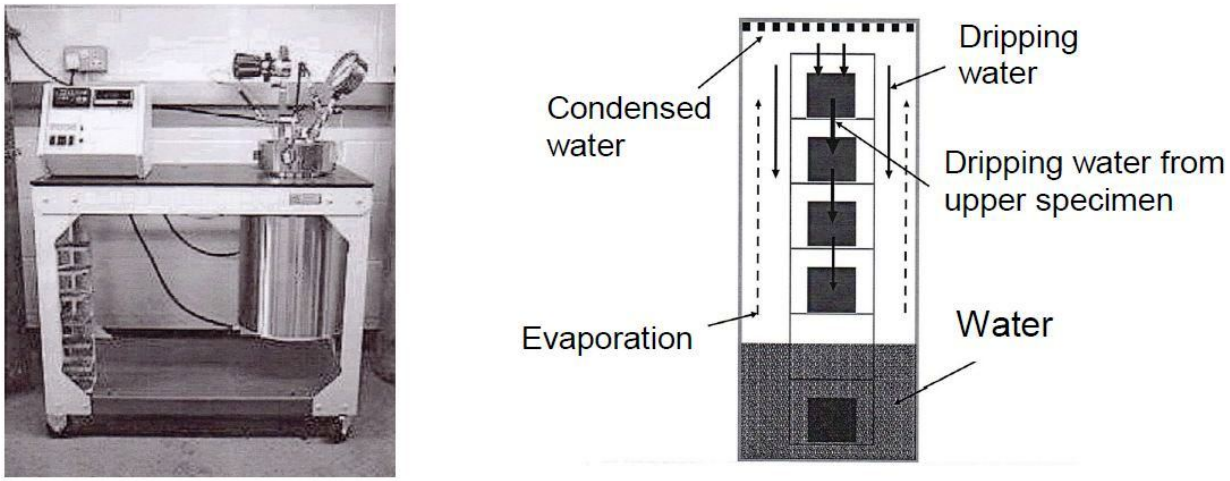

Figure A-10. Test set-up for asphalt mixture pressure aging and moisture conditioning (after Airey 2003).

A study conducted by Hachiya et al. (2003) introduced an accelerated method for the long-term aging of asphalt concrete. The procedure consists of two stages: First, asphalt mixture beams were aged in an oven at 70°C for eight hours to induce aging due to heat; and second, for the actual aging process, the beams were placed in an oven filled with pure oxygen at 60°C for 20 days. The effect of aging on the different properties of the asphalt concrete beams was examined. Flexural tests were performed to determine the mechanical properties of the asphalt mixture, and penetration tests, the softening point and the Fraass breaking point were used to evaluate the mechanical properties of the recovered asphalt binders. The Hachiya et al. study findings suggest that oxygen aging may properly simulate aging in the field. These researchers also concluded that the top 5 mm of the surface layer experienced the most aging during the aging procedure and that aging decreases with the depth of the pavement (Hachiya et al. 2003).

Collop et al. (2004) developed a procedure to inspect the aging/moisture sensitivity of a compacted coated macadam binder course. Moisturized cored samples were subjected to 2.1 Mpa air pressure at 85°C. The mechanical properties (stiffness moduli) of the samples were compared before and after the aging process (Collop et al. 2004).

One of the main shortcomings of PAV aging compared to oven aging is the amount of material that can be aged simultaneously. According to previous studies on loose mixture aging, in order to obtain uniform aging, a uniform thin layer of loose mix should be placed in the PAV, which reduces the capacity of the instrument to a very low level (around 1 kilogram) (Partl et al. 2013). A simple calculation can show that several PAV aging tests must be performed to obtain enough aged loose mixture for one standard large compacted specimen. Considering the standard PAV capacity, for compacted specimens, just one large asphalt mixture core (Ø100 mm × 150 mm) can fit vertically inside the chamber. However, if a smaller geometry for asphalt mixture cores is used, more specimens can be aged at once. Despite this capacity problem, it is believed that the air/oxygen pressure in the PAV can expedite aging and reduce the required time to achieve a certain level of aging in the asphalt mixture specimen. However, concern remains with respect to maintaining compacted specimen integrity during pressure aging and upon pressure release, which needs to be considered carefully when assessing PAV aging of compacted mix specimens.

Summary

Generally, the advantages and disadvantages of using loose and compacted asphalt mixtures can be summarized as outlined in Table A-9.

Table A-9. Comparison between loose mix and compacted specimens in the aging procedure

Loose Mix	Pros:	• *Homogenous aging in the mixture* • *Higher oxidation rate than compacted mix* • *Maintenance of specimen integrity a non-issue*
	Cons:	• *Difficulties associated with compaction of aged loose mix, which limits use for producing specimens for performance testing* • *Limited amount of materials can be aged in standard PAV chamber*
Compacted Specimen	Pros:	• *Can produce aged sample for performance tests if slumping is minimized through use of wire mesh*
	Cons:	• *Slower oxidation rate than loose mix* • *Integrity of the specimens is compromised at high temperatures and pressures due to slump and cracking upon pressure release* • *Oxidation gradients exist radially and along height of the specimen*

The comparison between aging in the oven and in a pressure oxidation vessel (e.g., a PAV) is summarized in Table 10.

Table 10. Comparison between oven and PAV aging methods

Oven Aging	Pros:	• *Available and easy to perform and control* • *Large amount of material can be aged simultaneously*
	Cons:	• *High variability among ovens, especially in terms of air drafting* • *More time needed to age materials in the oven than in the PAV* • *Maintenance of compacted specimen integrity is required, especially at high temperatures*
Pressure Aging	Pros:	• *Pressure can expedite the aging process* • *More reliable than oven aging due to less instrument variability between laboratories*
	Cons:	• *Due to limited capacity of the vessel, less material can be aged in each aging cycle unless new device is developed* • *Integrity of compacted samples during and after testing is a major concern*

Overview of Laboratory Aging Temperature

The oxidation of asphalt binder involves several independent and concurrent reactions. Temperature can affect the rate of oxidation, the binder species that are oxidized, and the nature of the oxidized species that are formed. Thus, temperature is a critical factor in laboratory simulations of long-term aging. Although increasing the aging temperature increases the rate of oxidation, it can also disrupt polar molecular associations and lead to the thermal decomposition of sulfoxides. Thus, accelerated aging of asphalt binder at significantly high temperatures may lead to a fundamentally different aged asphalt binder than asphalt aged in the field (at a lower temperature) (Branthaver et al. 1993). The literature indicates that the disruption of polar molecular associations and sulfoxide decomposition become critical at temperatures that exceed 100°C (Petersen 2009). Furthermore, aging at temperatures above 100°C can lead to asphalt mastic drain-down from the loose mix because asphalt binder has low viscosity values at elevated temperatures. Therefore, the effects of laboratory aging at temperatures over 100°C can

be divided into three categories: chemical effects, physicochemical effects, and binder/mastic drain-down, as shown in Figure A-11.

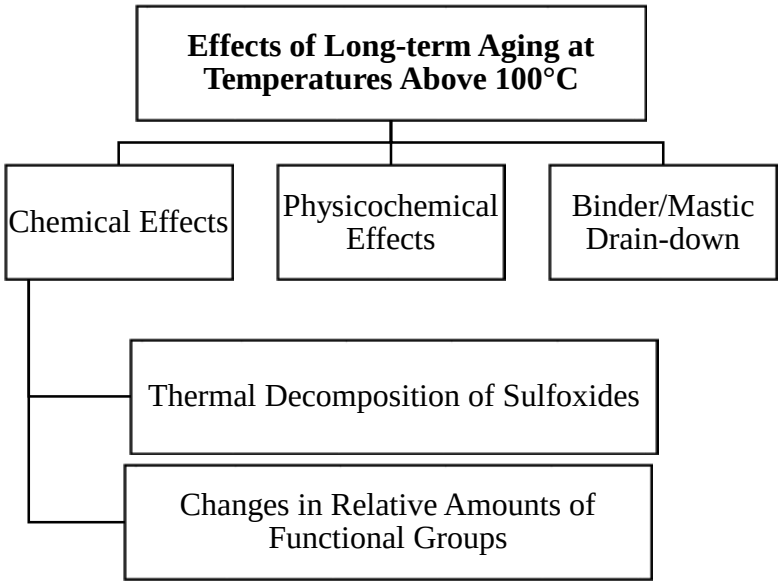

Figure A-11. Summary of effects of long-term aging at temperatures above 100°C.

Chemical Effects

Ketones and sulfoxides are the primary products of the oxidation of asphalt. In addition, minor amounts of carboxylic acids and dicarboxylic anhydrides are formed upon the oxidation of binders late in a pavement's service life (i.e., after significant oxidation has occurred). Anhydrides can also form from the condensation of oxidation products on adjacent side chains of aromatic ring systems (Petersen 2009). Figure A-12 presents a summary of the different chemical functional groups in asphalt molecules that are formed upon oxidative aging.

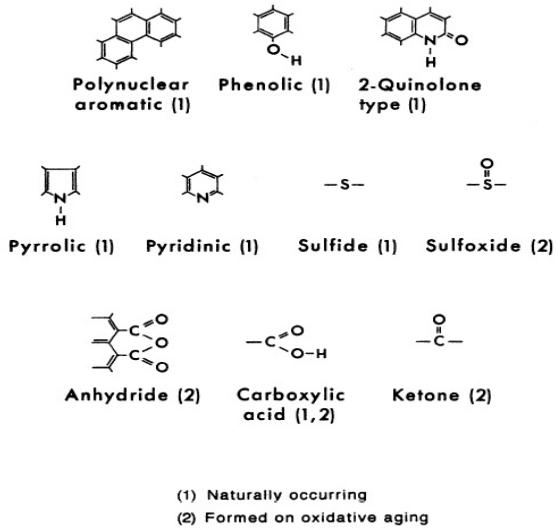

Figure A-12. Chemical functional groups in asphalt molecules normally present or formed during oxidative aging (Petersen 1984).

Petersen (2009) compared the relative amounts of different chemical functional groups that were formed during the oxidation of SHRP binder AAF-1 at two temperatures, 85°C and 113°C. Aging was conducted using thin films conditioned at ambient pressure. The results, shown in Figure A-13, demonstrate that a larger concentration of sulfoxides formed at the expense of ketones during the initial oxidation spurt at 85°C compared to 113°C. The right-hand graph in Figure A-13 shows that the relationship between rheology (dynamic viscosity) and sulfoxide concentration differs between the two aging temperatures, indicating fundamental differences in the oxidation reactions at 85°C and 113°C.

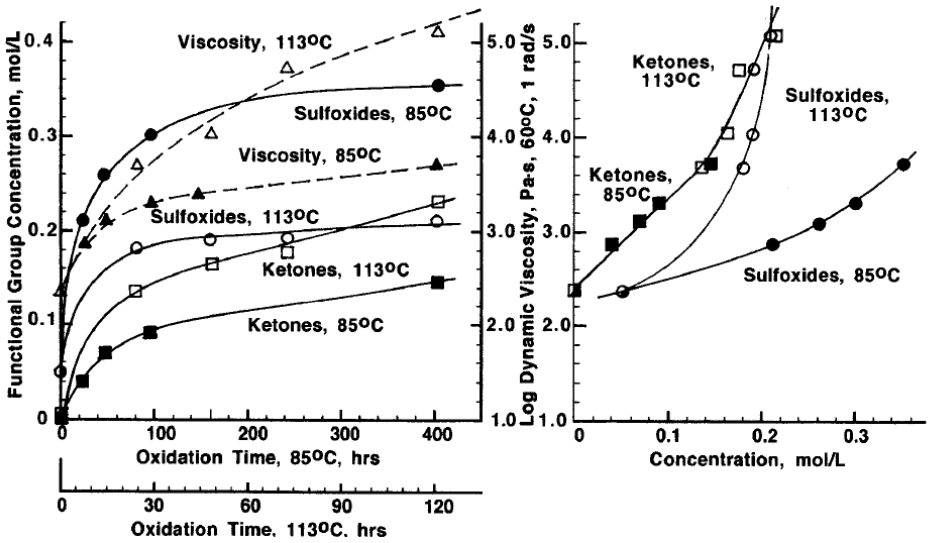

Figure A-13. Oxidative aging kinetic data and viscosity-functional group relationships for SHRP asphalt AAF-1 after thin film accelerated aging test (TFAAT) of oxidation as a thin film at atmospheric pressure (Petersen 2009).

Petersen and Harnsberger (1998) studied the effects of aging temperature on the sulfur content of eight SHRP asphalt binders. The results, shown in Figure A-14, correspond to the aging that occurred during the initial fast reaction period, also known as the 'spurt'. The ratio of sulfoxides to ketones differs based on whether the binder was aged at 85°C or 113°C. Generally, greater amounts of ketones were formed at the expense of sulfoxides at 113°C compared to 85°C. Petersen (2009) reported that the initial fast reaction spurt initially resulted from the reaction of oxygen with highly reactive perhydroaromatic hydrocarbons to form hydroperoxides. Then, the hydroperoxides could either react with the asphalt sulfides to form sulfoxides or decompose to form free radicals that participate in a subsequent oxidation reaction that involves benzylic carbon on aromatic rings to form ketones. Because hydroperoxides are thermally unstable, more free radicals are produced and fewer sulfoxides are formed at higher temperatures.

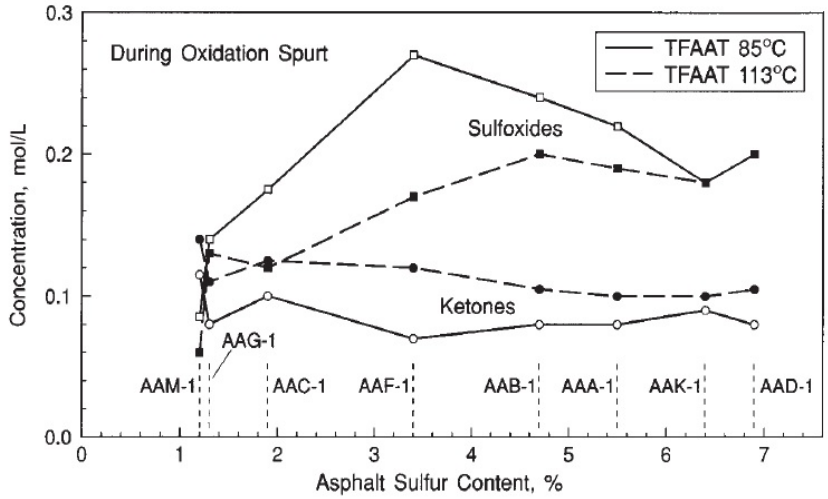

Figure A-14. Ketones and sulfoxides formed during oxidation spurt (fast reaction period) of eight SHRP binders during thin film accelerated aging test (TFAAT) of oxidation at atmospheric pressure (Petersen and Harnsberger 1998).

The other factor that may contribute to the decrease in the amount of sulfoxides that are formed relative to the ketones that are formed during the oxidation of asphalt at temperatures over 100°C is the thermal decomposition of the sulfoxides (Petersen et al. 1981, Herrington et al. 1994, Petersen 2009, Petersen and Glaser 2011, Glaser et al. 2013). Herrington et al. (1994) showed that the rate of asphalt sulfoxide decomposition can be significant. Figure A-15 presents a sulfoxide absorbance evolution with aging time at aging temperatures of 100°C and 130°C for typical asphalt. The results indicate that, although the concentration of sulfoxides increases with aging at 100°C, the sulfoxide concentration decreases after an aging duration of 50 hours at 130°C. This decrease in sulfoxide absorbance indicates that the rate of sulfoxide decomposition is greater than the rate of the formation of new sulfoxides upon oxidation.

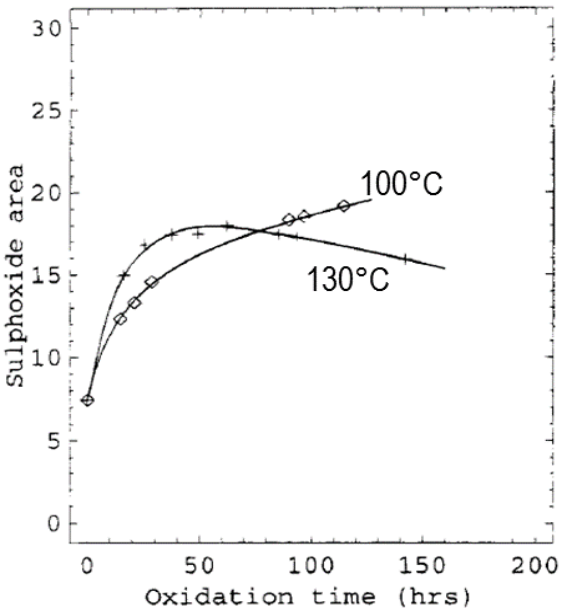

Figure A-15. Effect of oxidation duration and temperature on sulfoxide absorbance (Herrington et al. 1994).

Petersen (2009) further evaluated the thermal decomposition of sulfoxides in asphalt binder during oxidation. Sulfoxides form very rapidly during the initial oxidation and generally reach a constant concentration after prolonged aging, termed the 'steady state' concentration. For asphalt binder with low sulfur content, the steady state sulfoxide concentration results from the depletion of reactive sulfides. That is, all the sulfur that contains molecules becomes oxidized. However, in most asphalt binders with moderate to high sulfur contents, the occurrence of a steady state sulfur concentration is the net result of the sulfoxide formation from oxidation and sulfoxide loss through thermal decomposition. Petersen et al. (1981) provided evidence to support this phenomenon by evaluating the oxidation kinetics of Boscan asphalt with relatively high sulfur content (~5.5%). The Boscan asphalt was subjected to various oxidation temperatures and film thicknesses. Table A-11 presents the steady state concentrations of the sulfoxides that correspond to the different aging conditions. In both thin film (~0.0015 cm) and thick film (~0.5 cm) oxidation experiments, the steady state sulfoxide concentration decreased as the aging temperature increased. The decrease in the steady state sulfur concentration with an increase in the aging temperature indicates that, as the temperature increases, more of the sulfoxides decompose, which lowers the resultant steady state concentration of the sulfoxides.

Table A-11. Steady state concentrations of sulfoxides in Boscan asphalt under different oxidation conditions (Petersen et al. 1981)

Oxidation Method	Oxidation Temperature, °C	Steady State Sulfoxide Concentration, mol./L
Thin film on Teflon™ (~0.0015 cm)	25	> 0.46*
	113	0.40
	130	0.28
	163	0.16
Thick-film rolling thin-film oven (~0.5 cm)	113	0.21
	130	0.19
	163	0.15

* No steady state concentration was reached at the conclusion of the experiment because sulfoxide decomposition is negligible at 25°C.

Physicochemical Effects

The physicochemical interactions amongst the molecules in asphalt binder affect the temperature's sensitivity to oxidation and can alter the oxidation products that are formed when aging occurs at temperatures over 100°C. Petersen (2009) compared the kinetics of two SHRP binders: AAD-1 and AAG-1. These two binders are known to have different microstructures, with AAD-1 possessing less compatible chemistry and consequently a significant microstructure concentration compared to AAG-1. Although the two binders have different microstructure concentrations, Figure A-16 shows that the two binders exhibit similar oxidation kinetics for aging temperatures between 65°C and 85°C. However, the kinetics of the two binders are vastly different when the aging temperature exceeds 100°C. At temperatures over 100°C, the less compatible asphalt with high microstructure concentration (AAD-1) oxidizes much more rapidly than the more compatible asphalt with low microstructure concentration (AAG-1). The AAD-1 binder undergoes significant physicochemical disruption of its microstructure above 100°C, which increases the availability of molecules for oxidation and hence explains the observed trends.

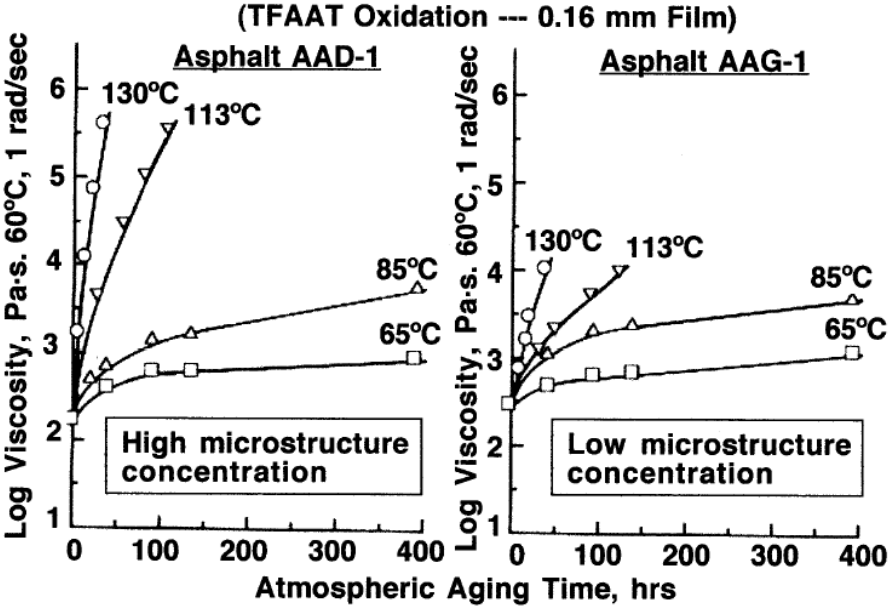

Figure A-16. Effects of temperature and component compatibility on age-hardening kinetics (Petersen 2009).

The literature review presented indicates that oxidation kinetics models that are derived based on results obtained at aging temperatures below 100°C cannot be extrapolated to predict oxidation kinetics at temperatures above 100°C (and vice versa) because the oxidation reactions are inherently different. Thus, although kinetics that correspond to temperatures below 100°C can be modeled using a simple Arrhenius type model, an additional model is needed to account for changes in the oxidation reaction in order to extrapolate to higher temperatures, thereby complicating modeling efforts to correlate loose mix aging times in the laboratory with field aging levels.

Mastic Drain-down

Braham et al. (2009) aged loose mixture in an oven at 135°C in an effort to simulate long-term aging efficiently. However, Braham et al. (2009) reported problems with mastic drain-down to the bottom of the aging pan during conditioning. Their study suggests that the drain-down was caused by the low viscosity of the asphalt binder at 135°C. Such loss of mastic is a significant concern for performance testing, as asphalt content plays a key role in mixture performance. Drain-down may decrease the uniformity of a mix and can cause a large loss of mastic due to the binder sticking to the aging pan. Braham et al. (2009) attempted to quantify the extent of the binder drain-down by comparing the mass of the aging pan (empty) before aging to that after aging and removing the aged loose mix in order to calculate the amount of drain-down. They calculated the percentage of drainage by first subtracting the initial empty pan weight from the final pan weight (i.e., the pan with drained materials) and then dividing the result by the initial total sample weight. The authors concluded that drain-down was not significant when the aging duration was less than 24 hours. However, the authors stated that the quantity of the material lost to the pan became significant as the aging time increased. Figure A-17 shows the

percentage of drain-down associated with aging loose mix prepared with PG 58-28 binder at 135°C for different durations in the Braham et al. (2009) study.

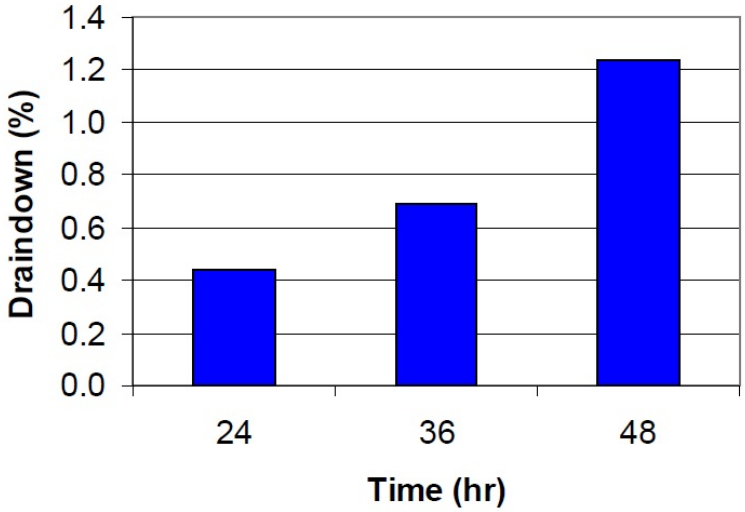

Figure A-17. Percentage of drain-down from mix M3 (PG 58-28) (Braham et al. 2009).

References

AASHTO, R30. (2002). *Standard Practice for Mixture Conditioning of Hot Mix Asphalt.*

Airey, G. D. (2003). State of the Art Report on Ageing Test Methods for Bituminous Pavement. *International Journal of Pavement Engineering, Vol. 4,* (No. 3), 165-176.

Airey, G. D., Choi, Y. K., Collop, A. C., and Elliot, R. C. (2003). *Development of an Accelerated Durability Assessment for High Modulus Base (HMB) Materials.* 6th RILEM symposium PTEMB'03. pp160-166.

Asphalt Research Consortium. (2011). *Quarterly Technical Progress Report.* Western Research Institute, October - December.

Bahia, H., and Anderson, D. (1995). *The Pressure Aging Vessel (PAV): A Test to Simulate Rheological Changes Due to Field Aging.* West Conshohocken, PA: ASTM Special Technical Publication 1241, Hardin, J.C., ed. American Society for Testing and Materials.

Bell, C. A. (1989). *Summary Report on Aging of Asphalt-aggregate Systems.* No. SHRP-A-305.

Bell, C. A., and Sosnovske, D. (1994). *Aging: Binder Validation.* Strategic Reshearch Program Report no. SHRP-A-384, National Research Council. Washington, DC.

Bell, C. A., AbWahab, Y., Cristi, R. E., and Sognovske, D. (1994). *Selection of Laboratory Aging.* SHRP-A-384, Strategic Highway Research. Washington, D.C.

Bell, C. A., Wieder, A. J., and Fellin, M. J. (1994). *Laboratory Aging of Asphalt-Aggregate Mixtures:Field Validation.* SHRP-A-390, Strategic Highway Research Program, National Research Council. Washington, D.C.

Bell, C. A., Fellin, M., and Wieder, A. (1994). Field Validation of Laboratory Ageing Procedures for Asphalt Aggregate Mixtures. *Journal of the Association of Asphalt Paving Technologists*, Vol. 63, pp 45-80.

Braham, A. F., W. G. Buttlar, T. R. Clyne, M. O. Marasteanu, and M. I. Turos (2009). The Effect of Long-term Laboratory Aging on Asphalt Concrete Fracture Energy. *Journal of the Association of Asphalt Paving Technologies*, Vol. 78.

Branthaver, J. F., J. C. Petersen, et al. (1993). *Binder Characterization and Evaluation – Vol. 2: Chemistry*. Strategic Highway Research Program (SHRP) Report No. SHRP-A-368, National Research Council, Washington, D.C.

Brown, S. F., and Scholz, T. V. (2000). Development of Laboratory Protocols for the Aging of Asphalt Mixtures. *I*, pp. vol. 1, pp. 83-90. 2nd Eurasphalt and Eurobitume Congress.

Casola, J. R. (2008). *Development of a Simple Procedure for Selecting Mixing and Compaction Temperatures.* Austin, TX: Association of Modified Asphalt Producers.

Collop, A., Choi, Y., Airey, G., and Elliott, R. (2004). *Development of a Combined Aging / Moisture Sensitivity Laboratory Test.* Vienna: 4th Euroasphalt and Eurobitume Congress.

Corbett, L. W., and Merz, R. E. (1975). *Asphalt Binder Hardening in the Michigan Test Road after 18 Years of Service.* Washington, D.C., pp. 27-34.: Transportation Research Record, 544, National Research Council.

De la Roche, C., Van de Ven, M., Van den Bergh, W., Gabet, T., Dubois, V., Grenel, J., and Porot, L. (2009). *Development of a Laboratory Bituminous Mixtures Aging Protocol.* Advanced Testing and Characterization of Bituminous Materials 331.

Farrar, M. J., Turner, T. F., Planche, J. P., Schabron, J. F., and Harnsberger, P. M. (2013). *Evolution of the Crossover Modulus with Oxidative Aging*. Washington, DC: Transportation Research Board.

Gatchalian, D., Masad, E., Chowdhury, A., and Little, D. (2006). Characterization of Aggregate Resistance to Degradation in Stone Matrix Asphalt Mixtures. *Transportation research record*, 55-63.

Glaser, R. R., Schabron, J. F., Turner, T. F., Planche, J. P., Salmans, S. L., and Loveridge, J. L. (2013). *Low Temperature Oxidation Kinetics of Asphalt Binders.* Washington, DC: Transportation Research Board.

Glover, C. J., Martin, A. E., Chowdhury, A., Han, R., Prapaitrakul, N., Jin, X., and Lawrence, J. (2008). *Evaluation of Binder Aging and its Influence in Aging of Hot Mix Asphalt Concrete: Literature Review and Experimental Design.* Texas: Report 0-6009-1.

Hachiya, Y., Nomura, K., and Chen, J. (2003). *Accelerated Aging Test for Asphalt Concretes.* Zurich: 6th RILEM Symposium PTEBM.

Hagos, E. (2008). *The Effect of Aging on Binder Proporties of Porous Asphalt Concrete.* PhD DiS 'SEP'I 'tZll'0nS, Delft University of Technology, the Netherlands.

Han, R. (2011). *Improvement to a Transport Model of Asphalt Binder Oxidation in Pavements: Pavement Temperature Modeling, Oxygen Diffusivity in Asphalt Binders and Mastics, and Pavement Air Void Characterization.* Collage Station, TX: Texas A&M University.

Harrigan, E. T. (2007). *Research Results Digest 324 - Simulating the Effects of Mot Mix Asphalt Aging for Performance Testing and Pavement Structural Design.* National Cooprative Highway Research Program.

Herrington, P. R., J. E. Patrick, and G. F. Ball (1994). Oxidation of Roading Asphalts. *Industrial and Engineering Chemistry Research,* Vol. 33 (11), pp. 2801-2809.

Hubbard, P., and Reeve, C. S. (1913). The Effect of Exposure on Bitumens. *Journal of Industrial and Engineering Chemistry,* 5(1), pp. 15-18.

Hurley, G. C., and Prowell, B. D. (2005). *Evaluation of Aspha-min® Zeolite for Use in Warm Mix Asphalt.* Auburn, Alabama: NCAT Report 05-04.

Hveem, F., Zube, E., and Skog, J. (1963). *Proposed New Tests and Specifications for Paving Grade Asphalt.* Proceedings of the Association of Asphalt Paving Technologists, Volume 32. AAPT, Minnesota, USA.

Jemison, H. B., Burr, B. L., Davison, R. R., Bullin, J. A., and Glover, C. J. (1992). Application and Use of the ATR, FT-IR Method to Asphalt Aging Studies. *Petroleum Science and Technology Journal,* 10(4), pp. 795-808.

Khalid, H. A., and Walsh, C. M. (2000). Relating Mix and Binder Fundamental Properties of Aged Porous Asphalt Materials. *Proceedings of the 2nd Eurasphalt and Eurobitume Congress, 1 , pp. 398-405.*

Kim, O. K., Bell, C., Wilson, J., and Boyle, G. (1986). *Effectof Moistureand Aging on AsphaltPavement Life, Part 2 - Effectof Aging.* FHWA-OR-RD-86-01-2, Final Report to Oregon Departmentof Transportationand the Federal Highway Administration.

Korsgaard, H. C., Blumensen, J., Sundahl, J., and Gonzales, C. (1996). Accelerated Ageing of Asphalt in Pressure Ageing Vessel. *Eurasphalt and Eurobitume Congress,* (p. VOLUME 1. PAPER E&E. 4.048). Strasbourg.

Kumar, A., and Goetz, W. (1977). Asphalt Hardening as Affected by Film thickness, Voids, and Permeability in Asphaltic Mixtures. *Proceedings, Association of Asphalt Paving Technologists*, (pp. Vol. 46, 571-605.).

Lee, D. Y., and Huang, R. J. (1973). Weathering of Asphalts as Characterized by Infrared Multiple Internal Reflection Spectra. *Journal of Applied Spectroscopy*, 27(6), pp. 419-490.

Liu, M., Lunsford, K. M., Davison, R. R., Glover, C., and Bullin, J. A. (1996). The Kinetics of Carbonyl Formation in Asphalt. *AlChE Journal*, 42(4), pp. 1069-1076.

Lunsford, K. M. (1994). *The effect of temperature and pressure on laboratory oxidized asphalt films with comparison to field aging.* College Station, TX: Texas A&M University.

Mirza, M. W., and Witczak, M. W. (1995). Development of Global Aging System for Short and Long Term Aging of Asphalt Cements. *Journal of the Association of Asphalt Paving Technologists, 64*, 393-430.

Mollenhauer, K., and Mouillet, V. (2011). *Re-road – End of Life Strategies of Asphalt Pavements.* European Commission DG Research.

Mouillet, V., Durrieu, J. L., Kister, J., and Martin, D. (2003). *Development of a New Methodology for Characterization of Polymer Modified Bitumens Aging by Infrared Microspectrometry Imaging.* Zurich: The 6th International RILEM Symposium, PTEBM.

Mugler, M. (1970). *Die veranderung der Bitumeneigenschaften wabrend der Verarbeitung und in Fertigen Belag.* Route et Traffic, 6.

Nicholls, C. (2006). *Analysis of Available Data for Validation of Bitumen Tests.* Forum of European National Highway Research Laboratories, ed. Cliff Nicholls, TRL. UK: Report on Phase 1 of the BiTVal Project, Forum of European National Highway Research Laboratories.

Partl, M. N., Bahia, H. U., Canestrari, F., De la Roche, C., Di Benedetto, H., Piber, H., and Sybilski, D. (2013). *Advances in Interlaboratory Testing and Evaluation of Bituminous Materials.* RILEM. RILEM.

Petersen, J. C. (1984). Chemical Composition of Asphalt as Related to Asphalt Durability: State of the Art. *Transportation Research Record* 999, pp. 13-30.

Petersen, J. C. (1993). Asphalt oxidation — an overview including a new model for oxidation proposing that physicochemical factors dominate the oxidation kinetics. *Fuel Sci Technol Int*, 11:57–87.

Petersen, J. C. (1998). A Dual, Sequential Mechanism for the Oxidation of Petroleum Asphalts. *Petroleum Science and Technology*.

Petersen, J. C. (2009). *A Review of the Fundamentals of Asphalt Oxidation.* Washington, D.C.: Transport Research Board.

Petersen, J. C., and Glaser, R. (2011). Asphalt Oxidation Mechanisms and the Role of Oxidation Products on Age Hardening Revisited. *12*, pp. 795 - 819. Lavoisier, Paris: Road Materials and Pavement Design.

Petersen, J. C., and Harnsberger, P. M. (1998). *Asphalt Aging: Dual Oxidation Mechanism and Its Interrelationships with Asphalt Composition and Oxidative Age Hardening.* Washington, D.C.: Transportation Research Record, 1638, National Research Council.

Petersen, J. C., Hansberger, P. M., and Robertson, R. E. (1996). Factors Affecting the Kinetics and Mechanisms of Asphalt Oxidation and the Realative Effects of Oxidation Products on Age Hardening. *Preprints of Papers, American Chemical Society, Division of Fuel Chemistry 41.CONF-960807*.

Petersen, J. C., S. M. Dorrence, M. Nazir, H. Plancher, and F. A. Barbour (1981). *Oxidation of Sulfur Compounds in Petroleum Residues: Reactivity-Structural Relationships.* American Chemical Society, Division of Petroleum Chemistry, Preprints (United States) 26, No. CONF-810813 (Vol. 2).

Piérard, N., and Vanelstraete, A. (2009). *Développement d'une méthode d'essai pour vieillir de manière accélérée les enrobés bitumineux en laboratoire.*

Prapaitrakul, N. (2009). *Toward and Improved Model of Asphalt binder Oxidation in Pavements.* Collage Station, TX: Texas A&M University.

Prapaitrakul, N., Han, R., Jin, X., and Glover, C. J. (2009). *A Transport Model of Asphalt Binder Oxidation in Pavements.* Road Materials and Pavement Design.

Read, J., and Whiteoak, D. (2003). *The Shell Bitumen Handbook. 5th Ed.* London: Thomas.

Reed, J. (2010). *Evaluation of the Effects of Aging on Asphalt Rubber Pavements.* Masters Thesis, PhD Dissertation., Arizona State University.

Reinke, G. (2003). Determination of Mixing and Compaction Temperature of PG Binders Using a Steady Shear Flow Test. *Presentation Made to the Superpave Binder Expert Task Group.* https://engineering.purdue.edu/~spave/old/Technical%20Info/Meetings/Binder%20ETG%20Sept%2003%20Las%20Vegas,%20NV/Reinke_MIX%20AND%20COMPACTINO%20INFO%20FOR%20ETG%209-15-03.pdf.

Such, C., Ballie, M., Lombardi, B., Migliori, F., Ramond, G., Samanos, J., and Simoncelli, J. P. (1997). *Susceptibilite au vieillissement des bitumen - Experimentation A08.* LCPC. Paris: Bitume, GNB - Groupe National.

Thurston, R., and Knowles, E. (1936). Oxygen Absorption Tests on Asphalt Constituents. *Journal of Industrial and Engineering Chemistry*, 28(1), pp88-91.

Tia, M., Ruth, B. E., Charai, C. T., Shiau, J. M., Richardson, D., and Williams, J. (1988). *Investigation of Original and In-service Asphalt Properties for the Development of Improved Specifications – Final Phase of Testing and Analysis.* Final Report, Engineering and Industrial Experiment Station. Gainesville, FL: Final Report, Engineering and Industrial Experiment Station.

Underwood, B. S., Sakhaei Far, M. S., and Kim, Y. R. (2010). *Using Limited Purchase Specification Tests to Perform Full Viscoelastic Characterization of Asphalt Binder.* ASTM Journal of Testing and Evaluation.

Van den Bergh, W. (2009). *The Development of an Artificially Aged Asphalt Mixture (in Dutch): Artificial Aged Asphalt mixture.* Gent, Belgium: In: Belgian Road Congress.

Van den Bergh, W. (2011). *The Effect of Aging on Fatigue and Healing Properties of Bituminous Mortars.* Ph.D Thesis, Delft University of Technology, Delft University.

Van Gooswilligen, G., De Bats, F., and Harrison, T. (1989). Quality of Paving Grade Bitumen - A Practical Approach in Terms of Functional Tests. *Proc. 4th Eurobitume Symp.*, pp. 290-297.

Van Oort, W. P. (1956). Durability of Asphalt – It's Aging in the Dark. *Journal of Industrial and Engineering Chemistry*.

Von Quintas, H., Scherocman, J., Kennedy, T., and Hughes, C. (1992). *Asphalt Aggregate Mixture Analysis System (AAMAS).* NCHRP. NCHRP 9-6(1).

West, R. C., Watson, D. E., Turner, P. A., and Casola, J. R. (2010). *Mixing and compaction temperatures of asphalt binders in hot-mix asphalt.* National Cooperative Highway Research Program. No. Project 9-39.

Wright, J. R. (1965). Weathering: Theoretical and Practical Aspects of Asphalt Durability. In *Chapter 8 in Bituminous Materials: Asphalts, Tars and Pitches* (p. Volume II). New York: Ed. A.J. Hoiberg. Interscience Publishers.

Yildirim, Y., Soaimanian, M., and Kennedy, T. (2000). *Mixing and Compaction Temperatures for Hot Mix Asphalt.* University of Texas, Center for Transportation Research, Research Report #1250-5.

APPENDIX B

Previous Studies of Modeling Asphalt Binder Aging in Pavements

To prepare an aged compacted specimen in the lab that represents a specific time on the road, climate, depth within the pavement, and level of air voids requires a solid understanding of binder oxidation kinetics and diffusion. Modeling the extent of oxidation in a pavement requires 'tracking' the property with respect to time, which is related directly to the oxidation level in the pavement. Asphalt binder is the asphalt mixture constituent that undergoes oxidative aging; hence, the oxidation of a pavement is best tracked using binder properties, because the mixture is subjected to other factors, including mechanical degradation that is caused by traffic loading, thermal-induced stress, and moisture, all of which could confound test results. In the following sections, the binder properties that are used to measure the extent of oxidation are referred to as *aging index properties* (AIPs). A review of relevant information regarding AIPs, oxidation kinetics modeling, and diffusion modeling is presented.

Aging Index Properties (AIPs)

Asphalt binder AIPs can be divided into two main categories: 1) chemical functional groups and 2) rheological parameters. The following sections discuss the AIPs that fall into these two categories. Chemical functional groups can be used to track the oxygen uptake of asphalt binders directly. Rheological properties are advantageous because they do not require IR spectroscopy (Glaser et al. 2013a). Underwood et al. (2010) presented laboratory aging data that suggest that the rheology and aging kinetics of asphalt binders are linked. An important advantage of the evolution of a model that is based on rheological parameters as an AIP is its ability to relate to the mechanical properties of polymer-modified binders. When using chemical functional groups as AIPs, the chemistry of the base binder oxidation and concurrent oxidation and degradation of the polymer is extremely complex and makes it more difficult to relate the model to mechanical properties.

Chemical Functional Groups

Fourier transform infrared (FTIR) spectroscopy can be used to analyze the chemical functional groups that constitute asphalt binder. The FTIR spectrometer simultaneously collects spectral data within a wide spectral range (400 cm^{-1} to 4000 cm^{-1}). Peaks in the spectral data can be used to detect the chemical functional groups. Functional groups that contain oxygen include carbonyl and sulfoxides. Hence, changes in the concentration of carbonyls and sulfoxides can be applied to the AIPs to measure the extent of oxygen uptake in the asphalt binder (Han 2011). The extent of the oxidation reaction in asphalt binders usually is tracked by following the infrared peak at wave number 1700 cm^{-1} (1650 cm^{-1} to 1820 cm^{-1}) that typically is assigned to carbonyl (Prapaitrakul 2009, Petersen 2009, Han 2011).

The carbonyl chemical functional group has long been used to indicate the level of asphalt oxidation. The linear relationship between the log viscosity increase and the carbonyl formation during asphalt oxidation is well established (Petersen 2009). The ketone functional group is the major component of the carbonyl IR absorption region. Ketone formation

sufficiently changes the polarity of the associated aromatic ring components, which leads to an increase in the asphaltene fraction, thereby increasing viscosity (Petersen 2009, Petersen et al. 2011).

The other major oxidation product that is readily identified via IR spectroscopy is the sulfoxide functional group. The effects of sulfoxides have received less consideration in the past, primarily because sulfoxides that form at high temperatures during oxidative aging conditioning thermally decompose, which made sulfoxide concentrations an unreliable, variable measure. However, an expanded and more fundamental understanding of the role of sulfoxide formation on physical properties during oxidative age hardening is presented by Petersen et al. (2011). Figure B-1 shows the relationship between the sum of ketones and sulfoxides and the log viscosity increase for oxidative aging from the Petersen et al. study. The analysis shows that the alcohols that are produced have a similar effect on viscosity increase as the ketones, and because they are more polar than ketones, they have a significant effect on the increase in viscosity, especially for high sulfur asphalts. Taking into consideration that ketones and sulfoxides form at different rates for different asphalts, the ratio between the ketone and sulfoxide formation rates is highly source-dependent. For example, binders extracted from different sources will have different sulfur contents, and this parameter will change the rate of sulfoxide formation. Then, the ratio between sulfoxide formation versus ketone formation will be binder source-dependent (Petersen et al. 2011). It should be noted that the absorbance peaks are direct measurements taken from the FTIR spectrum band, whereas the area-based measurements require numerical integration under the absorbance spectrum. The absorbance peak-based AIP is the easiest AIP to determine and it may involve less error or bias with regard to the method of calculation compared to the area-based AIPs.

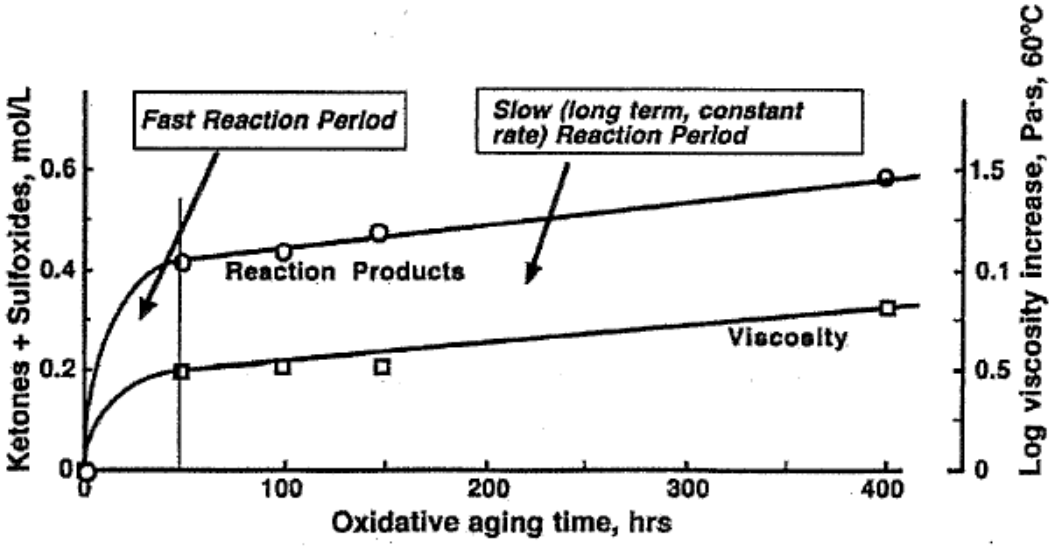

Figure B-1. Kinetics of ketones plus sulfoxide formation and viscosity increase during the dual oxidation mechanism for SHRP asphalt AAB-1, PAV-aged at 80°C (Petersen et al. 2011).

Rheological Parameters

Although chemical groups can be used to track oxygen uptake directly, and hence, can track the oxidation in asphalt binders, FTIR spectrometry is not a standard test procedure for characterizing asphalt. Moreover, the chemical functional groups provide little indication of the implications of oxidation on the rheological properties of interest. This limitation has prompted researchers to consider the use of the following rheological properties as AIPs:

Limiting Zero Shear Complex Viscosity (η_o^*)

Also known as *limiting viscosity*, has been used as an AIP. The limiting viscosity is defined as the plateau at low frequencies that is determined from a viscosity mastercurve. This property is independent of frequency or shear rate for unmodified binders (Han 2011). Furthermore, this property has been linked to carbonyl content for both neat and polymer-modified asphalt binders using Equation B-1 (Han 2011).

$$\ln(\eta_o^*) = HS.CA + m \tag{B-1}$$

where

η_o^* = asphalt binder limiting viscosity,
HS = hardening susceptibility,
CA = carbonyl content, and
m = log-viscosity intercept, where *HS* and *m* are asphalt binder-dependent.

Dynamic Shear Modulus (G)*

The dynamic shear modulus (*G**) is a property that can be measured directly and used to track the rheological changes caused by oxidation. The use of the *G** as an AIP is advantageous because it is a direct output of the DSR and is the most commonly used parameter that relates the physical properties of asphalt binder to asphalt pavement performance. Oxidative age hardening affects the *G** most significantly at high temperatures and/or low frequencies, as shown in Appendix E of this report.

Crossover Modulus (G^*_c)

The crossover modulus (G^*_c) is defined as the *G** value that corresponds to the reduced frequency where the storage modulus (*G'*) and loss modulus (*G"*) mastercurves cross (i.e., where the phase angle equals 45°), as shown in Figure B-2. The crossover modulus is a parameter that is found in the widely applied Christensen-Anderson (CA) model (Christensen and Anderson 1992) and has been proposed as an AIP to study the evolution of oxidative aging in asphalt binders (Farrar et al. 2013). Several different methods have been proposed for calculating the crossover modulus (e.g., data smoothing, interpolation, and curve fitting).

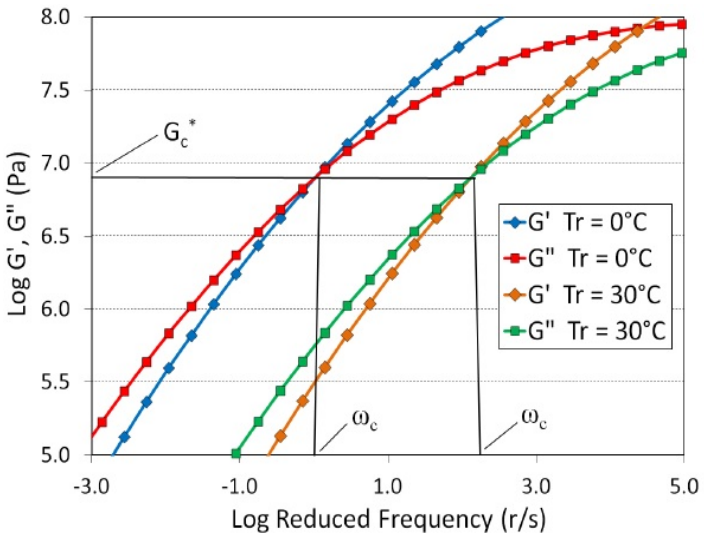

Figure B-2. Crossover modulus and frequency at two reference temperatures.

Oxidative aging leads to a decrease in the crossover modulus (*G*c*) value. To achieve a positive relationship with the aging duration, the inverse of the log of the crossover modulus (1/log *G*c*) is used as a rheological AIP (Farrar et al. 2013). Figure B-3 depicts that a linear relationship is found between the oxygen uptake and 1/log *G*c* for a given binder.

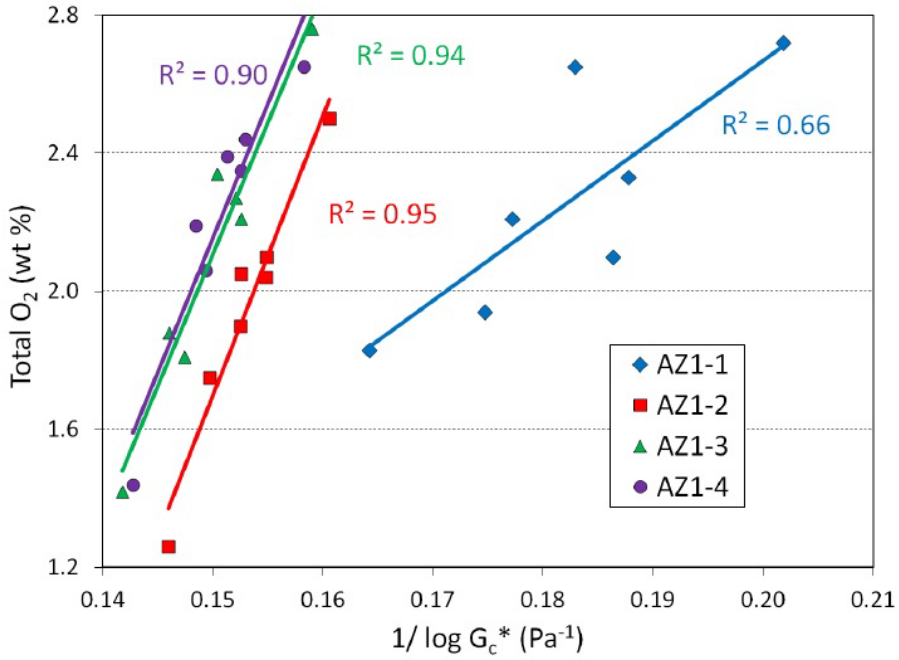

Figure B-3. Observed approximate linear relationship between oxygen uptake and the inverse of the log crossover modulus for the recovered binders from loose mix collected during construction and cores collected at 4 and 9 years after construction.

Zero Shear Viscosity (*ZSV*). Zero shear viscosity (*ZSV*) also was considered as a rheological AIP. *ZSV* is defined as the viscosity when the shear rate reaches zero (Binard et al. 2004, Brio et al. 2009). Marasteanu and Anderson (2002) proposed a method to estimate *ZSV* from frequency

sweep test results. In their method, the Christensen-Anderson-Marasteanu (CAM) model, (i.e., Equation B-2), has to be fitted to the frequency sweep test results. If the parameter *m* in the CAM model is larger than one, the CAM model is shifted to a reference temperature of 60°C by dividing the crossover modulus value by the time-temperature shift factor that corresponds to 60°C.

$$G^* = \frac{G_g^*}{[1+(f\ /\ f_c)^k]^{m/k}} \tag{B-2}$$

where

G^*_g = glassy modulus (Pa),
f_c = location parameter with dimensions of frequency (rad/s),
f = reduced frequency (rad/s),
m = CAM model shift factor, and
k = CAM model parameter.

Then, the Cox-Merz rule, shown in Equation B-3, is applied to convert the G^* value to viscosity.

$$G^*/\omega = \text{Viscosity} \tag{B-3}$$

Lastly, the limit of the function, as the frequency goes to zero, is used to obtain the *ZSV*, as shown in Equation B-4.

$$ZSV = \frac{G_g^*}{\omega_{c,refT=60°C}}\left(\frac{(m-1)^{m-1}}{m^m}\right)^{1/k} \tag{B-4}$$

where $\omega_{c,ref\,T=60°C}$ is the crossover frequency at the reference temperature (rad/s). If $m < 1$, then the CAM model is refitted to the data with $m = 1$, and the same algorithm is applied.

Glover-Rowe (G-R) Parameter

The Glover-Rowe (*G-R*) parameter also was used as a rheological AIP. The *G-R* parameter was proposed by Rowe based on his analysis of Glover et al.'s (2005) work on low temperature ductility (King et al. 2012). Glover et al. (2005) used the Maxwell mechanical analog model to derive a rheological parameter that is related to ductility, i.e., $G'/(\eta'/G')$, termed the 'Glover parameter'. This parameter has been proposed by Glover et al. (2005) as an indicator of pavement cracking potential. Rowe et al. (2014) simplified Glover's parameter to arrive at Equation B-5.

$$\frac{G^*(\cos\delta)^2}{\sin\delta} \tag{B-5}$$

where

G^* = dynamic shear modulus measured at 15°C and 0.005 rad/s (Pa), and
δ = phase angle measured at 15°C and 0.005 rad/s (°).

Testing at 0.005 rad/s is not possible. Therefore, the *G** and phase angle values at a reduced frequency that corresponds to 15°C and 0.005 rad/s should be determined from the *G** and phase angle mastercurves constructed from temperature-frequency sweep DSR testing and frequency-temperature shift factors.

Oxidation Kinetics

All asphalt materials exhibit relatively similar kinetics, with an initial fast reaction period, also known as *spurt*, followed by a slower reaction period that has an approximately constant rate (Petersen et al. 1996, Petersen 1998, Petersen et al. 2011, Prapaitrakul 2009, Han 2011). The hydrocarbon chemical reactions that occur during these two reaction periods are known to be fundamentally different (Petersen 1998). During the spurt, sulfoxides are the major oxidation product and cause an increase in viscosity. During the slower reaction period, ketones are the major product and drive the increase in viscosity (Petersen et al. 1996). Highly reactive hydrocarbon precursors of limited concentration react with oxygen during the fast reaction period to form hydroperoxides. Then, these hydroperoxides react primarily with the asphalt sulfides to form sulfoxides. When all of the highly reactive hydrocarbons are exhausted, the reaction proceeds at an approximately constant rate. Then, a classical free radical hydrocarbon chain reaction takes over during the slow, approximately constant reaction period (Petersen et al. 1996). Figure B-4 shows the two oxidation reaction periods at 113°C for SHRP asphalt AAG-1, the first hyperbolic kinetic oxidation curve with an initial rapid period of ketones and sulfoxide formation followed by lower (approximately constant) reaction rate (Prapaitrakul 2009, Petersen et al. 2011).

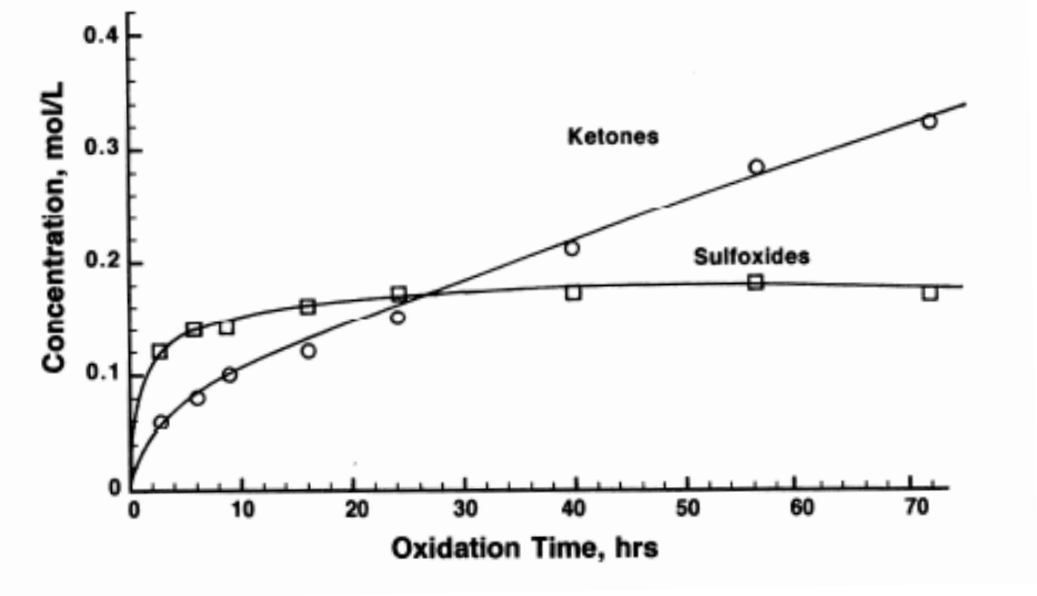

Figure B-4. Kinetic Oxidation of SHRP asphalt AAG-1 at 113°C (Petersen 2009).

The Arrhenius equation, presented as Equation B-6, describes the temperature dependency of the oxidation rate (Prapaitrakul 2009).

$$r = AP^{\alpha} \exp\left(\frac{-E_a}{RT}\right) \quad \text{(B-6)}$$

where

r = rate of the reaction,
A = frequency (pre-exponential) factor (s^{-1}),
P = absolute oxygen pressure,
α = reaction order with respect to oxygen pressure,
E_a = activation energy,
R = universal gas constant, or ideal gas constant, and
T = temperature (Kelvin).

When carbonyl content is used as an AIP, the kinetics models reveal a wide range of binder-specific Arrhenius parameters (Petersen 2009). However, when carbonyl + sulfoxide contents were used as an AIP in a recent study by the WRI to track the oxidation reaction, a simple dual mechanism model was used successfully to fit the oxidation of the 12 asphalt binders evaluated that originated from a wide variety of sources. The fitting used the same Arrhenius parameters for all 12 binders studied, with only one adjustable parameter, which represents the quantity of the fast reaction reactive material $C_{fast,o}$. Equation B-7 shows the model that was used to fit the isothermal data to determine the rate constants and amount of reactive material for each binder studied (Glaser et al. 2013b). If the Arrhenius parameters, shown in Equation B-8, can be applied universally, a single aging trial at a single temperature may be performed to characterize the oxidation kinetics for unmodified binders (Glaser et al. 2013b).

$$P = C_{fast,o}(1-\frac{k_2}{k_1})(1-e^{-k_1 t}) + k_2 C_{fast,o} t + P_o \quad \text{(B-7)}$$

where

P = reaction products,
$C_{fast,o}$ = fast reaction reactive material,
k_1 = temperature-dependent parameters of fast reaction paths,
k_2 = temperature-dependent parameters of slow reaction paths, and
t = time.

$$k'_1 = A_1 \exp\left(\frac{-E_{a,1}}{RT}\right)$$
$$k'_2 = A_2 \exp\left(\frac{-E_{a,2}}{RT}\right) \quad \text{(B-8)}$$

where

$A_{1,2}$ = Arrhenius pre-exponential constant, and
$E_{a,1,2}/R$ = Arrhenius activation energy divided by gas constant.

Effect of Temperature above 100°C on Oxidative Aging

The oxidation of asphalt binder involves several independent and concurrent reactions. Temperature can affect the rate of oxidation, the binder species that are oxidized, and the nature of the oxidized species that are formed. Thus, temperature is a critical factor in laboratory simulations of long-term aging. Although increasing the aging temperature increases the rate of oxidation, which is a desirable attribute, it can also disrupt polar molecular associations and lead to the thermal decomposition of sulfoxides. Thus, accelerated aging of asphalt binder at significantly high temperatures may lead to a fundamentally different aged asphalt binder than asphalt aged in the field (at a lower temperature) (Branthaver et al. 1993). The literature indicates that the disruption of polar molecular associations and sulfoxide decomposition become critical at temperatures that exceed 100°C (Petersen 2009). Furthermore, aging at temperatures above 100°C can lead to asphalt mastic drain-down from the loose mix because asphalt binder has low viscosity values at elevated temperatures. Therefore, the effects of laboratory aging at temperatures over 100°C can be divided into three categories: chemical effects, physicochemical effects, and binder/mastic drain-down, as shown in Figure B-5.

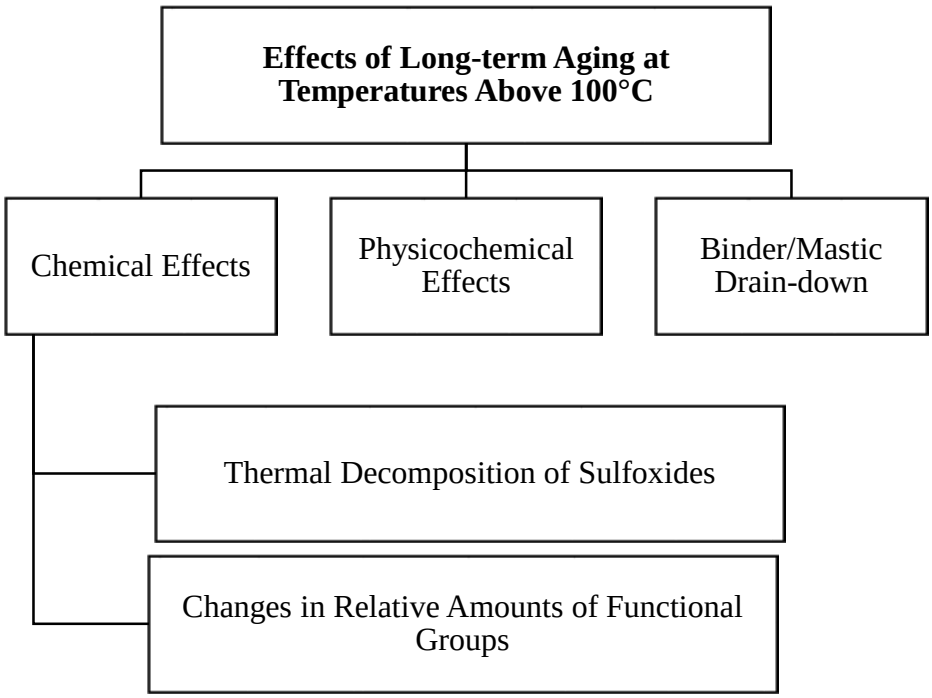

Figure B-5. Summary of effects of long-term aging at temperatures above 100°C.

Chemical Effects

Petersen (2009) compared the relative amounts of different chemical functional groups that were formed during the oxidation of Strategic Highway Research Program (SHRP) binder AAF-1 at two temperatures, 85°C and 113°C. Aging was conducted using thin films conditioned at ambient pressure. The results, shown in Figure B-6, demonstrate that a larger concentration of sulfoxides formed at the expense of ketones during the initial oxidation spurt at 85°C compared to 113°C. The right-hand graph in Figure B-6 shows that the relationship between rheology (dynamic viscosity) and sulfoxide concentration differs between the two aging temperatures, indicating fundamental differences in the oxidation reactions at 85°C and 113°C.

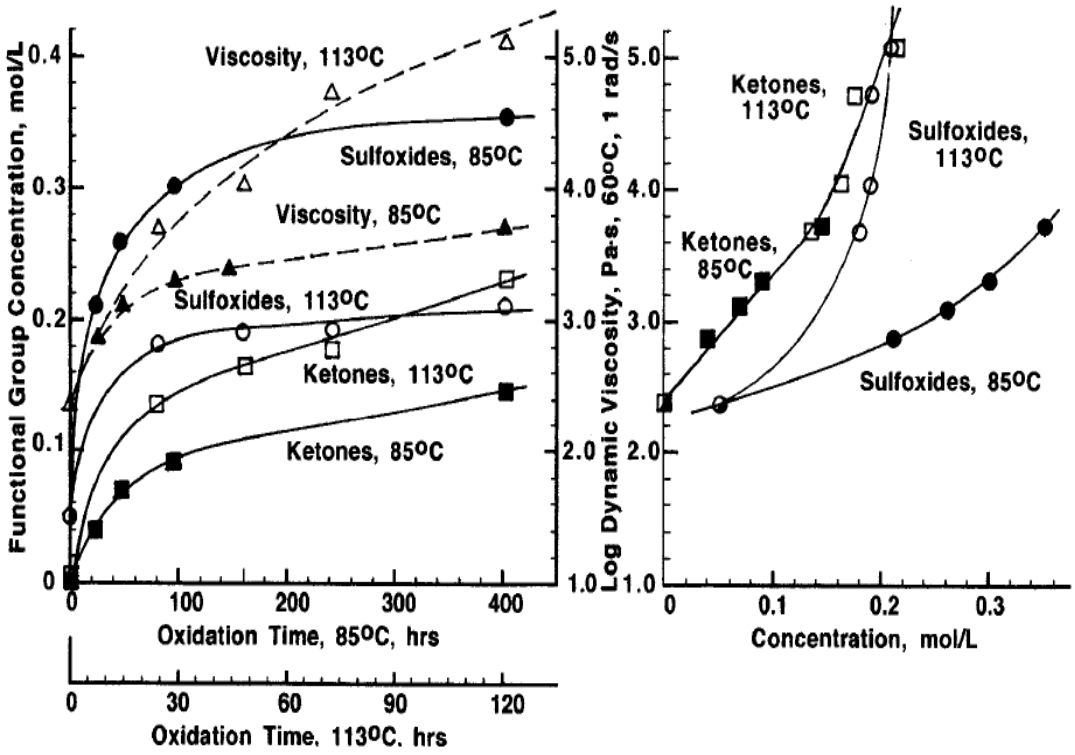

Figure B-6. Oxidative aging kinetic data and viscosity-functional group relationships for SHRP asphalt AAF-1 after thin film accelerated aging test (TFAAT) of oxidation as a thin film at atmospheric pressure (Petersen 2009).

Petersen and Harnsberger (1998) studied the effects of aging temperature on the sulfur content of eight SHRP asphalt binders. The results, shown in Figure B-7, correspond to the aging that occurred during the initial fast reaction period, also known as the 'spurt'. The ratio of sulfoxides to ketones differs based on whether the binder was aged at 85°C or 113°C. Generally, greater amounts of ketones were formed at the expense of sulfoxides at 113°C compared to 85°C. Petersen (2009) reported that the initial fast reaction spurt initially resulted from the reaction of oxygen with highly reactive perhydroaromatic hydrocarbons to form hydroperoxides. Then, the hydroperoxides could either react with the asphalt sulfides to form sulfoxides or decompose to form free radicals that participate in a subsequent oxidation reaction that involves benzylic

carbon on aromatic rings to form ketones. Because hydroperoxides are thermally unstable, more free radicals are produced and fewer sulfoxides are formed at higher temperatures.

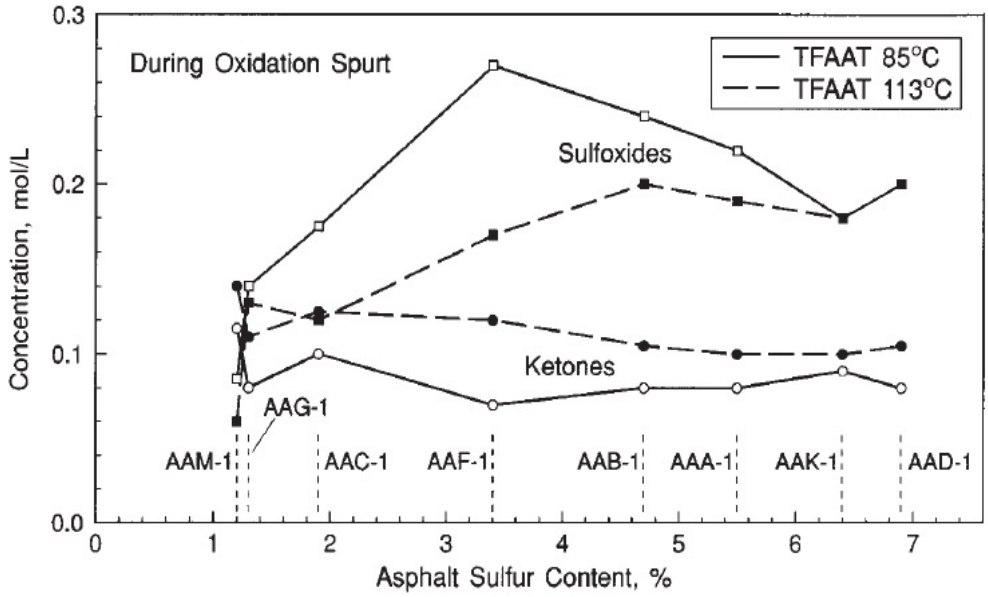

Figure B-7. Ketones and sulfoxides formed during oxidation spurt (fast reaction period) of eight SHRP binders during thin film accelerated aging test (TFAAT) of oxidation at atmospheric pressure (Petersen and Harnsberger 1998).

The other factor that may contribute to the decrease in the amount of sulfoxides that are formed relative to the ketones that are formed during the oxidation of asphalt at temperatures over 100°C is the thermal decomposition of the sulfoxides (Petersen et al. 1981, Herrington et al. 1994, Petersen 2009, Petersen and Glaser 2011, Glaser et al. 2013b). Herrington et al. (1994) showed that the rate of asphalt sulfoxide decomposition can be significant. Figure B-8 presents a sulfoxide absorbance evolution with aging time at aging temperatures of 100°C and 130°C for typical asphalt. The results indicate that, although the concentration of sulfoxides increases with aging at 100°C, the sulfoxide concentration decreases after an aging duration of 50 hours at 130°C. This decrease in sulfoxide absorbance indicates that the rate of sulfoxide decomposition is greater than the rate of the formation of new sulfoxides upon oxidation.

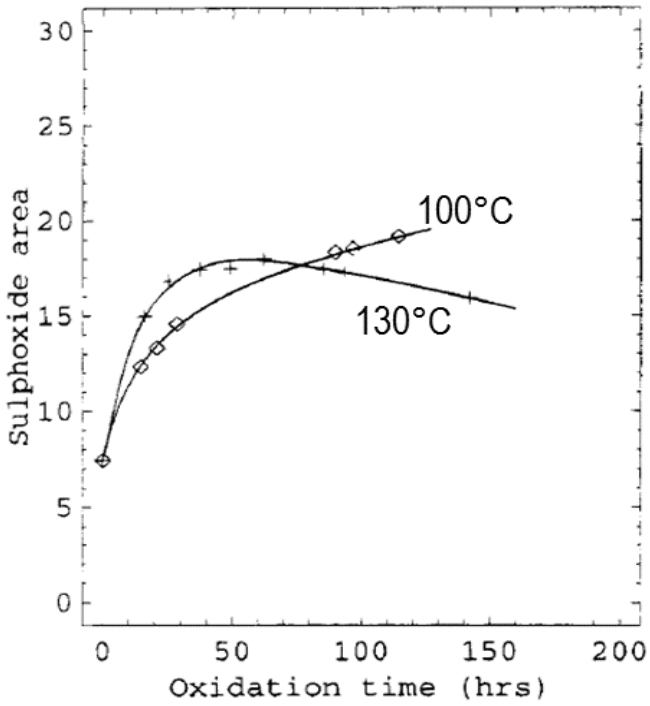

Figure B-8. Effect of oxidation duration and temperature on sulfoxide absorbance (Herrington et al. 1994).

Petersen (2009) further evaluated the thermal decomposition of sulfoxides in asphalt binder during oxidation. Sulfoxides form very rapidly during the initial oxidation and generally reach a constant concentration after prolonged aging, termed the 'steady state' concentration. For asphalt binder with low sulfur content, the steady state sulfoxide concentration results from the depletion of reactive sulfides. That is, all the sulfur that contains molecules becomes oxidized. However, in most asphalt binders with moderate to high sulfur contents, the occurrence of a steady state sulfur concentration is the net result of the sulfoxide formation from oxidation and sulfoxide loss through thermal decomposition. Petersen et al. (1981) provided evidence to support this phenomenon by evaluating the oxidation kinetics of Boscan asphalt with relatively high sulfur content (~5.5%). The Boscan asphalt was subjected to various oxidation temperatures and film thicknesses.

Table B-1 presents the steady state concentrations of the sulfoxides that correspond to the different aging conditions. In both thin film (~0.0015 cm) and thick film (~0.5 cm) oxidation experiments, the steady state sulfoxide concentration decreased as the aging temperature increased. The decrease in the steady state sulfur concentration with an increase in the aging temperature indicates that, as the temperature increases, more of the sulfoxides decompose, which lowers the resultant steady state concentration of the sulfoxides.

Table B-1. Steady state concentrations of sulfoxides in Boscan ssphalt under different oxidation conditions (Petersen et al. 1981)

Oxidation Method	Oxidation Temperature, °C	Steady State Sulfoxide Concentration, mol./L
Thin film on Teflon™ (~0.0015 cm)	25	> 0.46*
	113	0.40
	130	0.28
	163	0.16
Thick-film rolling thin-film oven (~0.5 cm)	113	0.21
	130	0.19
	163	0.15

* No steady state concentration was reached at the conclusion of the experiment because sulfoxide decomposition is negligible at 25°C.

Physicochemical Effects

The physicochemical interactions amongst the molecules in asphalt binder affect its temperature sensitivity to oxidation and can alter the oxidation products that are formed when aging occurs at temperatures over 100°C. Petersen (2009) compared the kinetics of two SHRP binders: AAD-1 and AAG-1. These two binders are known to have different microstructures, with AAD-1 possessing less compatible chemistry and consequently a significant microstructure concentration compared to AAG-1. Although the two binders have different microstructure concentrations, Figure B-9 shows that the two binders exhibit similar oxidation kinetics for aging temperatures between 65°C and 85°C. However, the kinetics of the two binders are vastly different when the aging temperature exceeds 100°C. At temperatures over 100°C, the less compatible asphalt with high microstructure concentration (AAD-1) oxidizes much more rapidly than the more compatible asphalt with low microstructure concentration (AAG-1). The AAD-1 binder undergoes significant physicochemical disruption of its microstructure above 100°C, which increases the availability of molecules for oxidation and hence explains the observed trends.

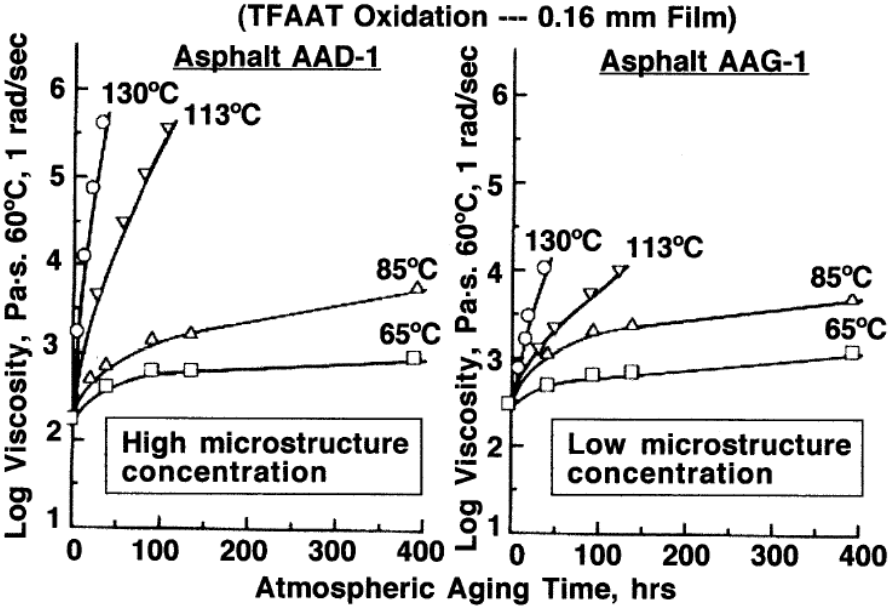

Figure B-9. Effects of temperature and component compatibility on age-hardening kinetics (Petersen 2009).

The literature review presented indicates that oxidation kinetics models that are derived based on results obtained at aging temperatures below 100°C cannot be extrapolated to predict oxidation kinetics at temperatures above 100°C (and vice versa) because the oxidation reactions are inherently different. Thus, although kinetics that correspond to temperatures below 100°C can be modeled using a simple Arrhenius type model, an additional model is needed to account for changes in the oxidation reaction in order to extrapolate to higher temperatures, thereby complicating modeling efforts to correlate loose mix aging times in the laboratory with field aging levels.

Mastic Draindown

Braham et al. (2009) aged loose mixture in an oven at 135°C in an effort to simulate long-term aging efficiently. However, Braham et al. (2009) reported problems with mastic drain-down to the bottom of the aging pan during conditioning. Their study suggests that the drain-down was caused by the low viscosity of the asphalt binder at 135°C. Such loss of mastic is a significant concern for performance testing, as asphalt content plays a key role in mixture performance. Drain-down may decrease the uniformity of a mix and can cause a large loss of mastic due to the binder sticking to the aging pan. Braham et al. (2009) attempted to quantify the extent of the binder drain-down by comparing the mass of the aging pan (empty) before aging to that after aging and removing the aged loose mix in order to calculate the amount of drain-down. They calculated the percentage of drainage by first subtracting the initial empty pan weight from the final pan weight (i.e., the pan with drained materials) and then dividing the result by the initial total sample weight. The authors concluded that drain-down was not significant when the aging duration was less than 24 hours. However, the authors stated that the quantity of the material lost to the pan became significant as the aging time increased. Figure B-10 shows the percentage of drain-down

associated with aging loose mix prepared with PG 58-28 binder at 135°C for different durations in the Braham et al. (2009) study.

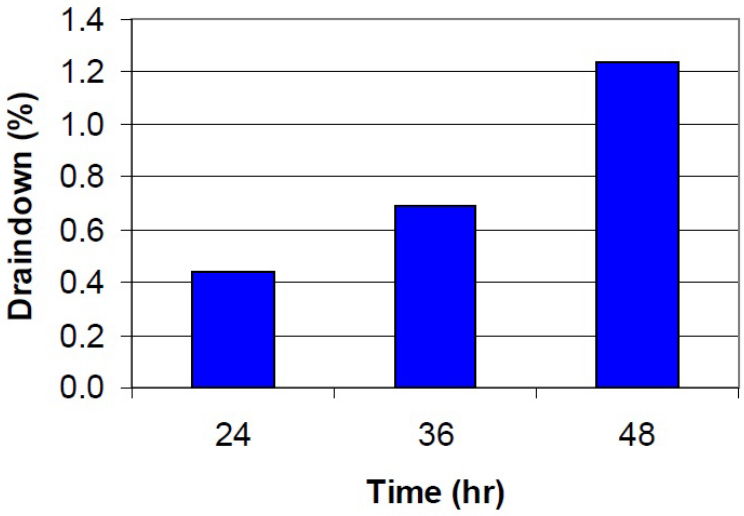

Figure B-10. Percentage of drain-down from mix M3 (PG 58-28) (Braham et al. 2009).

Effect of Mineral Filler on Aging Susceptibility of Asphalt Mixtures

The oxidation reaction is affected by the physicochemical interactions between the asphalt binder and the aggregate (Moraes and Bahia 2015, Wu et al. 2014, Petersen 2009, Little et al. 2006, Recasens et al. 2005, Huang et al. 2002, Jones 1997, Petersen et al. 1987). The mineral filler has the greatest specific surface area of the aggregate blend and thus, contributes most significantly to physicochemical interactions. Physicochemical interactions lead to the adsorption of polar components of the binder onto filler surfaces. Adsorbed components do oxidize. Figure B-11 demonstrates the effect of different aggregate types on aging indices as a ratio of GPC molecular weight of samples after 24 hours of PAV and unaged samples (Moraes and Bahia 2015). Where LH1 is hard limestone and GH1 is hard granite. While Figure B-12 demonstrates the effect of different aggregate types on aging index in terms of complex moduli of recovered binders after compaction and after long-term aging (Wu et al. 2014).

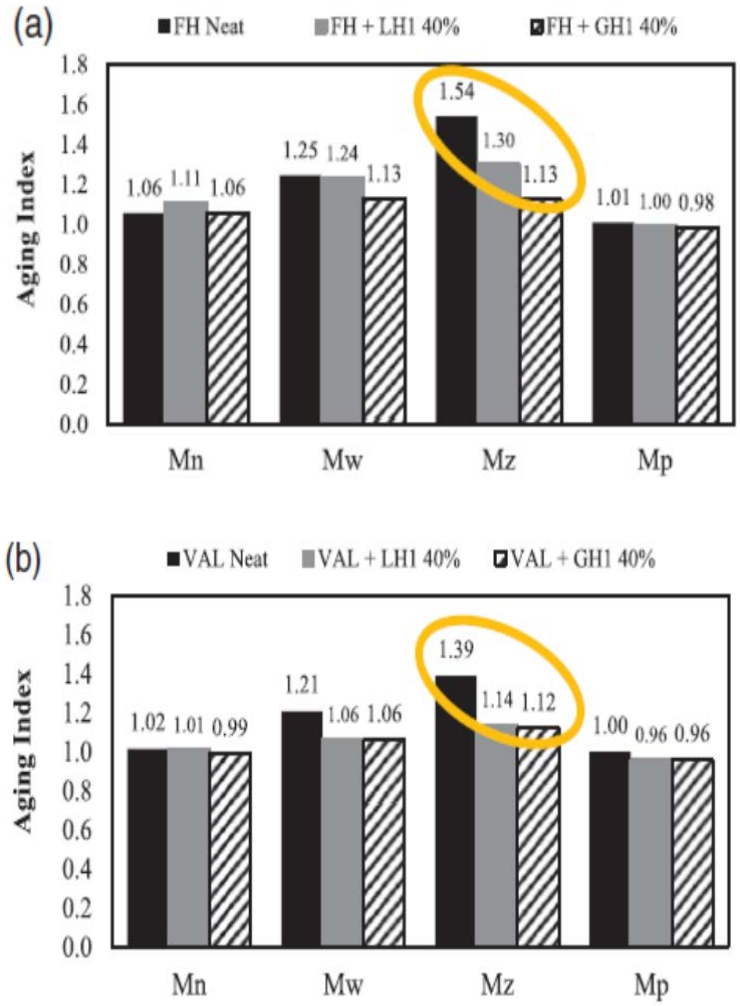

Figure B-11. Aging indices of GPC molecular weight of: (a) FH base binder and mastics and (b) VAL base binder and mastics (Moraes and Bahia 2015).

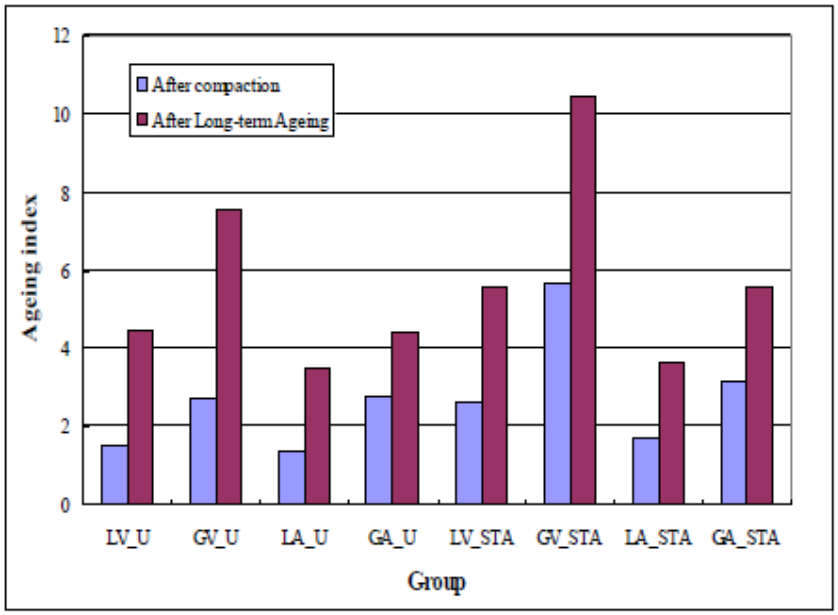

Figure B-12. Aging Indices in Terms of Complex Moduli of Binders Recovered from Mixtures; where letter L refers to limestone mixtures and letter G refers to granite mixtures (Wu et al. 2014).

The literature demonstrates that hydrated lime reduces oxidative aging more significantly than conventional mineral fillers as shown by the results presented in Figure B-13 (Petersen et al. 1987) and Figure B-14 (Jones 1997).

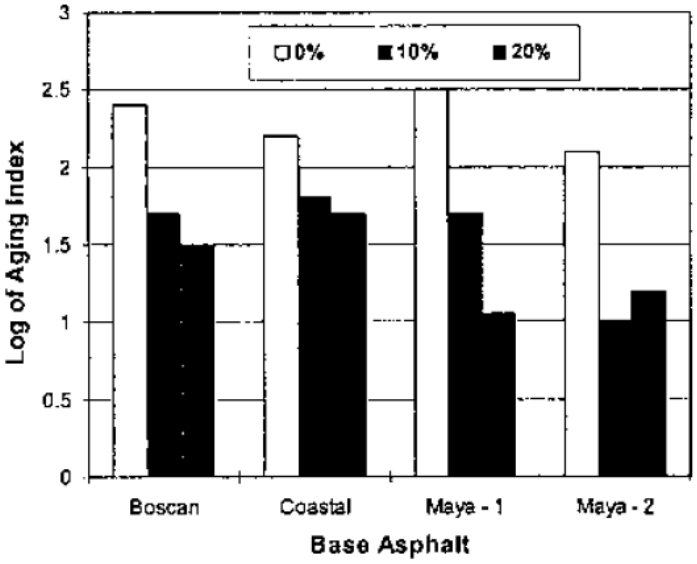

Figure B-13. Effect of hydrated lime in reducing aging index of asphalt binders (Petersen et al. 1987).

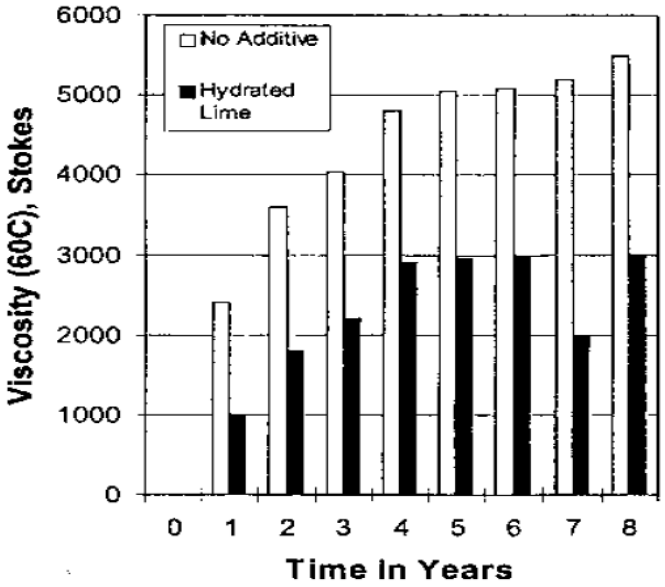

Figure B-14. Field data demonstrating the effect of hydrated lime on the hardening of asphalt binder based on Utah data (Jones 1997).

Empirical Models for Asphalt Binder Aging in Pavements

The *global aging system* (GAS) model (Mirza and Witczak 1995) is an empirical model that allows for the prediction of the change in binder viscosity as a function of age, given the mean annual air temperature (MAAT), and also considers the aging gradient with pavement depth. The model assumes a hyperbolic aging function that predicts a decreasing rate of viscosity with an increase in age (generally consistent with the observations made for the two-stage oxidation kinetics model discussed previously), under the assumption that most age hardening occurs within the first ten years of a pavement's service life. The GAS model is summarized in Equations B-9 and B-10.

$$\log\log(\eta_{aged}) = \frac{\log\log(\eta_{t=0}) + At}{1 + Bt} F_v \quad \text{(B-9)}$$

$$\log\log(\eta_{aged,z}) = \frac{\eta_{aged}(4+E) - E \times \eta_{t=0}(1-4z)}{4(1+E \times z)} F_v \quad \text{(B-10)}$$

where

η_{aged} = aged viscosity (centipoise),
$\eta_{t=0}$ = viscosity at mix/laydown (centipoise),
A and B = functions of the temperature and MAAT for the location of interest and $\eta_{t=0}$,
F_v = optional air void content adjustment factor,
t = time in months,
z = depth, and
E = function of MAAT.

The simplicity of the GAS model makes it an attractive option. However, the GAS model has been criticized for the following reasons:

1) The form of the GAS model implemented into the MEPDG does not account for aging 1.5 inches below the pavement surface (Mirza and Witczak 1995, Prapaitrakul 2009).
2) The model does not account directly for differences in asphalt binder kinetics among binder types.
3) The method used to account for air void content is based on a relatively small set of conditions, which is the reason this adjustment factor is considered optional (Mirza and Witczak 1995).
4) Prapaitrakul expressed concern over the unrecorded recovery method used to obtain binders from the field in developing the GAS model, because solvent recovery processes can leave residual solvent in the extracted binder, which leads to an effective softening and, hence, potentially leading to erroneously low viscosity values (Prapaitrakul 2009).

Despite these criticisms, the GAS model has been useful in the MEPDG and in other research studies. Its success and practical usage can be linked to its use of simple and easy-to-identify parameters.

Fundamental Models for Asphalt Binder Aging in Pavements

A preliminary fundamentals-based, one-dimensional combined asphalt oxidation kinetics and diffusion model was developed at Texas A&M University. This model is referred to as the *transport model* (Lunsford 1994). Lunsford's foundational work on the transport model (1994) combines a mathematical model of asphalt oxygen diffusion and reaction kinetics, as shown in Equation B-11, with Fick's law of diffusion, as presented in Equation B-12.

$$\left(\frac{\partial C_{O_2}}{\partial t}\right) = -\nabla N_{O_2} - r_{O_2} \tag{B-11}$$

where

C_{O2} = concentration of oxygen (mol. /m^3),
N_{O2} = oxygen diffusion flux (mol.m^{-2}.s^{-1}), and
r_{O2} = oxygen depletion rate.

$$N_{O_2} = -D_{O_2} \nabla C_{O_2} \tag{B-12}$$

where

D_{O2} = diffusion coefficient of oxygen (m^2.s^{-1}) and
∇ = gradient operator.

However, Lunsford's initial work did not include the effect of aggregate and void structure on diffusion; hence, approximate values were used as the oxygen diffusivity coefficients for the asphalt binders. In addition, the framework did not include a pavement temperature model (Prapaitrakul 2009).

Prapaitrakul et al. (2009) expanded on the work of Lunsford (1994) to overcome these deficiencies. The Prapaitrakul et al. diffusion model is based on three interlinked processes: 1) the diffusion of oxygen into the asphalt binder mastic in the pavement, 2) heat transfer into the pavement that results in temperature variations with depth and time, and 3) asphalt binder oxidation kinetics. Modeling these processes was facilitated by quantifying the air void distribution in the mixture, which dictates the availability of oxygen for the binder (Prapaitrakul et al. 2009).

Figure B-15 provides a depiction of the Prapaitrakul overall approach (Prapaitrakul 2009). This improvement to the original transport model was developed in a cylindrical coordinate system that is able to capture the effects of air void structure on pavements and include those effects in the model calculations. The use of cylindrical coordinates is based on the assumption that oxygen in asphalt concrete exists in air channels that extend through the pavement depth and is replenished from the thermal cycle within the pavement that leads to excess oxygen for the oxidation reaction. The model also is based on the assumption that the partial pressure of oxygen at the pore surface equals the partial pressure of oxygen in air (approximately 0.2 atm).

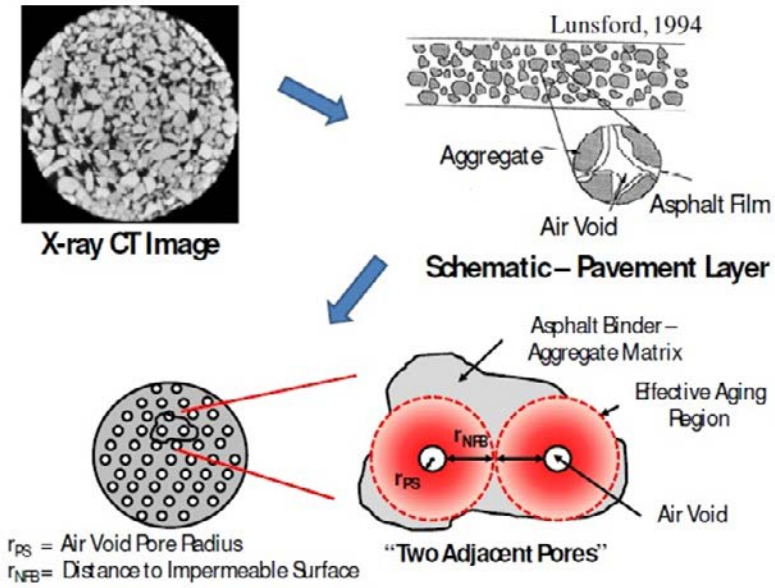

Figure B-15. Texas A&M University oxygen transport model, proposed by Prapaitrakul et al. (2009).

As part of the Asphalt Research Consortium (ARC) project, a more recent study by Han (2011) built upon the work of Prapaitrakul by modeling diffusion as two interlinked steps: 1) the diffusion/flow of oxygen from the atmosphere above the pavement into the interconnected air voids in the pavement (termed *vertical transport*) and 2) the diffusion of oxygen from the air voids to the adjoining asphalt-aggregate matrix (termed *horizontal transport*) where it reacts with the asphalt binder. Equation B-13 summarizes the vertical transport sub-model, which replaces the aforementioned assumption made by Prapaitrakul that oxygen partial pressure at the pore surface at any given depth equals the oxygen partial pressure in air (0.2 atm). Equation B-14 expresses the sub-model for horizontal oxygen diffusion. These steps are modeled mathematically to calculate the oxidation rate for a finite asphalt-aggregate matrix layer for each

air void. Taking in consideration that Equation B-13 is used for a single void geometry, this function would need to be repeated multiple times for the different air void geometries. The bulk oxidation rate for a pavement layer then is calculated as the average of the oxidation rates calculated for each air void.

$$\frac{\partial P}{\partial t} = 0.2\frac{\partial P}{\partial z} + A \times r_{O_2} \tag{B-13}$$

where

P = oxygen partial pressure,
A = proportion of modeled cross-section that is void space,
r_{O2} = rate of oxygen consumption, and
z = depth along diffusion channel.

$$\frac{\partial P}{\partial t} = \frac{1}{r}\frac{\partial}{\partial r}(rD_{O_2}\frac{\partial P}{\partial r}) + (\frac{cRT}{h})r_{CA} \tag{B-14}$$

where

r = diffusion distance (in cylindrical coordinate system),
D_{O2} = oxygen diffusivity in asphalt binder,
c = conversion factor from oxygen partial pressure units to concentration units in asphalt binder,
R = gas constant,
T = absolute temperature,
h = Henry's law constant, and
r_{CA} = rate of carbonyl uptake.

It is should be noted that the model calculations provide a range of oxidation rates, not a single value, depending on the upper or lower limit of the oxygen partial pressure, P_{av}, in a given pore. The higher oxidation rates are based on the assumption that convective flow through the pavement pores is sufficient to maintain oxygen partial pressure at 0.2 atm. The lower rate calculation is based on the assumption that the replenishment of oxygen in the pores is achieved only via the diffusion of oxygen from the pavement surface (Asphalt Research Consortium 2011).

Figure B-16 provides an overall picture of the four sub-models developed at Texas A&M University that comprise the transport model. Many of the required inputs for the sub-models are not standard test methods. For instance, X-ray computed tomography (CT) was used in this model to measure sophisticated air void structure properties, such as the air void radius and its frequency of existence within the pavement, to be used as inputs for the vertical transport sub-model. Because taking these measurements is extremely challenging, many assumptions had to be made, even with the X-ray CT. Also, FTIR spectrometry was used extensively to obtain binder-specific kinetics parameters (such as AP^{α}, E, HS, and m) as inputs for the oxidation kinetics sub-model. Thus, if this model is used in the current project, efforts will be made to develop surrogate means to obtain these inputs.

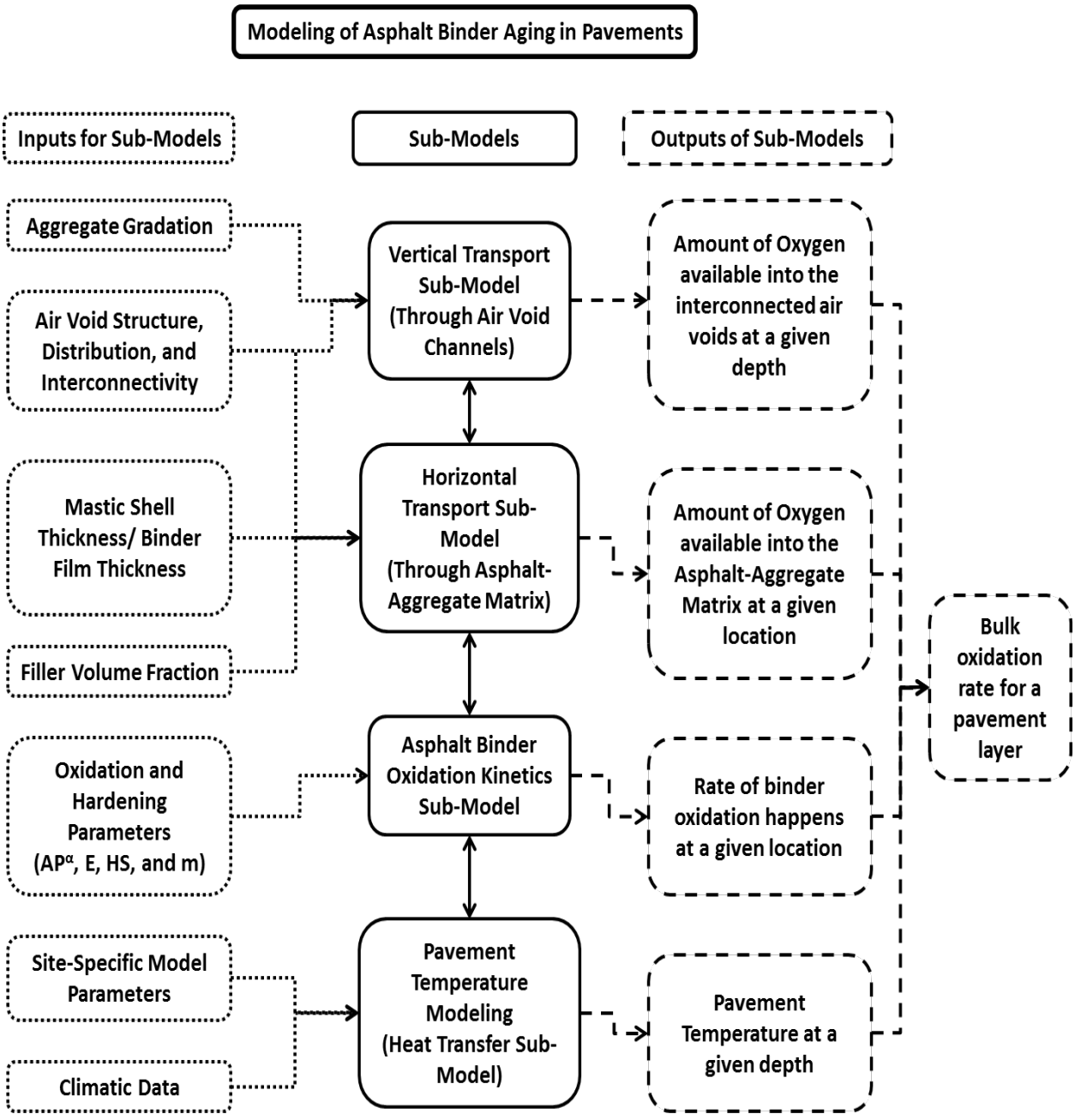

Figure B-16. Diagram of required inputs and resulting outputs of each sub-model developed at Texas A&M University.

The asphalt binder oxidation kinetics sub-model developed at Texas A&M University does not consider the aforementioned dual oxidation kinetics; instead, it considers an initial jump assumption that allows the model to consider only the second slower reaction following the initial fast reaction (Han 2011).

The field validation of the Texas A&M University transport model was part of the ARC project. The predicted versus measured oxidation rates obtained from the field cores were compared using six pavement sites in Texas and Minnesota. The pavement sections used in this study and the corresponding results are summarized in Table B-2,

Table B-3 and in Figure B-17. The oxidation rates measured in the field agree well with the predicted oxidation rates, with a few exceptions for newly constructed pavements where the rate of the asphalt binder oxidation is likely still governed by the initial rapid reaction (i.e., spurt). For those sections, the oxidation rates were underestimated significantly due to the use of the slower, constant reaction rate assumption used in the model (Han 2011). Despite the under-prediction of the oxidation levels in the newer pavements, in general, the fundamentals-based model provides a very good prediction of the field measurements, which suggests that the model captures the critical elements that affect asphalt binder oxidation in pavements (Asphalt Research Consortium 2011).

Table B-2. Field sites studied in the ARC study (Han 2011)

District (State)	Highway	Thickness (inch)	PG (modifier)	Binder Supplier	AAV (%)	Cons.	1st Coring	2nd Coring
Laredo (TX)	US277	2.5	70-22 (SBS)	Valero-C	7.27	2008	07/2008	09/2009
Lufkin (TX)	US69	2	70-22 (SBS)	Marlin	7.91	2003	02/2005	06/2008
Bryan (TX)	US290	2.5	64-22 (Un)	Eagle	12.44	2002	10/2005	08/2008
Waco (TX)	IH35 #5	3	70-22 (SBS)	Alon	5.86	2003	10/2005	08/2008
Amarillo (TX)	US54	2.5	70-28 (SBS)	Alon	7.33	1998	12/2004	07/2008
Laredo (TX)	IH35 #4	2	70-22 (SBS)	Valero-C	2.01	2007	--	06/2008
Metro Area (MN)	I-94	4.5	AC-120(Un)	--	4.81	1993	11/2004	11/2008

Table B-3. Comparison of measured and modeled field oxidation rates (Han 2011)

STATES	Site	Oxidation rate modeled (CA/year)		Bulk oxidation rate measured (CA/year)
		Maximum	Minimum	
MN	Cell 1	0.0200	0.0195	0.0256
TX	US277-LRD	0.0465	0.0451	0.0705
	US69-LFK	0.0258	0.0255	0.0370
	IH35-LRD #4	0.0384	0.0245	---
	US290-BRY	0.0651	0.0620	0.0671
	IH35-WAC #4	0.0264	0.0243	0.0340
	US54-AMR	0.1117	0.0994	0.0935

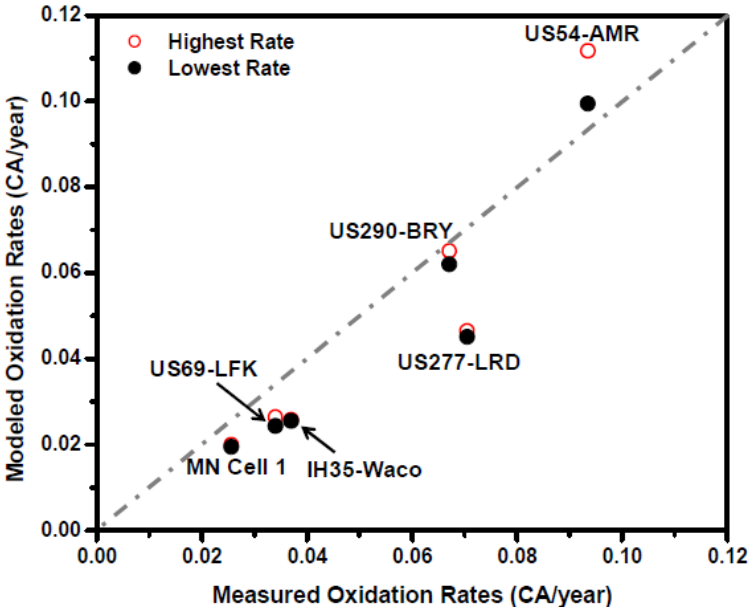

Figure B-17. Graphical comparison of measured and modeled field oxidation rates (Han 2011).

According to Han (2011), the Transport model is still in the initial stage of development, and the model calibration and validation steps are ongoing. Furthermore, the transport model has some additional constraints. It currently requires detailed information about air void content and distribution as well as the temperature gradient along the depth at a higher level of accuracy than can be provided by available databases, including the Enhanced Integrated Climatic Model (EICM).

Summary

In summary, rheological and chemical AIPs were presented for tracking oxidation levels. Rheological AIPs are advantageous in that they reflect mechanical behavior and negate the need for FTIR. However, past kinetics modeling efforts have focused on chemical AIPs. A kinetics model based on tracking the carbonyl + sulfoxides chemical functional group that takes into account the dual oxidation kinetics (initial fast reaction followed by a slower reaction) and requires a single, material-dependent parameter was presented. A review of the GAS and Texas A&M University pavement aging models was presented. The GAS model is relatively simple to implement but as significant limitations. The transport model developed at Texas A&M University is more fundamental but lacks validation and requires detailed information that may limit practical implementation. In addition, the effect of aging at temperatures higher than 100°C as the effect of mineral fillers on the oxidative reaction mechanisms were discussed.

References

American Association of State Highway and Transportation Officials (AASHTO), *Standard Practice for Mixture Conditioning of Hot Mix Asphalt,* AASHTO R 30, Washington, D.C. (2010).

Asphalt Research Consortium. *Quarterly Technical Progress Report.* Western Research Institute, October – December. (2011).

Binard, C., D. Anderson, L. Lapalu, and J. P. Planche. "Zero shear viscosity of modified and unmodified binders." *Proceedings of the 3rd Eurasphalt & Eurobitume Congress, Vienna,* 236 (2) (2004), pp. 1721–33.

Braham, A. F., W. G. Buttlar, T. R. Clyne, M. O. Marasteanu, and M. I. Turos, "The Effect of Long-term Laboratory Aging on Asphalt Concrete Fracture Energy." *Journal of the Association of Asphalt Paving Technologies*, Vol. 78 (2009).

Branthaver, J. F., J. C. Petersen, R. E. Robertson, J. J. Duvall, S. S. Kim, P. M. Harnsberger, T. Mill, E. K. Ensley, F. A. Barbour, and J. F. Scharbron, *Binder Characterization and Evaluation – Vol. 2: Chemistry*, Strategic Highway Research Program, SHRP-A-368, National Research Council, Washington, D.C. (1993).

Biro, S., T. Gandhi, and S. Amirkhanian. "Determination of zero shear viscosity of warm asphalt binders." *Construction and Building Materials*, 23(5) (2009), pp. 2080-2086.

Christensen, D. W., and D. A. Anderson. "Interpretation of dynamic mechanical test data for paving grade asphalt cements". *Journal of the Association of Asphalt Paving Technologists*, V. 61 (1991).

Farrar, M. J., T. F. Turner, J. P. Planche, J. F. Schabron, and P. M. Harnsberger, "Evolution of the Crossover Modulus with Oxidative Aging" Washington, DC: Transportation Research Board. (2013).

Glaser, R., J. Schabron, T. Turner, J. P. Planche, S. Salmans, and J. Loveridge, "Low-Temperature Oxidation Kinetics of Asphalt Binders." *Transportation Research Record: Journal of the Transportation Research Road*, No. 2370, (2013a), pp. 63-68.

Glaser, R., T. F. Turner, J. L. Loveridge, S. L. Salmans, and J. P. Planche, *Fundamental Properties of Asphalts and Modified Asphalts III*, Quarterly Technical Report, Federal Highway Administration (FHWA), Contract No. DTFH61-07-D-00005. (2013b).

Glover, C. J., A. E. Martin, A. Chowdhury, R. Han, N. Prapaitrakul, X. Jin, and J. Lawrence, *Evaluation of Binder Aging and its Influence in Aging of Hot Mix Asphalt Concrete: Literature Review and Experimental Design,* Report 0-6009-1. Texas Transportation Institute, College Station, Texas. (2008).

Glover, C. J., R. R. Davison, C. H. Domke, Y. Ruan, P. Juristyarini, D. B. Knorr, and S. H. Jung. "*Development of a New Method for Assessing Asphalt Binder Durability with Field Validation*." No. FHWA/TX-05/1872-2, (2005).

Han, R. *Improvement to a Transport Model of Asphalt Binder Oxidation in Pavements: Pavement Temperature Modeling, Oxygen Diffusivity in Asphalt Binders and Mastics, and Pavement Air Void Characterization.* Collage Station, TX: Texas A&M University. (2011).

Herrington, P. R., J. E. Patrick, and G. F. Ball, "Oxidation of Roading Asphalts." *Industrial and Engineering Chemistry Research*, Vol. 33, No. 11 (1994) pp. 2801-2809.

Huang, S. C., J. C. Petersen, R. Robertson, and J. Branthaver, "Effect of Hydrated Lime on Long-Term Oxidative Aging Characteristics of Asphalt." *Transportation Research Record: Journal of the Transportation Research Board*, No. 1810, Transportation Research Board of the National Academies, Washington, D.C. (2002) pp. 17-24.

Jones, G. M., "The Effect of Hydrated Lime on Asphalt in Bituminous Pavements" NLA Meeting, Utah DOT, Utah, USA. (1997).

King, G., M. Anderson, D. Hanson, and P. Blankenship. "Using black space diagrams to predict age-induced cracking." *7th RILEM International Conference on Cracking in Pavements*. Springer Netherlands, (2012), pp. 453-463.

Little, D. N., J. A. Epps, and P. E. Sebaaly, *Hydrated Lime in Hot Mix Asphalt*, National Lime Association. (2006).

Lunsford, K. M. (1994). *The effect of temperature and pressure on laboratory oxidized asphalt films with comparison to field aging.* College Station, TX: Texas A&M University.

Marasteanu, M. O., and D. A. Anderson. "Determination of asphalt binder's viscosity from other rheological parameters." *Ninth International Conference on Asphalt Pavements*, (2002).

Mirza, M. W. and M. W. Witczak, "Development of Global Aging System for Short and Long Term Aging of Asphalt Cements." *Journal of the Association of Asphalt Paving Technologists*, Vol. 64 (1995) pp. 393-430.

Moraes, R. and H. U. Bahia, "Effect of Mineral Filler on Changes in Molecular Size Distribution of Asphalt during Oxidative Aging." *Road Materials and Pavement Design*, Vol. 16 (2015), pp. 55-72.

Petersen, J. C. "Chemical Composition of Asphalt as Related to Asphalt Durability: State of the Art." *Transportation Research Record* 999, (1984), pp. 13-30.

Petersen, J. C., "A Dual, Sequential Mechanism for the Oxidation of Petroleum Asphalts." *Petroleum Science and Technology*, Vol. 16, No. 9-10 (1998), pp. 1023-1059.

Petersen, J. C., "A Review of the Fundamentals of Asphalt Oxidation: Chemical, Physicochemical, Physical Property, and Durability Relationships." *Transportation Research Board, Transportation Research Circular (E-C140)*, National Research Council, Washington, D.C. (2009).

Petersen, J. C. and R. Glaser, "Asphalt Oxidation Mechanisms and the Role of Oxidation Products on Age Hardening Revisited." *Road Materials and Pavement Design*. Vol. 12, No. 4 (2011) pp. 795 - 819.

Petersen, J. C. and P. M. Harnsberger, "Asphalt Aging: Dual Oxidation Mechanism and Its Interrelationships with Asphalt Composition and Oxidative Age Hardening." *Transportation Research Record*, 1638, National Research Council, Washington, D.C. (1998) pp. 47-55.

Petersen, J. C., P. M. Harnsberger, and R. E. Robertson, "Factors Affecting the Kinetics and Mechanisms of Asphalt Oxidation and the Relative Effects of Oxidation Products on Age Hardening" Preprints of Papers, American Chemical Society, Division of Fuel Chemistry, Vol. 41, No. CONF-960807. (1996).

Petersen, J. C., S. M. Dorrence, M. Nazir, H. Plancher, and F. A. Barbour. *Oxidation of Sulfur Compounds in Petroleum Residues: Reactivity-Structural Relationships*. American Chemical Society, Division of Petroleum Chemistry, Preprints (United States) 26, No. CONF-810813, Vol. 2 (1981).

Petersen, J. C., H. Plancher, and P. M. Harnsberger. "Lime Treatment of Asphalt to Reduce Age Hardening and Improve Flow Properties." *Association of Asphalt Paving Technologists*, Vol. 56 (1987).

Petersen, J. C. and R. Glaser. "Asphalt Oxidation Mechanisms and the Role of Oxidation Products on Age Hardening Revisited." *Road Materials and Pavement Design*, Vol. 12 (4) (2011), pp. 795-819.

Prapaitrakul, N. *Toward and Improved Model of Asphalt binder Oxidation in Pavements*. Collage Station, TX: Texas A&M University. (2009).

Prapaitrakul, N., Han, R., Jin, X., and Glover, C. J. "A Transport Model of Asphalt Binder Oxidation in Pavements." *Road Materials and Pavement Design*, (2009).

Recasens, R., A. Martínez, F. Jiménez, and H. Bianchetto, "Effect of Filler on the Aging Potential of Asphalt Mixtures." *Transportation Research Record: Journal of the Transportation Research Board*, No. 1901 (2005), pp. 10-17.

Rowe, G. M., G. King, G., and M. Anderson. "The influence of binder rheology on the cracking of asphalt mixes in airport and highway projects." *Journal of Testing and Evaluation, Vol. 42*(5) (2014), pp. 1-10.

Underwood, B. S., M. S. Sakhaei Far, and Y. R. Kim, “Using Limited Purchase Specification Tests to Perform Full Viscoelastic Characterization of Asphalt Binder.” *ASTM Journal of Testing and Evaluation.* (2010).

Wu, J. T., W. P. Han, G. Airey, and N. I. M. Yusoff, “The Influence of Mineral Aggregates on Bitumen Ageing.” *International Journal of Pavement Research and Technology,* Vol. 7, No. 2 (2014) pp. 115-123.

APPENDIX C

Evaluation of the Sensitivity of the Mechanical Properties of Asphalt Concrete to Asphalt Binder Oxidation

Introduction

When asphalt binder is blended with aggregate and compacted into an asphalt mixture, complex interactions occur that ultimately yield the observed behaviors of that asphalt mixture. These interactions are related to two phenomena; physico-chemical interaction between the asphalt and aggregate and structural factors related to the aggregate skeleton and internal load paths. Together these factors mean that there is not a one-to-one relationship between changes in binder properties and changes in mixture behavior. In fact, the relationship between binder and mixture modulus is temperature and frequency dependent with low temperatures showing the least sensitivity to binder properties and high temperatures showing the greatest sensitivity. Also, this level of sensitivity is not uniquely related to the asphalt binder, but also to the various characteristics of the mixture (aggregate type, gradation, volumetric contents, etc.) (Table C-1).

Table C-1. Study materials and their description

Notation	Notation Description	Binder			Aggregate		Gradation			Air Voids (%)	
		B1	B2	B3	A1	A2	G1	G2	G5	4.5	7.5
B1	PG 58-28 (Unmodified)	X									
B2	PG 64-22 (Unmodified)		X								
B3	PG 70-28 (SBS)			X							
A1	Limestone				X						
A2	Granite					X					
G1	Coarse Gradation						X				
G2	Fine Gradation							X			
G5	Fine Plus Gradation								X		
B1A1G2	Mastic: V_c = 26.6%	X			X			X			
B1A2G1	Mastic: V_c = 25.8%	X				X	X				
B1A2G2	Mastic: V_c = 24.1%	X				X		X			
B2A2G1	Mastic: V_c = 25.8%		X			X	X				
B2A2G2	Mastic: V_c = 24.1%		X			X		X			
B3A1G2	Mastic: V_c = 26.6%			X	X			X			
B3A2G2	Mastic: V_c = 24.1%			X		X		X			
B2A2G1-F-7.5	FAM: AC = 15.4%		X			X	X				X
B2A2G2-F-7.5	FAM: AC = 15.4%		X			X		X			X

B2A2G2-F-4.5	FAM: AC = 15.4%		X		X		X		X
B1A2G2-F-4.5	FAM: AC = 11.2%	X			X		X		X
B2A2G5-F-4.5	FAM: AC = 15.3%		X		X			X	X
B3A2G5-F-4.5	FAM: AC = 15.3%			X	X			X	X

[a] Percent passing G1 FAM gradation is 0.6 mm = 100%; 0.3 mm = 60%; 0.15 mm = 26%; and 0.075 mm = 9%

[b] Percent passing G2 FAM gradation is 0.6 mm = 100%; 0.3 mm = 61%; 0.15 mm = 28%; and 0.075 mm = 11%

[c] Percent passing G5 FAM gradation is 0.6 mm = 100%; 0.3 mm = 65%; 0.15 mm = 36%; and 0.075 mm = 12.9%

[d] V_c = Volume content of filler in mastic.

[e] AC = Percentage asphalt content in FAM.

The main objective of the sensitivity study is to evaluate the sensitivity of the asphalt concrete mixture behavior to changes in asphalt binder aging. This objective is accomplished using a multiscale evaluation approach. The approach separates the effects of the aggregate-binder physico-chemical interactions from those caused by air voids and physical aggregate interactions. The research thus involves experiments on the asphalt binder (to establish baseline properties), asphalt mastic (to consider the physico-chemical aspects), and asphalt mortar (to consider the air voids and aggregate interaction effects). The FAM (Fine Aggregate Matrix) consists of asphalt binder, filler, and fine particles smaller than approximately 1.18 mm to 0.6 mm depending on the mixture type. Underwood (2011) showed that a substantial amount of the total internal structure that exists within asphalt concrete mixture resulted from the structural configuration of the FAM, and thus experiments with this FAM could provide useful insight into the behaviors of asphalt concrete.

The testing plan as shown in Table C-1 summarizes the different binder, mastic, FAM combinations that have been tested. The naming convention used in Table C-1 indicates the asphalt binder type (B1, B2, or B3), the aggregate source (A1 or A2), the gradation (G1 through G5), and whether the material is a mastic or FAM (F). The experimental plan involved creating mastics and FAM in the laboratory using asphalt binders that have been pre-aged to a level corresponding to an approximate in service aging time of 0, 7, 15, and 22 years (this process is described later in this section). The exact aging temperatures corresponding to the aging times are discussed in the section below. Table C-2 shows the test conditions (age levels and air void contents) performed on these study materials. Testing consisted of dynamic modulus and fatigue, both of which are also described later in this appendix.

Table C-2. Tests performed on the study materials

Group	FAM Name	Mastic/Binder Name	Air Voids (%)	Asphalt Aging Levels (years)
A-1	B2A2G1-F	--	7.5	0, 7, 15, 22
	B2A2G2-F	--	4.5, 7.5	0, 7, 15, 22
A-2	B1A2G2-F	--	4.5	0, 7, 22
	B2A2G5-F	--	4.5	0, 22
	B3A2G5-F	--	4.5	0, 22
A-3	--	B1	N/A	0, 7, 15, 22
	--	B2	N/A	0, 7, 15, 22
	--	B3	N/A	0, 7, 15, 22
	--	B2A2G1	N/A	0, 7, 22
	--	B2A2G2	N/A	0, 7, 15,22
	--	B3A2G2	N/A	0, 7, 22
	--	B1A2G1	N/A	0, 7, 22
	--	B1A2G2	N/A	0, 7, 15, 22
	--	B3A1G2	N/A	0, 7, 15, 22
	--	B1A1G2	N/A	0, 7, 15, 22

Aging Methodology

The experimental plan for this study involved creating mastics and FAM using asphalt binders that were pre-aged to levels that represent in service aging time of 7, 15, and 22 years of aging. The process of creating these pre-aged asphalts begins with first aging in Rolling Thin Film Oven (RTFO) at 163°C for 85 minutes. Then, depending on the binder grade and the desired oxidation level, they were subjected to 20 hours of conditioning in a pressure aging vessel (PAV). For B1 the temperatures for 7, 15, and 22 years were 89, 97, and 104°C; for B2 the temperatures were 91, 101, and 107°C; and for B3 they were 90, 98, and 103°C.

The aging temperatures were estimated from the regression model developed in the NCHRP 09-23 study, Equation C-1. This equation predicts the required PAV temperature, T_{PAV}, to simulate a specified aging time, t_{aging} (in years), for a given location. Additional terms needed to predict this temperature include viscosity of RTFO residue at 60°C, $\eta_{RTFO,60°C}$, as constructed air void content of the mixture (VA_{orig}, assumed equal to 7%), and mean annual air temperature (*MAAT*), which is expressed in degrees Fahrenheit. It can be observed that both Equations C-1 and C-2 are the same, but are simply rearranged to provide the quantity of interest.

$$T_{PAV} = \left[\begin{array}{l} \left(2.132432 + 0.193560 \left(\log\log \eta_{RTFO,60^\circ C} \right)^2 MAAT \right) \times \\ \ln\left(t_{aging} \times 12 \right) + 109.9632 - 78.2945 \left(\log\log \eta_{RTFO,60^\circ C} \right)^2 \end{array} \right] \left(0.445445 \times VA_{orig}^{0.378370} \right) \qquad \text{(C-1)}$$

$$t_{aging} = \exp\left(\frac{\frac{T_{PAV}}{\left(0.445445 \times VA_{orig}^{0.378370}\right)} - 109.9632 + 78.2945\left(\log\log\eta_{RTFO,60^\circ C}\right)^2}{\left(2.132432 + 0.193560\left(\log\log\eta_{RTFO,60^\circ C}\right)^2 MAAT\right)}\right)^{\frac{1}{12}} \quad \text{(C-2)}$$

Correlation between PG Grade and MAAT

It is also recognized that viscosity and *MAAT* values are correlated, specifically that asphalt binder used in regions with high *MAAT* is more likely to have a high viscosity and those used where *MAAT* is low are more likely to have low viscosity. This correlation can be seen by subjectively comparing a map of the high temperature PG grade distribution to a map of *MAAT* values across the country, Figure C-1. The precise relationship is established by identifying correlation between the climate based PG grade and *MAAT* since viscosity can be predicted from PG grade (ARA, 2004). Two sets of data are obtained for this purpose; 1) the 98% reliability based PG grades and latitude/longitude of all available weather stations (7358 stations) in LTPPBindV3.1 and 2) the Global Historical Climatology Network (GHCN) data (Willmott and Matsura, 2009). The GHCN database contains monthly average temperatures at a 0.5° latitude and longitude precision, which was processed to calculate MAAT using Equation C-3.

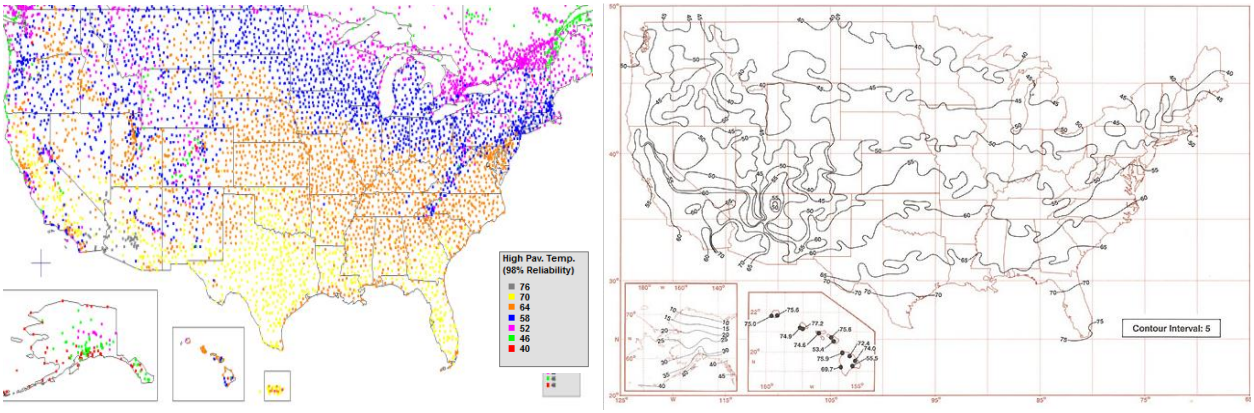

(a) (b)

Figure C-1. (a) Distribution of high temperature PG grades across the United States and (b) MAAT distribution for the United States (Source: LTTPBind and NOAA).

$$MAAT = \frac{1}{365}\sum_{i=1}^{12} MMAT_i\left(D_i\right) \quad \text{(C-3)}$$

where; *MMAT* is mean monthly air temperature, *D* is the number of days in a month, and *i* is an index to denote the month. In this calculation, February is assumed to have 28 days.

This database was then interpolated using MATLAB to determine the *MAAT* temperature at the exact latitude and longitude of the weather stations extracted from LTPPBind. The results were verified by comparing a selection of interpolated *MAAT* values to those from the NOAA National Climatic Data Center database. One weather station from each state (except Hawaii)

was selected. Generally, these sites corresponded to the airport for the state capital, but in some cases an alternative location was chosen in order to ensure correspondence between the NOAA and LTPPBind weather stations. The results of this analysis are shown in Figure C-2 where it is seen that the NOAA and interpolated *MAAT* values agree with a high degree of correlation and modest bias (*Se*/*Sy*). The largest exceptions to this agreement exist at the extreme high temperature (Phoenix, AZ) and extreme low temperature (Juneau, AK) and can be related to the use of different periods of record in the NOAA and GHCN databases (10 years versus 39 years). The slight bias (approximately 0.5°C) in this data can likewise be attributed to the differences in evaluation period for the two datasets.

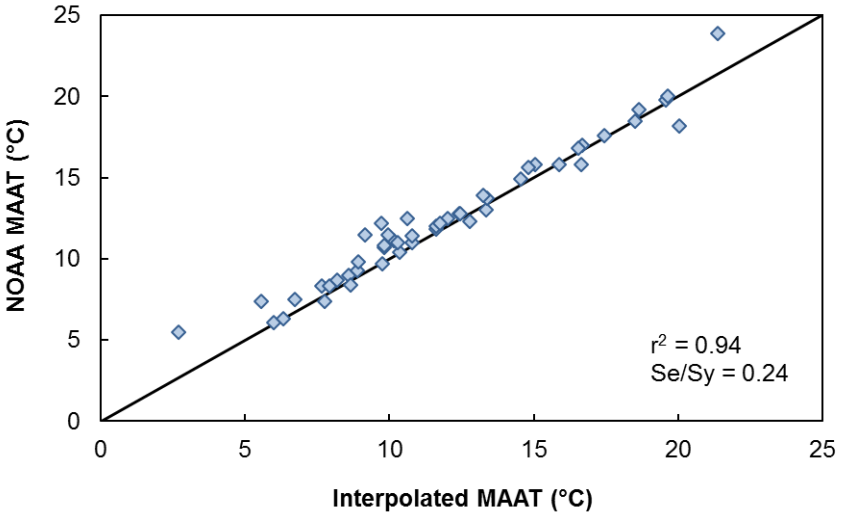

Figure C-2. Verification of interpolated MAAT values.

Once MAAT was estimated for all data points in the GHCN database, values were interpolated to the exact latitude and longitude of the weather stations extracted from LTPPBind. The results were verified by comparing a selection of interpolated *MAAT* values to those from National Oceanic and Atmospheric Administration's National Climatic Data Center (NCDC) database. The compiled *MAAT* values for each weather station were grouped by PG grade and an analysis of average and standard deviation was performed. The results are summarized in Figure C-3 with error bars representing the 95% confidence interval for MAAT. As expected, increases in this value are associated with increases in both the high temperature PG grade and decreases in the differences between high and low temperature PG grade. The data shown in this figure suggests that the likely *MAAT* values for B1, B2, and B3 are 8.3, 12.8, and 11.1°C, which is subsequently input to Equation C-1 to predict T_{PAV}.

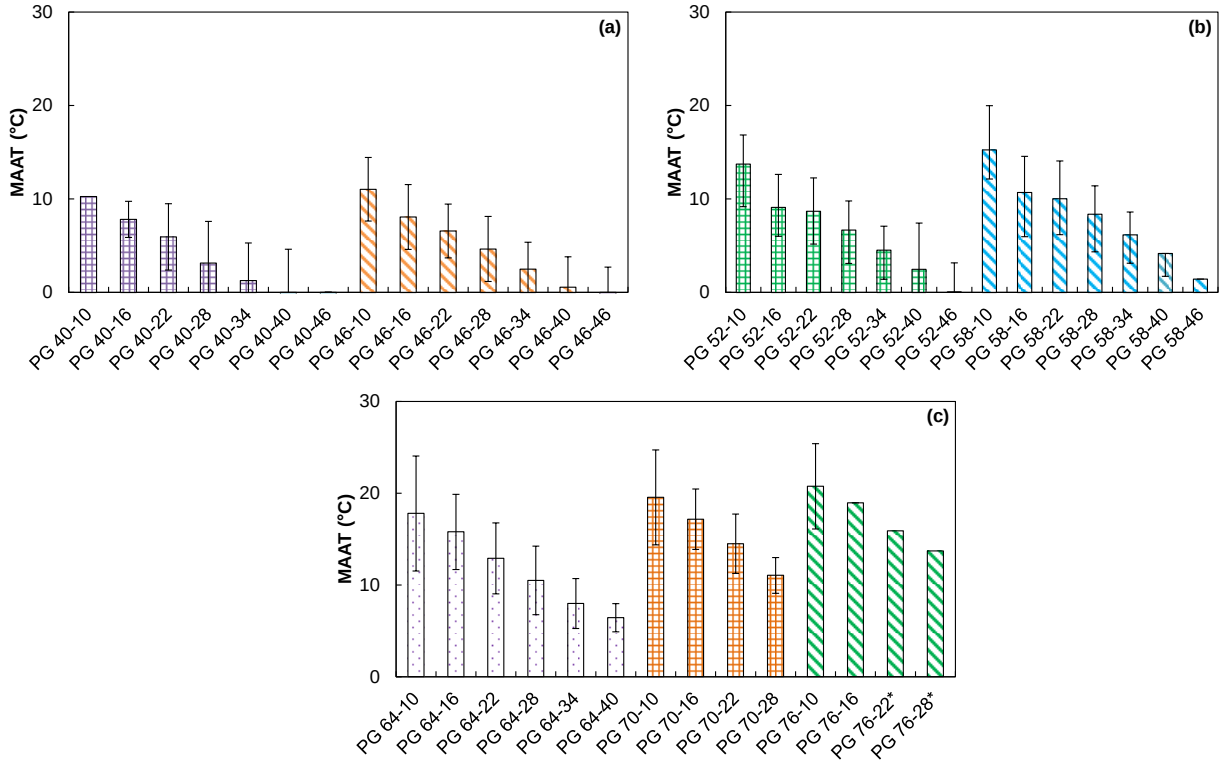

Figure C-3. MAAT by PG grade of asphalt; (a) PG 40-10 to PG 46-46; (b) PG 52-10 to PG 58-46; and (c) PG 64-10 to PG 76-16.

Estimating Aging Time and Temperature

Next, the data from Figure C-3 is used with Equation C-2 to predict the likely in-service aging times for the standard PAV aging temperatures (90°, 100°, and 110°C). Similarly, the data is used with Equation C-1 to predict the T_{PAV} that would correspond to 7, 15, and 22 years of service. The data is first compiled by binder type for the 95 percent confidence interval *MAAT* values (to the nearest 10°F bin) in Table C-3 and Table C-4. In Table C-5 the exact upper and lower 95th percentile of *MAAT* are used for each asphalt to provide a range of permissible T_{PAV} values to simulate 7, 15, and 22 years of service. There are three items of note regarding these tables and the analysis:

- The viscosity values for each of these binder grades are obtained from established temperature susceptibility relationships presented elsewhere (ARA, 2004).
- The standard AASHTO M320 PAV aging temperature for each binder is highlighted in gray in Table C-3.
- The PG grades for the asphalt binder in the sensitivity study are highlighted in gray in Table C-4 and Table C-5.

Table C-3. Summary of calculated simulation times for PG binder grades by likely MAAT regions

PG Grade	MAAT and Time Simulated for Standard Temperatures (years)																	
	-4°C (25°F)			2°C (35°F)			7°C (45°F)			13°C (55°F)			18°C (65°F)			24°C (75°F)		
	T_{PAV} (°C)			T_{PAV} (°C)			T_{PAV} (°C)			T_{PAV} (°C)			T_{PAV} (°C)			T_{PAV} (°C)		
	90	100	110	90	100	110	90	100	110	90	100	110	90	100	110	90	100	110
PG 46-46	18	201	2309	7	53	401												
PG 46-40				6	49	381	3	19	113									
PG 46-34				6	45	364	3	18	109									
PG 52-46	9	66	456	9	66	456	5	24	126									
PG 52-40				9	64	450	5	24	125									
PG 52-34				9	61	436	4	23	123	3	11	48						
PG 52-28							4	22	120	2	11	47						
PG 52-22							4	22	120	2	11	47						
PG 52-16							4	21	118	2	11	47						
PG 52-10										2	11	47	2	6	23			
PG 58-40				12	78	508	6	28	135									
PG 58-34							6	27	134	3	13	50						
PG 58-28							6	27	134	3	13	50						
PG 58-22							6	27	133	3	13	50	2	7	24			
PG 58-16							6	27	133	3	13	50	2	7	24			
PG 58-10										3	13	50	2	7	24	2	7	24
PG 64-40							7	31	143	4	14	53						
PG 64-34							7	32	144	4	14	53						
PG 64-28							7	32	145	4	14	53	2	8	25			

PG 64-22				4	14	53	2	8	25			
PG 64-16				4	14	53	2	8	25			
PG 64-10				4	15	53	3	8	25	2	5	14
PG 70-28				5	16	55	3	8	25			
PG 70-22				5	16	55	3	8	25			
PG 70-16							3	9	25	2	5	14
PG 70-10							3	9	25	2	5	14
PG 76-16							3	9	26	2	5	14
PG 76-10							3	9	26	2	5	14

* PG 70-XX and above has an option for 110°C for desert climates

Table C-4. Summary of calculated T_{PAV} to achieve target aging levels for PG binder grades by likely MAAT regions

PG Grade	MAAT and PAV Aging Temperature (°C) for Simulated Ages																	
	-4°C (25°F)			2°C (35°F)			7°C (45°F)			13°C (55°F)			18°C (65°F)			24°C (75°F)		
	Pave. Age			Pave. Age			Pave. Age			Pave. Age			Pave. Age			Pave. Age		
	7	15	22	7	15	22	7	15	22	7	15	22	7	15	22	7	15	22
PG 46-46	86	89	91	90	94	96												
PG 46-40				91	94	96	94	99	101									
PG 46-34				91	95	97	95	99	101									
PG 52-46	84	88	89	88	92	94	92	97	99									
PG 52-40				89	93	95	93	97	100									
PG 52-34				89	93	95	93	97	100	97	102	105						
PG 52-28							93	98	100	97	102	105						
PG 52-22							93	98	100	97	102	105						
PG 52-16							93	98	100	97	102	105						
PG 52-10										97	102	105	101	107	110			
PG 58-40				87	91	93	91	96	99									
PG 58-34							91	96	99	96	101	104						
PG 58-28							91	96	99	96	101	104						
PG 58-22							91	96	99	96	101	104	100	106	109			
PG 58-16							91	96	99	96	101	104	100	106	109			
PG 58-10										96	101	104	100	106	109	104	111	115
PG 64-40							90	95	98	95	100	103						
PG 64-34							90	95	98	95	100	103						
PG 64-28							90	95	98	95	100	103	99	106	109			
PG 64-22										94	100	103	99	106	109			

PG 64-16				94	100	103	99	106	109		
PG 64-10				94	100	103	99	106	109	104	111	115
PG 70-28				94	100	103	98	105	109		
PG 70-22				93	99	103	98	105	109		
PG 70-16							98	105	109	103	111	115
PG 70-10							98	105	109	103	111	115
PG 76-16							97	105	108	103	111	115
PG 76-10							97	105	108	103	111	115

Table C-5. Range of permissible T_{PAV} to achieve target aging levels for PG binder grades

PG Grade	T_{PAV} (°C) Simulated Years in Service		
	7	15	22
PG 46-46	83-91	85-95	87-97
PG 46-40	88-92	91-96	93-98
PG 46-34	90-93	93-97	95-100
PG 52-46	84-91	87-95	88-97
PG 52-40	87-91	91-95	93-98
PG 52-34	89-93	93-98	95-100
PG 52-28	90-95	94-100	96-103
PG 52-22	92-97	96-102	98-104
PG 52-16	93-97	97-102	99-104
PG 52-10	95-101	99-107	102-110
PG 58-40	87-91	91-96	93-98
PG 58-34	88-93	93-98	95-101
PG 58-28	89-95	94-101	96-104
PG 58-22	91-97	95-102	98-105
PG 58-16	91-98	95-104	97-107
PG 58-10	95-100	101-106	103-109

PG Grade	T_{PAV} (°C) Simulated Years in Service		
	7	15	22
PG 64-40	88-91	93-96	95-98
PG 64-34	88-93	93-98	96-101
PG 64-28	90-96	95-102	97-105
PG 64-22	91-98	97-104	99-107
PG 64-16	94-100	99-107	102-111
PG 64-10	93-104	99-111	102-115
PG 70-28	90-94	96-100	99-103
PG 70-22	92-98	98-105	101-108
PG 70-16	94-100	101-107	104-111
PG 70-10	95-104	101-112	104-116
PG 76-16	98-98	105-105	109-109
PG 76-10	95-104	102-112	106-117

Recall that the decision to select 7, 15, and 22 years itself was somewhat arbitrary and intended to cover the appropriate range of in-service times. The above analysis demonstrates that an asphalt cement of a grade may be used in locations with different *MAAT* values. Based on these somewhat arbitrary definitions of time and the variability in *MAAT* and associated sensitivities to aging it is seen that there exists overlap in the ranges of T_{PAV} for each simulation period. Considering this fact, the research team chose to establish the laboratory aging conditions for the experimental program based on the following rules;

1. Set the T_{PAV} for the 7-year simulation equal to the lowest statistically determined T_{PAV} range for that asphalt grade,
2. Set the T_{PAV} for the 22-year simulation equal to the largest statistically determined T_{PAV} range for that asphalt grade, and
3. Set the T_{PAV} for the 15-year simulation equal to the middle value (to the nearest whole degree Celsius) of the statistically determined T_{PAV} range values for that asphalt grade.

Following these rules sets the T_{PAV} values for the study asphalts as given in Table C-6.

Table C-6. PAV aging temperatures used for sensitivity study

PG Grade	Binder Name	T_{PAV} (°C)		
		Simulated Years in Service		
		7	15	22
PG 64-22	B1	91	101	107
PG 70-28	B2	90	98	103
PG 58-28	B3	89	97	104

High Temperature PG Grade of Aged Binders

After conducting the PAV aging, testing was performed on the aged asphalt binders to determine their high temperature performance grade. Strain sweep experiments were first performed on binders B1, B2 and B3 at all three aging levels to establish a suitable strain level with which to run the experiment to ensure that the test remained within the linear viscoelastic region. The strains for the strain sweep experiment ranged from 0.005% to 50%. Based on the results from the strain sweep experiment, it was decided to perform the tests for grade determination at 0.5% strain level, which is low enough to remain in the linear viscoelastic range and large enough to avoid instrument measurement errors.

The modulus of the aged binder samples was measured at 10 rad/s at the initial binder PG grade temperature and then six degree increments (e.g., for B1 testing began at 58°C then went to 64°C, 70°C, etc.). These temperature increments continued until the sample failed the criteria of $|G^*|/\sin\delta \geq 2.2$kPa. In order to calculate the continuous PG grade, the parameter $|G^*|/\sin\delta$ was plotted against temperature and the relationship was fit to an exponential curve as shown in Figure C-4. The continuous PG grade of the sample was then found by interpolation. In the case of B3-22, which is shown in Figure C-4 this process yielded a high temperature continuous PG grade of 87. All grades found by interpolation were rounded to the nearest whole number. The continuous grades of all aged binders under B1, B2, and B3 are graphically presented in Figure C-5, Figure C-6, and Figure C-7 respectively and summarized in Table C-7. Table C-7 also includes the convention PG grade for each binder case as well.

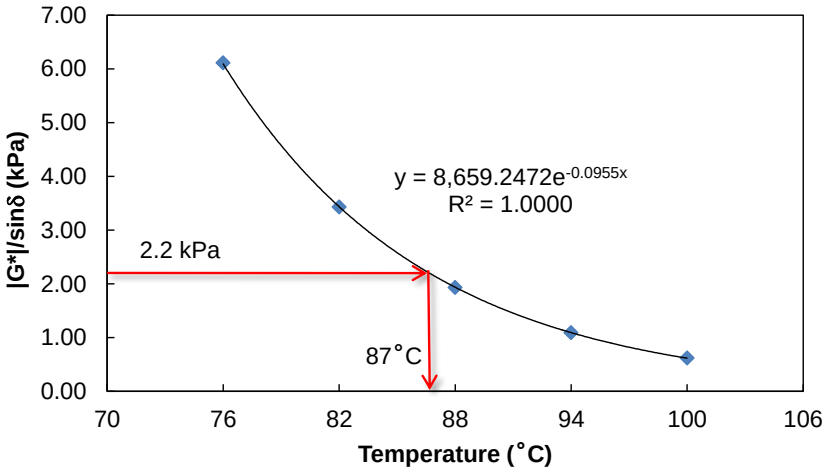

Figure C-4. Exponential data fit of |G*|/sinδ vs. temperature for B3-22.

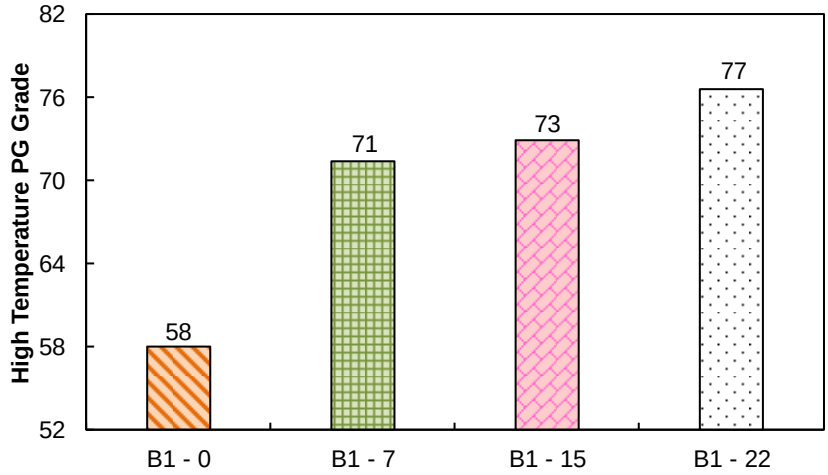

Figure C-5. Continuous PG grades of B1 binder at 7, 15, and 22 years aging levels.

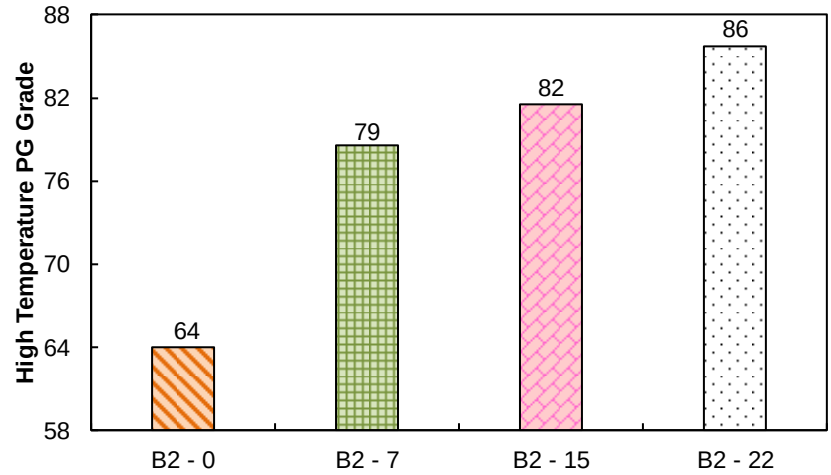

Figure C-6. Continuous PG grades of B2 binder at 7, 15, and 22 years aging levels.

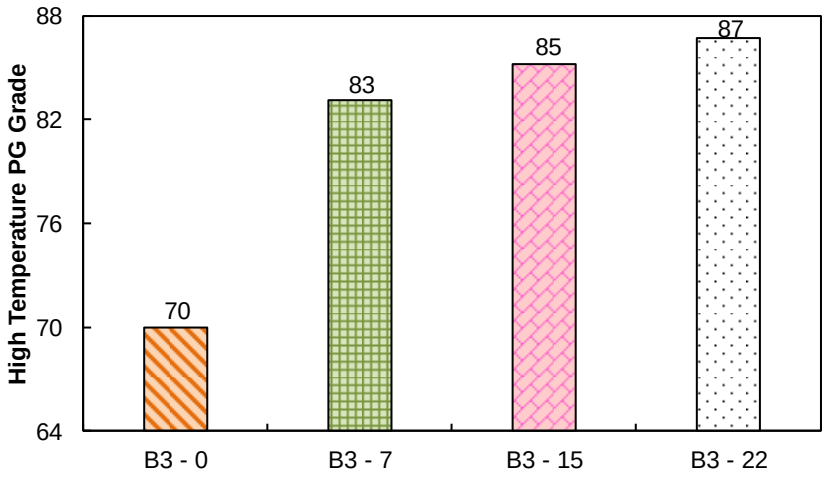

Figure C-7. Continuous PG grades of B3 binder at 7, 15, and 22 years aging levels.

Table C-7. Summary of the conventional and continuous PG grades characterized for the aged binders

Binder Type	Aging Level (years)	Conventional PG Grade	Continuous PG Grade
B-1	7	76	71
	15	76	73
	22	82	77
B-2	7	82	79
	15	82	82
	22	88	86
B-3	7	88	83
	15	88	85
	22	88	87

Experimental Characterization

Binder and Mastic

Mix Design and Sample Preparation

Once the pre-aging process was complete, asphalt binder was either prepared for testing, or mixed with aggregate to create mastic or FAM. For the asphalt binder, testing material was first cooled from PAV temperature to room temperature and then re-heated to the temperature used to mix mastic and FAM. After reaching the proper mixing temperature, binder was poured into small 60 mL tins for storage and future testing. The purpose in these two steps was to replicate any additional aging that would be induced during the mastic or FAM mixing process.

For A1 aggregate, the mix design for the G2 gradation was provided by the supplier and the same was used. The G1 and G2 gradations developed for A2 aggregate were first checked to be in accordance with the Superpave guidelines. Trials were performed to determine the

optimum binder content for this gradation and the corresponding G_{mm} was measured. The percentage of aggregate used in the mastics varied by aggregate type and target gradation as summarized in Table C-1.When creating mastic samples, the pre-aged asphalt binder was first heated to the mixing temperature and then combined with sub-0.075 mm aggregate by using a mechanical mixer. The prepared mastic samples were then poured into smaller 30 ml containers and stored in a refrigerator for further testing.

Test Methods

Dynamic Modulus

Temperature and frequency sweeps were conducted at 10, 20, 30, 40 and 54°C and at a frequency range of 30 - 0.1 Hz. Prior to all testing a strain sweep experiment was conducted and the tests were performed at strain levels below the linear viscoelastic limit, but above the resolution limits of the equipment (100 – 400 με). Tests were conducted from low temperature to high temperature and from high frequency to low frequency. The modulus and phase angle values used in subsequent calculations were taken directly from the test equipment's internal calculation; however, the quality of the torque and encoder signals were monitored continuously throughout the testing to ensure that the calculated results were representative of the test.

After experimental characterization of the dynamic modulus, a form of the Christensen-Anderson-Marasteanu (CAM) model in Equation C-4 was used to develop the master curves. A second order quadratic equation as shown in Equation C-5 was used to estimate the shift factor a_T.

$$\left|G^*\right| = \frac{10^g}{\left(1+\left(\frac{\omega_c}{\omega_R}\right)^k\right)^{\frac{m_e}{k}}} \tag{C-4}$$

$$\log\left(a_T\right) = \alpha_1 \left(T - T_R\right)^2 + \alpha_2 \left(T - T_R\right) \tag{C-5}$$

where; $|G^*|$ is the dynamic shear modulus (Pa), 10^g is the binder glassy modulus (Pa) (determined through optimization), ω_c is the crossover frequency (rad/s) (a fitting coefficient), m_e and k are fitting coefficients, T is the test temperature (°C), T_R is the reference temperature (°C), and α_1 and α_2 are the time-temperature shift factor function fitting coefficients.

The mastercurves for binder B2, and its corresponding mastic B2A2G2 is shown in Figure C-8. Similarly, mastercurves were developed for all the binders and mastics shown in Table C-11. All the remaining mastercurves are provided in appendix. The trend from all the mastercurves is clear that the modulus increases with aging level. Based on the modulus results, the next step was to quantify oxidation.

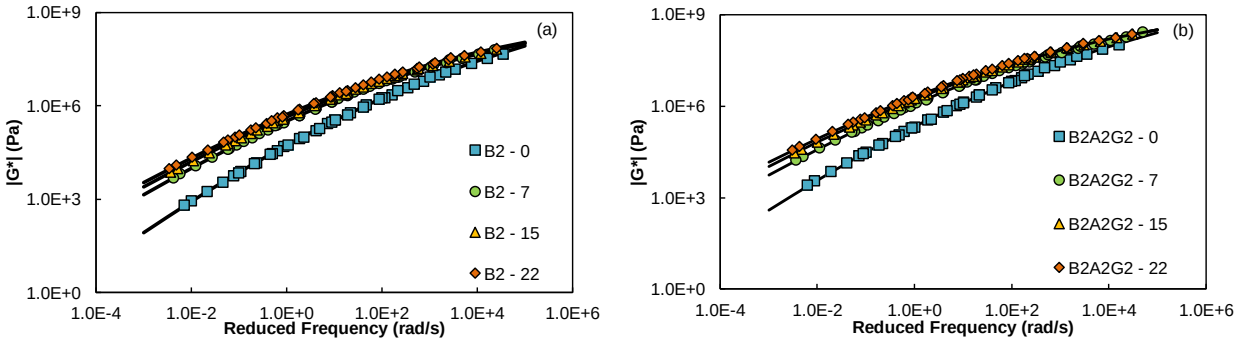

Figure C-8. Mastercurves for (a) binder B2 and (b) mastic B2A2G2 at different aging levels.

Oxidation in the current study is quantified in multiple ways. The simplest metric is based on the ratio of moduli values before and after aging and is referred to as aging ratio (*AR*) in this report. As shown in Equation C-6, it is the mathematical ratio of $|G^*|$ or $|E^*|$ after aging to the value before aging. It is calculated at multiple temperatures (T_j) and frequencies (ω_i) to gain a complete picture of the impacts of oxidation. For comparison across different study materials a singular frequency was required and 10 rad/s was chosen for this purpose.

$$AR = \begin{cases} \left(\dfrac{|G^*|\left(\omega_i, T_j\right)_{after\ aging}}{|G^*|\left(\omega_i, T_j\right)_{before\ aging}} \right) & mastic\ and\ binder \\ \left(\dfrac{|E^*|\left(\omega_i, T_j\right)_{after\ aging}}{|E^*|\left(\omega_i, T_j\right)_{before\ aging}} \right) & FAM \end{cases} \qquad \text{(C-6)}$$

The discussion of aging ratios across the three material scales for B2 binder is provided in the subsequent section.

Fatigue Test and Analysis

Strain controlled time sweep experiments were performed on the study materials to assess the fatigue properties and to characterize the continuum damage model. It should be noted that the tests were carried out at single temperature, 13°C and at two zero-to-peak strain levels, which were 6% and 7.5% for the B3 binder and 2.5% and 4% for B3A2G2 and B3A1G2 mastics. The temperature of 13°C was selected after a consideration for the edge flow phenomenon. The phenomenon which is more likely to occur in softer materials was evaluated using the unaged B1 binder, which has the lowest modulus among the materials in the test matrix.

The fatigue failure criteria adopted for the present study is that where a drop in the phase angle is observed during the experiment. The corresponding cycle number at the phase angle drop is the number of cycles to failure for the material at that strain level. A schematic of the phase angle drop is shown in below in Figure C-9. The strain levels tested and the number of cycles to failure for the binders and mastics at the different aging levels are tabulated in Table C-8. It should be noted that the values shown are the average of two replicates.

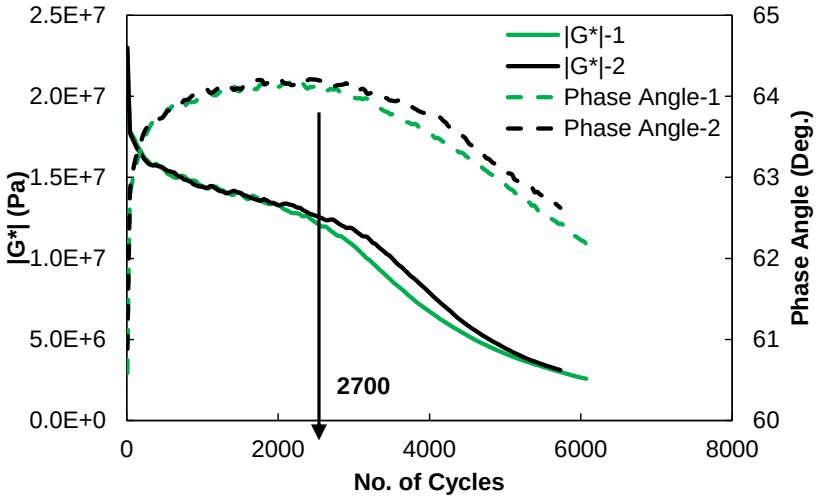

Figure C-9. Schematic showing the phase angle drop and the number of cycles to failure determination.

Table C-8. Number of cycles to failure for B1, B2, B3 and their associated mastics at different strain levels

Sample	1.25%	2.5%	4%	5.0%	6%	7.5%
B1-0	-	30250	-	4650	-	-
B1-7	-	-	-	28100	-	5950
B1-15	-	-	-	24250	-	7100
B1-22	-	-	-	31000	-	10800
B1A1G2-0	-	15000	-	2600	-	-
B1A1G2-7	-	25250	-	2375	-	-
B1A1G2-15	-	27350	-	1750	-	-
B1A2G2-0	-	11900	-	1600	-	-
B1A2G2-7	-	15200	-	920	-	-
B1A2G2-15	-	24238	-	1900	-	-
B1A2G2-22	-	16600	-	1530	-	-
B1A2G1-0	-	8463	-	1122	-	-
B1A2G1-7	-	6800	-	1090	-	-
B1A2G1-22	-	5450	-	1195	-	-
B2-0	-	39500	-	6340	-	-
B2-7	-	33500	-	3150	-	-
B2-15	-	12200	-	2550	-	-
B2-22	-	-	-	3682	-	-
B2A2G2-0	-	8180	-	1430	-	-
B2A2G2-7	34500	5250	-	-	-	-
B2A2G2-15	24500	2950	-	-	-	-
B2A2G2-22	-	3000	-	-	-	-
B3-0	-	-	-	-	24000	12350
B3-7	-	-	-	-	234250	122500
B3-15	-	-	-	-	189048	65508
B3-22	-	-		-	112500	63500

B3A2G2-0	-	139500	33550	-	-	-
B3A2G2-7	-	242625	68910	-	-	-
B3A2G2-22	-		60292	-	-	-

The general interpretation of the N_f varied from binder to binder. It was seen that among B1 binders and mastics the fatigue life increased with increase in aging level. Among B2 binders and mastics the general interpretation was that the fatigue life decresed with increase in aging level. However, interesting results are obtained for B3 binder and mastics. The values of N_f for B3 and B3A2G2 are plotted in the form of bar charts and shown in Figure C-10 and Figure C-11. For both B3 binder and B3A2G2 mastic it is seen that the fatigue life increases from control to 7 years aging condition. However, with further increase in aging level i.e. at 15 and 22 years the fatigue life decreased.

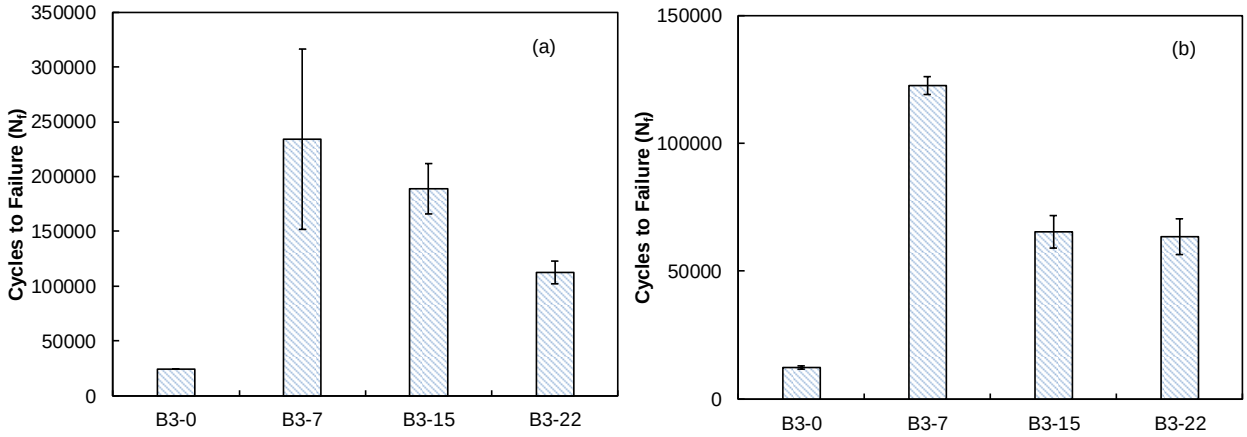

Figure C-10. Variation of N_f at different aging levels for B3 binder at: (a) 6% and (b) 7.5% strain levels.

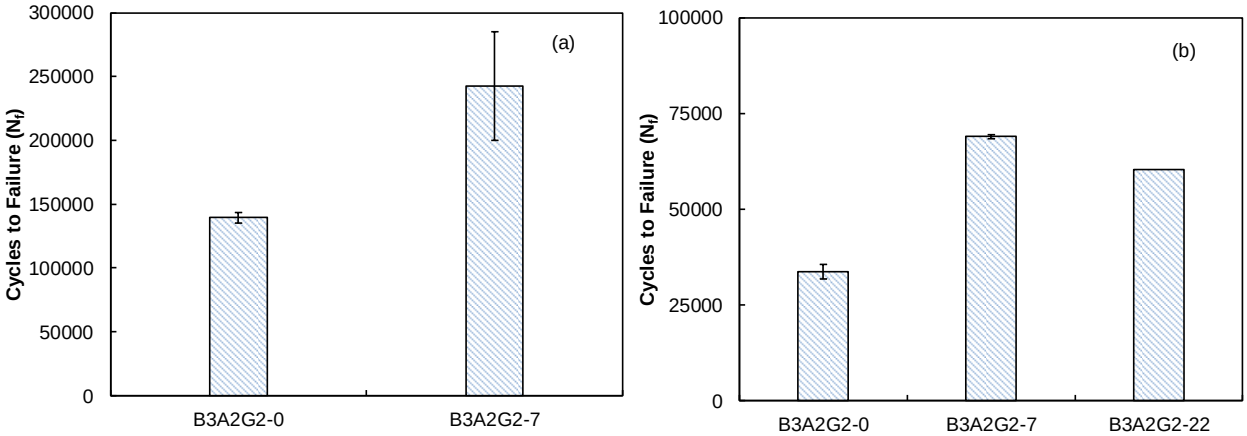

Figure C-11. Variation of N_f at different aging levels for B3A2G2 mastic at: (a) 2.5% and (b) 4% strain levels.

It should be recalled that B3 is a polymer modified binder, graded as PG 70-28. Comparisons made across binders in the same class of mastics i.e. A2G2 at 2.5% strain level shows that the B3A2G2 at 0 years had N_f almost 17 times higher than that of B2A2G2-0 and 12 times

higher than that of B1A2G2-0. At 7 years aging condition, the N_f of B3A2G2 is 46 times higher than B2A2G2-7 and 16 times higher than B1A2G2-7. Clearly, polymer modification does have a positive effect on cycles to failure. The increase in N_f from 0 years to 7 years aging condition can be attributed to a theory developed by Jahangir et al. (2015) which states that aging reduces the modulus gradient or the mismatch within different phases in the binder microstructure. It is understood that crack initiation in asphalt binder may occur at the interface of such phases, with greater modulus mismatch between the phases leading to early cracking or reduced fatigue resistance. Having a lower modulus mismatch, delays the occurrence of cracking, thus higher fatigue life. However, this explanation does not adequately explain why N_f at higher aging levels decreases for B3 binder.

Underwood (2011) applied the S-VECD model to evaluate the fatigue performance of the asphalt binders at strain levels that were not tested and also to more systematically evaluate the cause of the unexpected binder and mastic fatigue performance with aging (Underwood 2011). The S-VECD model is based on the same S-VECD method that is applied to asphalt concrete mixtures, with exceptions to account for the greater nonlinear viscoelastic response of binders and the torsional loading that is applied to asphalt binders and mastics. In torsional loading, loading is referred to as either positive displacement (clockwise rotation) or negative displacement (counter-clockwise rotation). The damage that occurs in torsional loading is likely due to anti-plane shearing.

The S-VECD model formulation that was used to model asphalt binder and mastic behavior in this study is shown in Equations C-7 through C-14. The most important functional relationship in the model is the one between pseudo stiffness (*C*) and damage (*S*). The parameter *C* represents the loss in modulus value that occurs as the test progresses, *S* is the damage parameter that represents the amount of damage that occurs due to cracking, and the functional relationship between the two variables represents the fundamental interaction between material integrity and damage. The importance of this function is that it has been shown to be independent of strain amplitude and frequency and, thus, when characterized can be used to predict behavior under many other conditions that were not used directly in the characterization.

$$C = \frac{\tau}{\gamma^R * DMR}, \; for \xi \le \xi_p \tag{C-7}$$

$$C = C^* = \frac{\tau_{0,pp}}{\gamma^R * DMR}, \; for \xi \ge \xi_p \tag{C-8}$$

$$\gamma^R \; = \; \gamma^R \; = \; \frac{h_1}{G_R} \int_0^{\xi} G(\xi' \; - \; \tau') \frac{dh_2 \gamma}{d\tau'} d\tau', \; for \xi \; \le \; \xi_p \tag{C-9}$$

$$\left(\gamma^R_{0,pp}\right)_{cyclei} \; = \; \frac{1}{G_R} * \left((\gamma_{0,pp})_i \; * \left| G^* \right|_{NL} \right) for \xi \; > \; \xi_p \tag{C-10}$$

$$dS = (dS_{Transient})_{timestepj} = \left(-\frac{DMR}{2} (\gamma^R)_j^{\,2} \Delta C_j \right)^{\frac{\alpha}{1+\alpha}} * (\Delta \xi)_j^{1/\alpha}, \; for \xi \le \xi_p \tag{C-11}$$

$$dS = (dS_{Cyclic})_{cyclei} = \left(-\frac{DMR}{2} (\gamma_{0,pp}{}^R)^2 \Delta C_i \right)^{\frac{\alpha}{1+\alpha}} * (\Delta \xi_p * \mathrm{B}_1)_j^{1/1+\alpha}, \; for \xi > \xi_p \tag{C-12}$$

$$B_1 = f_R \int_{\xi_i}^{\xi_f} (f(\xi))^{2\alpha} * d\xi \tag{C-13}$$

$$f(\xi) = -\frac{1}{2}\cos(\omega\xi) + \frac{(\tau_{peak})_i + (\tau_{valley})_i}{2\left[(\tau_{peak})_i - (\tau_{valley})_i\right]} \tag{C-14}$$

where; C is the pseudo stiffness in the first half of the first loading cycle, C^* is the pseudo stiffness during the remainder of the test, DMR is a normalization parameter given by Equation C-15, τ is the torsional stress amplitude, $\tau_{0,pp}$ is the torsional stress amplitude (peak to peak), γ^R is the pseudo strain, $\gamma^R_{0,pp}$ is the pseudo strain (peak to peak), $\gamma_{0,pp}$ is the peak-to-peak strain, h_1 and h_2 are nonlinear functions, $G(\xi')$ is the strain-dependent relaxation modulus, ξ' is the strain-dependent reduced time variable, G_R is the reference shear modulus, $|G^*|_{NL}$ is the nonlinear viscoelastic modulus, ξ_P is the reduced pulse time, $dS_{Transient}$ is the early portion of damage calculation, dS_{Cyclic} is the remaining portion of damage calculation, α is the factor that relates to viscoelastic time dependence, B_1 is the shape factor, ω is the angular frequency, τ_{peak} is the largest stress value within cycle i, and τ_{valley} is the smallest stress value within cycle i.

$$DMR = \frac{|G^*|_{fingerprint}}{|G^*|_{LVE}} \tag{C-15}$$

The inputs for this model were obtained from temperature-frequency sweep tests (linear viscoelastic properties), time sweep (strain-controlled fatigue) tests, and repeated stress sweep (RSS) tests (to obtain nonlinear viscoelastic properties). The torque and displacement inputs from the time sweep tests were obtained using a stand-alone data acquisition system created in LabVIEW that is able to acquire a data point approximately every 0.001 second. The Prony coefficients (relaxation modulus and creep compliance) to be used for the model were obtained from the temperature-frequency tests via collocation. Strain-level nonlinearity in the binder/mastic RSS tests was determined for the test materials at 13°C. Details regarding the RSS test are explained in Underwood and Kim (2014). Figure C-12 presents a schematic representation of the loading history employed in the RSS test. The loading history can consist of multiple groups, with each group consisting of a finite number of blocks that have incremental stress levels. These stress levels are constant within a group, but increase from one group to another.

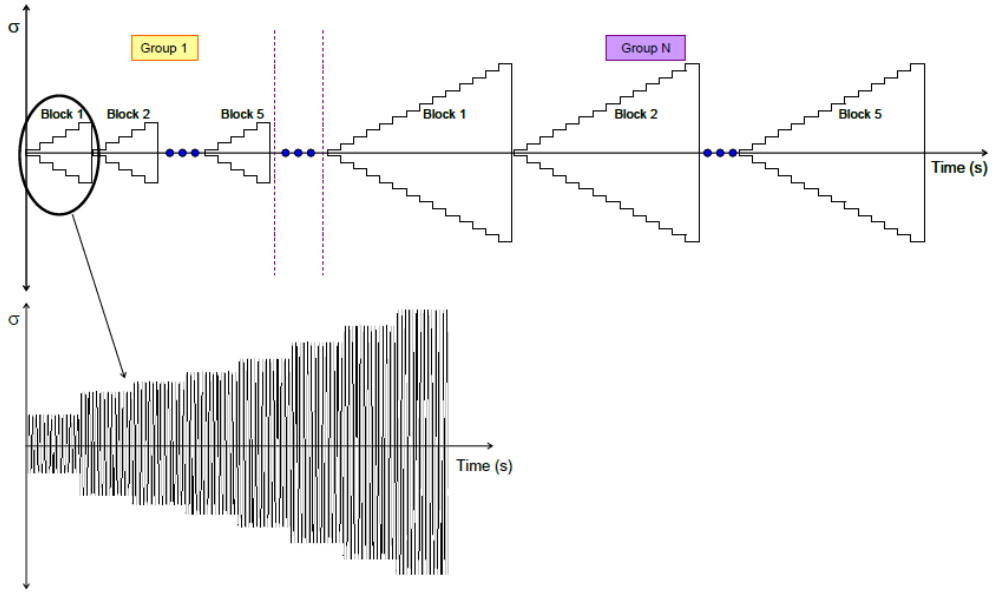

Figure C-12. Schematic of repeated stress sweep test loading history.

In the present study, two loading groups are considered. Loading group 1 consists of two blocks and loading group 2 consists of five blocks. Figure C-13 presents an example of the modulus response patterns for the loading groups. The different series shown in the figure correspond to a particular loading group (G) and block (B). $|G^*|$ is the primary property of interest in the RSS test and is denoted as $|G^*|_{RSS}$. This parameter in turn is affected by other mechanisms in addition to nonlinear viscoelasticity, and thus, additional steps must be taken to isolate only the nonlinear viscoelastic effects. The term $|G^*|_{NL}$ is used in the present study to reflect only the nonlinear viscoelastic component of the $|G^*|_{RSS}$. Equation C-16 is used to distinguish $|G^*|_{NL}$ from $|G^*|_{RSS}$. This step, along with important observations from Figure C-13, is explained in the following paragraphs.

$$\left|G^*\right|_{NL} = \frac{\left|G^*\right|_{RSS}}{F} \tag{C-16}$$

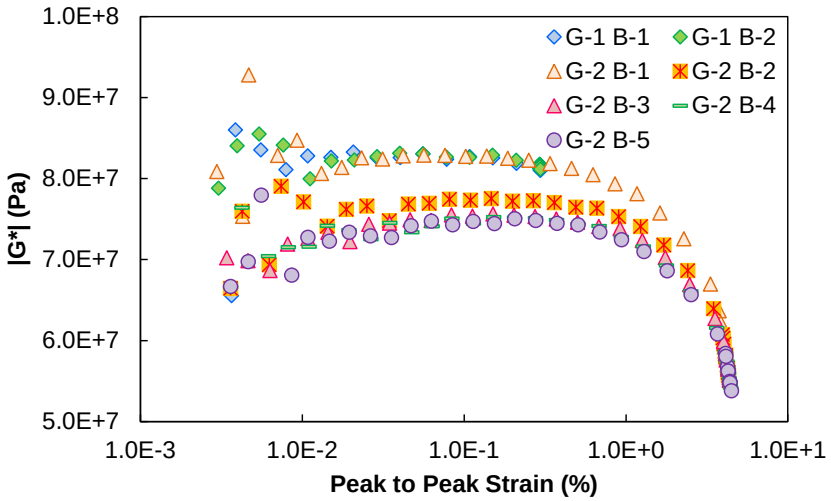

Figure C-13. Typical modulus responses of RSS loading group as seen in B1A2G2-7 mastic.

The important observations that can be made from Figure C-13 are as follows.

- For both loading groups, the modulus value decreases with an increase in strain level.
- No permanent change in the material is seen during group 1 loading, as the material response is the same for G-1 B-1 and G-1 B-2.
- For group two, some permanent change in the material can be seen, but this change is not fully permanent, as the modulus values at the beginning of blocks 2 through 5 are higher than the modulus value at the end of the preceding block. For example, the modulus value at the beginning of block G-2 B-4 is higher than the modulus value at the end of G-2 B-3.
- The reduction in modulus value is not fully recoverable because the modulus value at the smallest strain levels decreases from block to block. For example, compare the modulus value at the beginning of block G-2 B-2 to that at the beginning of block G-2 B-3.
- After approximately three block repetitions, the balance between modulus recovery and permanent modulus change becomes stable. For example, compare the vertical distance between G-2 B-1 and G-2 B-3 to the vertical distance between G-2 B-3, G-2 B-4, and G-2 B-5.

Underwood and Kim (2014) postulated that the reduction in modulus value can be attributed partly to the nonlinear viscoelastic response of the material, whereas the pattern of apparent partial recovery can be attributed to microstructural damage. This damage will cause a proportional change in the modulus such that |G*|NL and |G*|RSS, the modulus values obtained from the RSS test, are related to each other, as shown in Equation C-16. The proportionality constant F is expected to evolve slowly and its value will change only from one block to another. However, within a block, its value for different strains is assumed to be the same as long as the |G*|RSS data collapse into a single function for subsequent blocks.

To understand the role of this F variable, the G1 loading results shown in Figure C-13 should be examined. The group test results (G-1 B-1 and G-1 B-2) are unaffected by the damage. Thus, F would be equal to one. Group one tests are insufficient to characterize |G*|NL as they extend only up to small strain levels of about 0.3 percent. However, group two loadings go to higher strain levels and the vertical separation of the modulus responses between the blocks

suggests that F is not equal to one for all loading blocks. The overlap of G-2 B-3, G-2 B-4, and G-2 B-5 provides an opportunity to separate nonlinearity from damage. Underwood and Kim (2014) hypothesized that this type of overlap indicates that a minimum amount of damage occurs during G-2 B-3 loading, and the authors assumed that the damage is now constant for all strain levels in blocks four and five. The value of F for G-2 B-5 was determined by calculating the ratio of |G*|RSS for this block between 0.01 percent and 0.1 percent from G-1 B-1 between 0.01 percent and 0.1 percent. Upon calculating F, Equation C-16 was used to calculate |G*|NL. The results from the RSS tests for all the materials are denoted as a ratio of the value of |G*|NL at block G-2 B-5 to the average value of |G*|RSS for G-1 B-1 between 0.01 percent and 0.1 percent where the material is still in the linear viscoelastic region.

Once the nonlinear viscoelastic response is characterized, it can be used along with the measured time, stress, and strain values, and Equations C-7 through C-14 to characterize the damage characteristic curves for the different materials. These curves are shown in

Figure **C-14** through Figure C-17. The data in these figures represent the best fit function from the individual replicate data and are shown only up to the average damage at failure for each of these tests.

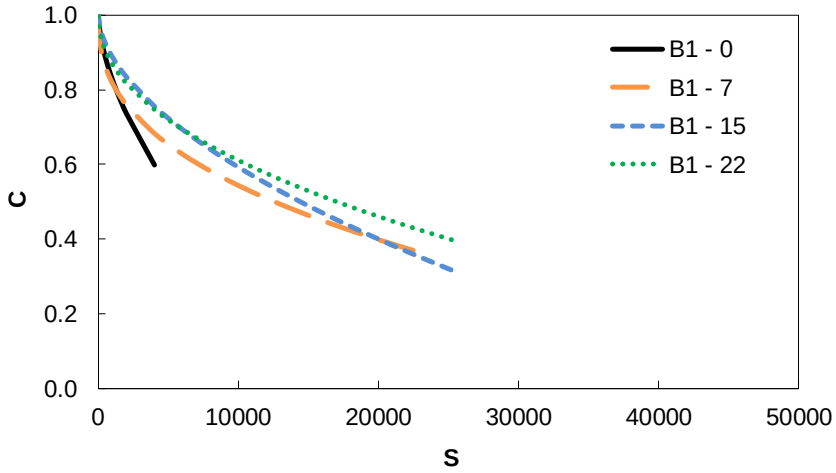

Figure C-14. C vs. S curve for B1 binder at different aging levels.

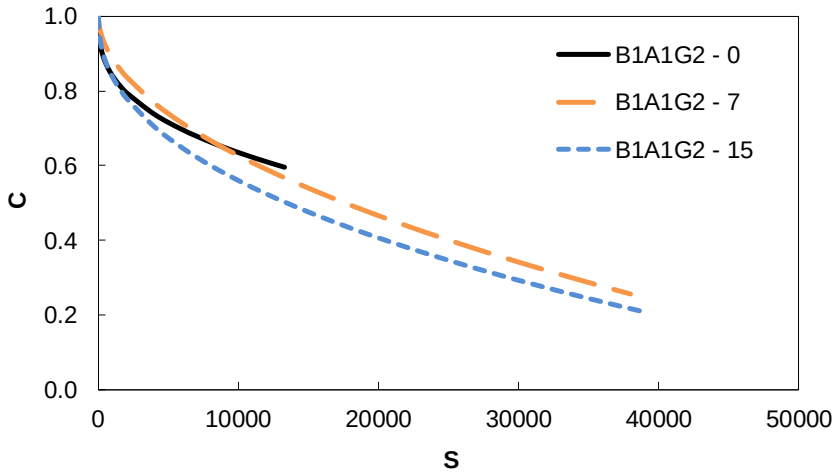

Figure C-15. C vs. S curve for B1A1G2 mastic at different aging levels.

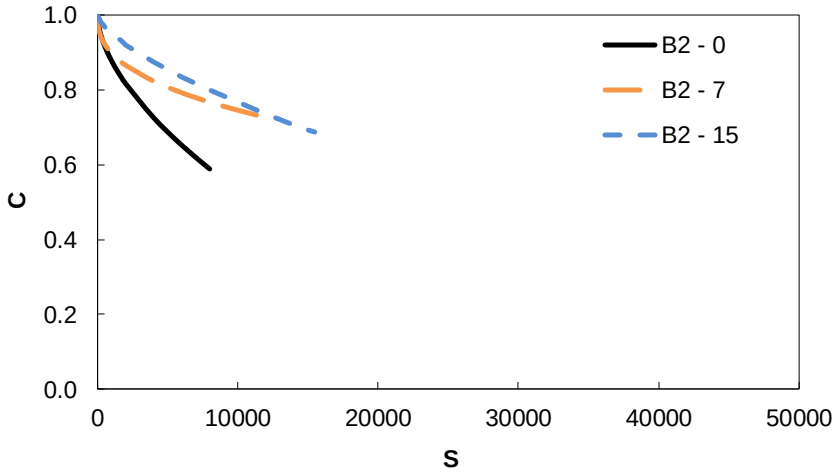

Figure C-16. C vs. S curve for B2 binder at different aging levels.

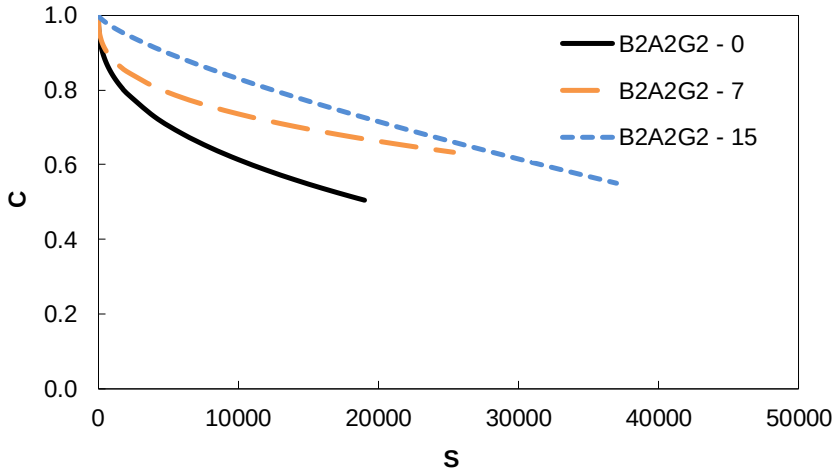

Figure C-17. C vs. S curve for B2A2G2 mastic at different aging levels.

The common observation that can be made for both the B1- and B2-based materials is that the level of damage at failure increases with an increase in aging level. However, to draw conclusions about the fatigue behavior of these materials, it is important to consider the *C* value at failure for these materials. For the B1-based binders and mastics, shown in

Figure **C-14** and Figure C-15, it is observed that the aged mastics and binders fail at a lower pseudo stiffness, *C*, than the unaged binders and mastics. This finding suggests that aged materials provide better resistance to fatigue damage than unaged materials, which is contrary to the common belief that fatigue resistance decreases with an increase in aging level. Also, among the aging levels, these figures show that materials at an aging level of 15 years exhibit better resistance to fatigue than those at 7 years, as they fail at a lower *C* value. However, for B1 binder at 22 years, this failure occurs at a higher *C* value than for B1 (7 years).

The reason for this trend reversal could be related to the natural variability of the tests, and thus, the differences would not be statistically significant. The general trend obtained from the *C* versus *S* approach adds support to the findings that are based on N_f value. These trends show that for the B1 binders and corresponding mastics, longer aging results in better resistance to fatigue. For the B2-based binders and mastics shown in Figure C-16 and Figure C-17, the unaged materials fail at a lower pseudo stiffness value than the aged materials. This finding is in direct contradiction to the observations made from the B1 binders. However, it is seen that within the aging levels, the materials that correspond to 15 years of aging have lower *C* values at failure than the materials that correspond to 7 years of aging.

Overall, the results from the binder and mastic fatigue tests show that fatigue performance across aging levels is a strong function of the type of binder being used. Some proof for the trends observed, especially with regard to the increased fatigue resistance with aging for the B1 binders, is available in unpublished literature by Jahangir et al. (2015). That study states that aging reduces the modulus gradient or the mismatch between the distinct phases in the binder microstructure. It is understood that crack initiation usually occurs at the interface of such phases, with a greater modulus mismatch between the phases leading to early cracking or reduced fatigue resistance. Having less modulus mismatch delays the occurrence of cracking, thus leading to a longer fatigue life.

Fatigue life simulations were carried out binders B1, B2, B3 and its corresponding A2G2 suite of mastics. Simulated data for B2 and B2A2G2 are presented in Figure C-18 and Figure C-19. These failure envelopes were used to calculate the sensitivity of binder and mastic fatigue to oxidation, which will be discussed in detail in the sensitivity assessment sections. One of the main observations from these envelopes is that noticeable change in fatigue life occurs from 0 to 7 years and 7 to 15 years, however with further increase in aging level, there is minimal change in fatigue life. The strain values at 10,000 and 100,000 cycles to failure obtained from these simulations were used to develop a sensitivity parameter, that was be used to quantify the sensitivity of binder and mastic fatigue properties to asphalt binder oxidation.

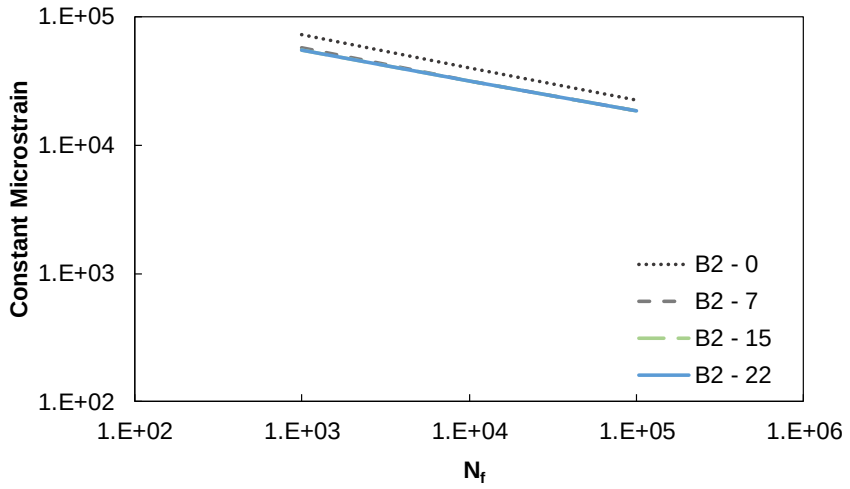

Figure C-18. C-value at failure based failure envelope for binder B2.

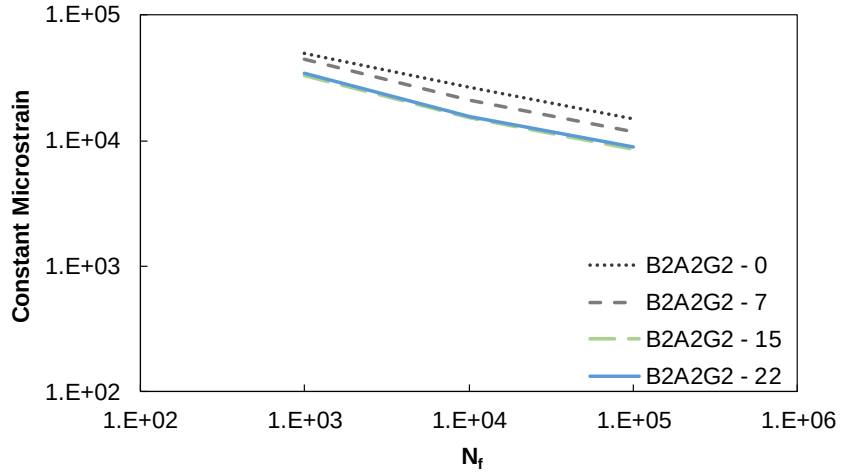

Figure C-19. C-value at failure based failure envelope for mastic B2A2G2.

Fine Aggregate Matrix (FAM)

Mix Design and Sample Preparation

The compositional design for A2G2-F class of FAM materials was developed based on the mixture design provided by NCSU for A2G2. For the A2G1-F and A2G5-F class of FAM materials the compositional design was developed based on the mixture design developed by ASU. FAM gradation for all three gradations G1, G2, and G5 are provided in Table C-1. Preparation and instrumentation is explained in detail in the subsequent sections. The samples cored from this plug had air voids close to samples from 7.5% air void case, thus were not considered for testing.

Aged binder for the FAM samples was pre-aged as done in the case of the mastics. This aged binder was blended with aggregate in a conventional bucket mixer, after which the blended FAM mix was poured into compaction mold and kept inside the oven until reaching compaction temperature. After reaching the correct temperature, FAM plugs were compacted in the Superpave gyratory compactor. After the FAM plugs had cooled, test specimens were first

extracted by coring and cutting and then instrumented with linear variable displacement transducers (LVDTs). The cored samples measured 20 mm in diameter and were cut to a height of 50 mm. The samples in this study were subjected to tension-compression loading and so all samples were glued to end platens prior to testing as shown in Figure C-20. Specialized gluing jigs that ensured proper vertical alignment were built and gluing was performed using Devcon 5 minute epoxy. Due to the sample size, only two sets of LVDTs were mounted and these were separated by 180°. The FAM LVDTs were MHR 010 (± 0.254 mm span) with a gauge length of 25 mm. FAM samples were tested using a BOSE Electro Force 3330 (±3 kN capacity) electromechanical load frame for |*E**|.

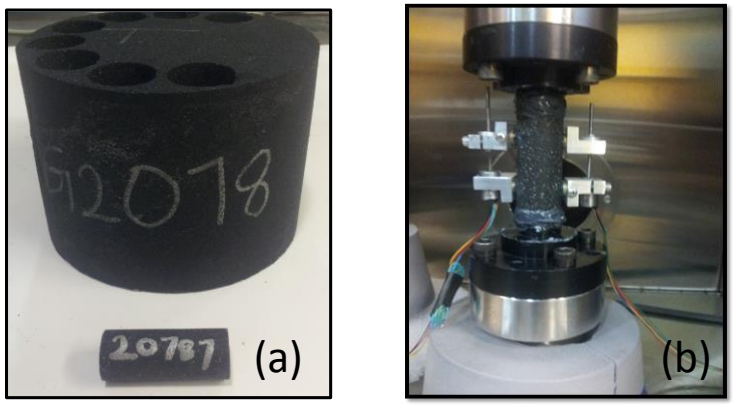

Figure C-20. FAM plug with sample cored and cut and (b) instrumented FAM sample.

Test Methods

Dynamic Modulus

The dynamic modulus test was conducted in tension-compression mode at target test temperatures of -10, 4.4, 20.4, 30.5 and 38.6°C and at 20, 10, 5, 1, 0.5, and 0.1 Hz. The load amplitude was varied by temperature and frequency to maintain an on-specimen strain magnitude between 60 and 80 με. To ensure accurate comparisons between binder, mastic, and FAM samples, a thermal calibration was performed prior to all testing. FAM samples were prepared to replicate the FAM that exists in mixtures with air void contents of 4.5% and 7.5%. Since FAM represents only a portion of the total mixture volume, its air void content was higher than the mixture air void content that it was representing. For example, for B2A2G2-F These target FAM air voids for mix air voids of 4.5% and 7.5% were 6.5% and 11% respectively.

Figure C-21 to Figure C-23 shows the replicated modulus data for FAM B1A2G2 along with the average representative mastercurve. In Figure C-27 only the mastercurves at the different aging levels and at 4.5% air void content are plotted together in log-log and semi-log space respectively.

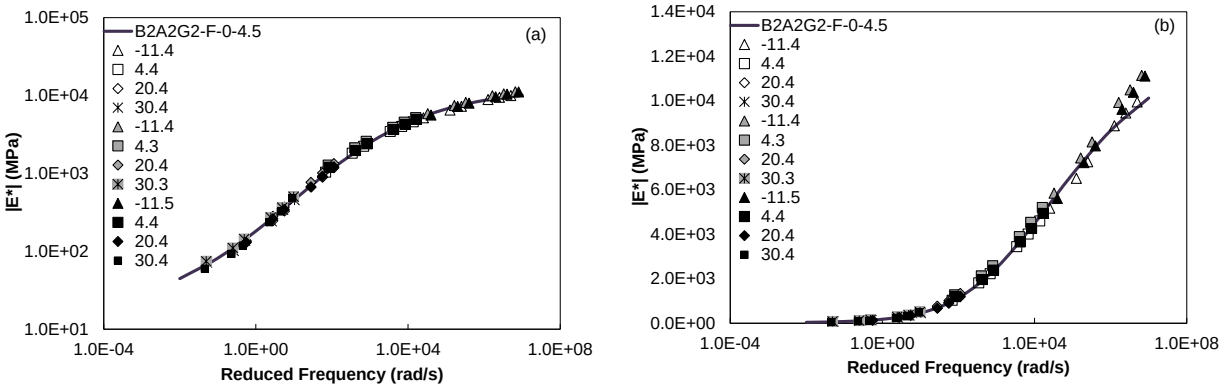

Figure C-21. Mastercurve for B2A2G2-F-0-4.5 showing modulus replicate data at different testing temperatures (°C) in: (a) log-log space and (b) semi-log space.

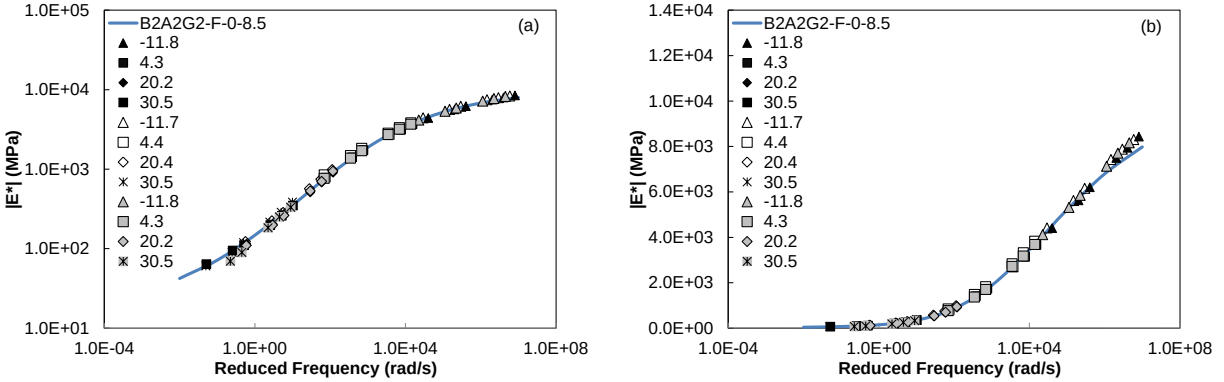

Figure C-22. Mastercurve for B2A2G2-F-0-7.5 showing modulus replicate data at different testing temperatures (°C) in: (a) log-log space and (b) semi-log space.

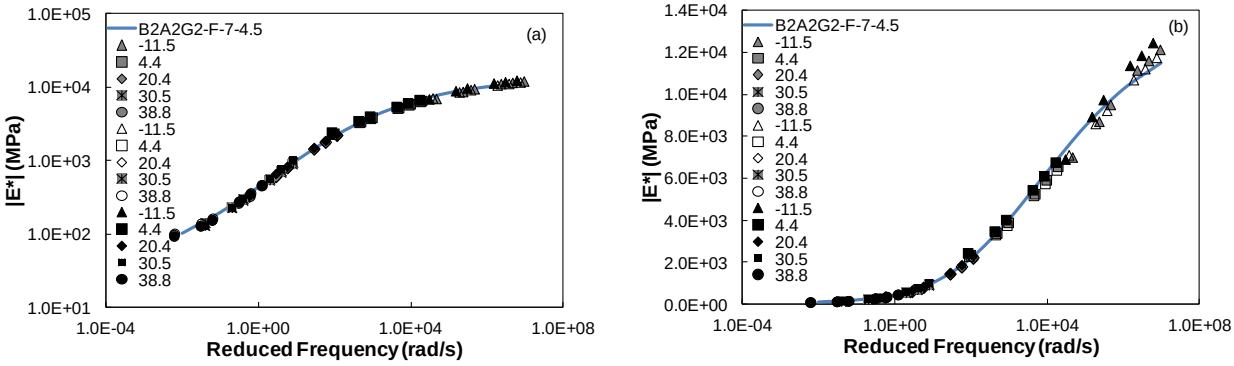

Figure C-23. Mastercurve for B2A2G2-F-22-4.5 showing modulus replicate data at different testing temperatures (°C) in: (a) log-log space and (b) semi-log space.

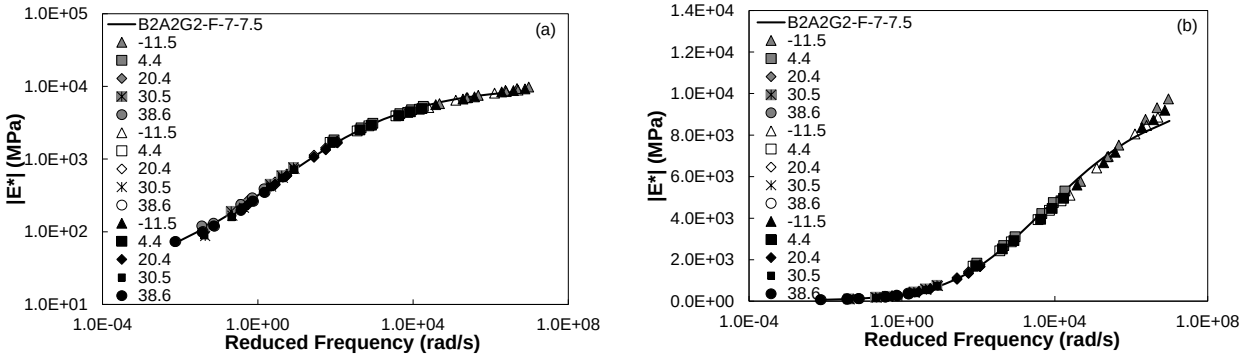

Figure C-24. Mastercurve for B2A2G2-F-22-7.5 showing modulus replicate data at different testing temperatures (°C) in: (a) log-log space and (b) semi-log space.

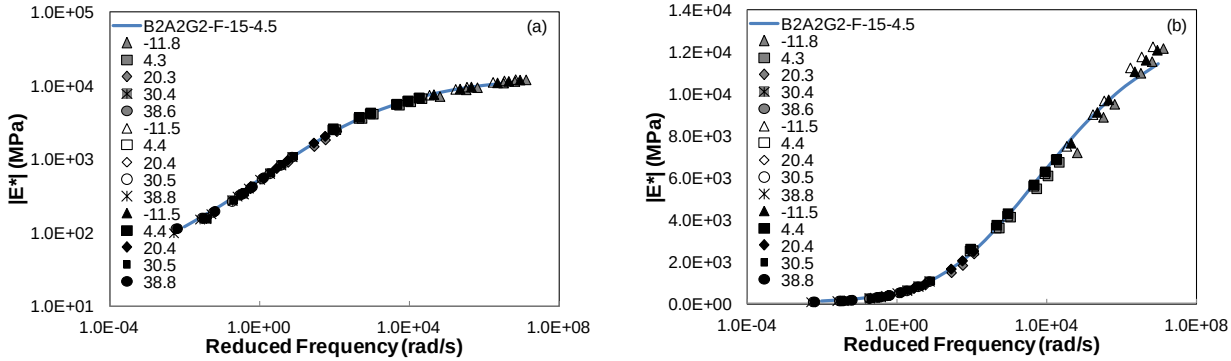

Figure C-25. Mastercurve for B2A2G2-F-15-4.5 showing modulus replicate data at different testing temperatures (°C) in: (a) log-log space and (b) semi-log space.

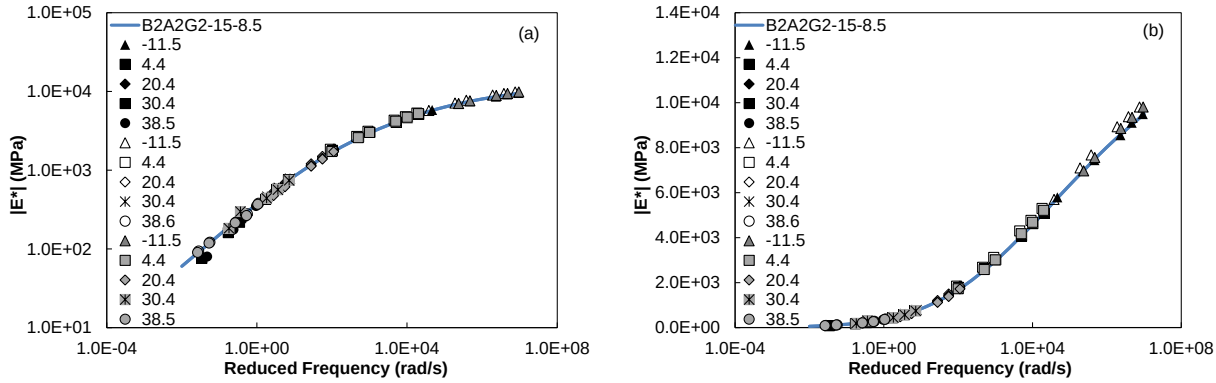

Figure C-26. Mastercurve for B2A2G2-F-15-7.5 showing modulus replicate data at different testing temperatures (°C) in: (a) log-log space and (b) semi-log space.

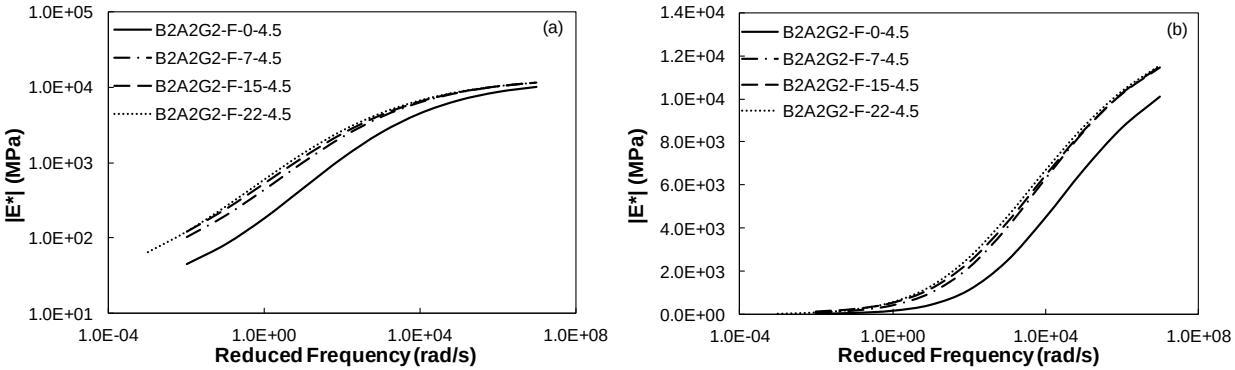

Figure C-27. Modulus Mastercurves for FAM, B2A2G2-F at 4.5% air voids for different aging levels in: (a) log-log space and (b) semi-log space.

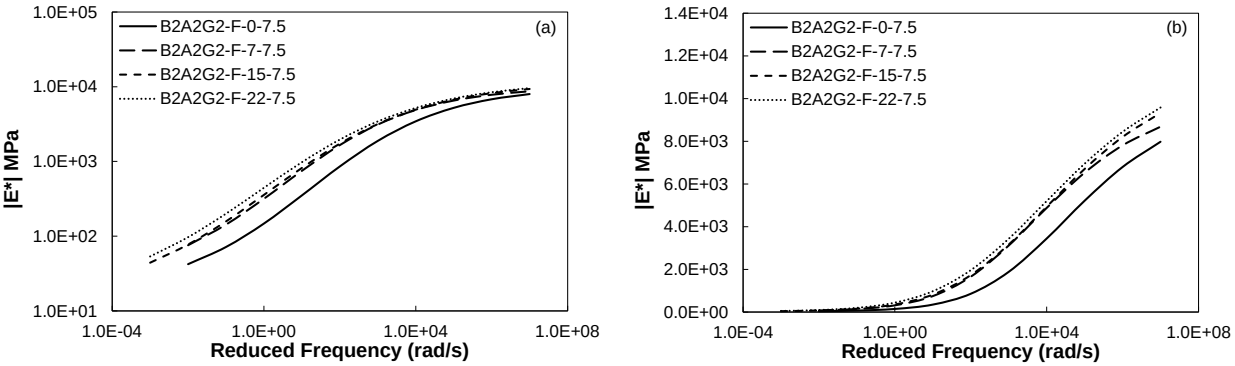

Figure C-28. Modulus Mastercurves for FAM, B2A2G2-F at 7.5% air voids for different aging levels in: (a) log-log space and (b) semi-log space.

The results from the dynamic modulus tests rank per aging levels. The general trend of the mastercurves, is like that observed in case of the mastics, wherein the mastercurves at different aging levels are parallel at intermediate to high temperatures and taper in together at low temperatures. The aging ratios (*AR*) for the binder B2, mastic B2A2G2 and FAM B2A2G2-F-4.5/7.5 are presented in Table C-9 and Figure C-29. FAM is seen to produce an apparent mitigation of the relative stiffening caused by binder oxidation. Also, the apparent mitigation in FAM is greater than the mastics. The general trend that is observed is that binder shows a larger increase in *AR* than mastic and FAM. This is due to the dual influences that aggregate particles impart with respect to mitigation of aging effects on modulus and overall stiffening. Also, *AR* increases with increase in temperature, which can be attributed to greater binder mobility resulting in greater influences from oxidation products at higher temperatures. The dual influences hinder sensitivity analysis based purely on *AR*. To better quantify sensitivity, a procedure based on crossover modulus was applied and will be discussed in the next section.

Table C-9. Aging ratios of B2 binder and B2A2G2 mastic and B2A2G2-F FAM samples at different aging conditions

Material	AR_{10}	AR_{20}	AR_{30}
B2-0	1.00	1.00	1.00
B2-7	2.69	4.33	6.12
B2-15	3.24	5.63	8.40
B2-22	3.52	6.77	11.01
B2A2G2-0	1.00	1.00	1.00
B2A2G2-7	2.36	3.22	4.02
B2A2G2-15	3.02	4.27	5.47
B2A2G2-22	3.06	4.58	6.19
B2A2G2-F-0-4.5	1.00	1.00	1.00
B2A2G2-F-7-4.5	2.74	4.43	6.12
B2A2G2-F-15-4.5	2.96	4.93	7.02
B2A2G2-F-22-4.5	2.99	5.55	8.69
B2A2G2-F-0-7.5	1.00	1.00	1.00
B2A2G2-F-7-7.5	1.86	2.11	1.94
B2A2G2-F-15-7.5	1.83	2.44	2.53
B2A2G2-F-22-7.5	2.24	2.78	2.84

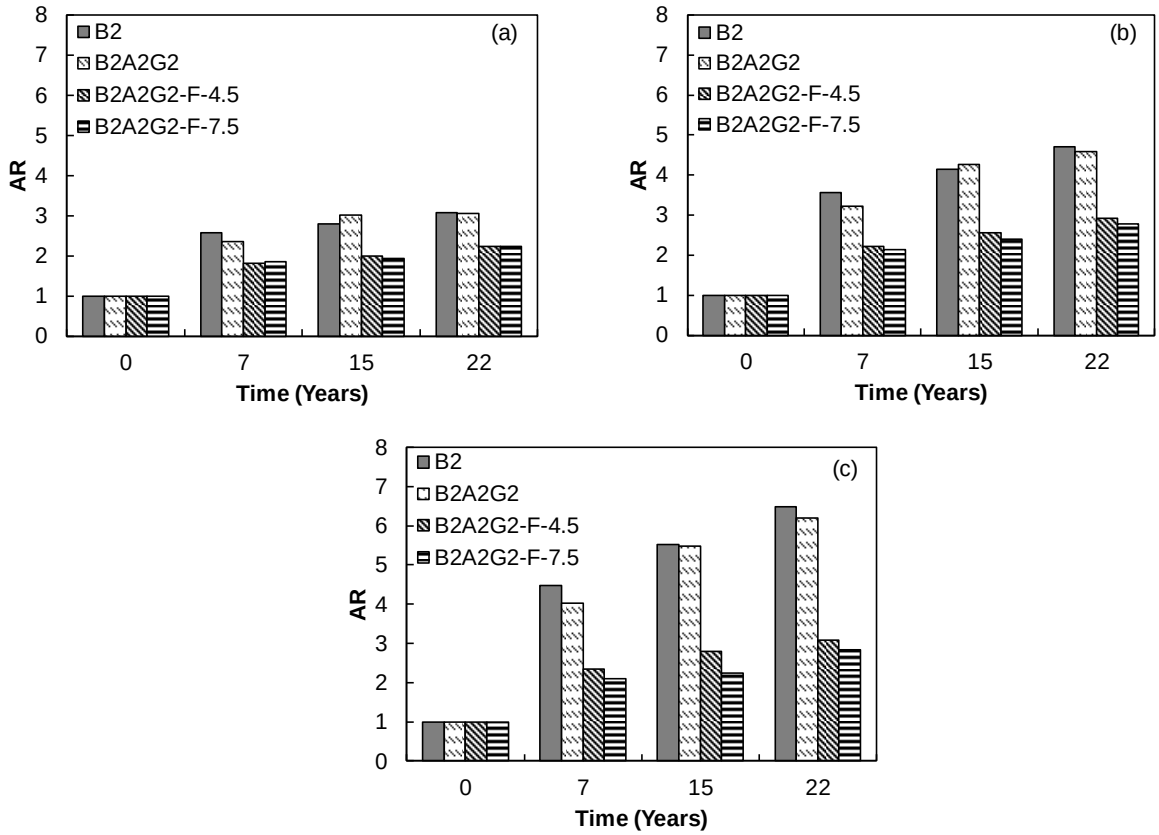

Figure C-29. Aging ratios of B2, B2A2G2, and FAM B2A2G2-F-4.5/7.5 for different aging conditions at 10 rad/s: (a) 10°C; (b) 20°C; (c) 30°C.

Fatigue Test and Analysis

Fatigue testing was conducted on FAM samples using the same equipment as the dynamic modulus test and at a test temperature of 18°C. Fingerprint testing was conducted at the same 18°C test temperature and 10 Hz frequency on all the samples before starting the fatigue test. The fatigue test on all the samples were conducted using constant actuator controlled strain at 18°C temperature and 10Hz frequency. During the testing on specimen strain was measured using the installed LVDTs on the sample. Testing was conducted on three replicates from each aging level at different strain levels. The target strain levels were set to reach a fatigue life of approximately 10000, 50000 and 100000 cycles. The number of cycles to failure for all the tested FAM materials are presented in Table C-10.

Table C-10. Experimental number of cycles to failure and on-specimen strain for FAM fatigue tests

Sample	4% AV		8% AV		Sample	4% AV	
	On-specimen micro strain	Number of failure cycles	On-specimen micro strain	Number of failure cycles		On-specimen micro strain	Number of failure cycles
B2A2G2-0-F	827	116818	724	62837	B1A2G2-0-F	785	37896
	1157	35656	886	107746		904	32058
	2031	8296	1500	7516		3620	2500
B2A2G2-7-F	627	126199	687	119263	B1A2G2-7-F	618	145187
	814	45449	782	54662		798	30343
	1160	11923	1190	17531		823	15462
B2A2G2-15-F	705	101954	767	96717	B1A2G2-22-F	564	138775
	755	47623	965	28724		684	52430
	960	16042	1362	6084		843	25319
B2A2G2-22-F	536	398934	711	118136	B3A2G5-0-F	1040	58958
	698	90688	883	12208		740	345741
	1128	7888	1040	12412		866	61707
B2A2G1-0-F	N/A		550	50448	B3A2G5-22-F	1169	123963
			586	92395		1180	46525
			967	15435		1320	18804
B2A2G1-7-F			581	105983	B2A2G5-0-F	725	141378
			692	46268		725	26025
			789	19056		995	7706
B2A2G1-15-F			588	95933	B2A2G5-22-F	1100	152563
			700	38677		903	39883
			787	14737		903	23690
B2A2G1-22-F			532	166353			
			684	34650			
			785	14028			

The fatigue test data was analyzed using simplified viscoelastic continuum damage theory (S-VECD). The S-VECD formulation and its functionality are explained in research paper by Underwood et.al. (2010). But in short some of model equations are described below.

1. The pseudo strain (ε^R) function in time and steady-state frequency domains;

$$\varepsilon^R = \frac{1}{E_R}\int_0^t E(t-\tau)\frac{d\varepsilon}{d\tau}d\tau$$
$$\varepsilon_0^R = \frac{1}{E_R}\left(|E^*|\times\varepsilon_0\right) \quad \text{(C-17)}$$

2. The pseudo strain energy density function, W^R;

$$W^R = \frac{1}{2}\left(\varepsilon^R\right)^2 C \quad \text{(C-18)}$$

3. The stress, σ, to ε^R relationship; and

$$\sigma = \frac{dW^R}{d\varepsilon^R} = C\times\varepsilon^R \quad \text{(C-19)}$$

4. The damage evolution law with respect to time and cycles

$$\left\{\begin{array}{l} \frac{dS}{dt} = \left(-\frac{\partial W^R}{\partial S}\right)^\alpha = \left(-\frac{1}{2}\left(\varepsilon^R\right)^2\frac{dC}{dS}\right)^\alpha \\ \frac{dS}{dN} = \left(-\frac{\partial W^R}{\partial S}\right)^\alpha = \left(-\frac{1}{2}\left(\varepsilon_0^R\right)^2\frac{dC}{dS}\right)^\alpha \frac{1}{f}K_1 \end{array}\right\} \quad \text{(C-20)}$$

where; $E(t)$ is the LVE relaxation modulus (kPa), τ is the integration term, t is the time (s), E_R is the reference modulus (taken as 1 kPa), α is the damage evolution rate, C is the pseudo stiffness (material integrity), S is the damage, and K_1 is the loading shape factor.

The result of the S-VECD model is the damage characteristic curve or the C vs. S curve. For the present study, C vs. S curves were developed for each aging level and air void content. Irrespective of strain levels these curves were found to collapse together at each of the aging levels. Once each replicate test was measured, the C-S curves were cumulatively fitted to the power function given in Equation C-21 below.

$$C = 1 - aS^b \quad \text{(C-21)}$$

The C vs. S fit functions for B2A2G1-F and B1A2G2-F are shown in Figure C-30 and Figure C-31 and from Figure C-30 it is seen that the pseudo stiffness values at failure increase with increase in aging level. FAM corresponding to 22 years had the highest C value at failure and the control case i.e. 0 years had the lowest C value at failure. This follows the well-known notion of softer materials lasting longer than the stiffer materials. Also, it is seen that aged samples sustained more damage than the control samples. However, in Figure C-31 the damage characteristic curves of B1A2G2-4.5 show a completely opposite trend wherein the FAM material corresponding to 22 years of aging had the least C value at failure and the one corresponding to 0 years, the highest. In Figure C-32, a clear modulus effect is seen in the C vs S

curves of B2A2G1-F and B2A2G2-F. FAM, B2A2G1-F, which corresponds to a coarser gradation possesses higher stiffness and had C values at failure higher than that of B2A2G2-F at same aging level. Similar trends at 22 years aging level are observed in Figure C-33 where B2A2G2-F is the stiffer material. The difference in C value at failure at 7 years and 0 years is very marginal, with B1A2G2-F having a slightly higher value.

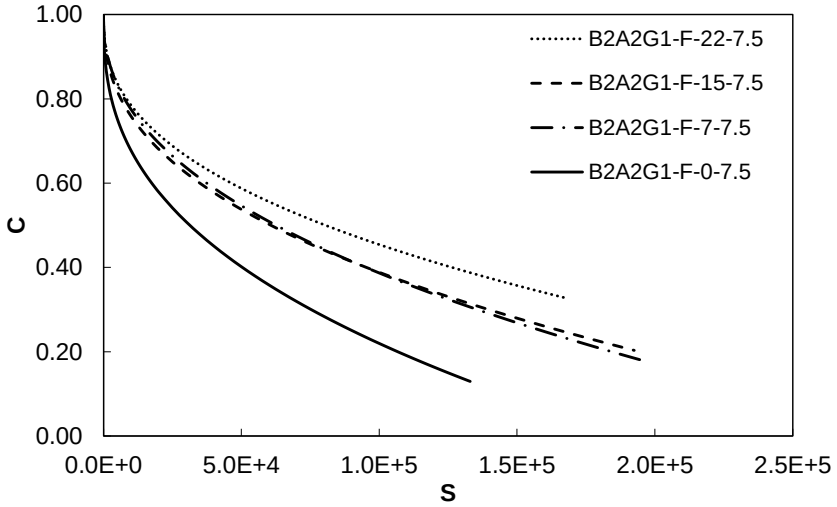

Figure C-30. Damage characteristic curve for B2A2G1-F at 7.5% air void content.

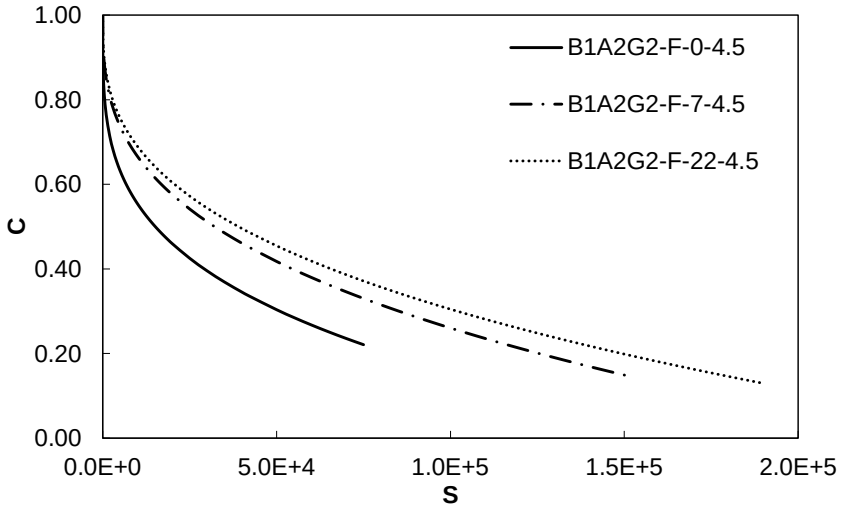

Figure C-31. Damage characteristic curve for B1A2G2-F at 4.5% air void content.

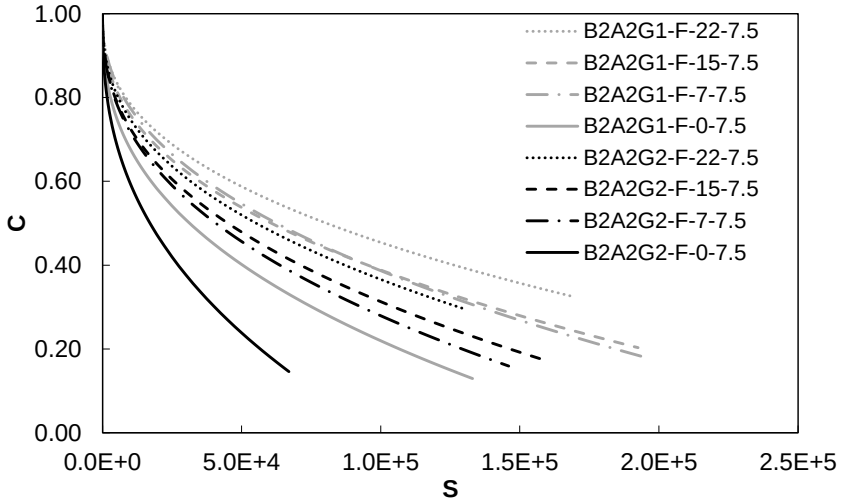

Figure C-32. Comparison of damage characteristic curves for B2A2G1-F and B2A2G2-F (AV= 7.5%).

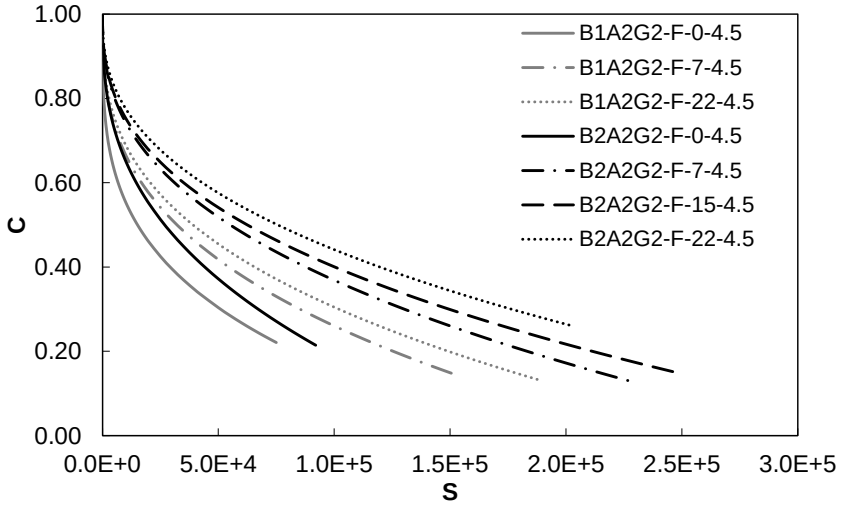

Figure C-33. Comparison of damage characteristic curves for B1A2G2-F and B2A2G2-F (AV= 4.5%).

Fatigue Life Simulation Analysis for FAM Materials Using the GR Approach

Damage curves alone are not sufficient to understand and predict the fatigue life of FAM. The damage curves and $|E^*|$ of FAM should be considered to evaluate the fatigue life. To gain additional information on fatigue performance, fatigue life of FAM samples at different aging levels and under constant strain conditions is predicted using the S-VECD model. Fatigue life prediction with the S-VECD model requires characterization of a failure criteria and here the rate of pseudo strain energy release (G^R) approach (Sabouri and Kim, 2014) was adopted. Replicate fatigue data (G^R and N_f) from each FAM were plotted together and fitted to an exponential Equation C-22, as shown in Figure C-34 through Figure C-36.

$$G^R = aN_f{}^b \tag{C-22}$$

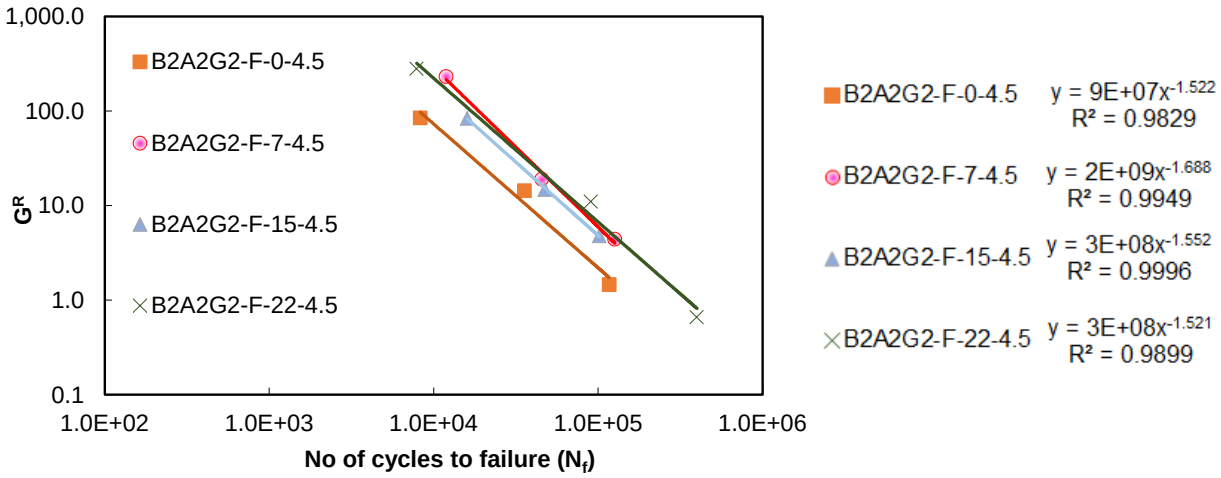

Figure C-34. G^R vs. N_f relationship for B2A2G2-F-4.5.

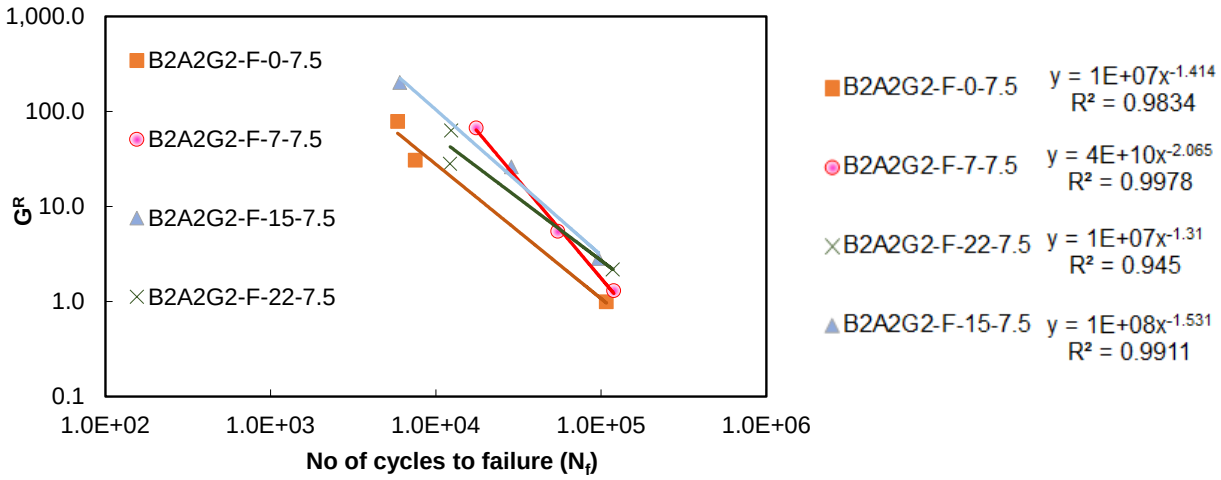

Figure C-35. G^R vs. N_f relationship for B2A2G2-F-7.5.

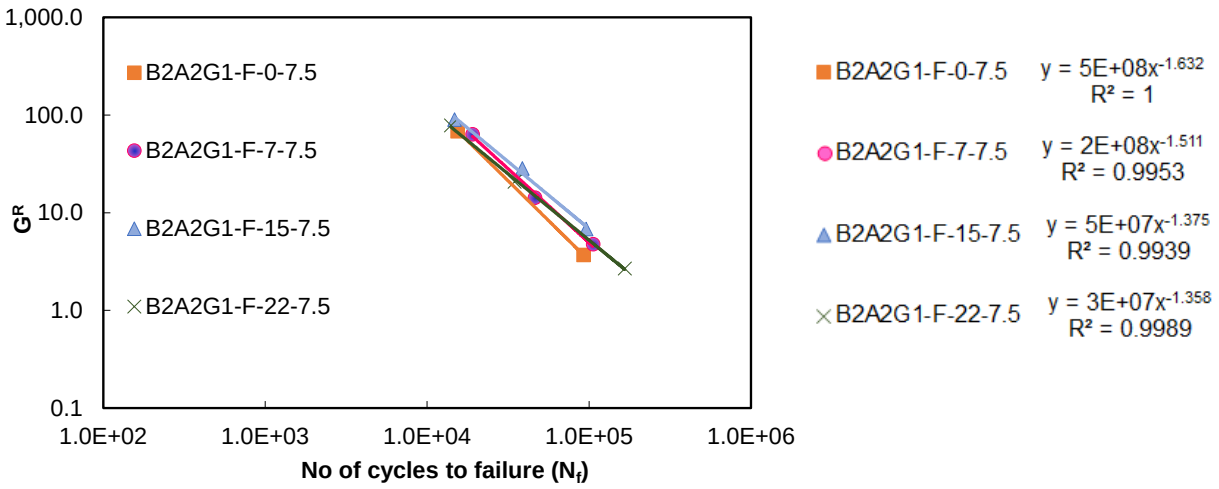

Figure C-36. G^R vs. N_f relationship for B2A2G1-F-7.5.

Failure criterion lines alone are not sufficient to predict the fatigue life of FAM materials and can be used only for an approximate comparison of the fatigue resistance of the FAM materials. The damage curves, failure criterion lines, and dynamic modulus value of a mixture should be considered to evaluate the fatigue life of FAM materials. Figure C-37 through Figure C-39 show the fatigue life plots determined using the S-VECD modeling Equation C-23 for different FAM materials at a test temperature of 18°C.

$$N_f = \left[\frac{\alpha - C_{12}\alpha + 1}{\alpha - C_{12}\alpha + 1 + C_{12}} \frac{C_{11}}{2a} \left[\left(\varepsilon_0 \right) \left(|E^*|_{LVE} \right) \right]^2 \times \left(\frac{(\alpha - C_{12}\alpha + 1)(C_{11}C_{12})^{\alpha} \left[\left(\varepsilon_0 \right) \left(|E^*|_{LVE} \right) \right]^{2\alpha} K_1}{f_{red} \times 2^{\alpha}} \right)^{\frac{C_{12}}{\alpha - C_{12}\alpha + 1}} \right]^{\frac{\alpha - C_{12}\alpha + 1}{(\alpha+1)(b+1) - C_{12}(\alpha + b\alpha + 1)}} \quad \text{(C-23)}$$

Figure C-37 shows the simulated fatigue life results for B2A2G2-4.5 FAM material at different aging levels. The figure shows that the unaged FAM material has a longer fatigue life than the FAM materials aged to 7 years, 15 years, and 22 years of aging. This trend corroborates the literature with regard to existing aged asphalt concrete materials. Similar trends also were observed for both B2A2G2-7.5 FAM (Figure C-38) and B2A2G1-7.5 FAM (Figure C-39) materials. However, the only abnormality found was in the case of the control material for the

B2A2G2-7.5 FAM. This material showed a shorter fatigue life at low strain levels than the other aged cases and a steep slope for the fatigue line.

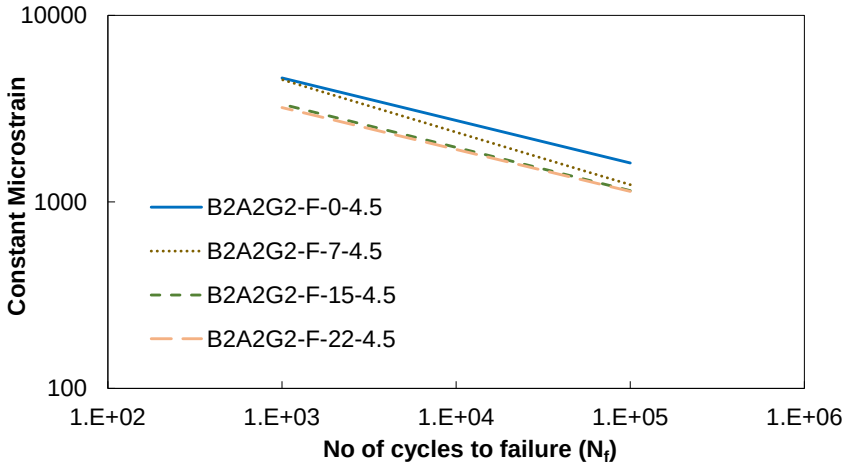

Figure C-37. G^R failure envelope for B2A2G2-F-4.5.

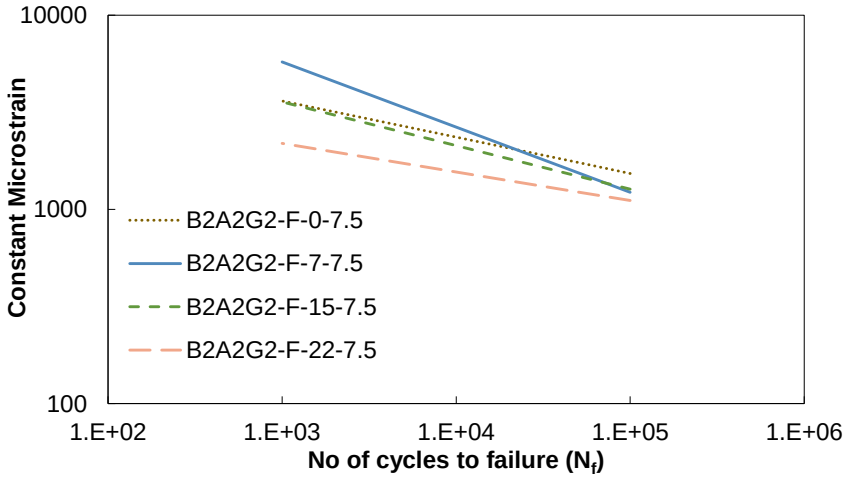

Figure C-38. G^R failure envelope for B2A2G2-F-7.5.

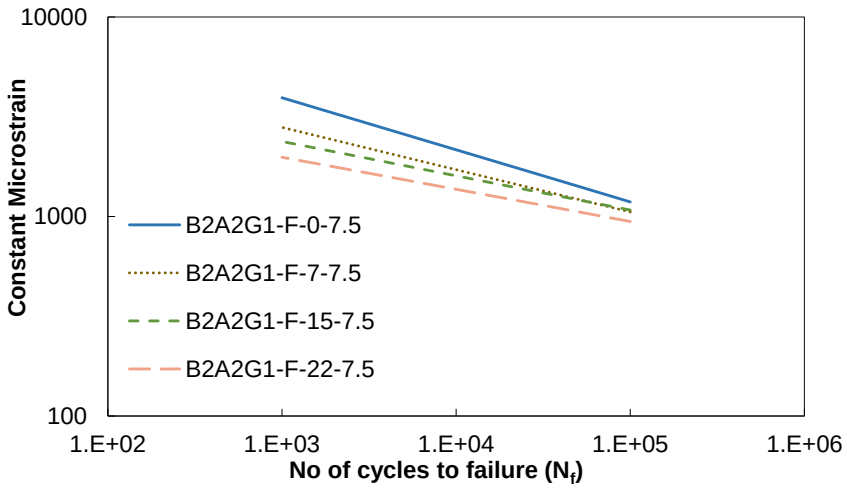

Figure C-39. G^R failure envelope for B2A2G1-F-7.5.

Sensitivity Assessment

Crossover Modulus Kinetics

The *AR* is a convenient parameter to quickly identify the mechanical effects of oxidation, especially when evaluated across a range of temperature and frequency combinations. However, drawing conclusions related to sensitivity based only on *AR* might be inappropriate. Consider an example of binder and its corresponding mastic. The differences in *AR* for the two materials reflect the influence of aggregate particles in stiffening the asphalt binder composite as well as any potentially mitigating physico-chemical surface reactions occurring between asphalt binder and aggregate. Because of this dual influence, care should be taken when directly comparing the differences in binder and mastic *AR* to compare the relative sensitivity of the two materials to oxidative aging products.

To overcome this limitation, it is necessary to define a second aging quantity related only to the oxidation in the asphalt binder. The parameter chosen for this purpose was based on crossover modulus, G^*_c, which is defined as the modulus when the phase angle is 45° (Farrar et al., 2013). It is related to the shape parameter in Christensen-Anderson model (Christensen and Anderson, 1992) or it can be identified through direct interpolation of the temperature and frequency sweep data. The latter approach was adopted here and involved first plotting the measured $|G^*|$ versus measured ϕ, then fitting the plot in the range of ϕ between 40° and 50°, and finally interpolating for 45° to compute G^*_c. The importance of using this quantity is that it has been shown to correlate to oxidation induced chemical changes in asphalt binder (Farrar et al., 2013). In the same work, it was also reported that the inverse of G^*_c varied with time according to a 2nd order rate law. In this rate law, two relevant crossover moduli are considered; G^*_c from the un-aged case, e.g., at t=0, G^*_{c0}, and crossover modulus at different oxidation times, G^*_{ct}.

The change in G^*_c over time, $G^*_{c0} \rightarrow G^*_{ct}$, is associated with some rate, r, which is mathematically described by Equation C-24.

$$r = -\frac{d\left[G_c^*\right]}{dt} \tag{C-24}$$

If this reaction obeys a 2nd order rate law, the rate can also be written as;

$$r = k\left[G_c^*\right]^2. \tag{C-25}$$

Then setting Equation C-24 equal to Equation C-25 and solving for time yields;

$$\frac{1}{G_{ct}^*} - \frac{1}{G_{c0}^*} = kt \Rightarrow \textit{Aging Parameter } = AP = kt. \tag{C-26}$$

Relationship between AR and AP

Thus, it follows from 2nd order aging kinetics that the difference in the inverse of these moduli over time is a direct indication of oxidation, thus as it is shown in Equation C-26, a second aging metric, *AP*, has been defined based on the difference in the inverse of these moduli. The primary purpose of this parameter is to establish the level of oxidation that has occurred in the asphalt binder. Since sensitivity entails identifying how strongly the mechanical properties of a composite are affected by chemical changes in asphalt binder, assessment of sensitivity involves combining *AR* and *AP* quantities. Mathematically, the aging sensitivity parameter (*ASP*) is defined to be the impact of a differential change in *AP* of the binder on *AR* of a binder, mastic, or FAM, Equation C-27. The *ASP* can be determined directly by cross-plotting *AR* of the binder or mastic or FAM with the aging parameter from the asphalt binder. Since *AR* and *AP* vary with temperature and frequency, *ASP* also varies by temperature and frequency.

$$ASP = \frac{d(AR_{mastic\ or\ binder})}{d\left(AP_{binder}\right)} \tag{C-27}$$

The *ASP* from Equation C-27 is determined by cross-plotting *AR* of the binder, mastic, or FAM with *AP* from asphalt binder, as shown in Figure C-40, which is an example of B1 binder and its corresponding mastic and FAM.

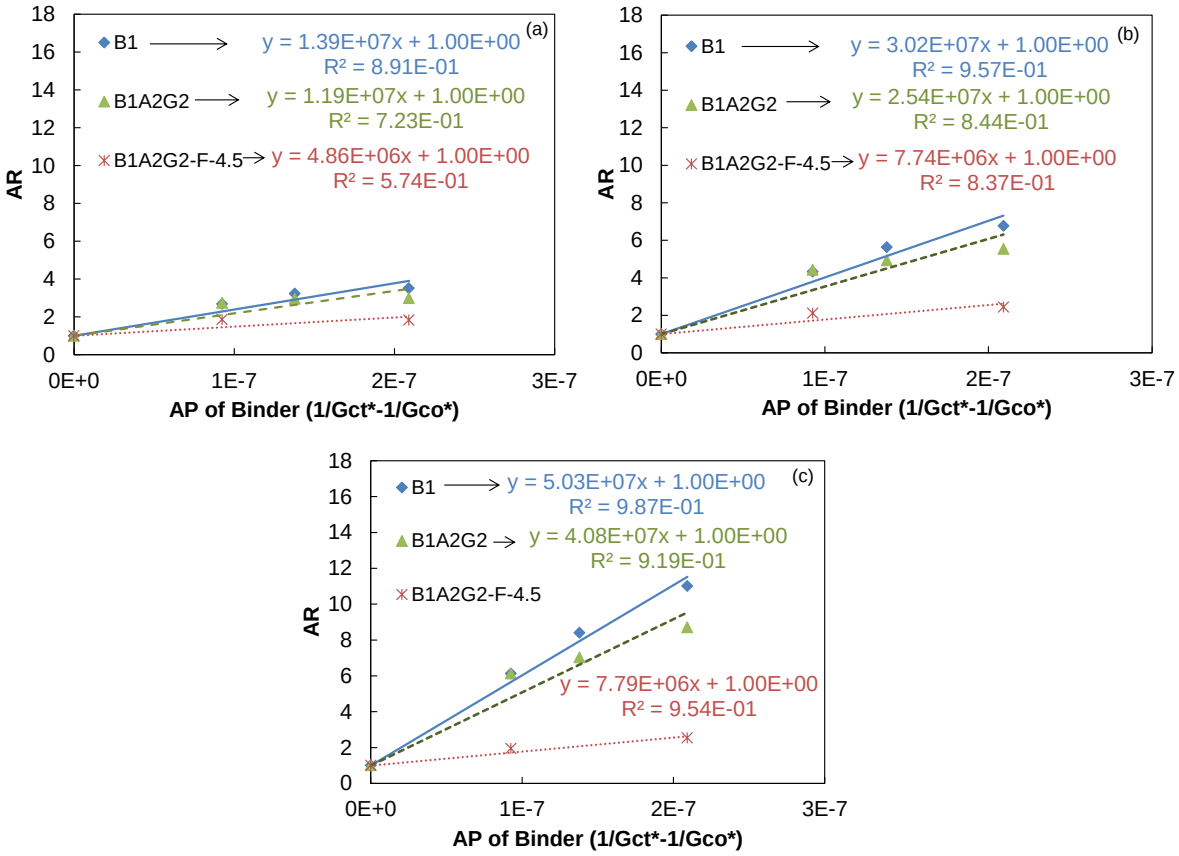

Figure C-40. Relationship between *AR* of Binder B1, Mastic B1A2G2, FAM B1A2G2-F-4.5, to *AP* of B1 for different aging conditions at 10 rad/s: (a) 10°C; (b) 20°C; (c) 30°C.

Since asphalt binder is pre-aged, *AP* of the binder in mastic and FAM is identical and equal to what was measured for the non-mixed asphalt binder. The *ASP's* for materials shown in the figure are slopes of the respective trendlines, which for B1, B1A2G2, and B1A2G2-F-4.5 are 1.39×10^7, 1.19×10^7, and 4.86×10^7 respectively at 10°C. The slopes differ with respect to temperature and are shown in Figure C-21. Through Figure C-21 inferences on sensitivity can be made by comparing the proximity of mastics and FAM trendlines to that of binder. In this study sensitivity is defined as how changes in the binder properties are correlated to the changes in the mechanical properties of mastic and FAM. Greater proximity, as in case of B1A2G2, indicates greater sensitivity of mechanical properties of B1A2G2 to oxidation of binder B1 and lower proximity, as in case of FAM B1A2G2-F-4.5 indicates otherwise. Although, these observations can be quantified, generalization based on the goals of the study is difficult to achieve through this approach.

Sensitivity Assessment Approaches

Recall that the motivation for this study is to identify the accuracy with which laboratory aging processes should replicate in-service/field aging. In this case sensitivity can be viewed from two perspectives; 1) how accurately does *AP* of binder need to be matched to achieve a chosen level of accuracy in mechanical properties of AC or FAM and 2) what is the expected

accuracy in mechanical properties of a material for a given a level of accuracy in matching *AP* of a binder. Both approaches have been evaluated for different levels of accuracy as detailed below.

Approach 1: How accurately should the laboratory process replicate binder AP in order to match in-service/field aging of asphalt mixture mechanical properties?

To evaluate how accurately the laboratory process should replicate the binder AP to achieve specific level of accuracy in mechanical properties of AC, consider the effect of an arbitrary change in AR on AP. For this purpose, let AR1 be a given aging ratio of the material (binder, mastic, or FAM) at one aging level (indicated by AP1). Since there exists linear relationship between AP and AR with an intercept of one and a slope equal to ASP, AP1 can be calculated by Equation C-28.

$$AP_1 = \frac{(AR_1 - 1)}{ASP} \tag{C-28}$$

Next consider a second aging ratio, AR2, which represents aging ratio after a percentage change (denoted as x),

$$AR_2 = AR_1\left(1 + \frac{x}{100}\right) \tag{C-29}$$

In this case AP2 is defined as the aging parameter corresponding to AR2, and can be calculated as,

$$AP_2 = \frac{(AR_2 - 1)}{ASP} \tag{C-30}$$

The accuracy required for AP of a binder to match AR of a mix within a predetermined level of accuracy, x, is determined by first selecting AR1. Then, a value of x is assumed and substituted into Equation C-29 to find AR2. Finally, Equations C-28 and C-30 are used to calculate AP1 and AP2 respectively. The percent difference between AP1 and AP2, Equation C-31, represents the accuracy of binder that need to be achieved in laboratory to match the mix AR with in the given accuracy of x. These calculations are performed at each of the temperatures and frequencies evaluated, for each of 7, 15, and 22 years aging conditions, and at a range of AR accuracy.

$$\%Difference_{AP} = \frac{(AP_2 - AP_1)}{AP_1} \times 100 \tag{C-31}$$

The above described procedure is used for calculating the sensitivity of AP for given accuracy in the AR for different binders, mastics and FAM materials tested in this study. The results for B2 and two of its corresponding mastics and FAM are presented in Figure C-41(a). The data presented in this figure represents the accuracy required in matching the binder AP to achieve a 20% accuracy in AR. Note that for the sake of brevity only the 20% accuracy case is shown in the figure, but the conclusions and observations below were developed based on analysis covering a range of accuracy from 1-20%. The required accuracy in binder AP for the

entire 1-20% range of accuracies in AR are tabulated in Table C-11. Figure C-41(a) should be read as follows, if a laboratory procedure can estimate AP of binder B2 at 22 years aging level within approximately 35% then it can be ensured that the resultant modulus of B2A2G2-F-7.5 at 22 years and 10°C will be within 20% of its true modulus. Results are shown at only 10°C and 30°C as they are lowest and highest common temperatures for which experimental data were available. They also demonstrate the lowest and highest observed sensitivities in the dataset. A frequency of 10 rad/s is used in this analysis, but comparable results are obtained at other frequencies. The main observations from this data are:

- Lower accuracy is required in matching binder *AP* when needed to replicate aged mechanical properties at larger length scales. For example, mastics require a higher accuracy in *AP* than FAM to match an assumed accuracy of *AR*.
- The accuracy required in *AP* increases with increase in aging level, i.e., a more accurate *AP* must be achieved at 22 years aging level than at 15 or 7 years aging levels to match an assumed accuracy of *AR*.
- Higher temperatures require *AP* to be more closely matched. Although not shown here the inverse statement occurs with respect to frequency, as the frequency decreases the *AP* must be matched more closely.
- Fine graded (G2) mastics and FAM, Figure C-41(a), require higher accuracy in *AP* than coarse graded (G1) materials, Figure C-41(b).
- Although not shown in Figure C-41, FAM materials containing 4.5% air voids require higher accuracy in *AP* than FAM materials containing 7.5% air voids.
- It is observed from Figure C-41(c) that, B1 binder mastics require a greater accuracy in *AP* than those prepared with B2, which in turn require a greater accuracy than those prepared with B3. A2G2 was the only class of mastics that was in common among the three binders. The relationship also holds true for any two sets of binders as well as shown in Figure C-41(d). For example, binders B1 and B2 in class A2G1 and binders B1 and B3 in class A1G2.
- It is observed that the ratio of required accuracy in *AP* to the resultant accuracy in *AR* varies from 1.1 to 1.9 for binders and mastics and from 1.5 to 3.6 for FAM. This ratio is independent of the value of assumed accuracy in *AR*, e.g., it includes results from analysis with other values of *x* that are not explicitly shown in Figure C-41 but tabulated in Table C-11. A ratio equal to 1 indicates that the required accuracy in *AP* matches the assumed accuracy in *AR* and higher the ratio, lower is the accuracy required in *AP* to match assumed accuracy in *AR*.

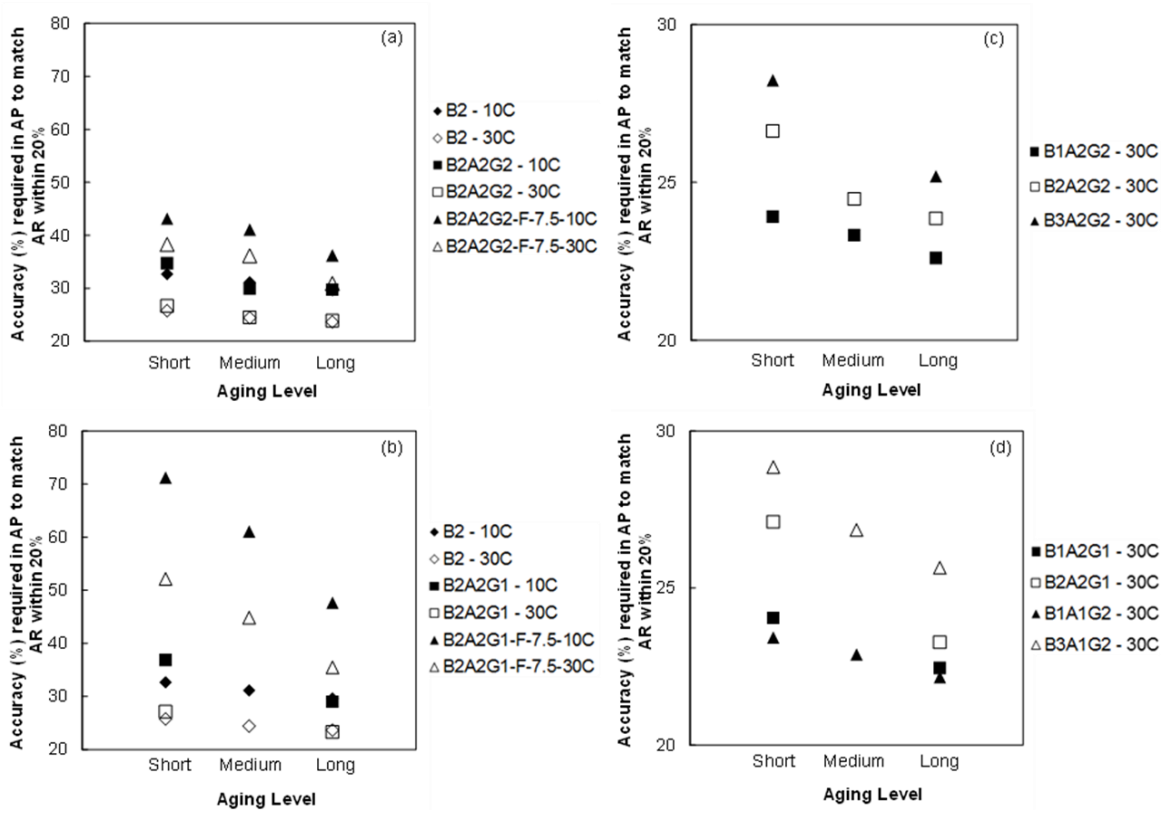

Figure C-41. Accuracy required in binder *AP* to match *AR* within 20% for (a) B2A2G2 based materials; (b) B2A2G1 based materials; (c) A2G2 mastics; and (d) A2G1 and A1G2 mastics.

Table C-11. Accuracy (%) required in binder *AP*, to match the mechanical property (*AR*) within 1, 2, 10, and 20% at 10, and 30°C.

Material	Aging Level (years)	Accuracy Required in *AP* to match *AR* within							
		1% at 10˚C	1% at 30˚C	2% at 10˚C	2% at 30˚C	10% at 10˚C	10% at 30˚C	20% at 10˚C	20% at 30˚C
B1	7	1.59	1.20	3.18	2.39	15.92	11.95	31.83	23.91
	15	1.45	1.14	2.89	2.27	14.46	11.35	28.93	22.70
	22	1.40	1.10	2.79	2.20	13.97	11.00	27.94	22.00
B2	7	1.63	1.29	3.27	2.57	16.33	12.87	32.66	25.75
	15	1.56	1.22	3.11	2.44	15.56	12.21	31.11	24.42
	22	1.48	1.18	2.96	2.36	14.81	11.82	29.62	23.64
B3	7	1.88	1.38	3.77	2.75	18.85	13.77	37.70	27.55
	15	1.78	1.28	3.55	2.57	17.75	12.85	35.50	25.70
	22	1.58	1.21	3.16	2.41	15.81	12.07	31.63	24.13
B1A1G2	7	1.48	1.17	2.97	2.34	14.83	11.71	29.66	23.42
	15	1.45	1.14	2.89	2.29	14.46	11.44	28.93	22.89
	22	1.38	1.11	2.76	2.22	13.79	11.08	27.58	22.16
B1A2G1	7	1.58	1.20	3.15	2.40	15.75	12.02	31.51	24.04
	15	N/A	N/A	N/A	N/A	N/A	N/A	N/A	N/A
	22	1.43	1.12	2.86	2.25	14.30	11.23	28.61	22.45
B1A2G2	7	1.57	1.20	3.15	2.39	15.75	11.95	31.49	23.91
	15	1.51	1.17	3.02	2.33	15.10	11.66	30.20	23.32
	22	1.50	1.13	3.01	2.26	15.03	11.30	30.05	22.60
B2A2G1	7	1.84	1.36	3.69	2.71	18.43	13.55	36.86	27.10
	15	N/A	N/A	N/A	N/A	N/A	N/A	N/A	N/A
	22	1.45	1.16	2.90	2.33	14.50	11.63	28.99	23.27
B2A2G2	7	1.74	1.33	3.47	2.66	17.35	13.31	34.71	26.62
	15	1.50	1.22	2.99	2.45	14.95	12.24	29.90	24.47
	22	1.49	1.19	2.97	2.39	14.85	11.93	29.71	23.85
B3A1G2	7	1.95	1.44	3.90	2.88	19.52	14.42	39.05	28.85
	15	1.79	1.34	3.57	2.68	17.87	13.42	35.75	26.85
	22	1.68	1.28	3.36	2.56	16.80	12.82	33.61	25.65
B3A2G2	7	1.81	1.41	3.63	2.82	18.13	14.12	36.26	28.23
	15	N/A	N/A	N/A	N/A	N/A	N/A	N/A	N/A
	22	1.58	1.26	3.17	2.52	15.85	12.60	31.70	25.19
B2A2G1-F-7.5	7	3.56	2.61	7.12	5.21	35.60	26.06	71.20	52.13
	15	3.05	2.24	6.11	4.48	30.53	22.42	61.05	44.85
	22	2.38	1.77	4.76	3.55	23.82	17.73	47.65	35.45
B2A2G2-F-7.5	7	2.16	1.91	4.31	3.82	21.57	19.12	43.14	38.25
	15	2.05	1.81	4.11	3.61	20.53	18.06	41.07	36.11
	22	1.81	1.54	3.62	3.09	18.09	15.45	36.18	30.89
B2A2G2-F-4.5	7	2.21	1.74	4.42	3.49	22.12	17.43	44.24	34.86
	15	2.00	1.56	4.00	3.12	19.99	15.59	39.99	31.17
	22	1.80	1.48	3.60	2.96	18.01	14.81	36.02	29.62

B1A2G 2-F-4.5	7	2.16	2.07	4.32	4.13	21.59	20.67	43.18	41.35
	15	N/A	N/A	N/A	N/A	N/A	N/A	N/A	N/A
	22	2.20	1.65	4.40	3.30	22.01	16.52	44.02	33.03

Approach 2: How accurately can asphalt mixture properties be matched at different levels of AP accuracy?

To answer second sensitivity related question, consider the effect of an arbitrary error in *AP* of binder on *AR of* asphalt mix. Like in the derivation to answer the first question, let AR_1 be a given aging ratio of the material (binder, mastic, or FAM) and AP_1 be *AP* at AR_1. The relationship between AP_1 and AR_1 is given by Equation C-28. Next consider a second aging parameter, AP_2, which represents the aging parameter after a percentage error (denoted as *y*) is factored in,

$$AP_2 = AP_1\left(1 + \frac{y}{100}\right) \tag{C-32}$$

In this case AR_2 is defined as the aging ratio corresponding to AP_2, and can be calculated as;

$$AR_2 = (AP_2 \times ASP) + 1 \tag{C-33}$$

The percent difference between AR_1 and AR_2, Equation C-34, represents the resulting error in *AR* because of the arbitrary percentage error in *AP*.

$$\%Error_{AR} = \frac{(AR_2 - AR_1)}{AR_1} \times 100 \tag{C-34}$$

The above procedure is used to answer the second question for several materials tested in this study. The results of this analysis for B2 and two of its corresponding mastics and FAM are presented in Figure C-42 and Table C-12 The data presented in this figure shows the resulting error in AR of asphalt material due to a given percentage error in AP of binder, which in this case is set at 20%. The data from Figure C-42(a) should be interpreted as follows, if error in matching AP of binder B2 at 7 years aging level is 20% then the resultant error in AR at 7 years aging level at 30°C for binder B2 is 15.5%, mastic B2A2G2 is 15.0%, but for FAM B2A2G2-F-7.5 it is only approximately 10.5%. This shows that for a fixed accuracy in AP the error in estimated mechanical properties would be less for FAM than for binders and mastics. Since the analysis relies on the same ASP values as in Approach 1, other major findings with respect to impacts from temperature, gradation, and binder aggregate interactions essentially remain the same.

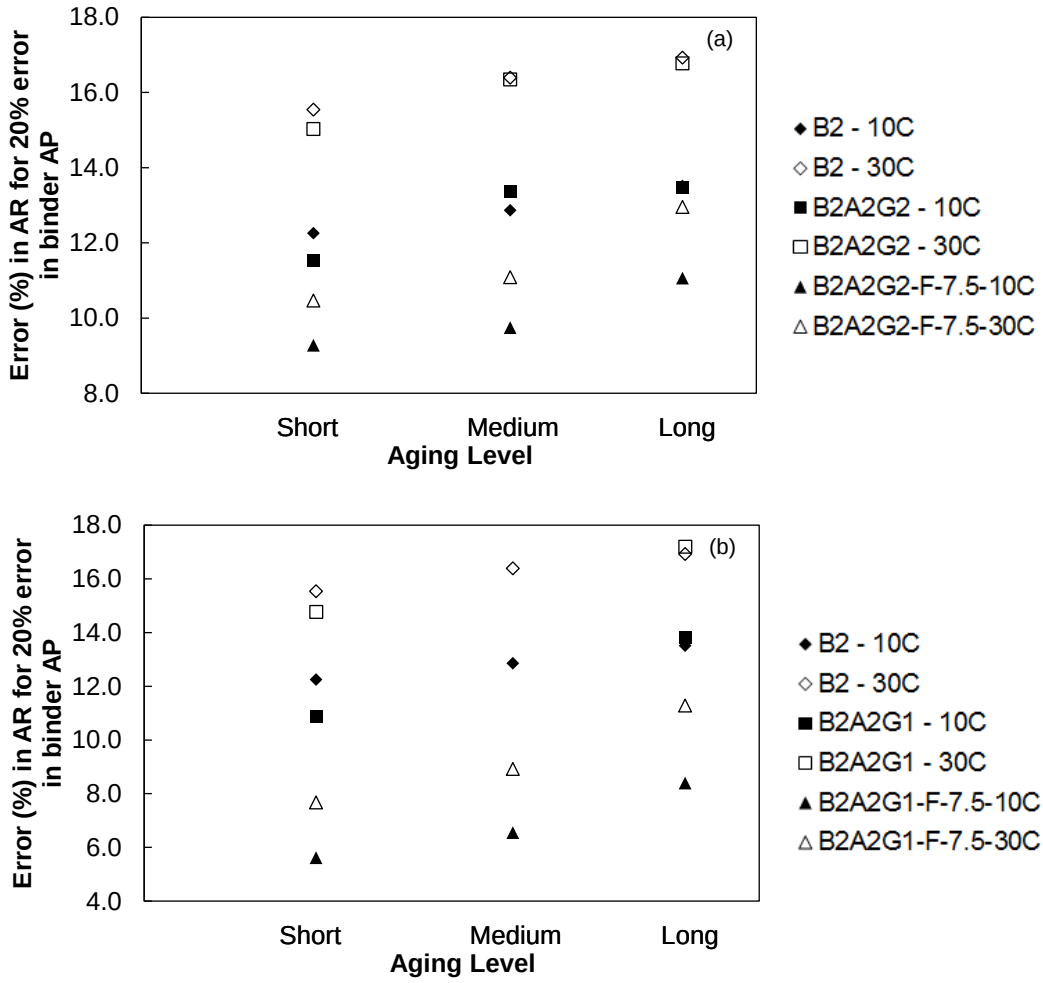

Figure C-42. Error (%) in mechanical property (*AR*) due to 20% error in binder *AP* for (a) B2A2G2 based materials; and (b) B2A2G1 based materials.

Table C-12. Error (%) in mechanical property (*AR*) due to 1, 2, 10, and 20% error in binder *AP* at 10°C and 30°C

Material	Aging Level (Years)	The Resulting Error in AR when the Error in AP is							
		1% at 10˚C	1% at 30˚C	2% at 10˚C	2% at 30˚C	10% at 10˚C	10% at 30˚C	20% at 10˚C	20% at 30˚C
B1	7	0.63	0.84	1.26	1.67	6.28	8.37	12.57	16.73
	15	0.69	0.88	1.38	1.76	6.91	8.81	13.83	17.62
	22	0.72	0.91	1.43	1.82	7.16	9.09	14.32	18.18
B2	7	0.61	0.78	1.22	1.55	6.12	7.77	12.25	15.54
	15	0.64	0.82	1.29	1.64	6.43	8.19	12.86	16.38
	22	0.68	0.85	1.35	1.69	6.75	8.46	13.51	16.92
B3	7	0.53	0.73	1.06	1.45	5.31	7.26	10.61	14.52
	15	0.56	0.78	1.13	1.56	5.63	7.78	11.27	15.57
	22	0.63	0.83	1.26	1.66	6.32	8.29	12.65	16.58
B1A1G2	7	0.67	0.85	1.35	1.71	6.74	8.54	13.49	17.08
	15	0.69	0.87	1.38	1.75	6.91	8.74	13.83	17.48
	22	0.73	0.90	1.45	1.80	7.25	9.02	14.51	18.05
B1A2G1	7	0.63	0.83	1.27	1.66	6.35	8.32	12.70	16.64
	15	N/A	N/A	N/A	N/A	N/A	N/A	N/A	N/A
	22	0.70	0.89	1.40	1.78	6.99	8.91	13.98	17.82
B1A2G2	7	0.64	0.84	1.27	1.67	6.35	8.37	12.70	16.73
	15	0.66	0.86	1.32	1.72	6.62	8.58	13.24	17.15
	22	0.67	0.88	1.33	1.77	6.66	8.85	13.31	17.70
B2A2G1	7	0.54	0.74	1.09	1.48	5.43	7.38	10.85	14.76
	15	N/A	N/A	N/A	N/A	N/A	N/A	N/A	N/A
	22	0.69	0.86	1.38	1.72	6.90	8.60	13.80	17.19
B2A2G2	7	0.58	0.75	1.15	1.50	5.76	7.51	11.53	15.02
	15	0.67	0.82	1.34	1.63	6.69	8.17	13.38	16.34
	22	0.67	0.84	1.35	1.68	6.73	8.38	13.46	16.77
B3A1G2	7	0.51	0.69	1.02	1.39	5.12	6.93	10.24	13.87
	15	0.56	0.74	1.12	1.49	5.59	7.45	11.19	14.90
	22	0.60	0.78	1.19	1.56	5.95	7.80	11.90	15.59
B3A2G2	7	0.55	0.71	1.10	1.42	5.52	7.08	11.03	14.17
	15	N/A	N/A	N/A	N/A	N/A	N/A	N/A	N/A
	22	0.63	0.79	1.26	1.59	6.31	7.94	12.62	15.88
B2A2G1-F-7.5	7	0.28	0.38	0.56	0.77	2.81	3.84	5.62	7.67
	15	0.33	0.45	0.66	0.89	3.28	4.46	6.55	8.92
	22	0.42	0.56	0.84	1.13	4.20	5.64	8.40	11.28
B2A2G2-F-7.5	7	0.46	0.52	0.93	1.05	4.64	5.23	9.27	10.46
	15	0.49	0.55	0.97	1.11	4.87	5.54	9.74	11.08
	22	0.55	0.65	1.11	1.29	5.53	6.47	11.05	12.95
B2A2G2-F-4.5	7	0.45	0.57	0.90	1.15	4.52	5.74	9.04	11.48
	15	0.50	0.64	1.00	1.28	5.00	6.42	10.00	12.83
	22	0.56	0.68	1.11	1.35	5.55	6.75	11.11	13.51

B1A2G 2-F-4.5	7	0.46	0.48	0.93	0.97	4.63	4.84	9.26	9.67
	15	N/A	N/A	N/A	N/A	N/A	N/A	N/A	N/A
	22	0.45	0.61	0.91	1.21	4.54	6.05	9.09	12.11

Modulus Sensitivity (|G*| Based)

During the course of the study, it was also of interest to find sensitivity of mechanical property (*AR*) of mastics and FAM not to *AP*, which is a calculated quantity, but to |*G**| directly. Figure C-43 below shows *ASP* values calculated based on linear assumption of the *AR* vs |*G**| plot. The linear approximation with *AP* still holds good. Hence, all the calculations presented for *AR* vs *AP*, including those in approaches 1 and 2, will be equivalent to a |*G**| based assessment also. Thus, the sensitivity values presented in Table C-11 and Table C-12 will not change for |*G**| based sensitivity assessment.

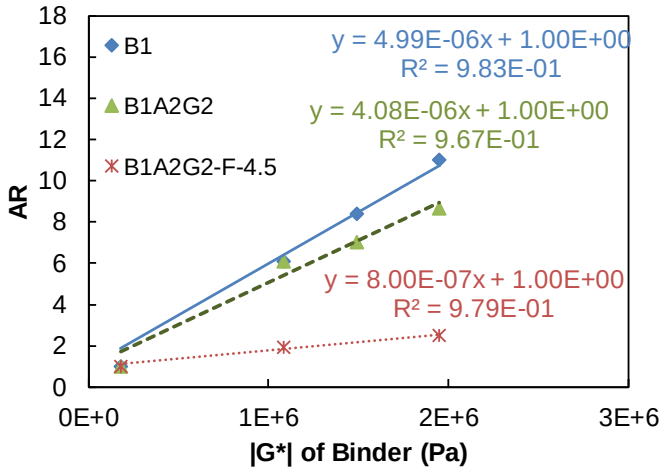

Figure C-43. Relationship between *AR* of Binder B1, Mastic B1A2G2, FAM B1A2G2-F-4.5, to |*G| of B1 for different aging conditions at 10 rad/s and 30°C.**

Sensitivity of Binder and Mastic Fatigue to Binder Oxidation

The strain ratio (*SR*), shown in Equation C-35, was used to evaluate the fatigue sensitivity of the FAM materials as a function of the aging parameter (*AP*) of the binder. This *SR* parameter is based on the ratio of the strain level (*SL*) that is required to achieve a given number of failure cycles.

$$SR = \frac{SL_{after\ aging}}{SL_{before\ aging}} \quad \text{(C-35)}$$

The *SR* was calculated at two levels of number of cycles to failure. One at 10,000 cycles and another at 100,000 cycles. The *SR* values were calculated for the binders B1, B2, and B3 and their corresponding A2G2 suite of mastics as this mastic was common to all the three binders. The relationship between *SR* and *AP* was fit using a polynomial, Equation C-36, where *A*, *B*, and *C* are the fitting parameters. The relationships and coefficients of the fitting are shown in Figure C-44 and Figure C-45.

$$SR = A \times AP^2 + B \times AP + C \tag{C-36}$$

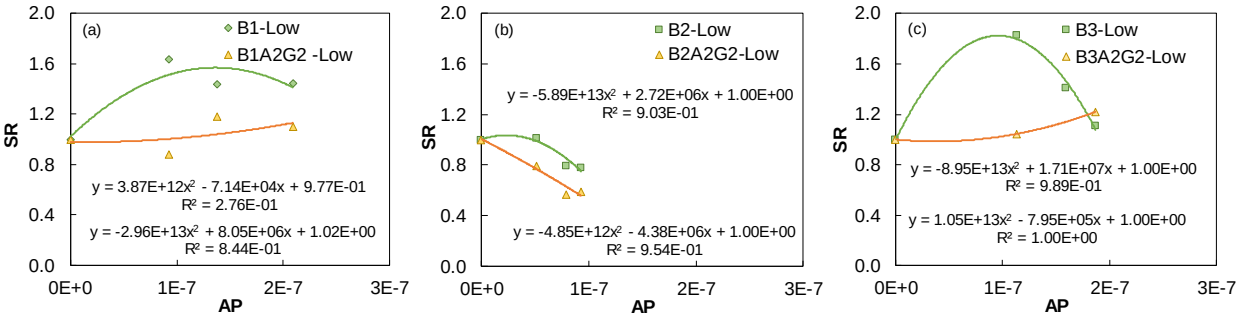

Figure C-44. Relationship between strain ratio (*SR*) at 10,000 cycles and AP of corresponding binder for (a) B1 and B1A2G2; (b) B2 and B2A2G2; and (c) B3 and B2A2G2.

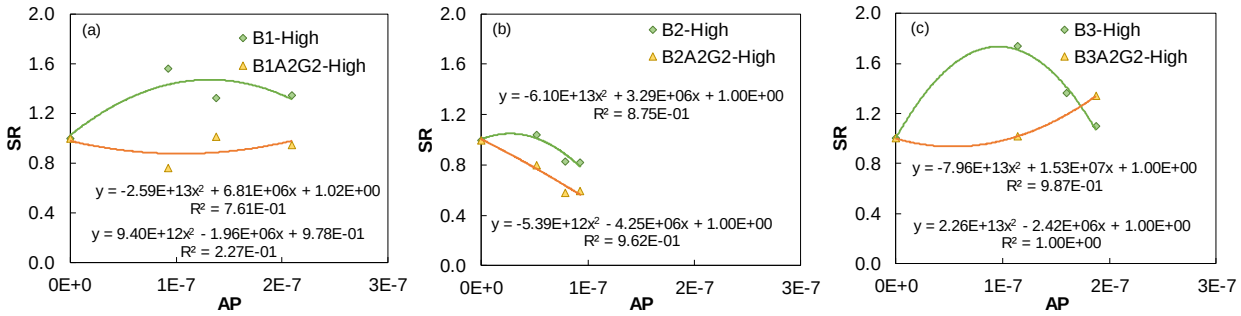

Figure C-45. Relationship between strain ratio (*SR*) at 100,000 cycles and AP of corresponding binder for (a) B1 and B1A2G2; (b) B2 and B2A2G2; and (c) B3 and B2A2G2.

The fitted polynomial equation that corresponds to each binder/mastic was used to calculate the sensitivity of the *SR* with respect to the change in the *AP* of the binder. For this purpose, let SR_1 be a given strain ratio of the material (binder or mastic) and AP_1 be the aging parameter at SR_1. Next, consider a second aging parameter, AP_2, and its corresponding strain ratio, SR_2 (determined directly from Equation C-36. AP_2 represents the aging parameter after a percentage error (denoted as *y*) is factored in, see Equation C-37.

$$AP_2 = AP_1\left(1 + \frac{y}{100}\right) \tag{C-37}$$

The change in *SR* for the corresponding change in *AP* is calculated by Equation C-38.

$$\%Error_{SR} = \frac{(SR_2 - SR_1)}{SR_1} \times 100 \tag{C-38}$$

The percentage error values as calculated from Equation C-38 for the materials shown in Figure C-44 are presented in Table C-13 for 10,000 cycles to failure, in Table C-14for 100,000 cycles to failure, and in graphical form in Figure C-46.

Table C-13. Error (%) in mechanical property (*SR*) at 10,000 cycles to failure due to 1, 2, 10, and 20% error in binder *AP*

Material	Aging Level (Years)	The Resulting Error in *SR* at 10,000 cycles when the Error in AP is			
		1%	2%	10%	20%
B1	7	0.16	0.31	1.41	2.48
	22	0.65	1.32	7.33	16.49
B1A2G2	7	0.03	0.07	0.42	1.00
	22	0.47	0.94	4.99	10.69
B2	7	0.18	0.36	1.91	4.14
	22	1.02	2.05	10.77	22.88
B2A2G2	7	0.33	0.66	3.31	6.65
	22	0.88	1.76	8.86	17.87
B3	7	0.26	0.54	3.40	8.51
	22	4.73	9.56	51.68	113.08
B3A2G2	7	0.26	0.53	2.77	5.90
	22	0.65	1.31	6.84	14.45

Table C-14. Error (%) in mechanical property (*SR*) at 100,000 cycles to failure due to 1, 2, 10, and 20% error in binder *AP*

Material	Aging Level (Years)	The Resulting Error in SR at 100,000 cycles when the Error in AP is			
		1%	2%	10%	20%
B1	7	0.13	0.25	1.14	1.98
	22	0.65	1.32	7.29	16.30
B1A2G2	7	0.02	0.04	0.14	0.10
	22	0.42	0.86	4.63	10.10
B2	7	0.15	0.31	1.69	3.71
	22	0.95	1.92	10.11	21.55
B2A2G2	7	0.32	0.64	3.24	6.51
	22	0.86	1.73	8.70	17.56
B3	7	0.20	0.40	2.49	6.19
	22	2.56	5.18	27.98	61.16
B3A2G2	7	0.31	0.62	3.33	7.23
	22	0.85	1.71	9.03	19.23

The data presented in Table C-13 should be interpreted as follows. If the error in matching *AP* at 7 years aging level for binder B1 is 10%, then the resultant error in the

mechanical property *SR* for binder B1 is 1.41%, and for mastic B1A2G2 it is 0.42%. Similar results can be seen with binders B2, B3, and their corresponding mastics. This result shows that resultant error (for a fixed error in AP) is lower in mastics than binders. The only exception to the trend is B2 and B2A2G2 at 7 years. This can also be inferred as the required accuracy in *AP* for a fixed error in *SR* will be lower for mastics than asphalt binders. This finding is consistent to the findings with respect to modulus sensitivity, where it is found that the required accuracy in *AP* for a fixed error in *AR* reduces with increasing length scales. The error values increase with aging level. Thus, the mechanical properties of binders/mastics at higher aging levels need to be more accurately matched. In comparison to the error values obtained from the modulus based sensitivity, the values are very comparable. Thus, the general conclusion that can be made is that the resulting error in the mechanical properties of mastics (*AR* or *SR*) is either lower or equates to observed error in binder properties (*AP*).

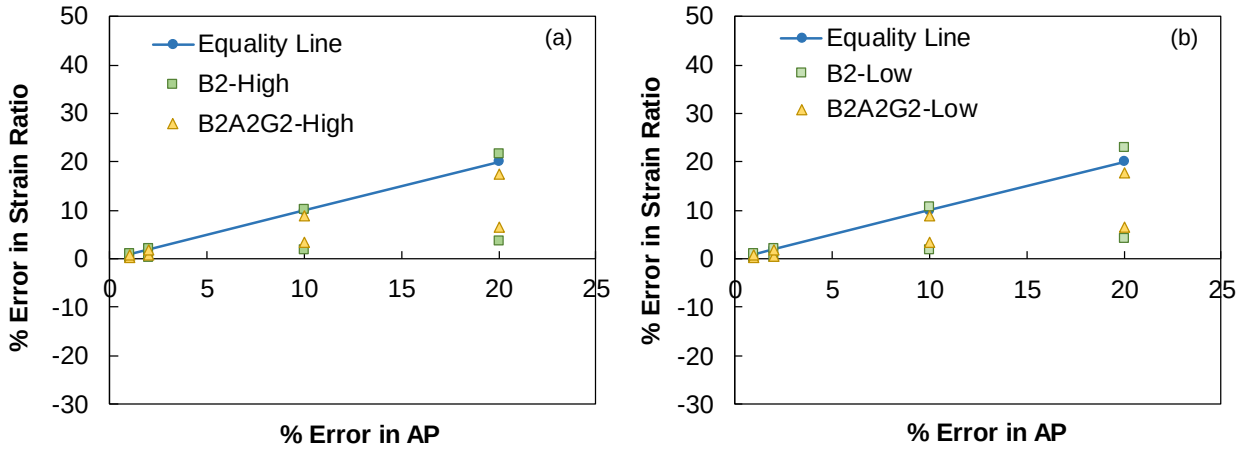

Figure C-46. Sensitivity of strain ratio of B2 and B2A2G2 a given percentage error in the aging parameter for (a) high number of failure cycles and (b) low number of failure cycles.

Sensitivity of FAM Fatigue to Binder Oxidation

The *SR*, Equation C-35, was also used to evaluate the fatigue sensitivity of the FAM materials as a function of the aging parameter (*AP*) of the binder. In this analysis, both a low failure cycle condition (20,000 cycles) and a high failure cycle condition (90,000) were chosen. Once the *SL* values were obtained, the *SR* values calculated from Equation (12) and corresponding *AP* of the binder were plotted and fitted to a polynomial equation, as shown in Figure C-47.

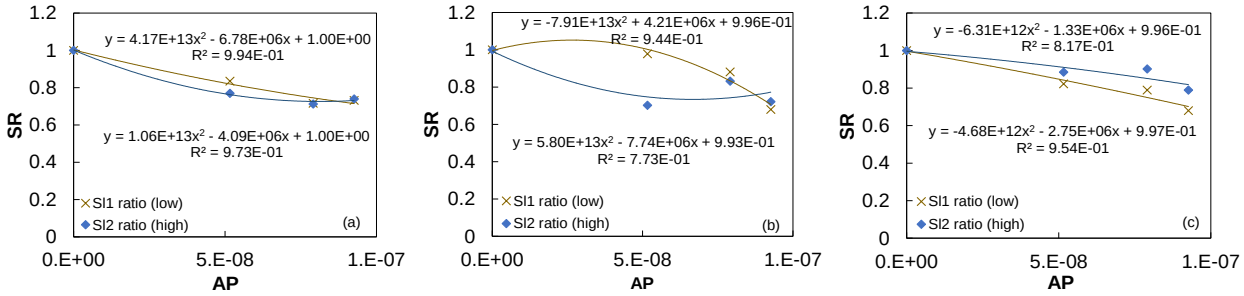

Figure C-47. Relationship between strain ratio (SR) and aging parameter (AP) for (a) B2A2G2-F-4.5, (b) B2A2G2-F-7.5, and (c) B2A2G1-F-7.5.

The fitted polynomial equation that corresponds to each FAM mix was used to calculate the sensitivity of the SR with respect to the change in the AP of the binder as was done for the mastics. The sensitivity of the *SR* of the FAM for a given percentage error in the *AP* is calculated for both high and low numbers of failure cycles, as shown in Figure C-48(a) and (b), respectively.

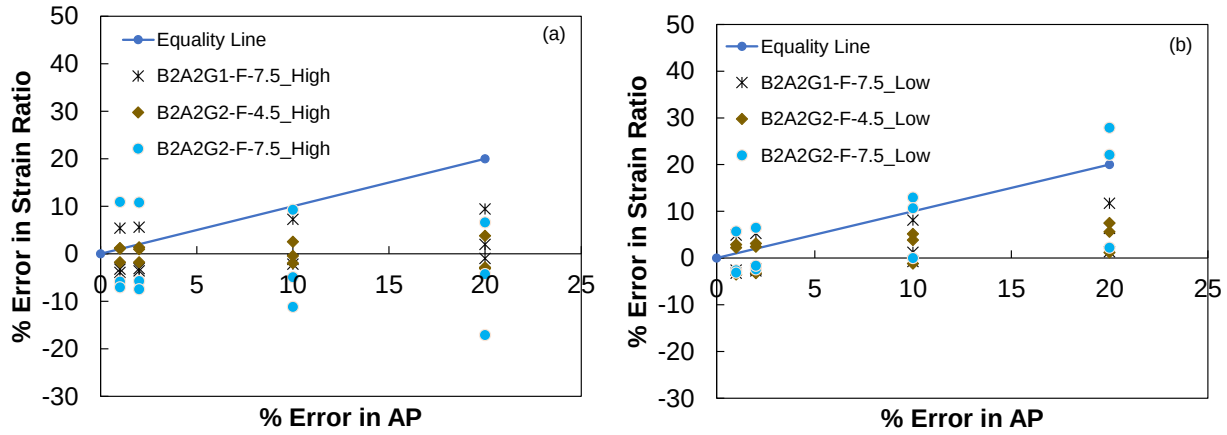

Figure C-48. Sensitivity of strain ratio of FAM for a given percentage error in the aging parameter for (a) high number of failure cycles and (b) low number of failure cycles.

Figure C-48 shows the equality lines that represent the same quantity of error in the *SR* for a given percentage error in the *AP* of the binder. For example, if the error in the *AP* of the binder is 10 percent, then the corresponding percentage error in the SR is also 10 percent. These lines are plotted to show how the percentage error in the *SR* is sensitive to the error in the *AP* of the binder. Sensitivity analysis of all the FAM mixtures was conducted at fixed *AP* percentage errors of 1, 2, 5, 10 and 20%. Because the relationship between the *AP* of a binder and the corresponding *SR* of a FAM is represented by a polynomial function, the sensitivity of the *SR* does not increase significantly even though the error in the *AP* increases. For example, in Figure C-48, in the case of 'B2A2G2-F-4.5_Low', the error in the *SR* increased only from 2.2 percent to 5.6 percent for 1 percent to 20 percent increase in the error of the *AP*. Similarly, for 'B2A2G2-F-4.5_High', the error in the *SR* increased only from 1.2 percent to 3.6 percent for an increase in the *AP* error from 1 percent to 20 percent. Similar observations were made for all the other FAM materials, except for the B2A2G2-F-7.5 material that shows a significant increase in sensitivity of the *SR* at 15 and 22 years of aging cases from 5.7 percent to 22.1 percent for an increase in the *AP* error from 1 percent to 20 percent. Figure C-48 shows that the B2A2G2-F-7.5 material has a

larger curvature than the other materials, which causes an overall higher sensitivity of the *SR* to the error in the *AP* of the binder. From the sensitivity analysis study, it can be stated that the fatigue life is not as sensitive as the *AR* to the error in the *AP* of binder. At this point, it can be inferred that, for FAM materials, sensitivity with respect to the modulus is the factor that governs the overall sensitivity of the phenomenon.

However, from the FAM fatigue sensitivity study some generalized conclusions can be made. Finer gradation, higher air void content and higher PG grade are the factors that are more sensitive to the *SR* with unit change in *AP* of the binder. As higher air void content and stiffer binder grades are prone to less fatigue resistance, the same factors are also contributing more to sensitivity in fatigue behavior for a unit change in *AP* of binder.

Research Comparisons

To understand the factors contributing to differences in sensitivity, the binder, mastic, and FAM experimental results are compared in a pairwise way. Figure C-49 shows the various comparisons that are made to address first order effects, which are aggregate, and binder source, as well as the interaction effects. Comparisons are made based on the *AP* – to – *AR* relationship described above.

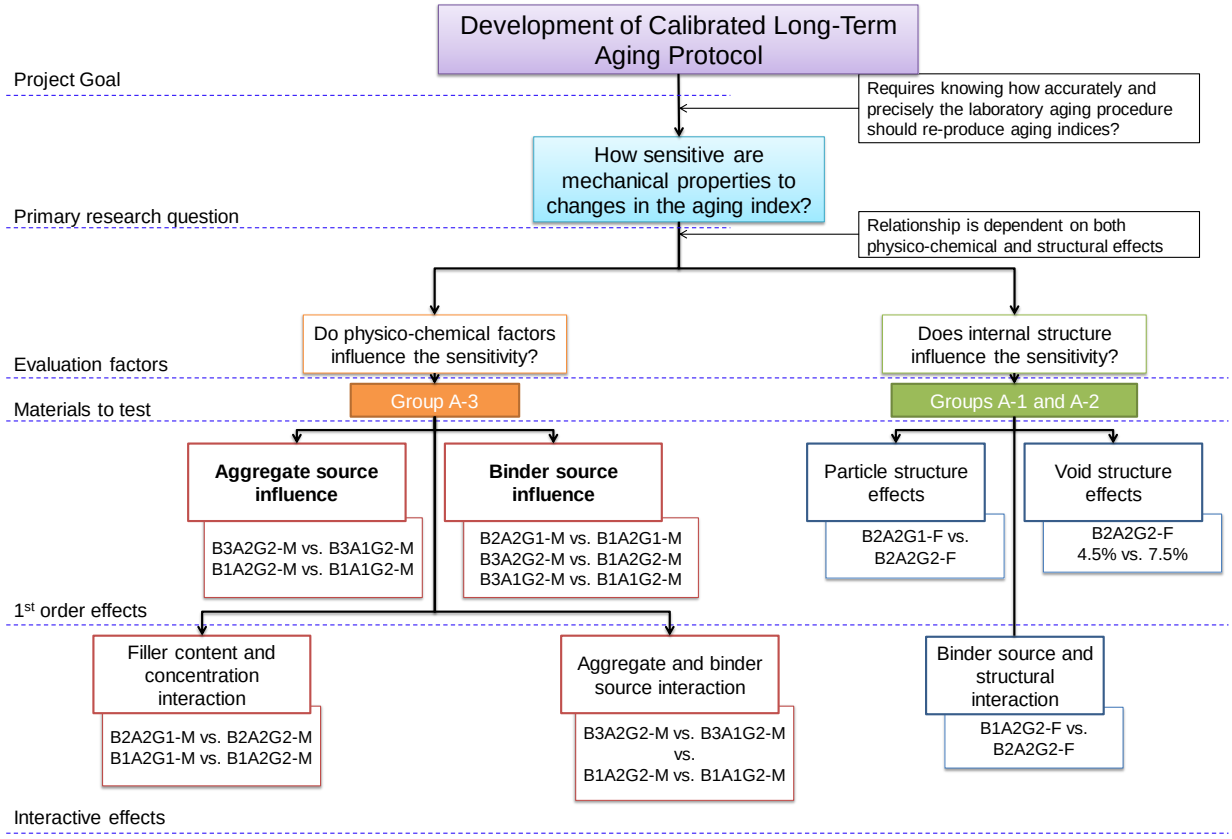

Figure C-49. Summary of subtask 3.4 research comparisons and goal.

Mastic Comparisons

The sensitivity data from approach 1 and 2 are shown in Table C-11 and Table C-12 respectively. Consider the temperature of 10˚C for both approaches and for approach 1 assume the accuracy required in material *AR* is 10% and for approach 2 assume the error in *AP* as 10%. The value 10% is chosen as a representative value here because in the field of asphalt concrete testing, 10% is often used as a reasonable estimate for variability in experimentation and for prediction accuracies. All data shown here for mastic comparisons will be based on these assumed conditions, but others were evaluated through the course of the study and the same conclusions can be drawn.

Binder Source Influence
B1A2G1 vs B2A2G1

The sensitivity data from approach 1 and 2 are presented in Table C-15 and Table C- 16. The general interpretation from both approaches is that mastics prepared with binder B1 are more sensitive than mastics prepared with binder B2. Also, it is seen that the difference in sensitivities between the mastics is reduces with increase in aging level. Thus, it can be concluded that binder influences on sensitivity are more profound at lower aging levels.

Table C-15. Accuracy required in binder *AP* to match material *AR* with assumed accuracy for B1A2G1 and B2A2G1

Material	Aging (years)	Accuracy Required in AP to match AR within							
		1%		2%		10%		20%	
		10˚C	30˚C	10˚C	30˚C	10˚C	30˚C	10˚C	30˚C
B1A2G1	7	1.58	1.20	3.15	2.40	15.75	12.02	31.51	24.04
	22	1.43	1.12	2.86	2.25	14.30	11.23	28.61	22.45
B2A2G1	7	1.84	1.36	3.69	2.71	18.43	13.55	36.86	27.10
	22	1.45	1.16	2.90	2.33	14.50	11.63	28.99	23.27

Table C- 16. The resulting errors in *AR* of materials for an assumed error in binder *AP* for B1A2G1 and B2A2G1

Material	Aging (years)	The Resulting Error in AR when the Error in AP is							
		1%		2%		10%		20%	
		10˚C	30˚C	10˚C	30˚C	10˚C	30˚C	10˚C	30˚C
B1A2G1	7	0.63	0.83	1.27	1.66	6.35	8.32	12.70	16.64
	22	0.70	0.89	1.40	1.78	6.99	8.91	13.98	17.82
B2A2G1	7	0.54	0.74	1.09	1.48	5.43	7.38	10.85	14.76
	22	0.69	0.86	1.38	1.72	6.90	8.60	13.80	17.19

B1A2G2 vs B3A2G2

The sensitivity data from approach 1 and 2 are presented in Table C-17 and Table C-18 respectively. Even in this comparison the mastic prepared with B1 binder is found to be more sensitive than that prepared with B3 binder. Even in this case, the difference in sensitivities reduces with increase in aging level.

Table C-17. Accuracy required in binder *AP* to match material *AR* with assumed accuracy for B1A2G2 and B3A2G2

Material	Aging (years)	Accuracy Required in AP to match AR within							
		1%		2%		10%		20%	
		10˚C	30˚C	10˚C	30˚C	10˚C	30˚C	10˚C	30˚C
B1A2G2	7	1.57	1.20	3.15	2.39	15.75	11.95	31.49	23.91
	15	1.51	1.17	3.02	2.33	15.10	11.66	30.20	23.32
	22	1.50	1.13	3.01	2.26	15.03	11.30	30.05	22.60
B3A2G2	7	1.81	1.41	3.63	2.82	18.13	14.12	36.26	28.23
	22	1.58	1.26	3.17	2.52	15.85	12.60	31.70	25.19

Table C-18. The resulting errors in *AR* of materials for an assumed error in binder *AP* for B1A2G2 and B3A2G2

Material	Aging (years)	The Resulting Error in AR when the Error in AP is							
		1%		2%		10%		20%	
		10˚C	30˚C	10˚C	30˚C	10˚C	30˚C	10˚C	30˚C
B1A2G2	7	0.64	0.84	1.27	1.67	6.35	8.37	12.7	16.73
	15	0.66	0.86	1.32	1.72	6.62	8.58	13.24	17.15
	22	0.67	0.88	1.33	1.77	6.66	8.85	13.31	17.70
B3A2G2	7	0.55	0.71	1.10	1.42	5.52	7.08	11.03	14.17
	22	0.63	0.79	1.26	1.59	6.31	7.94	12.62	15.88

B1A1G2 vs B3A1G2

The sensitivity data from approach 1 and 2 are presented in Table C-19 and Table C-20 respectively. The change in aggregate from A2 to A1 does not change the interpretation regarding higher sensitivity of B1. However, the magnitude of difference in sensitivities between the two mastics is higher than that observed with A2 aggregate and G2 gradation.

Table C-19. Accuracy required in binder *AP* to match material *AR* with assumed accuracy for B1A1G2 and B3A1G2

Material	Aging (years)	Accuracy Required in AP to match AR within							
		1%		2%		10%		20%	
		10˚C	30˚C	10˚C	30˚C	10˚C	30˚C	10˚C	30˚C
B1A1G2	7	1.48	1.17	2.97	2.34	14.83	11.71	29.66	23.42
	15	1.45	1.14	2.89	2.29	14.46	11.44	28.93	22.89
	22	1.38	1.11	2.76	2.22	13.79	11.08	27.58	22.16
B3A1G2	7	1.95	1.44	3.90	2.88	19.52	14.42	39.05	28.85
	15	1.79	1.34	3.57	2.68	17.87	13.42	35.75	26.85
	22	1.68	1.28	3.36	2.56	16.80	12.82	33.61	25.65

Table C-20. The resulting errors in *AR* of materials for an assumed error in binder *AP* for B1A1G2 and B3A1G2

Material	Aging (years)	The Resulting Error in AR when the Error in AP is							
		1%		2%		10%		20%	
		10˚C	30˚C	10˚C	30˚C	10˚C	30˚C	10˚C	30˚C
B1A1G2	7	0.67	0.85	1.35	1.71	6.74	8.54	13.49	17.08
	15	0.69	0.87	1.38	1.75	6.91	8.74	13.83	17.48
	22	0.73	0.90	1.45	1.80	7.25	9.02	14.51	18.05
B3A1G2	7	0.51	0.69	1.02	1.39	5.12	6.93	10.24	13.87
	15	0.56	0.74	1.12	1.49	5.59	7.45	11.19	14.9
	22	0.60	0.78	1.19	1.56	5.95	7.80	11.90	15.59

B2A2G2 vs B3A2G2

The sensitivity data from approach 1 and 2 are presented in Table C-21 and Table C-22 respectively. From approach 1 mastic prepared with B2 binder requires higher precision in binder *AP* for fixed *AR*, than those prepared with B3 binder. Thus, it can be inferred that the sensitivity of the mechanical properties to binder oxidation is higher for B2A2G2 than B3A2G2.

Table C-21. Accuracy required in binder *AP* to match material *AR* with assumed accuracy for B2A2G2 and B3A2G2

Material	Aging (years)	Accuracy Required in AP to match AR within							
		1%		2%		10%		20%	
		10˚C	30˚C	10˚C	30˚C	10˚C	30˚C	10˚C	30˚C
B2A2G2	7	1.74	1.33	3.47	2.66	17.35	13.31	34.71	26.62
	15	1.5	1.22	2.99	2.45	14.95	12.24	29.9	24.47
	22	1.49	1.19	2.97	2.39	14.85	11.93	29.71	23.85
B3A2G2	7	1.81	1.41	3.63	2.82	18.13	14.12	36.26	28.23
	22	1.58	1.26	3.17	2.52	15.85	12.60	31.70	25.19

Table C-22. The resulting errors in *AR* of materials for an assumed error in binder *AP* for B2A2G2 and B3A2G2

Material	Aging (years)	The Resulting Error in AR when the Error in AP is							
		1%		2%		10%		20%	
		10˚C	30˚C	10˚C	30˚C	10˚C	30˚C	10˚C	30˚C
B2A2G2	7	0.58	0.75	1.15	1.5	5.76	7.51	11.53	15.02
	15	0.67	0.82	1.34	1.63	6.69	8.17	13.38	16.34
	22	0.67	0.84	1.35	1.68	6.73	8.38	13.46	16.77
B3A2G2	7	0.55	0.71	1.10	1.42	5.52	7.08	11.03	14.17
	2	0.63	0.79	1.26	1.59	6.31	7.94	12.62	15.88

Some of the important observations from binder source comparisons are:

1. The mechanical properties of the mastics prepared with softer binders will be more sensitive to oxidation than those prepared with stiffer binders.
2. For two mastics containing same aggregate and gradation but different binder, the magnitude of difference in sensitivities reduces with increase in aging level.

Overall, it can be said that binder source does influence the sensitivity of mechanical properties of mastic to binder oxidation. However, the degree of influence is also affected by the type of aggregate present.

Aggregate Source Influence

B1A2G2 vs. B1A1G2

As seen from Table C-23 and Table C-24 mastic prepared with aggregate A1 requires greater precision in binder *AP* than the B1A2G2 mastic, which is prepared with A2 aggregate. From approach 2 it is seen that for 10% error in binder *AP*, the error in mechanical properties is higher for B1A1G2 mastic than B1A2G2 mastic. However, the differences between the two mastics are very marginal and are unlikely to be significant. The effect of aggregate source in cognizance with binder B1 can be considered weak or very marginal.

Table C-23. Accuracy required in binder *AP* to match material *AR* with assumed accuracy for B1A1G2 and B1A2G2

Material	Aging (years)	Accuracy Required in AP to match AR within							
		1%		2%		10%		20%	
		10˚C	30˚C	10˚C	30˚C	10˚C	30˚C	10˚C	30˚C
B1A1G2	7	1.48	1.17	2.97	2.34	14.83	11.71	29.66	23.42
	15	1.45	1.14	2.89	2.29	14.46	11.44	28.93	22.89
	22	1.38	1.11	2.76	2.22	13.79	11.08	27.58	22.16
B1A2G2	7	1.57	1.20	3.15	2.39	15.75	11.95	31.49	23.91
	15	1.51	1.17	3.02	2.33	15.10	11.66	30.20	23.32
	22	1.50	1.13	3.01	2.26	15.03	11.30	30.05	22.60

Table C-24. The resulting errors in *AR* of materials for an assumed error in binder *AP* for B1A1G2 and B1A2G2

Material	Aging (years)	The Resulting Error in AR when the Error in AP is							
		1%		2%		10%		20%	
		10˚C	30˚C	10˚C	30˚C	10˚C	30˚C	10˚C	30˚C
B1A1G2	7	0.67	0.85	1.35	1.71	6.74	8.54	13.49	17.08
	15	0.69	0.87	1.38	1.75	6.91	8.74	13.83	17.48
	22	0.73	0.90	1.45	1.80	7.25	9.02	14.51	18.05
B1A2G2	7	0.64	0.84	1.27	1.67	6.35	8.37	12.70	16.73
	15	0.66	0.86	1.32	1.72	6.62	8.58	13.24	17.15
	22	0.67	0.88	1.33	1.77	6.66	8.85	13.31	17.70

B3A2G2 vs. B3A1G2

The sensitivity data from approach 1 and 2 are shown in Table C-25 and Table C-26 respectively. Using approach 1 we see that higher accuracy is required in binder *AP* for mastics prepared with B3 binder and A2 aggregate than those prepared with A1 aggregate. From approach 2 we see that error in *AR* for fixed error in *AP* will be higher for mastics prepared with A2 aggregate. As seen with the mastics of B1 binder, the difference between the sensitivities is very low (1-2%), suggesting that for mastics prepared with same binder, the influence of different aggregate source on sensitivity is marginal.

Table C-25. Accuracy required in binder *AP* to match material *AR* with assumed accuracy for B3A1G2 and B3A2G2

Material	Aging (years)	Accuracy Required in AP to match AR within							
		1%		2%		10%		20%	
		10˚C	30˚C	10˚C	30˚C	10˚C	30˚C	10˚C	30˚C
B3A1G2	7	1.95	1.44	3.90	2.88	19.52	14.42	39.05	28.85
	15	1.79	1.34	3.57	2.68	17.87	13.42	35.75	26.85
	22	1.68	1.28	3.36	2.56	16.80	12.82	33.61	25.65
B3A2G2	7	1.81	1.41	3.63	2.82	18.13	14.12	36.26	28.23
	22	1.58	1.26	3.17	2.52	15.85	12.60	31.70	25.19

Table C-26. The resulting errors in *AR* of materials for an assumed error in binder *AP* for B3A1G2 and B3A2G2

Material	Aging (years)	The Resulting Error in AR when the Error in AP is							
		1%		2%		10%		20%	
		10˚C	30˚C	10˚C	30˚C	10˚C	30˚C	10˚C	30˚C
B3A1G2	7	0.51	0.69	1.02	1.39	5.12	6.93	10.24	13.87
	15	0.56	0.74	1.12	1.49	5.59	7.45	11.19	14.90
	22	0.60	0.78	1.19	1.56	5.95	7.80	11.90	15.59
B3A2G2	7	0.55	0.71	1.10	1.42	5.52	7.08	11.03	14.17
	22	0.63	0.79	1.26	1.59	6.31	7.94	12.62	15.88

Filler Content and Concentration Interaction

B1A2G1 vs. B1A2G2

The sensitivity data from approach 1 and 2 are presented in Table C-27 and Table C-28 respectively. From both approaches it is seen that for mastics prepared with binder B1, gradation does not have a big impact on sensitivity of mechanical properties to oxidation. The only noticeable finding is that coarser gradations have a greater sensitivity at higher aging levels.

Table C-27. Accuracy required in binder *AP* to match material *AR* with assumed accuracy for B1A2G1 and B1A2G2

Material	Aging (years)	Accuracy Required in AP to match AR within							
		1%		2%		10%		20%	
		10˚C	30˚C	10˚C	30˚C	10˚C	30˚C	10˚C	30˚C
B1A2G1	7	1.58	1.2	3.15	2.40	15.75	12.02	31.51	24.04
	22	1.43	1.12	2.86	2.25	14.30	11.23	28.61	22.45
B1A2G2	7	1.57	1.20	3.15	2.39	15.75	11.95	31.49	23.91
	15	1.51	1.17	3.02	2.33	15.10	11.66	30.20	23.32
	22	1.50	1.13	3.01	2.26	15.03	11.30	30.05	22.60

Table C-28. The resulting errors in *AR* of materials for an assumed error in binder *AP* for B1A2G1 and B1A2G2

Material	Aging (years)	The Resulting Error in AR when the Error in AP is							
		1%		2%		10%		20%	
		10˚C	30˚C	10˚C	30˚C	10˚C	30˚C	10˚C	30˚C
B1A2G1	7	0.63	0.83	1.27	1.66	6.35	8.32	12.7	16.64
	22	0.70	0.89	1.40	1.78	6.99	8.91	13.98	17.82
B1A2G2	7	0.64	0.84	1.27	1.67	6.35	8.37	12.70	16.73
	15	0.66	0.86	1.32	1.72	6.62	8.58	13.24	17.15
	22	0.67	0.88	1.33	1.77	6.66	8.85	13.31	17.70

B2A2G1 vs. B2A2G2

The sensitivity data from approach 1 and 2 are presented in Table C-29 and Table C-30 respectively. For the mastics prepared with binder B2, it is seen that mastic with finer gradation (G2) is sensitive at lower aging levels and the mastic with coarser gradation is sensitive at higher aging levels. The latter observation was true for mastics made with B1 binder also. Overall, the difference in sensitivities between the gradations was less than 1% at low as well as high levels for both binder types. Thus, it is unlikely that it would be significantly affect the sensitivity of mechanical properties to binder oxidation.

Table C-29. Accuracy required in binder *AP* to match material *AR* with assumed accuracy for B2A2G1 and B2A2G2

Material	Aging (years)	Accuracy Required in AP to match AR within							
		1%		2%		10%		20%	
		10˚C	30˚C	10˚C	30˚C	10˚C	30˚C	10˚C	30˚C
B2A2G1	7	1.84	1.36	3.69	2.71	18.43	13.55	36.86	27.10
	22	1.45	1.16	2.90	2.33	14.5	11.63	28.99	23.27
B2A2G2	7	1.74	1.33	3.47	2.66	17.35	13.31	34.71	26.62
	15	1.50	1.22	2.99	2.45	14.95	12.24	29.90	24.47
	22	1.49	1.19	2.97	2.39	14.85	11.93	29.71	23.85

Table C-30. The resulting errors in *AR* of materials for an assumed error in binder *AP* for B2A2G1 and B2A2G2

Material	Aging (years)	The Resulting Error in AR when the Error in AP is							
		1%		2%		10%		20%	
		10˚C	30˚C	10˚C	30˚C	10˚C	30˚C	10˚C	30˚C
B2A2G1	7	0.54	0.74	1.09	1.48	5.43	7.38	10.85	14.76
	22	0.69	0.86	1.38	1.72	6.90	8.60	13.80	17.19
B2A2G2	7	0.58	0.75	1.15	1.50	5.76	7.51	11.53	15.02
	15	0.67	0.82	1.34	1.63	6.69	8.17	13.38	16.34
	22	0.67	0.84	1.35	1.68	6.73	8.38	13.46	16.77

Aggregate and Binder Source Interaction
(B3A2G2 vs. B3A1G2) vs. (B1A2G2 vs. B1A1G2)

From Table C-23 it can be seen that for the mastics prepared with binder B1, those containing A1 aggregate have a greater sensitivity than those containing A2 aggregate. However, when we look at Table C-25, the trends are reversed. The mastics in Table C-25 are prepared with B3 binder and it is seen that mastics containing A2 (granite) aggregate have a greater sensitivity than those containing A1 (limestone) aggregate. The data in these tables show that there is an interaction between binder and aggregate sources and that no two binders interact the same way with a particular aggregate type. Another example of the aggregate binder interaction can be explained by observing the data in Table C-17 and Table C-19. The difference in sensitivities for B1A1G2 and B3A1G2 in Table C-19 are in the range of 3-5%, whereas the difference in sensitivities for B1A2G2 and B3A2G2 in Table C-17 are in the range of 1-3%.

FAM Comparisons

Particle Structure Effects (B2A2G1-F vs. B2A2G2-F)

The sensitivity data from approach 1 and 2 are presented in Table C-31 and Table C-32 respectively. It can be easily inferred from Table C-31 that the FAM materials possessing finer aggregate gradation exhibit greater sensitivity. The effect of gradation can be more easily observed in FAM than in mastics, as the magnitude of difference in sensitivities is in the order of 5-15%.

Table C-31. Accuracy required in binder *AP* to match material *AR* with assumed accuracy for B2A2G1-F and B2A2G2-F

Material	Aging (years)	Accuracy Required in AP to match AR within							
		1%		2%		10%		20%	
		10˚C	30˚C	10˚C	30˚C	10˚C	30˚C	10˚C	30˚C
B2A2G1-F-7.5	7	3.56	2.61	7.12	5.21	35.60	26.06	71.20	52.13
	15	3.05	2.24	6.11	4.48	30.53	22.42	61.05	44.85
	22	2.38	1.77	4.76	3.55	23.82	17.73	47.65	35.45
B2A2G2-F-7.5	7	2.16	1.91	4.31	3.82	21.57	19.12	43.14	38.25
	15	2.05	1.81	4.11	3.61	20.53	18.06	41.07	36.11
	22	1.81	1.54	3.62	3.09	18.09	15.45	36.18	30.89

Table C-32. The resulting errors in *AR* of materials for an assumed error in binder *AP* for B2A2G1-F and B2A2G2-F

Material	Aging (years)	The Resulting Error in AR when the Error in AP is							
		1%		2%		10%		20%	
		10˚C	30˚C	10˚C	30˚C	10˚C	30˚C	10˚C	30˚C
B2A2G1-F-7.5	7	0.28	0.38	0.56	0.77	2.81	3.84	5.62	7.67
	15	0.33	0.45	0.66	0.89	3.28	4.46	6.55	8.92
	22	0.42	0.56	0.84	1.13	4.2	5.64	8.40	11.28
B2A2G2-F-7.5	7	0.46	0.52	0.93	1.05	4.64	5.23	9.27	10.46
	15	0.49	0.55	0.97	1.11	4.87	5.54	9.74	11.08
	22	0.55	0.65	1.11	1.29	5.53	6.47	11.05	12.95

It can be concluded that the sensitivity of mechanical properties to binder oxidation is higher for fine graded FAM mixtures than coarse graded FAM mixtures.

Void Structure Effects (B2A2G2-F, 4.5% vs 7.5%)

The sensitivity data from approach 1 and 2 are presented in Table C-33 and Table C-34 respectively. It is observed from these tables that FAM material containing higher void percentage, B2A2G2-F-7.5 is more sensitive than B2A2G2-F-4.5. However, the difference in the sensitivities is small; suggesting that sensitivity of mechanical properties to oxidation of binder is a weak function of the percentage air voids. It should be recalled that the FAM samples were fabricated using binder that was pre-aged at 7, 15 and 22 years aging levels and that no aging has been performed once the sample has been fabricated. In other words, the effect of these air voids should not be confused with the effect of air voids on an unaged mixture that is subjected to oxidation.

Table C-33. Accuracy required in binder *AP* to match material *AR* with assumed accuracy for B2A2G2-F-7.5 and B2A2G2-F-4.5

Material	Aging (years)	Accuracy Required in AP to match AR within							
		1%		2%		10%		20%	
		10˚C	30˚C	10˚C	30˚C	10˚C	30˚C	10˚C	30˚C
B2A2G2-F-7.5	7	2.16	1.91	4.31	3.82	21.57	19.12	43.14	38.25
	15	2.05	1.81	4.11	3.61	20.53	18.06	41.07	36.11
	22	1.81	1.54	3.62	3.09	18.09	15.45	36.18	30.89
B2A2G2-F-4.5	7	2.21	1.74	4.42	3.49	22.12	17.43	44.24	34.86
	15	2.00	1.56	4.00	3.12	19.99	15.59	39.99	31.17
	22	1.80	1.48	3.60	2.96	18.01	14.81	36.02	29.62

Table C-34. The resulting errors in *AR* of materials for an assumed error in binder *AP* for B2A2G2-F-7.5 and B2A2G2-F-4.5

Material	Aging (years)	The Resulting Error in AR when the Error in AP is							
		1%		2%		10%		20%	
		10˚C	30˚C	10˚C	30˚C	10˚C	30˚C	10˚C	30˚C
B2A2G2-F-7.5	7	0.46	0.52	0.93	1.05	4.64	5.23	9.27	10.46
	15	0.49	0.55	0.97	1.11	4.87	5.54	9.74	11.08
	22	0.55	0.65	1.11	1.29	5.53	6.47	11.05	12.95
B2A2G2-F-4.5	7	0.45	0.57	0.9	1.15	4.52	5.74	9.04	11.48
	15	0.50	0.64	1.00	1.28	5.00	6.42	10.00	12.83
	22	0.56	0.68	1.11	1.35	5.55	6.75	11.11	13.51

Binder Source and Structural Interaction (B1A2G2-F vs. B2A2G2-F)

The sensitivity data from approach 1 and 2 are presented in Table C-35 and Table C-36. It can be seen that at lower aging levels for the aggregate structure A2G2, FAM prepared with B1 binder has a greater sensitivity, but at higher aging levels FAM prepared with B2 binder has higher sensitivity. It can be said that the effects of binder source and aggregate interaction are seen only at higher aging levels where the magnitude of difference in the sensitivities was higher.

Table C-35. Accuracy required in binder *AP* to match material *AR* with assumed accuracy for B1A2G2-F-4.5 and B2A2G2-F-4.5

Material	Aging (years)	Level of Accuracy for Material AR							
		1%		2%		10%		20%	
		10˚C	30˚C	10˚C	30˚C	10˚C	30˚C	10˚C	30˚C
B1A2G2-F-4.5	7	2.16	2.07	4.32	4.13	21.59	20.67	43.18	41.35
	22	2.20	1.65	4.40	3.30	22.01	16.52	44.02	33.03
B2A2G2-F-4.5	7	2.21	1.74	4.42	3.49	22.12	17.43	44.24	34.86
	15	2.00	1.56	4.00	3.12	19.99	15.59	39.99	31.17
	22	1.80	1.48	3.60	2.96	18.01	14.81	36.02	29.62

Table C-36. The resulting errors in *AR* of materials for an assumed error in binder *AP* for B1A2G2-F-4.5 and B2A2G2-F-4.5

Material	Aging (years)	The Resulting Error in AR when the Error in AP is							
		1%		2%		10%		20%	
		10˚C	30˚C	10˚C	30˚C	10˚C	30˚C	10˚C	30˚C
B1A2G2-F-4.5	7	0.46	0.48	0.93	0.97	4.63	4.84	9.26	9.67
	22	0.45	0.61	0.91	1.21	4.54	6.05	9.09	12.11
B2A2G2-F-4.5	7	0.45	0.57	0.90	1.15	4.52	5.74	9.04	11.48
	15	0.50	0.64	1.00	1.28	5.00	6.42	10.00	12.83
	22	0.56	0.68	1.11	1.35	5.55	6.75	11.11	13.51

Summary Based on Research Comparisons

Following is the summary from the comparisons to evaluate the effect of different variables on the sensitivity of modulus to binder oxidation

For Mastics

1. *Aggregate source influence*: For mastics prepared with B1 binder, those containing A1 aggregate were more sensitive. For mastics prepared with B3, those containing A2 aggregate were more sensitive. However, the differences between the two mastics are very marginal and are unlikely to be significant.
2. *Binder source influence*: Some of the important observations from binder source comparisons are:
    a. The mechanical properties of the mastics prepared with softer binders will be more sensitive to oxidation than those prepared with higher modulus binders.
    b. For two mastics containing the same aggregate and gradation but different binder, the magnitude of difference in sensitivities reduces with increase in aging level.
    c. Overall, it can be said that binder source does influence the sensitivity of mechanical properties of mastic to binder oxidation. However, the degree of influence is also affected by the type of aggregate present.

3. *Filler content and concentration interaction*: The difference in sensitivities between the gradations was less than 1% for both binder types. Thus, it is unlikely that filler content would substantially affect the sensitivity of mechanical properties of mastic to binder oxidation for dense graded mixtures.
4. *Aggregate and binder source interaction*: The isolated influences of aggregate and binder sources show that there is an interaction between binder and aggregate sources and that no two binders interact the same way with a particular aggregate type.

For FAM

1. *Particle structure effects*: The sensitivity of mechanical properties to binder oxidation is higher for fine graded FAM mixtures than coarse graded FAM mixtures. The effect of gradation can be more easily observed in FAM than in mastics.
2. *Void structure effects*: It is found that the FAM materials containing higher void percentage are more sensitive than those containing lower voids. However, the difference in the sensitivities is small; suggesting that sensitivity of mechanical properties to oxidation of binder is a weak function of the percentage air voids.
3. *Binder source and structural interaction*: The effects of binder source and aggregate interaction are seen only at higher aging levels, where for A2 aggregate and G2 gradation B2 binder was found to be more sensitive than B1 binder.

Conclusions

The main goal of this study was to estimate the sensitivity of the mechanical properties of asphalt concrete to asphalt binder oxidation. In this regard, experimental characterization was performed at multiple length scales. Testing was performed on asphalt binder to establish baseline properties, on asphalt mastic to consider physico-chemical aspects, and FAM to consider air voids and aggregate interaction effects. Dynamic modulus and fatigue experiments were run on these materials at different levels of oxidation. Subsequently, these experiments were analyzed to determine how sensitive the material response was to binder oxidation. Based on these experiments and the requisite analysis, the following conclusions are made:

- The accuracy levels required in the binder aging parameter (either |G*| or difference of inverse of crossover modulus) to match mixture aging ratios at 1%, 10%, and 20% levels of accuracy are 1.5 – 3.6%, 14.8 – 35.6%, and 29.6 – 71.2% respectively. Stated differently to a given error in matching the aging parameter of the asphalt binder will result in approximately 28-67% of this error in matching the properties of the mixture.
- The accuracy levels required in the binder aging parameter to match the mastic aging ratio at 1%, 10%, and 20% levels of accuracy are 1.1 – 1.9%, 11.1 – 19.5%, and 22.2 – 39% respectively. Again stated differently, a given error in matching the aging parameter of the asphalt binder will result in approximately 50-90% of this error in matching the properties of the mastic.
- The specific level of sensitivity is dependent upon the specific type of aggregate used and to a lesser extent the aggregate gradation adopted with limestone aggregates and fine gradations being more sensitive.

The significance of these findings is two-fold. First, they demonstrate with a unique laboratory experiment that the properties of asphalt concrete are not proportionally sensitive to changes in asphalt binder modulus. Second, they show that for a laboratory aging procedure to replicate the impacts of binder oxidation on the modulus of asphalt concrete with a given level of accuracy (say 10%), the desired binder oxidation can be replicated at accuracy of between 15 and 36%. Conversely if a laboratory aging procedure is found to match the in-service level of binder oxidation with certain amount of error (say 10%), then the expected error in in the resulting modulus of an asphalt mixture tested after being subjected to that laboratory process will be 6.7 – 2.8%.

References

Applied Research Associates (ARA). (2004). *2002 Design Guide: Design of New and Rehabilitated Pavement Structures*. Final Report for NCHRP 1-37A Project, National Cooperative Highway Research Program. National Research Council. Washington, D.C.

Christensen, D.W. and D.A. Anderson (1992). Interpretation of Mechanical Test Data for Paving Grade Asphalt Cements. *Journal of the Association of Asphalt Paving Technologists*, Vol. 61, pp. 67-116.

Farrar, M.J., T.F. Turner, J.P. Planche, J.F. Schabron, and P.M. Harnsberger (2013). Evolution of the Crossover Modulus with Oxidative Aging: A Method to Estimate the Change in Viscoelastic Properties of an Asphalt Binder with Time and Depth on the Road. *Transportation Research Record: Journal of the Transportation Research Board*, Vol. 2370, pp. 76-83.

Jahangir, R., D. Little and A. Bhasin (2015). Evolution of Asphalt Binder Microstructure due to Tensile Loading Determined using AFM and Image Analysis Techniques. *International Journal of Pavement Engineering*, Vol. 16, No. 4, pp. 337-349.

Sabouri, M. and Y.R. Kim (2014). Development of a Failure Criterion for Asphalt Mixtures under Different Modes of Fatigue Loading. *Transportation Research Record: Journal of the Transportation Research Board*, Vol. 2447, pp. 117-125.

Underwood, B.S., Kim, Y.R., and M.N. Guddati (2010). Improved Calculation Method of Damage Parameter in Viscoelastic Continuum Damage Model. *International Journal of Pavement Engineering*, Vol. 11, No. 6, pp. 459-476.

Underwood, B.S. (2011). Multiscale Constitutive Modeling of Asphalt Concrete. Ph.D. Dissertation, North Carolina State University, Raleigh, NC.

Underwood, B.S. and Y.R. Kim (2014). A Four Phase Micro-Mechanical Model for Asphalt Mastic Modulus. *Mechanics of Materials*, Vol. 75, pp. 13-33.

Willmott, C.J. and K. Matsura (2009). Terrestrial Air Temperature and Precipitation: Monthly Climatologies (1950-2005). Online. <http://climate.geog.udel.edu/~climate/html_pages/Global2_Clim/README.global2_clim.html>. Accessed: February 2014.

APPENDIX D

Evaluation of Different Chemical and Rheological Aging Index Properties

Introduction

Asphalt binder is an organic end product that reacts with oxygen in the environment. The oxidation of asphalt binder is a physicochemical reaction that causes permanent hardening and reduces the flexibility of the asphalt binder. Consequently, oxidation increases a pavement's susceptibility to cracking under traffic loading and thermal stress. Thus, given the importance of asphalt binder oxidation to pavement performance, it is imperative to define practical aging index properties (AIPs) that can be used effectively to determine oxidation levels. The AIPs then can be used to calibrate kinetics diffusion models and, by extension, be used within pavement performance prediction models. For an AIP to be effective, it must be easy to quantify and must relate directly to oxidative aging in an asphalt binder. AIPs generally are divided into two main categories: chemical functional groups and rheological parameters. Although numerous AIPs have been proposed in the literature, a comprehensive paper that examines the chemistry-based and rheology-based AIPs that best correlate to binder oxidation levels is currently missing.

The chemistry-based AIPs provide the most direct indicators of oxygen uptake and can be measured using Fourier transform infrared spectroscopy (FTIR) techniques. Carbonyls and sulfoxides are the two primary chemical functional groups that are produced upon oxidation of asphalt binder. The carbonyl chemical functional group has long been used to indicate the level of oxidation within asphalt binder (Petersen 2009). The ketone functional group is the major component of the carbonyl infrared absorption region. Ketone formation changes the polarity of the associated aromatic ring components within an asphalt binder, which leads to an increase in the asphaltene content, thereby increasing viscosity (Petersen 2009, Petersen and Glaser 2011). The production of sulfoxides by the oxidation of asphalt has received less attention in the past. However, Petersen and Glaser (2011) conducted a thorough study to understand the effect of sulfoxide formation on oxidative age hardening in asphalt binders. Their work demonstrated that the sulfoxides produced during oxidation have a significant impact on viscosity, especially for high sulfur content asphalts. Chemical AIPs have been represented by both absorbance peaks (e.g., Petersen 2009, Petersen and Glaser 2011) and areas (e.g., Han, 2012, Jin et al. 2011, Lamontage et al. 2001, Zhang et al. 2011).

Different rheological-based AIPS also have been introduced and include, for example, the crossover modulus, low shear viscosity, etc. (Petersen 2009, Underwood et al. 2010, Farrar et al. 2013). Rheological AIPs are advantageous over chemical AIPs because they do not require infrared spectroscopy devices and can be correlated more directly to the mechanical properties of an asphalt mixture than chemical AIPs (Glaser et al. 2013). However, a comprehensive study to determine the rheological properties that relate most directly to the chemical changes caused by oxidation is currently missing in the literature.

Objectives

The objectives of this study are to:

- Evaluate different chemical AIPs based on their sensitivity to oxidation.
- Evaluate the relationship between rheological AIPs and the chemical changes induced by oxidation.
- Identify suitable chemical and rheological AIPs for tracking the oxidation of asphalt.

Test Method and Analysis Procedure

Table D-1 presents details about the six asphalt mixtures evaluated and the aging trials conducted in this study. The materials encompass a wide range of binder types. All of the mixtures were subjected to laboratory loose mixture aging and were fabricated using original, component materials.

Table D-1. Summary of different aging trials

Material Source	Binder	Aging Temperature (°C)	Aging Duration
NC	PG 64-22	70	10, 12, 35 days
		85	8, 10, 15 days
		95	10, 17, 26 days
FHWA ALF Control	PG 70-22	70	10, 35 days
		95	12, 14, 18 days
FHWA ALF SBS-LG	PG 70-28 (SBS-modified)	70	10, 35 days
		85	8, 10, 20 days
		95	8, 10, 18, 22 days
SHRP AAD-1	PG 58-28	70	10, 18, 21 days
		95	10, 15, 27 days
SHRP AAG-1	PG 58-10	70	10, 18 days
		95	10, 15, 22, 27 days
WesTrack	PG 64-22	70	12, 18 days
		95	10, 15, 20 days

To evaluate the changes in the chemical and rheological AIPs in terms of oxidation, the loose mixtures were subjected to laboratory aging at multiple temperatures and for various durations in an oven under ambient pressure. To prepare the loose mixtures for long-term aging, the component materials were combined according to the original mix design and subjected to short-term aging at 135°C for four hours in accordance with AASHTO R 30. A mix design was not available for the SHRP AAD-1 and SHRP AAG-1 binders. Therefore, these SHRP binders

were combined with the FHWA ALF (Federal Highway Administration Accelerated Load Facility) aggregate according to the FHWA ALF mix design.

The short-term aged loose mixture was spread in a single layer in metal trays such that the thickness of the mix was equal to or less than the largest aggregate size in the mix. The thin layer of loose mixture was used to ensure homogenous exposure to the heat and oxygen during the laboratory aging process. Also, it was assumed that using a thin layer of asphalt loose mix would expedite oxidative aging in the binder film, as most of the mixture was in direct contact with circulating hot air. Three aging temperatures, 70°C, 85°C, and 95°C, were used for long-term aging the loose mixtures. Samples were collected at different time intervals for binder extraction and recovery and subsequent AIP testing to track the oxidation levels. The micro-extraction and recovery method developed by the Western Research Institute (WRI) (Farrar et al. 2015) was used to obtain the binder samples from the aged loose mixtures.

Micro-Extraction and Recovery

Qualitative micro-extraction and recovery of the asphalt binder from the asphalt mixtures was accomplished following a proposed AASHTO specification prepared by the WRI (Farrar et al. 2015). This procedure uses a solvent mixture of toluene and ethanol (85:15) for extraction and recovery. The mixture sample size is limited to 200 g to produce approximately 10 g of asphalt binder per extraction, which is adequate for both the FTIR with attenuated total reflectance (FTIR-ATR) sampling technique and dynamic shear rheometer (DSR) testing. In order to prevent further aging of the binder sample during the extraction and recovery procedure, a rotary evaporator balloon was subjected to vacuum pressure of 80.0 ± 0.7 kPa (600 ± 5 mm of Hg) under nitrogen gas. The extraction and recovery process consists of the application of temperatures ranging from 70°C to 170°C at different stages. FTIR-ATR testing was conducted following extraction and recovery to ensure that no residual solvent was evident.

Measurement of Aging Index Properties (AIPs)

The chemical and rheological AIPs were measured using FTIR-ATR spectrometry and DSR tests, respectively. The micro-extraction and recovery process was conducted in order to collect asphalt binder from loose mixtures for the AIP measurements. Summaries of the of FTIR and DSR procedures follow.

FTIR-ATR Spectroscopy

FTIR-ATR spectroscopy allows absorbance data to be collected within a wide spectral range (400 cm^{-1} to 4000 cm^{-1}). Peaks in the spectra can be used to detect the presence of chemical functional groups. In this study, the ATR spectra were collected using 64 scans at a resolution of 4 cm^{-1} with a minimum of two replicates. For each binder, all replicates under different conditions were normalized to the same absorbance value at wave number 1375 cm^{-1}. This wave number was selected for normalization because absorbance is not affected by the level of oxidation. The chemical AIPs evaluated in this study are the carbonyl area (CA), carbonyl plus sulfoxide area (C+S area), and carbonyl plus sulfoxide peaks (C+S peaks). Changes in the carbonyl and sulfoxides peaks were tracked at wave numbers 1702 cm^{-1} and 1032 cm^{-1}, respectively. The carbonyl areas were determined according to the area under the FTIR

absorbance curves from wave numbers 1650 cm^{-1} to 1820 cm^{-1}. The sulfoxide areas were determined according to the area under the FTIR absorbance curve from wave numbers 1000 cm^{-1} to 1050 cm^{-1}. The trapezoidal rule was used to determine numerically the area under the band between the specified wave number ranges. It should be noted that the absorbance peaks are direct measurements taken from the FTIR spectrum band, whereas the area-based measurements require numerical integration under the absorbance spectrum. The absorbance peak-based AIP is the easiest AIP to determine and involves less error or bias with regard to the method of calculation compared to the area-based AIPs.

Dynamic Shear Rheometer Procedure

Frequency sweep testing was conducted at frequencies ranging from 0.1 Hz to 30 Hz at multiple temperatures (5°C, 20°C, 35°C, 50°C, and/or 64°C) in an ARG-2 DSR from TA Instruments. The tests were conducted using an 8-mm parallel plate spindle with a strain amplitude of 1 percent. The four rheological AIPs that were calculated using the DSR are described in the following.

Dynamic Shear Modulus (G*)

The dynamic shear modulus (G^*) is a property that can be measured directly and used to track the rheological changes caused by oxidation. The use of the G^* as an AIP is advantageous because it is a direct output of the DSR and is the most commonly used parameter that relates the physical properties of asphalt binder to asphalt pavement performance. This study found that oxidative age hardening affects the G^* most significantly at high temperatures and/or low frequencies, which is demonstrated by the asphalt binder mastercurves presented in Figure D-1. The results shown in Figure D-1 correspond to a single-source asphalt binder (FHWA ALF-SBS) that had been conditioned to produce various age levels. The figure shows that at lower reduced frequencies (and correspondingly, higher temperatures), the differences among the G^* values are most significant. Therefore, the G^* value at 64°C and 10 rad/s was selected as one of the rheological AIPs to evaluate herein.

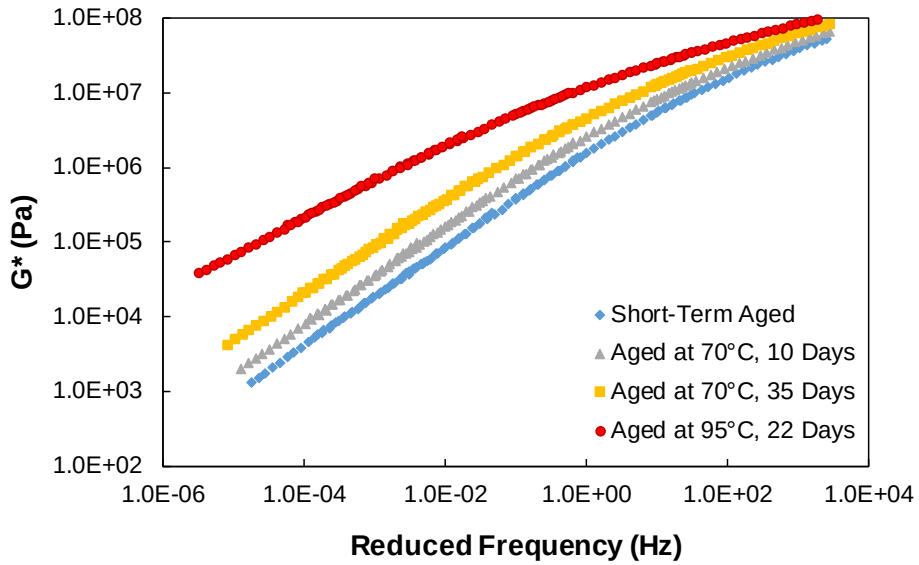

Figure D-1. Comparison between dynamic shear modulus (G*) mastercurves for asphalt binders extracted and recovered from FHWA ALF-SBS asphalt mixture aged at different levels.

Crossover Modulus (G*c)

The crossover modulus (*G*c*) is defined as the *G** value that corresponds to the reduced frequency where the storage modulus (*G'*) and loss modulus (*G"*) mastercurves cross (i.e., where the phase angle equals 45°). The crossover modulus is a parameter that is found in the widely applied Christensen-Anderson (CA) model (Christensen and Anderson 1992) and has been proposed as an AIP to study the evolution of oxidative aging in asphalt binders (Farrar et al. 2013). Several different methods have been proposed for calculating the crossover modulus (e.g., data smoothing, interpolation, and curve fitting). In this study, the method developed by Farrar et al. (2013) was applied. This method determines the crossover modulus as follows:

1. Examine the data in black space and remove any spurious points. Such points are particularly troublesome at the highest test frequencies.
2. Use the Christensen-Anderson-Marasteanu (CAM) model to pre-smoothen the *G** data and obtain mastercurves for both the *G** and phase angle.
3. Sort the measured data points according to reduced frequency in ascending order.
4. Apply a polynomial fit of the black space plot (phase angle versus logarithm of *G**) to the as-measured data in the neighborhood of 45° (40° to 50°).
5. Interpolate the polynomial fit for the crossover modulus by finding the value of *G** when the phase angle is exactly 45°.

Figure D-2 presents the crossover modulus values estimated from a black space diagram for the binder extracted and recovered from the FHWA ALF SBS loose mixture after 20 days of conditioning at 85°C. As shown in Figure D-2, the binder is not perfectly thermorheologically simple, thus leading to differences in the data obtained from different isotherms. Therefore, the

estimation of the crossover modulus value requires interpolation between the data that correspond to different isotherms within the black space diagram. Consequently, the determination of the crossover modulus may be subject to more variability than is the case for parameters that are direct measurements (e.g., *G**).

Oxidative aging leads to a decrease in the crossover modulus (*G*c*) value. To achieve a positive relationship with the aging duration, the inverse of the log of the crossover modulus (1/log *G*c*) is used as a rheological AIP (Farrar et al. 2013). Farrar et al. (2013) found a linear relationship is found between the oxygen uptake and 1/log *G*c* for a given binder.

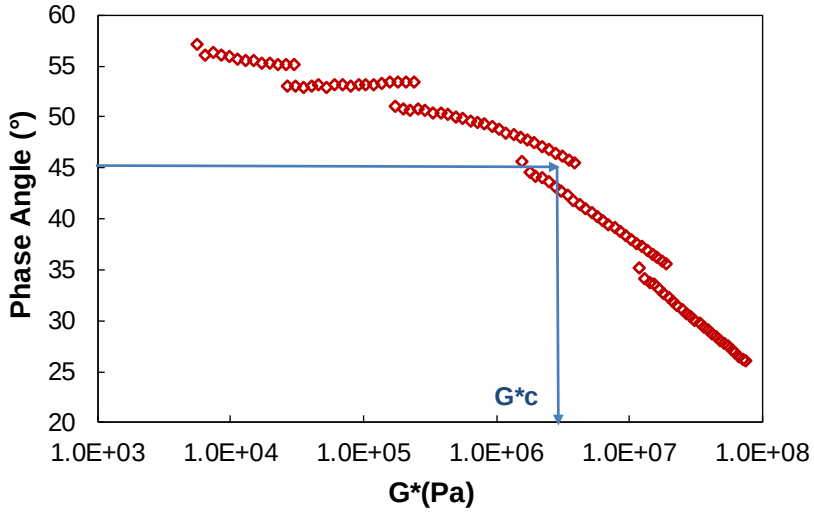

Figure D-2.Crossover modulus (G*c) values for binders extracted and recovered from FHWA ALF SBS loose mix after 20 days of aging at 85°C.

Zero Shear Viscosity (ZSV)

Zero shear viscosity (*ZSV*) also was considered as a rheological AIP in this study. *ZSV* is defined as the viscosity when the shear rate reaches zero (Binard et al. 2004, Brio et al. 2009). *ZSV* can be determined from creep or frequency sweep testing. In this study, frequency sweep test results were used to estimate *ZSV* values using the method proposed by Marasteanu and Anderson (2002). To apply their method, the Christensen-Anderson-Marasteanu (CAM) model, (i.e., Equation D-1), was fitted to the frequency sweep test results. If the parameter *m* in the CAM model is larger than one, the CAM model is shifted to a reference temperature of 60°C by dividing the crossover modulus value by the time-temperature shift factor that corresponds to 60°C.

$$G^* = \frac{G_g^*}{[1+(f\ /\ f_c)^k]^{m/k}} \qquad \text{(D-1)}$$

where

G^*_g = glassy modulus (Pa),

f_c = location parameter with dimensions of frequency (rad/s),

f = reduced frequency (rad/s),

m = CAM model shift factor, and
k = CAM model parameter.

Then, the Cox-Merz rule, shown in Equation D-2, is applied to convert the G^* value to viscosity.

$$G^*/\omega = \text{Viscosity} \tag{D-2}$$

Lastly, the limit of the function, as the frequency goes to zero, is used to obtain the *ZSV*, as shown in Equation D-3.

$$ZSV = \frac{G_g^*}{\omega_{c,refT=60°C}} \left(\frac{(m-1)^{m-1}}{m^m} \right)^{1/k} \tag{D-3}$$

where $\omega_{c,ref\,T=60°C}$ is the crossover frequency at the reference temperature (rad/s).
If $m < 1$, then the CAM model is refitted to the data with $m = 1$, and the same algorithm is applied.

Glover-Rowe (G-R) Parameter

The Glover-Rowe (*G-R*) parameter also was evaluated in this study as a rheological AIP. The *G-R* parameter was proposed by Rowe based on his analysis of Glover et al.'s (2005) work on low temperature ductility (King et al. 2012). Glover et al. (2005) used the Maxwell mechanical analog model to derive a rheological parameter that is related to ductility, i.e., $G'/(\eta'/G')$, termed the 'Glover parameter'. This parameter has been proposed by Glover et al. (2005) as an indicator of pavement cracking potential. Rowe et al. (2014) simplified Glover's parameter to arrive at Equation D-4.

$$\frac{G^*(\cos\delta)^2}{\sin\delta} \tag{D-4}$$

where
G^* = dynamic shear modulus measured at 15°C and 0.005 rad/s (Pa) and
δ = phase angle measured at 15°C and 0.005 rad/s (°).

Testing at 0.005 rad/s is not possible. Therefore, the G^* and phase angle values at a reduced frequency that corresponds to 15°C and 0.005 rad/s were determined from the G^* and phase angle mastercurves constructed from temperature-frequency sweep DSR testing and frequency-temperature shift factors.

Results

Evaluation of Chemical AIPs

The chemical AIPs were evaluated based on their correlation to the aging duration. Asphalt materials exhibit relatively similar kinetics, with an initial fast reaction period (also known as the *spurt*), followed by a slower reaction period that has an approximately constant rate

(Glaser et al. 2013a, Han 2012, Jin et al. 2011, Petersen 1998, Petersen et al. 1996). The focus herein is long-term aging. Therefore, the chemical AIPs were evaluated within the constant rate period because this period corresponds to higher age levels.

Figure D-3 presents comparisons of the three chemical AIPs evaluated (i.e., carbonyl area, C+S area, and C+S peaks) with respect to aging duration. The rate of oxidation is temperature-dependent. Therefore, the chemical AIPs measured from long-term aging at different temperatures for a given mixture are plotted separately. All of the data included in the analysis of the chemical AIPs correspond to aging trials where extracted and recovered binders were analyzed for at least three aging durations to compare the correlations. Conditions with fewer than three aging conditions were excluded from the evaluation. As shown in Figure D-3, generally all three chemical AIPs are strongly correlated with the aging duration. However, it can be noted that the effect of the sulfoxide functional group on the chemical AIP-based aging rates is of great importance. Although the C+S area and C+S peaks show very similar aging rates and rankings, the carbonyl area versus aging duration shows a different ranking of the materials. The literature indicates that sulfoxides have a significant effect on rheology, and thus, this observation suggests that it is important to consider the sulfoxide functional group when tracking oxidative aging. The C+S peaks versus aging duration graph exhibits the overall highest R^2 values. Furthermore, the C+S peaks can be calculated using the direct output of the ATR-FTIR data, whereas the calculation of the C+S area requires numerical integration under the infrared spectrum. Therefore, C+S peaks is an easy parameter to calculate and is not sensitive to the method chosen for the calculation. Thus, in this study C+S peaks was selected as the most promising chemical AIP identified and was used in the subsequent analysis of the rheological AIPs.

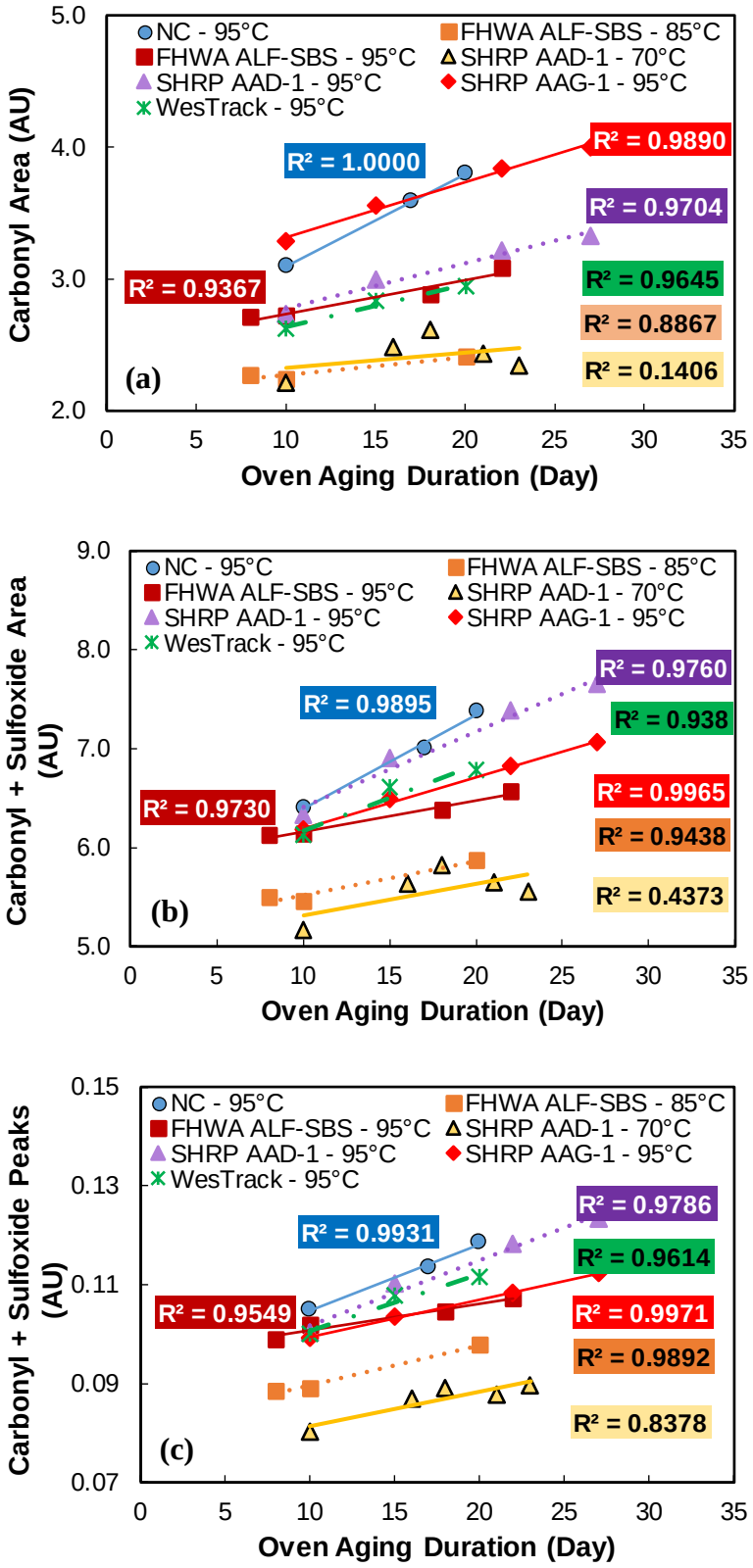

Figure D-3. Sensitivity of different chemical AIPs to aging duration: (a) carbonyl area, (b) C+S area, and (c) C+S peaks.

Evaluation of Rheological AIPs

The correlation between the rheological AIPs and C+S peaks for each mixture was used to evaluate the rheological AIPs. Data that correspond to different aging temperatures ranging from 70°C to 95°C were included in the evaluation. Past studies have demonstrated that the relationship between chemistry and rheology is not affected by aging temperature if the temperature is below 100°C (Petersen 2009, Yousefi Rad et al. 2017). Therefore, the data for multiple aging temperatures are included for each mixture evaluated.

Figure D-4 presents the correlations between log *G** at 64°C and 10 rad/s and C+S peaks for all of the mixtures evaluated. Each data point corresponds to a different aging duration and/or aging temperature. A log scale of the rheological parameters was used to produce a linear relationship to C+S peaks. The results demonstrate that *G** at 64°C and 10 rad/s is highly correlated with the chemical changes induced by oxidation for all of the mixtures evaluated.

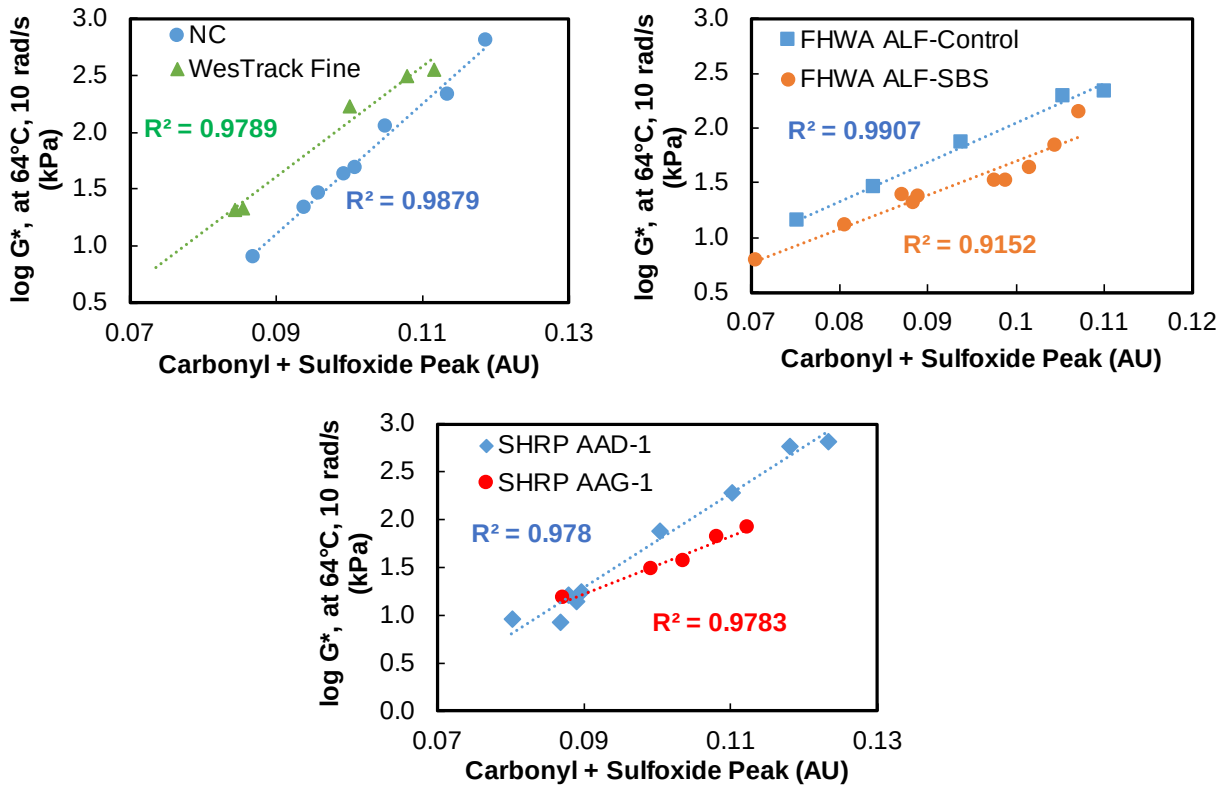

Figure D-4. Correlations between log G* at 64°C, 10 rad/s and C+S peaks for six mixtures.

Figure D-5 presents the correlations between 1/log *G*c* and C+S peaks. The results demonstrate that the crossover modulus is highly correlated with the chemical changes caused by oxidation. However, for certain highly aged mixtures, including the NC mix aged at 95°C for 20 days, FHWA ALF SBS aged at 95°C for 28 days, and SHRP AAD-1 aged at 95°C for 22 and 27 days, the *G*c* could not be estimated due to calculation difficulties and high variability. These difficulties and variability are caused by differences between the results from different isotherms in the black space, which led to inconsistent crossover modulus values from two test replicates.

In addition, Figure D-5 shows that the slopes of the 1/log *G*c* versus C+S peaks lines are very low for many of the mixtures evaluated. Thus, although a good correlation exists, the crossover modulus changes relatively little as the C+S peaks values change, thereby indicating that the crossover modulus is not very sensitive to oxidation.

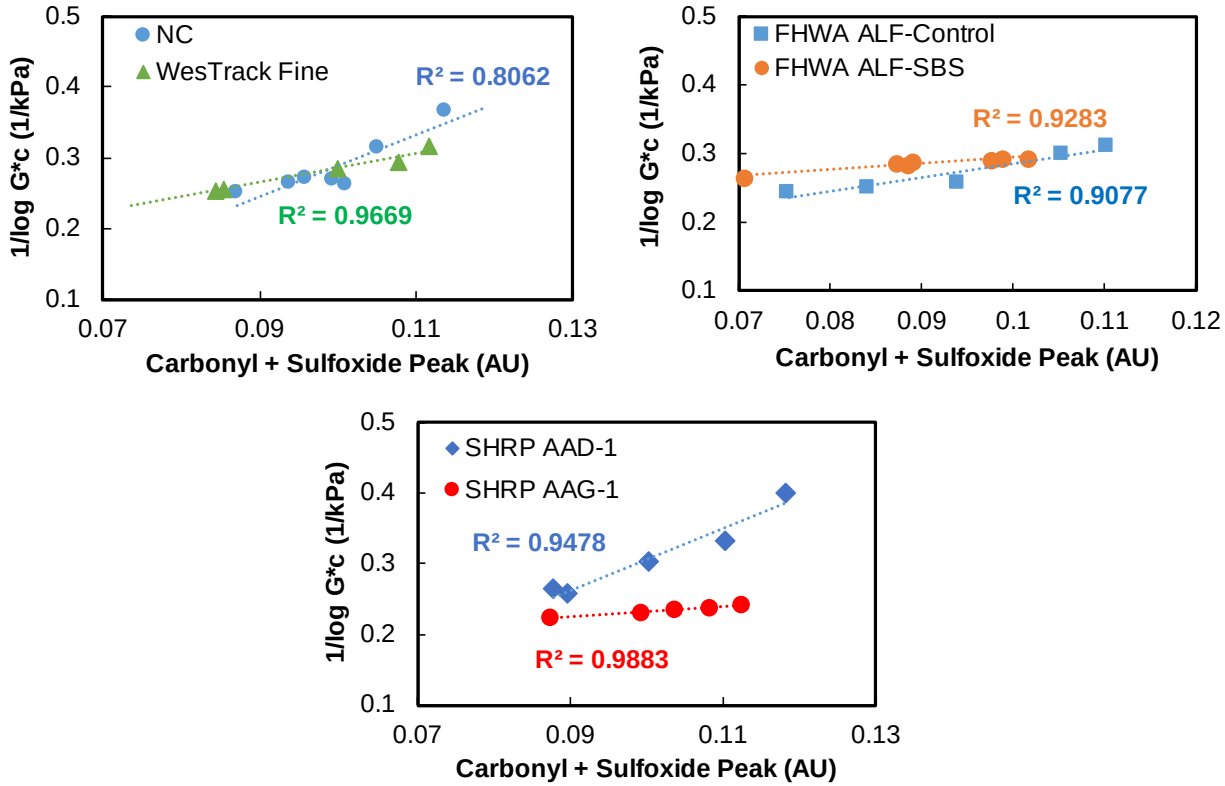

Figure D-5. Correlations between log 1/G*c and C+S peaks for six mixtures.

Figure D-6 presents the correlation between the *ZSV* at 60°C and C+S peaks for each mixture evaluated. It is noted that relatively significant differences among the *ZSV* values for different test replicates were observed for some asphalt binder samples, which was attributed to the variability involved in the extrapolation process to estimate the *ZSV* from *G** mastercurves. The same data that caused the variability in the ZSV values were used to calculate other rheological AIPs and resulted in considerably less variability, indicating the weakness of the ZSV parameter as a reliable AIP. These problematic data were not included in Figure D-6. The results in Figure D-6 demonstrate that *ZSV* is highly correlated with C+S peaks for all of the mixtures evaluated with the exception of FHWA ALF-SBS. Note that the FHWA ALF-SBS mixture is the only mixture in this study that contains polymer-modified binder.

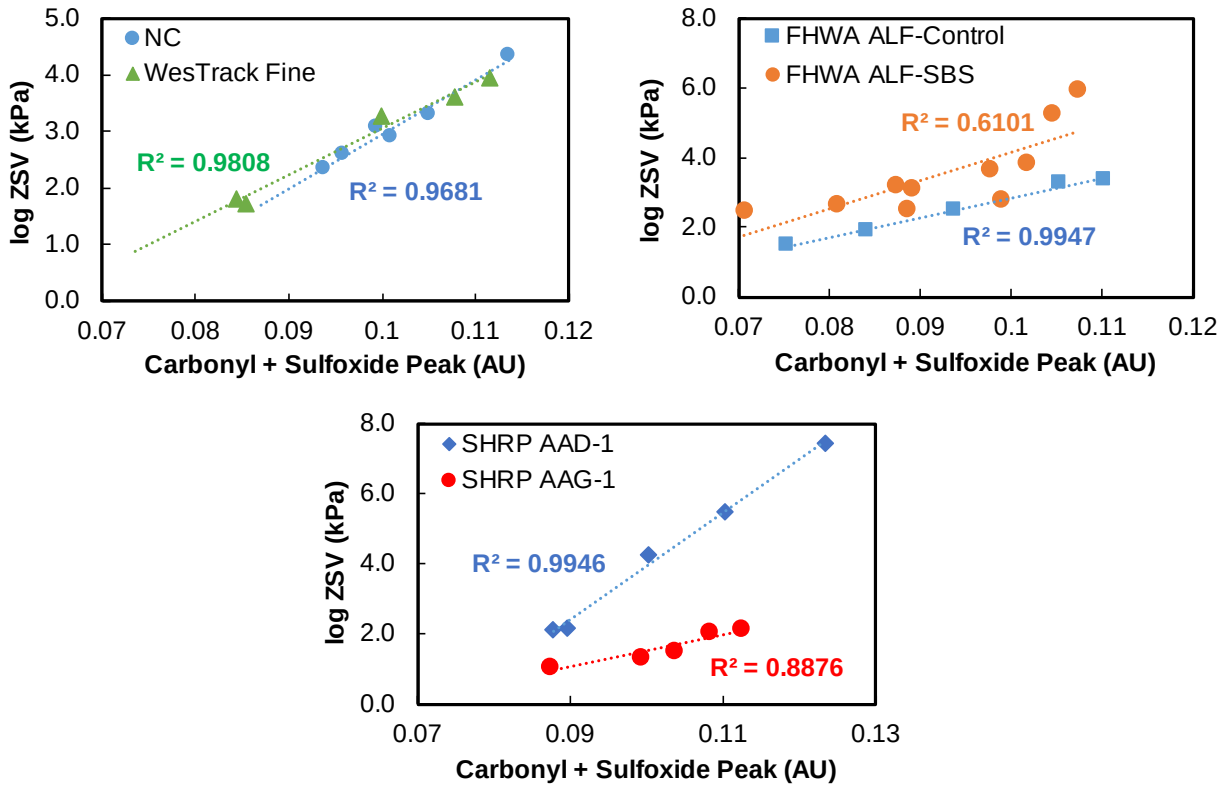

Figure D-6. Correlations between log ZSV at 60°C and C+S peaks for six mixtures.

Figure D-7 presents the correlation between the *G-R* parameter and C+S peaks for each of the mixtures evaluated. The results demonstrate that the *G-R* parameter is highly correlated with the chemical changes that result from oxidation for all of the mixtures evaluated.

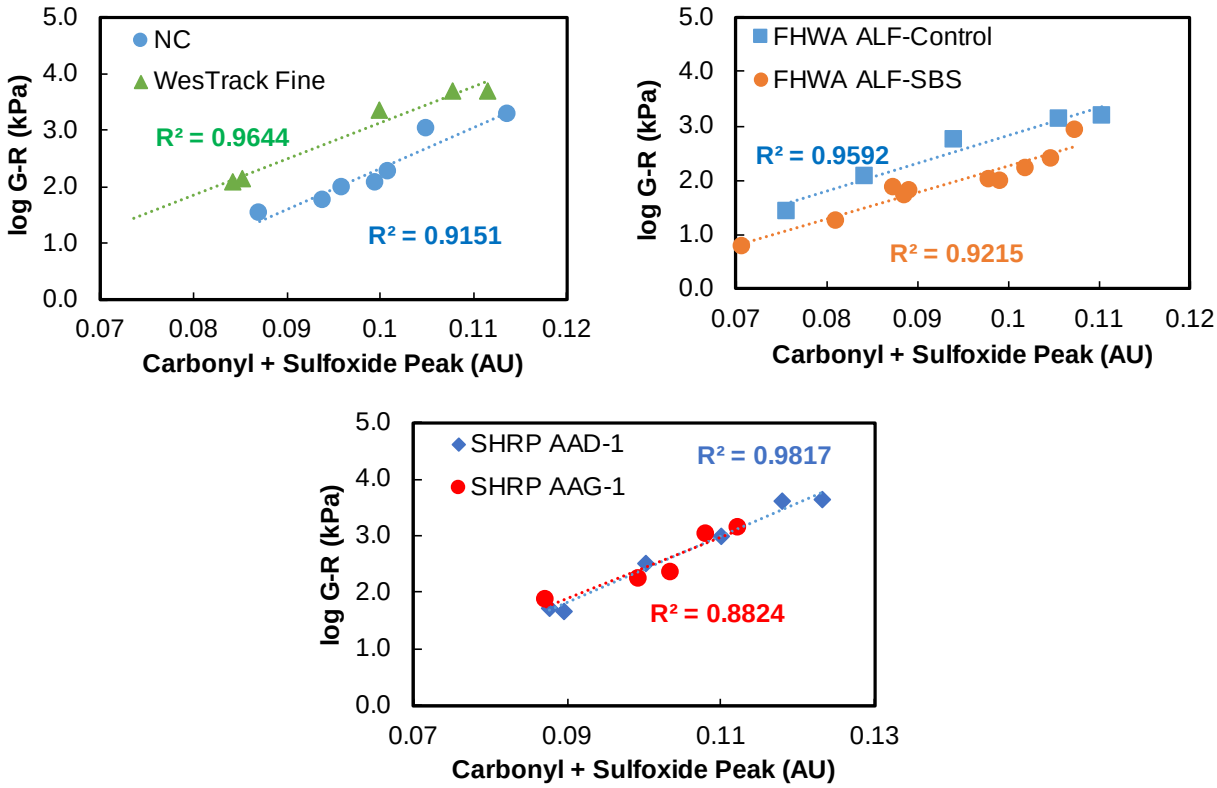

Figure D-7. Correlations between log G-R and C+S peaks for six mixtures.

Based on the results presented, the most promising rheological AIPs for tracking oxidation levels are *G** at 64°C and 10 rad/s and the *G-R* parameter. The *ZSV* and crossover modulus values proved problematic in some instances. The problems associated with *ZSV* and the crossover modulus are related to the interpolation and extrapolation of the data. In addition, the crossover modulus is less sensitive to the chemical changes caused by oxidation compared to the other rheological parameters evaluated. With the exception of the crossover modulus, all of the rheological AIPs evaluated correspond to low reduced frequencies. Low reduced frequencies are achieved by evaluating the properties either at a high temperature or at slow rates (i.e., low frequencies). Although the *G-R* parameter was evaluated at 15°C, it was evaluated at a very low frequency (0.005 rad/s) and, therefore, constitutes a relatively low reduced frequency within the mastercurve. For example, the condition of 15°C and 0.005 rad/s is equivalent to approximately 45°C and 10 rad/s based on typical binder time-temperature shift factors. Hence, the *G-R* parameter also represents high-temperature characteristics of the asphalt binder.

Figure D-8 presents the correlations between log *G** 64°C and 10 rad/s and log *G-R*. Figure D-8 shows that *G** at 64°C and 10 rad/s and the *G-R* parameter are highly correlated, indicating that either can be used effectively as an AIP. The *G-R* parameter requires frequency sweep testing at multiple temperatures and the fitting of both a mastercurve and time-temperature shift factor function to the rheological data because testing at 0.005 rad/s is not possible. In contrast, *G** at 64°C and 10 rad/s is a single-point measurement that can be acquired directly from testing at a single temperature and frequency. Therefore, the *G** at 64°C and 10 rad/s constitutes the most efficient and effective rheological AIP of those evaluated.

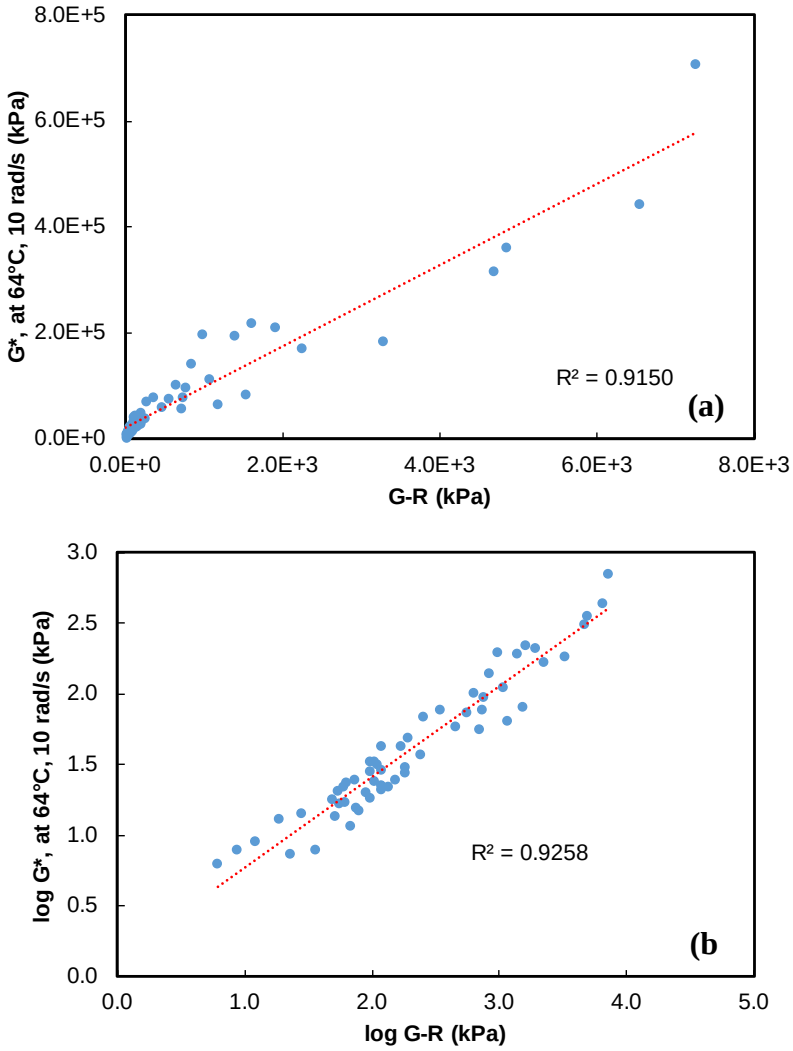

Figure D-8. Correlation between G* at 64°C and 10 rad/s and G-R parameter in (a) arithmetic scale and (b) log-log scale.

Conclusions and Recommendations

The main conclusions and recommendations drawn from this study are:

- The consideration of sulfoxides is critical when evaluating the chemical changes caused by oxidation in asphalt materials. Comparing the oxidation rates of different materials based on the combined effects of carbonyl and sulfoxide can lead to significantly different conclusions than when considering carbonyl alone. C+S peaks is an effective chemical AIP for tracking oxidation and can be obtained directly from FTIR-ATR spectrometry data.
- The two most promising rheological AIPs for tracking oxidation levels are *G** at 64°C and 10 rad/s and the *G-R* parameter. The *ZSV* and crossover modulus AIPs are problematic in some instances due to the required interpolation and/or extrapolation of the data used to determine the AIP values.

- The G* 64°C and 10 rad/s and the *G-R* parameter are highly correlated, indicating that either can be used effectively as an AIP. The *G-R* parameter requires frequency sweep testing at multiple temperatures and the fitting of a mastercurve and time-temperature shift factor function to the rheological data. In contrast, *G** at 64°C and 10 rad/s is a single-point measurement that can be acquired directly from testing at a single temperature and frequency. Therefore, the *G** at 64°C and 10 rad/s constitutes the most efficient, effective rheological AIP evaluated.

References

Anderson, R. M., King, G. N., Hanson, D. I., & Blankenship, P. B. (2011). Evaluation of the relationship between asphalt binder properties and non-load related cracking. *Journal of the Association of Asphalt Paving Technologists*, *80*.

Binard, C., Anderson, D., Lapalu, L., & Planche, J. P. (2004). Zero shear viscosity of modified and unmodified binders. *Proceedings of the 3rd Eurasphalt & Eurobitume Congress, Vienna*, 236 (2), 1721–33.

Biro, S., Gandhi, T., & Amirkhanian, S. (2009). Determination of zero shear viscosity of warm asphalt binders. *Construction and Building Materials*, 23(5), 2080-2086.

Christensen, D. W., & Anderson, D. A. (1992). Interpretation of dynamic mechanical test data for paving grade asphalt cements (with discussion). *Journal of the Association of Asphalt Paving Technologists*, 61.

Farrar, M., Turner, T., Planche, J. P., Schabron, J., & Harnsberger, P. (2013). Evolution of the crossover modulus with oxidative aging: Method to estimate change in viscoelastic properties of asphalt binder with time and depth on the road. *Transportation Research Record: Journal of the Transportation Research Board*, (2370), 76-83.

Farrar, M. J., Planche, J. P., Grimes, R. W., & Qin, Q. (2015). The Universal Simple Aging Test (USAT): Simulating short-and long term hot and warm mix oxidative aging in the laboratory. *Introduction to Unmanned Aircraft Systems*, 79.

Farrar, M. J., Grimes, R. W., Wiseman, S., & Planche, J. P. (2015). Asphalt Pavement–Micro-sampling and Micro-Extraction Methods. White paper.

Glaser, R., Schabron, J., Turner, T., Planche, J. P., Salmans, S., & Loveridge, J. (2013). Low-temperature oxidation kinetics of asphalt binders. *Transportation Research Record: Journal of the Transportation Research Board*, (2370), 63-68.

Glover, C. J., Davison, R. R., Domke, C. H., Ruan, Y., Juristyarini, P., Knorr, D. B., & Jung, S. H. (2005). *Development of a New Method for Assessing Asphalt Binder Durability with Field Validation*. No. FHWA/TX-05/1872-2).

Han, R. (2012). *Improvements to a Transport Model of Asphalt Binder Oxidation in Pavements: Pavement Temperature Modeling, Oxygen Diffusivity in Asphalt Binders and Mastics, and Pavement Air Void Characterization.* Doctoral dissertation, Texas A&M University, College Station, TX.

Jin, X., Han, R., Cui, Y., & Glover, C. J. (2011). Fast-rate–constant-rate oxidation kinetics model for asphalt binders. *Industrial & Engineering Chemistry Research*, 50(23), 13373-13379.

King, G., Anderson, M., Hanson, D., & Blankenship, P. (2012). Using black space diagrams to predict age-induced cracking. *7th RILEM International Conference on Cracking in Pavements*. Springer Netherlands, 453-463.

Lamontagne, J., Dumas, P., Mouillet, V., & Kister, J. (2001). Comparison by Fourier transform infrared (FTIR) spectroscopy of different ageing techniques: Application to road bitumens. *Fuel*, 80(4), 483-488.

Marasteanu, M. O., & Anderson, D. A. (2002, August). Determination of asphalt binder's viscosity from other rheological parameters. *Ninth International Conference on Asphalt Pavements*.

Petersen, J. C. (1998). A dual, sequential mechanism for the oxidation of petroleum asphalts. *Petroleum Science and Technology*, 16(9-10), 1023-1059.

Petersen, J. C. (2009). A review of the fundamentals of asphalt oxidation. *Transportation Research Circular* E-C140.

Petersen, J. C., & Glaser, R. (2011). Asphalt oxidation mechanisms and the role of oxidation products on age hardening revisited. *Road Materials and Pavement Design*, 12(4), 795-819.

Petersen, J., & Harnsberger, P. (1998). Asphalt aging: Dual oxidation mechanism and its interrelationships with asphalt composition and oxidative age hardening. *Transportation Research Record: Journal of the Transportation Research Board*, (1638), 47-55.

Petersen, J. C., Harnsberger, P. M., & Robertson, R. E. (1996). Factors affecting the kinetics and mechanisms of asphalt oxidation and the relative effects of oxidation products on age hardening. *Preprints of Papers, American Chemical Society, Division of Fuel Chemistry*, 41(CONF-960807).

Rowe, G. M., King, G., & Anderson, M. (2014). The influence of binder rheology on the cracking of asphalt mixes in airport and highway projects. *Journal of Testing and Evaluation*, *42*(5), 1-10.

Underwood, B. S., Far, M. S. S., & Kim, Y. R. (2010). Using limited purchase specification tests to perform full linear viscoelastic characterization of asphalt binder. *Journal of Testing and Evaluation*, 38(5), 558-566.

Yousefi Rad, F. Elwerdani, M., Castorena, C. & Kim, Y. R. (2017). Investigation of proper long-term laboratory aging temperature for performance testing of asphalt concrete. *Journal of Construction and Building Materials*.

Zhang, F., Yu, J., & Han, J. (2011). Effects of thermal oxidative ageing on dynamic viscosity, TG/DTG, DTA and FTIR of SBS-and SBS/sulfur-modified asphalts. *Construction and Building Materials*, 25(1), 129-137.

APPENDIX E

Factors Affecting Oxidation Reaction Mechanisms in Asphalt Concrete

Introduction

The accurate characterization and prediction of asphalt mixture properties in terms of the service life of a pavement are becoming more important factors as increasingly powerful pavement design and performance prediction methods are being implemented. Oxidative aging has long been recognized as a major distress mechanism of asphalt concrete pavements. Aging causes the material to stiffen and embrittle, which leads to a high potential for cracking. Pavement oxidation is a complex phenomenon that is affected by material properties, volumetric properties, climate, and structure. In addition, oxidation reaction mechanisms can be affected by temperature, material state, and external pressure. Sulfoxides can decompose and the microstructure can become compromised when the binder is subjected to high temperatures, which then affects oxidation products (Yousefi Rad et al. 2017, Petersen and Glaser 2011, Petersen 2009, Petersen and Harnsberger 1998, Herrington 1994). In addition, oxidation reactions can be diffusion- or kinetics-controlled, depending on the availability of oxygen to the asphalt binder within the asphalt concrete. Field oxidative aging is diffusion-controlled below the pavement surface because oxygen must percolate through the air void structure and asphalt binder film within the pavement (Das et al. 2015, Glaser et al. 2013, Dickinson 1984). In laboratory aging, the state of the asphalt during oxidation (i.e., as asphalt binder, loose mix, or compacted asphalt concrete), temperature, and pressure can all affect the degree to which the oxidation reaction is diffusion- versus kinetics-controlled (Petersen and Glaser 2011, Domke et al. 1997). An improved understanding of the factors that affect oxidation reactions will inform improved laboratory aging procedures and predictive oxidation models.

Asphalt binder is the asphalt concrete constituent that undergoes oxidative aging. Therefore, the oxidation of pavements is best characterized using asphalt binder properties. The binder properties that are used to measure the extent of oxidation are referred to as aging index properties (AIPs). AIPs generally are divided into two main categories: chemical functional groups and rheological parameters. Chemical functional groups provide an indication of the oxygen uptake and can be measured using Fourier transform infrared (FTIR) spectroscopy techniques (Petersen and Glaser 2011, Petersen 2009, Farrar et al. 2013). The rheological properties provide an indication of any change in the viscoelastic binder properties due to oxidation and can be measured using a dynamic shear rheometer (DSR).

The primary oxidation products in asphalt binders are ketones and sulfoxides, detected by carbonyl and sulfoxide IR absorption peaks. Ketone formation changes the polarity of the associated aromatic ring components, leading to an increase in the asphaltenes, which in turn increases viscosity (Petersen and Glaser 2011, Petersen 2009). Sulfoxides are polar and, hence, serve to increase asphalt binder viscosity (Petersen and Glaser 2011). The specific ketone and sulfoxides that are formed, combined with the physico-chemical interactions between the asphalt binder constituents, affect the binder rheology (Petersen 2009).

The relationship between chemical and rheological AIPs can be used to detect changes in oxidation reaction mechanisms. The relationship between chemical and rheological AIPs is unique

to a binder, given that the oxidation reaction mechanism is consistent. However, if the chemical oxidation products change, the relationship between the chemical and rheological AIPs will change, which can lead to performance consequences. Yousefi Rad et al. (2017) recently demonstrated that, even if the rheology of binders within asphalt mixtures is the same after long-term aging, chemical differences can affect the performance test results. Many researchers have studied the relationship between rheological and chemical AIPs (Petersen and Glaser 2011, Petersen 2009, Farrar et al. 2013, Elwardany et al. 2016, Morian et al. 2015, Glover et al. 2014, Morian et al. 2013, Petersen et al. 1996). However, past efforts have not elucidated the critical factors that affect oxidation products.

Objectives

The objectives of this study are to:

- Evaluate the effects of temperature, material state (i.e., binder, loose mixture, compacted mixture), and pressure on oxidation reaction mechanisms during laboratory aging.
- Evaluate the differences in the oxidation reaction mechanisms of laboratory-aged material versus field-aged material.

Experimental Plan

Table E-1 provides the specific details of the experimental plan. Laboratory-aged binder, laboratory-aged mixtures, and field cores were evaluated in this study.

Materials

Seven asphalt mixtures (detailed in Table E-1) were evaluated in this study. All mixtures were prepared using component aggregate and binder. The ‘NC’ mix is a typical North Carolina mix prepared with crushed granite. Two mixtures from an earlier Federal Highway Administration (FHWA) Accelerated Loading Facility (ALF) study also were evaluated. These ALF mixtures include unmodified binder and modified binder, prepared with the same source asphalt and same limestone aggregate (Gibson et al. 2012). Field cores from the ALF study also were analyzed in this study. Two WesTrack mixtures also were evaluated. Both WesTrack mixtures were prepared with PG 64-22 binder, but the binders were from different sources. The WesTrack 1995 mix is fine-graded whereas the WesTrack 1997 mix is coarse-graded. Both WesTrack mixtures were prepared with andesite and granite aggregate. WesTrack field cores also were analyzed. Two Strategic Highway Research Program (SHRP) binders were included in the testing due to their known differences in chemical composition and oxidative behavior (Petersen 2009). SHRP AAD-1 has high sulfur content (6.9%) and is highly structured (incompatible), leading to high temperatures and hardening susceptibility upon oxidation. SHRP AAG-1 has low sulfur content (1.3%) and is less structured (more compatible) than SHRP AAD-1. Therefore, SHRP AAD-1 is expected to be more susceptible to temperature sensitivity and hardening during oxidation than SHRP AAG-1.

Table E-1. Experimental plan: summary of different aging trials

Material Source	Material Type	Aging Test	Temperature (°C)	Pressure (MPa)	Duration
NC (PG 64-22)	Binder	RTFO	163	--	85 min
		RTFO + PAV	100	2.1	20 hr
		USAT	100	--	Various Durations
	Loose Mix	Oven	70, 85, 95	--	Various Durations
		PAV	85	2.1	Various Durations
	Compacted Specimen	Oven	85	--	Various Durations
ALF Control (PG 70-22)	Binder	RTFO	163	--	85 min
		RTFO + PAV	100	2.1	20 hr
		USAT	85	--	Various Durations
	Loose Mix	Oven	70, 85, 95	--	Various Durations
	Field Core	8 Years Old in McLean, VA			
ALF SBS LG (PG 70-28)	Binder	RTFO	163	--	85 min
		RTFO + PAV	100	2.1	20 hr
	Loose Mix	Oven	70, 85, 95, 135	--	Various Durations
	Field Core	8 Years Old in McLean, VA			
WesTrack 1995 (PG 64-22)	Loose Mix	Oven	70, 85, 95	--	Various Durations
	Field Core	19 Years Old in western Nevada (NV)			
WesTrack 1997 (PG 64-22)	Loose Mix	Oven	70, 85, 95	--	Various Durations
	Field Core	17 Years Old in western NV			
SHRP AAD-1	Binder	RTFO	163	--	85 min
		RTFO + PAV	100	2.1	20 hr

(PG 58-28)	Loose Mix	Oven	70, 85, 95, 135	--	Various Durations
SHRP AAG-1 (PG 58-10)	Loose Mix	Oven	70, 85, 95, 135	--	Various Durations

Aging Methods

Laboratory Aging of Asphalt Binders

Standard binder aging tests, i.e., rolling thin film oven (RTFO) tests and RTFO plus pressure aging vessel (PAV), i.e., RTFO+PAV tests, were performed using four binders (NC, ALF Control, ALF SBS, and SHRP AAD-1). The Universal Simple Aging Test (USAT), developed at the Western Research Institute (WRI), was performed using the NC and ALF Control binders. In the USAT method, hot binder is poured in casted slots of a metal plate to form 0.3-mm thick samples. The metal plates are placed in an oven on a level surface for aging. The USAT has been proposed as an alternative procedure to the conventional standard RTFO and PAV aging methods. The major feature of the USAT that distinguishes it from the other binder aging methods is the use of thin binder film (0.3-mm thick) that is expected to reduce the oxygen diffusion path and, hence, expedite oxidation (Farrar et al. 2015).

Laboratory Aging of Asphalt Mixtures

Both loose mixture aging and compacted specimen aging were performed in this study, as detailed in Table E-1. Prior to all long-term aging trials, the loose mix was short-term aged at 135°C for four hours as per AASHTO R 30 (2010). All seven mixtures were subjected to long-term aging in a loose mix state in a forced-draft oven at temperatures that were varied between 70°C and 135°C. In addition, the NC loose mixture was aged in the binder PAV at 85°C and 2.1 MPa pressure. In all the loose mix aging trials, the loose mixture was spread onto metal trays in a thin layer that was equal to the thickness of the mixture's nominal maximum aggregate size (NMAS) to maximize the availability of the oxygen to the binder. The long-term aged loose mix samples were collected at different intervals during the aging process to assess their oxidation levels. The NC mix also was subjected to compacted specimen aging at 85°C in an oven. These compacted specimens had 100-mm diameters and were 178-mm tall. Wire mesh supports were utilized to minimize specimen distortion of the compacted specimens under self-weight during aging. Compacted specimens typically are expected to experience a gradient in the oxidation level due to less availability of oxygen at the specimen's center compared to its periphery. Therefore, in this study, samples were extracted from the compacted specimens at various distances from the specimen periphery to minimize smearing the material data with differing oxidation levels.

Field-Extracted Material

In addition to laboratory aging trials, field cores were acquired from the FHWA ALF and WesTrack projects, as detailed in Table E-1. Field cores were sliced prior to the extraction and recovery of the binders to evaluate oxidation at multiple pavement depths.

Micro-Extraction and Recovery

A micro-extraction and recovery process was used to obtain asphalt binders from the aged mixtures (Farrar et al. 2015). The micro-extraction mixture sample size was 200 g, which allowed for approximately 10 g of asphalt binder as the resultant sample. A solvent mixture of toluene and ethanol (85:15) was used to dissolve the asphalt from the mixtures. After centrifugation, the asphalt-solvent solutions were separated in a rotary evaporator for approximately 2.5 hours under vacuum pressure of 80.0 ± 0.7 kPa. Nitrogen gas was used in place of oxygen to minimize oxidation during the recovery process. FTIR spectroscopy was performed using the recovered binder samples to ensure complete solvent removal prior to AIP testing.

Measurement of Aging Index Properties

FTIR Spectroscopy

Attenuated total reflectance (ATR) FTIR spectroscopy was performed to measure the chemical AIPs. This technique simultaneously collects absorbance data within a wide spectral range (400 cm-1 to 4000 cm-1). The ATR spectra were collected using 64 scans of each sample using a resolution of 4 cm-1. Peaks in the spectral data were used to detect the presence of chemical functional groups. A minimum of two replicates was used for each aging condition. Replicates were normalized to the same absorbance value at wave number 1375 cm-1, which is not affected by the level of oxidation. Changes in the concentration of the carbonyl and sulfoxides can be used to measure the extent of oxygen uptake in the asphalt (Petersen and Glaser 2011, Petersen 2009). In this study, changes in the carbonyl and sulfoxides peaks were tracked at wave numbers 1702 cm-1 and 1032 cm-1, respectively. In addition, the carbonyl and sulfoxide areas were measured as the areas under the FTIR absorbance curves at wave numbers ranging from 1650 cm-1 to 1820 cm-1 and 1000 cm-1 to 1050 cm-1, respectively. In this study, the carbonyl plus sulfoxide absorbance peak (referred to as ‘C+S’) was used as the primary chemical AIP because it encompasses the effects of both carbonyl and sulfoxide oxidation products. It was shown in Appendix D that C+S is generally the most reliable chemical AIP for evaluating both laboratory- and field-aged binders. In addition, the carbonyl area was used in limited analyses to evaluate the effects of sulfoxide decomposition when the aging temperature exceeds 100°C.

Dynamic Shear Rheometer

Temperature-frequency sweep tests were performed in a TA ARG2 DSR to measure the rheological properties of the extracted binders. The loading frequencies ranged from 0.1 Hz to 30 Hz. Temperatures ranged from 5°C to 64°C. Most of the tests were conducted using an 8-mm parallel plate set-up with a strain amplitude of 1 percent. However, lesser aged materials were tested using a 25-mm parallel plate set-up at 64°C. Data acquired from DSR testing can be

analyzed to obtain different rheological AIPs, including the crossover modulus, zero shear viscosity, and/or the dynamic shear modulus (G*) and phase angle at a given temperature and frequency. Appendix D compared different rheological AIPs and found that the dynamic shear modulus at a specific temperature and frequency can be used as a simple and reliable rheological AIP. The dynamic shear modulus can be measured directly and does not depend on a fitting algorithm or require extrapolation that can decrease reliability (Appendix D). The dynamic shear modulus value at 64°C and 10 Hz is used as the rheological AIP herein. The temperature of 64°C was selected because aging effects generally are most pronounced at high temperatures.

Effects of Laboratory Aging Temperature

Loose mix aging trials were performed to study the effects of the laboratory aging temperature on the oxidation reaction. It is well documented in the literature that laboratory aging temperatures above 100°C can alter oxidation kinetic mechanisms and cause degradation of the binder microstructure (Yousefi Rad et al. 2017, Petersen and Glaser 2011, Petersen 2009, Petersen and Harnsberger 1998, Herrington 1994). Therefore, the effects of the aging temperature were studied in two steps. First, the results of loose mix aging trials conducted at temperatures below 100°C were evaluated. Second, the effects of oxidation temperatures over 100°C were evaluated.

Aging Temperature below 100°C

Figure E-1 presents correlations between the rheological and chemical AIPs for binders extracted from laboratory-aged loose mixtures conditioned at 70°C, 85°C, and 95°C. Short-term aged loose mix results also are included for reference. In general, the results demonstrate a strong linear relationship between log G* and C+S that is independent of the laboratory aging temperature for each binder. However, note that the relationship between log G* and C+S is binder-dependent. The slope of the log G* versus C+S lines can be used to infer hardening susceptibility. SHRP AAG-1 demonstrates the highest slope, indicating that this binder hardens rapidly with oxidation. This finding matches expectations, because SHRP AAG-1 is known to be a highly structured asphalt. The ALF Control and ALF SBS lines have similar slopes. ALF Control and ALF SBS contain the same source binder, with the ALF SBS binder containing the addition of polymer as a modification. Thus, the results suggest that hardening susceptibility with oxidation is related to the base asphalt rather than to the modifier. Note that, although both WesTrack mixtures and the NC mix contain the same PG 64-22 binder, their hardening susceptibility varies, indicating that the binder source can have a significant impact on the oxidation susceptibility of binders, even if their performance grades are the same. Also note that the NC loose mix results correspond to oven aging durations that range from one day to 35 days. Oxidation generally progresses in two phases, commonly referred to as the initial spurt and the constant rate phase (Petersen and Glaser 2011). One day of aging is within the initial spurt whereas aging beyond several days will be within the constant rate phase. Thus, the results suggest that the relationship between chemistry and rheology is independent of the oxidation phase, which agrees with reports in the literature (Petersen and Glaser 2011).

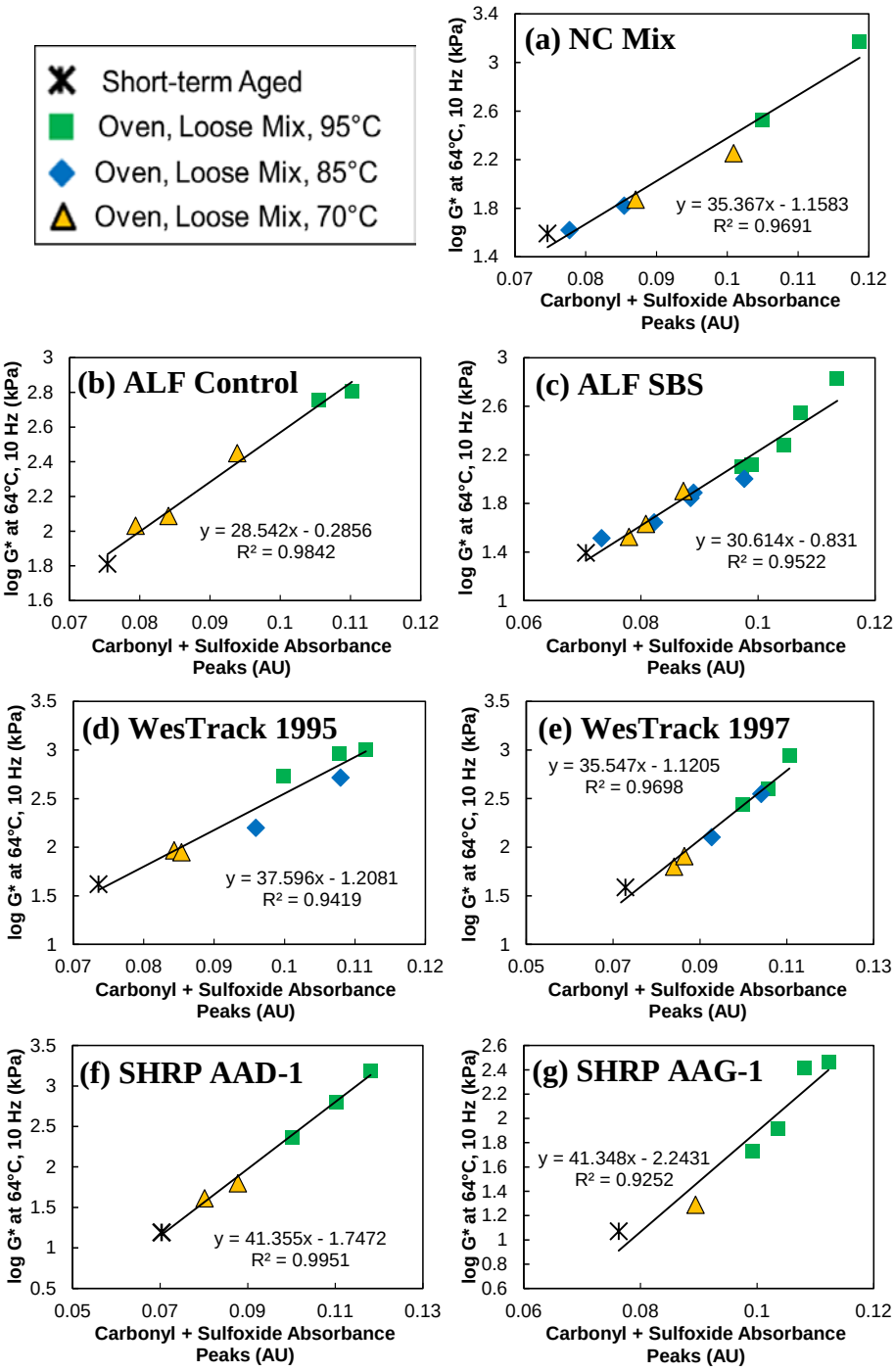

Figure E-1. Relationships between chemical and rheological AIPs for binders extracted and recovered from loose mixtures aged at different temperatures below 100°C (70°C to 95°C): (a) NC Mix, (b) ALF Control, (c) ALF SBS, (d) WesTrack 1995, (e) WesTrack 1997, (f) SHRP AAD-1, and (g) SHRP AAG-1.

Aging Temperatures that Exceed 100°C

Figure E-2 presents correlations between the rheological and chemical AIPs for binders extracted from the laboratory-aged loose mixtures, including those conditioned at 135°C. Note that only SHRP materials and FHWA ALF SBS were subjected to loose mix aging at 135°C. Here, both the C+S and carbonyl area are used as the chemical AIPs to allow for the assessment of sulfoxide decomposition. Figure E-2 demonstrates a clear shift in the relationship between log G* and C+S for SHRP AAD-1 and ALF SBS when the aging temperature is increased from 95°C to 135°C. Comparatively, a relatively small change in the relationship between the carbonyl area and log G* at 135°C is observed. These results suggest that sulfoxide decomposition is significant when SHRP AAD-1 and ALF SBS are aged at 135°C. Recall that SHRP AAD-1 has a high sulfur content and thus high potential for sulfoxide decomposition. Thus, the observed trends match expectations. The SHRP AAG-1 results shown in Figure E-2 (a) demonstrate only a minor shift in the relationship between log G* and C+S when the aging temperature is increased from 95°C to 135°C and show negligible effects of the aging temperature on the relationship between log G* and carbonyl area. Recall that SHRP AAG-1 is compatible with low sulfur content, and thus, these findings also match expectations.

The findings presented in Figure E-2 have important practical implications for laboratory aging. Several recent studies have proposed loose mix long-term aging at 135°C as an efficient alternative to the aging procedure recommended in current AASHTO specification (AASHTO R 30 2012, Blankenship 2015, Dukatz 2015, Braham et al. 2009). However, the results herein indicate that it is not possible to reflect both field chemistry and rheology using laboratory aging at temperatures that exceed 95°C. Yousefi Rad et al. (2017) demonstrated that the differences in binder chemistry that result from different aging temperatures can affect mixture performance even if the binder rheology is consistent between two mixtures.

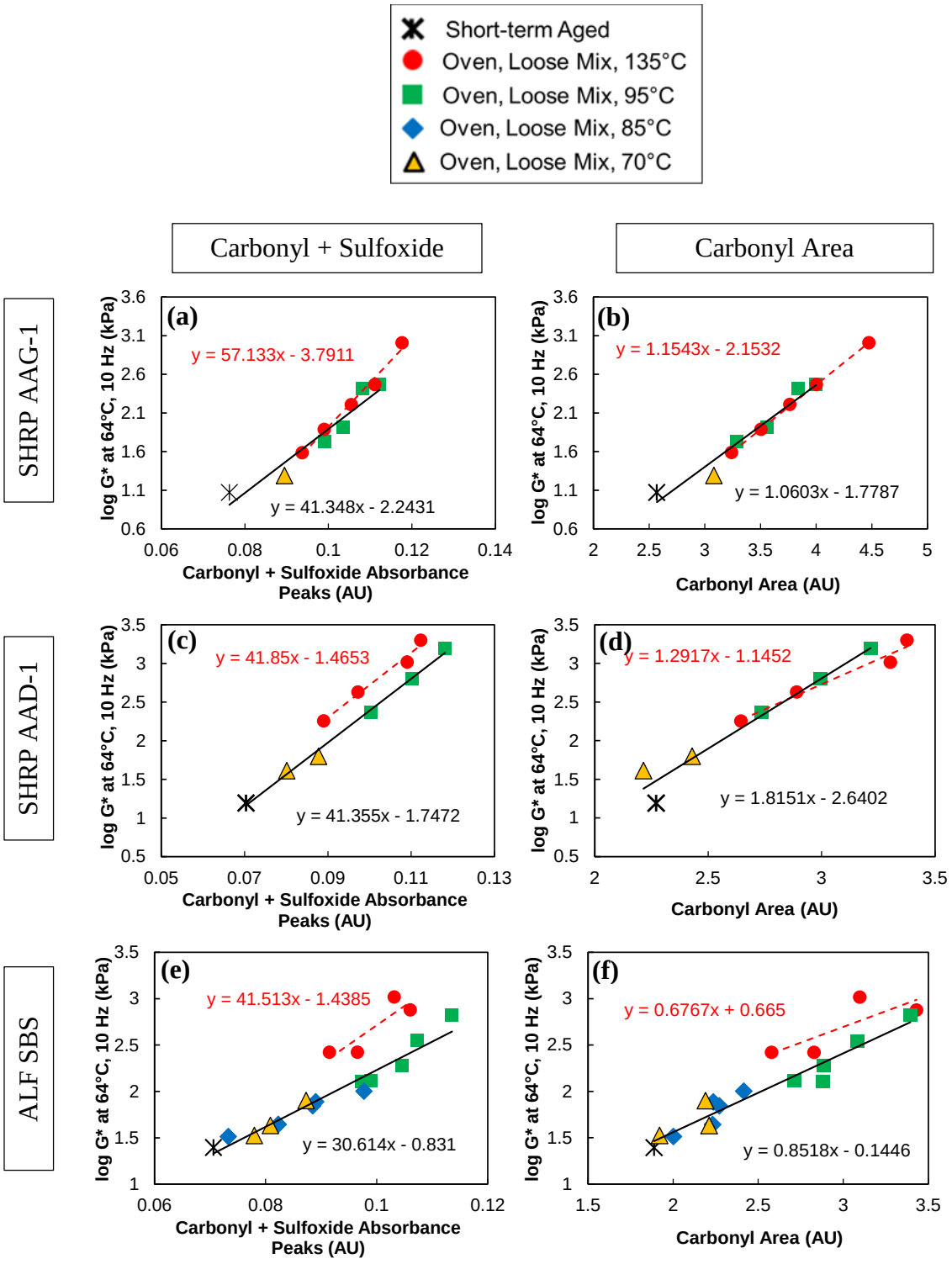

Figure E-2. Effects of aging temperatures above 100°C on the relationship between *log* G* and carbonyl + sulfoxide absorbance peaks: (a) SHRP AAG-1, (c) SHRP AAD-1, and (e) ALF SBS. Effects of aging temperature on the relationship between *log* G* and carbonyl absorbance area: (b) SHRP AAG-1, (d) SHRP AAD-1, and (f) ALF SBS.

Effects of Material State

Loose Mixture Aging vs. Compacted Specimen Aging

The state of the asphalt mixture during aging may impact the oxidation mechanisms. In compacted specimen aging, the oxidation reaction is expected to be diffusion-controlled. Oxygen must percolate through air voids and binder film in compacted specimens for the oxidation reaction to occur. As a result, the oxidation reaction in compacted specimens is expected to be limited by the local partial pressure of the oxygen within the specimen. Thus, compacted specimens experience oxidation gradients in accordance with the distance from the sample periphery (Elwardany et al. 2016). Loose mix aging is anticipated to be uniform and kinetics-controlled because the mixture is aged in thin layers, and thus, the binder has ample exposure to oxygen. Figure E-3 presents the correlations between the rheological and chemical AIPs for the binders extracted and recovered in compacted specimen aging trials conducted at 85°C and laboratory loose mix aging trials conducted at 70°C, 85°C, and 95°C. A clear difference is evident in the relationship between log G* and C+S in compacted specimen aging versus loose mix aging. It is speculated that this difference indicates that oxidation in compacted specimen aging is diffusion-controlled whereas the oxidation that takes place in loose mix aging is kinetics-controlled. However, it is not fully understood why diffusion-controlled oxidation leads to a reduction in hardening susceptibility. Thus, the chemical changes induced by a diffusion-controlled versus kinetics-controlled oxidation reaction merits investigation in future work.

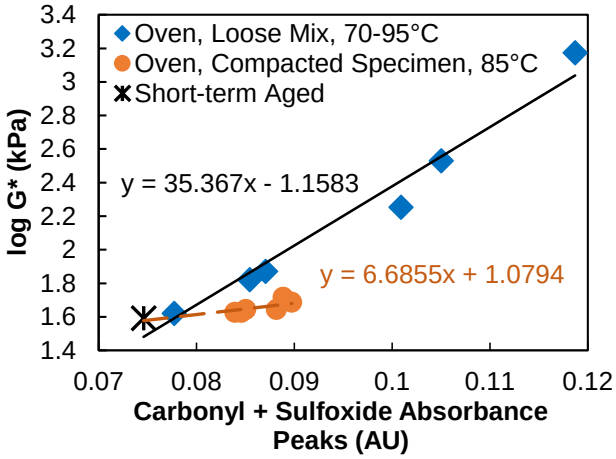

Figure E-3. Correlation between log G* and carbonyl plus sulfoxide peaks for binders extracted and recovered from different aging conditions.

Mixture Aging vs. Binder Aging

Oxidation mechanisms may be affected by factors such as the presence of aggregate, film thickness, and pressure. Therefore, the relationships between chemistry and rheology for loose mixture aging and binder aging were compared in this study.

USAT vs. Loose Mixture Aging

It can be assumed that both USAT binder aging and loose mixture aging are kinetics-controlled reactions. Farrar et al. (2015) proposed that the USAT procedure induces kinetics-controlled oxidation with no diffusion effects because the film thickness is small (300 μm). Similarly, loose mix aging is assumed to be kinetics-controlled because the film thickness of the binder on the aggregate likewise is small (less than 300 μm). Therefore, comparing USAT and loose mix test results can be used to elucidate the effects of the aggregate on the oxidation mechanisms. The selective adsorption of asphaltenes by the aggregate and filler can alter the oxidation mechanism because adsorbed asphaltenes are unavailable for oxidation (Petersen 2009). Figure E-4 (a) and (b) present correlations between the rheological and chemical AIPs obtained from USAT binder aging and loose mix oven aging for the NC mix and ALF Control mix, respectively. Loose mix oven aging trials were conducted at 70°C, 85°C, and 95°C. USAT aging was conducted at 100°C for the NC binder and 85°C for the ALF Control binder. Figure E-4 (a) demonstrates a potential difference in the relationship between chemistry and rheology but additional data are needed to draw a firm conclusion for the NC mixture. Figure E-4 (b) demonstrates relatively good agreement between the USAT and loose mix aging test results. Thus, these results indicate that the presence of aggregate has only a minor effect on the oxidation reaction.

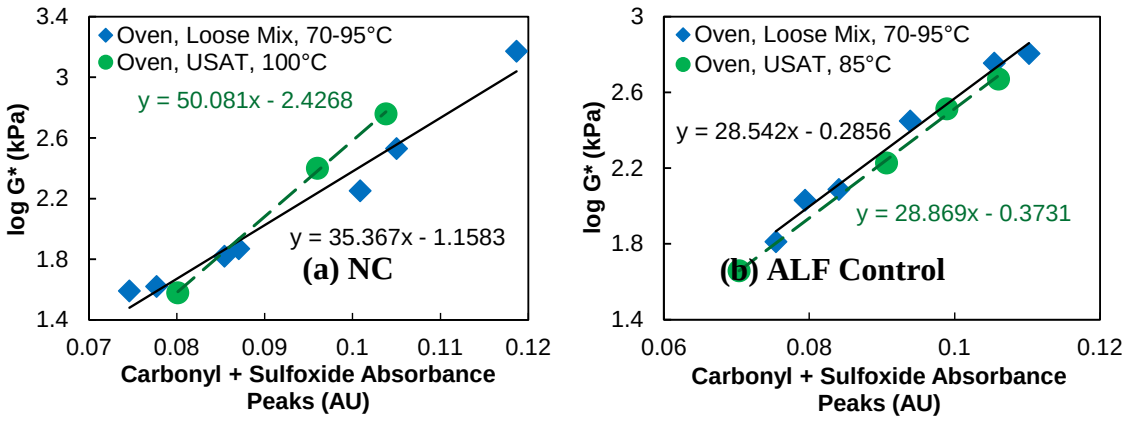

Figure E-4. Correlation between log G* and carbonyl plus sulfoxide peaks for loose mix aging and USAT binder aging: (a) NC Mix and (b) ALF Control.

Standard RTFO and PAV Aging vs. Loose Mix Aging

The relationships between rheology and chemistry in standard binder aging procedures (RTFO and PAV) were compared to those in loose mixture aging to allow for the general assessment of the ability of different binder aging procedures to reflect mixture aging. It should be noted that multiple factors may impact the differences in loose mix aging versus standard binder aging. Temperature, pressure, film thickness, and aggregate-asphalt interactions could all impact the results. As discussed, oxidative aging at temperatures that exceed 100°C can significantly impact the oxidation reaction. RTFO aging utilizes 163°C, which is significantly higher than the mixture short-term aging temperature (135°C). In addition, several research studies suggest that the application of pressure can alter the oxidation mechanism, which may impact the relative amounts of chemical functional groups formed upon oxidation, which in turn

affects the hardening susceptibility (Petersen and Glaser 2011, Domke et al. 1997). Therefore, comparisons between standard binder aging results and loose mix aging results cannot be used to identify the effects of individual factors on oxidation mechanisms.

Figure E-5 presents the correlations between the rheological and chemical AIPs for binders aged using standard RTFO and PAV procedures and binders extracted and recovered after laboratory loose mix aging conducted at 70°C, 85°C, and 95°C. The RTFO aging results tend to deviate from the trends of the other aging trials, which is speculated to be related to the relatively high temperature used in RTFO aging (163°C) compared to that used for mixture short-term aging (135°C), but could be related also to the effects of the aggregate in the mixture aging process, which are absent in binder aging. The results somewhat surprisingly indicate that the relationship between log G* and C+S for the RTFO+PAV aged binder is generally close to that of the binder extracted from aged loose mix. However, this finding does not necessarily imply good agreement between the oxidation reaction mechanisms, but rather a potential cancelling-out effect of the various factors that differ between standard binder aging and loose mix aging.

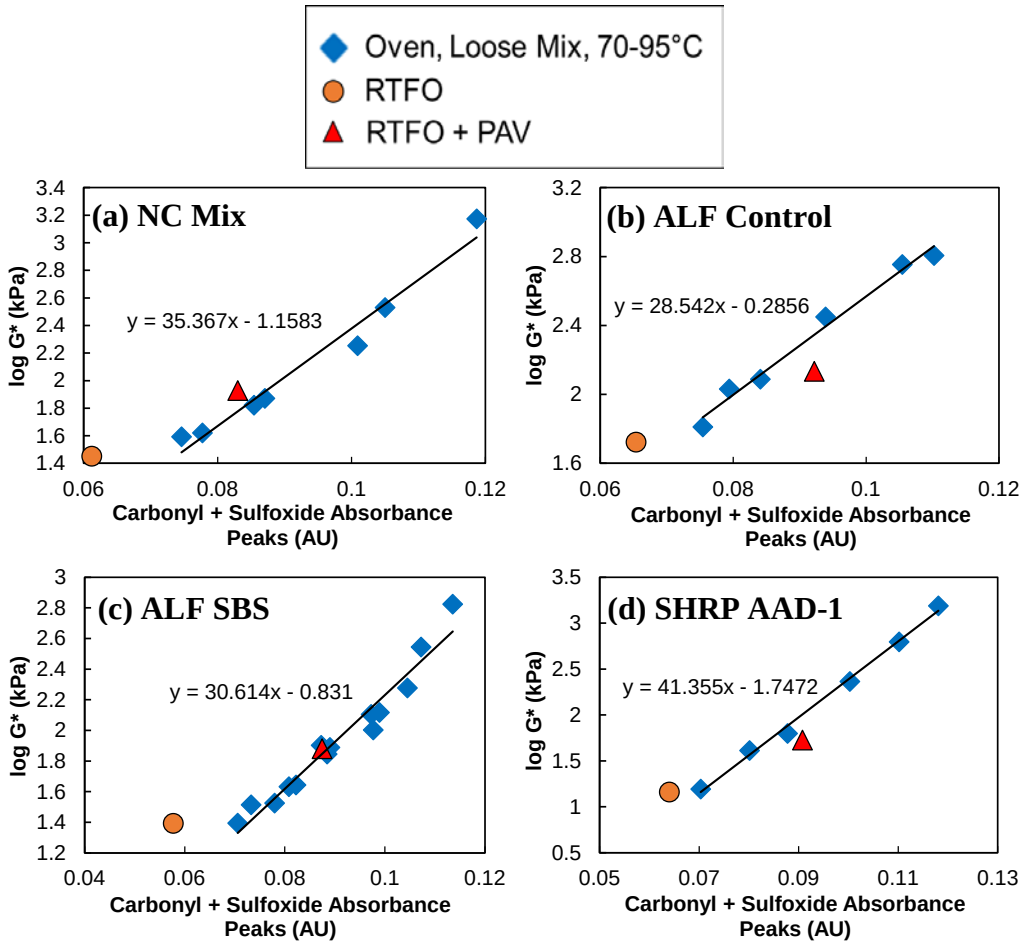

Figure E-5. Correlation between log G* and carbonyl plus sulfoxide peaks for loose mix aging versus standard binder RTFO and RTFO+PAV aging: (a) NC Mix, (b) ALF Control, (c) ALF SBS, and (d) SHRP AAD-1.

Effect of Pressure

As discussed, pressure may affect the relationship between rheology and chemistry. However, comparing the loose mixture aging results and the binder PAV aging results does not allow for a direct assessment of the effect of pressure on the oxidation mechanism. Therefore, a comparison of binders extracted from loose mix aged with and without the application of external pressure was made using the NC Mix to study the effects of pressure on oxidation products directly. Figure E-6 presents the results. The results indicate a clear difference in the relationship between log G* and C+S in oven aging versus pressure aging. These results also agree with past study results (Petersen and Glaser 2011, Domke et al. 1997). Petersen and Glaser (2011) suggested that oxidation occurs deeper in the microstructure of the binder when pressure is applied during aging, which has less effect on the rheology than the oxidation reactions that occur in the absence of external pressure. Thus, for a given C+S value, it is expected that the G* value would be lower for PAV-aged material than for oven-aged material.

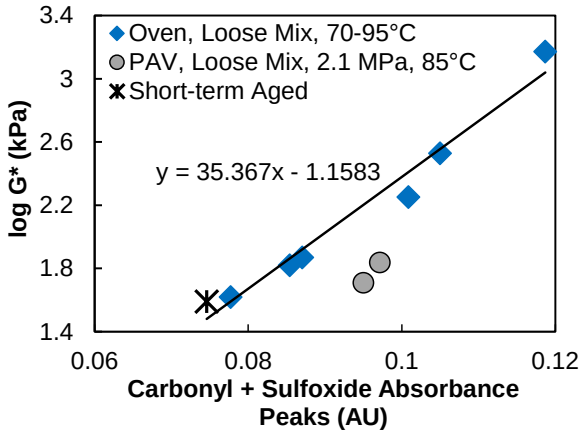

Figure E-6. Correlation between log G* and carbonyl plus sulfoxide absorbance peaks for loose mix aging with and without applied pressure.

Laboratory Aging vs. Field Aging

Laboratory and field aging may lead to differences in oxidation reaction mechanisms. Therefore, the relationships between *log* G* and C+S for binders extracted from laboratory-aged loose mix and binders extracted from varying depths of field cores were compared. Figure E-7 presents the results. Generally, the field results fall below the laboratory loose mix aging results. This finding is analogous to the findings presented in Figure E-3 where the compacted specimen results fall below the loose mix results. These results suggest that field oxidation is diffusion-controlled below the surface of the pavement, whereas loose mix aging is kinetics-controlled. Although the results for the binders extracted from the surface of field cores are generally close to the laboratory loose mix aging results, they also differ slightly from the laboratory aging results, indicating that other mechanisms may affect the field oxidation reaction. For example, ultraviolet photo-oxidation may affect the oxidation of the surface of pavements, which is an effect that is absent in laboratory aging (Das et al. 2014). Therefore, the possibility of fully replicating field-aged material in the laboratory is unlikely. However, the results also indicate that loose mix aging can be used to produce oxidized material that has the same rheology and

relatively similar chemistry to the surface of field-aged material, thereby allowing for reasonable performance testing and predictions of asphalt mixtures. Compacted specimen aging is not recommended because it leads to a gradient in oxidation with distance from the specimen periphery, which leads to variable properties in specimens and thus is problematic for performance testing and prediction (Elwardany et al. 2016). It remains to be proven or disproven whether compacted specimen aging better matches the field reaction mechanisms than loose mix aging. However, fully reflecting field conditions is probably impossible due to the potential effects of pavement structure, densification, and moisture.

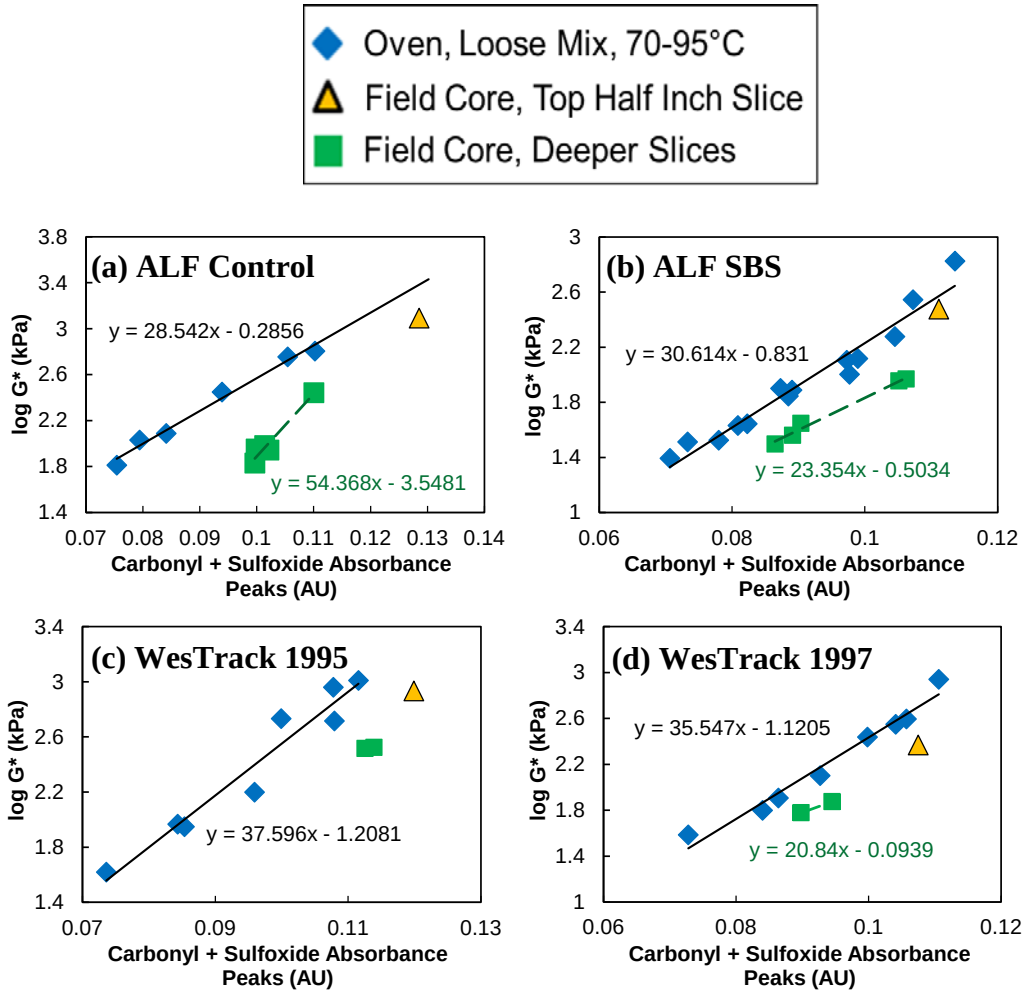

Figure E-7. Correlations between log G* and carbonyl plus sulfoxide peaks for binders extracted and recovered from laboratory loose mixtures aged at different temperatures below 100°C and binders extracted and recovered from different depths of in-service asphalt pavement: (a) ALF Control (8 years old), (b) ALF SBS (8 years old), (c) WesTrack 1995 (19 years old), and (d) WesTrack 1997 (17 years old).

Conclusions and Recommendations

The following conclusions and recommendations can be drawn from this study:

- The relationship between chemical and rheological AIPs can be used to identify changes in oxidation reaction mechanisms.
- The evaluation of loose mix aging at multiple temperatures indicates that a significant change in the relationship between binder rheology and chemistry occurs when the aging temperature is increased from 95°C to 135°C. This finding implies a change in the reaction mechanism, and therefore, laboratory aging above 95°C should be avoided. Laboratory aging at or below 95°C indicates no change in the reaction mechanism based on observed trends in the relationship between rheology and chemistry.
- The hardening susceptibility of asphalt binders, defined as the slope of the rheology versus chemistry AIP lines, depends on the asphalt binder source. Thus, binders with the same performance grade (PG) may age differently.
- The results indicate that the physico-chemical interaction between asphalt and aggregate has only a minor impact on oxidation reaction products. However, this finding should be verified using a broader set of materials in future work.
- The application of pressure leads to a change in the oxidation reaction mechanism. The results confirm the literature findings that an application of pressure leads to a decrease in hardening susceptibility.
- A comparison of binders extracted from laboratory-aged loose mixture, laboratory-aged compacted specimens, and field cores suggests that field aging is diffusion-controlled below the pavement surface. In addition, the oxidation at the pavement surface differs from that of laboratory-aged loose mixture even though both the pavement surface and laboratory-aged loose mix are speculated to experience kinetics-driven oxidation. This result suggests that ultraviolet photo-oxidation and/or other field variables affect pavement oxidation, which cannot be easily replicated in the laboratory.

References

American Association of State Highway and Transportation Officials (AASHTO), *Standard Practice for Mixture Conditioning of Hot Mix Asphalt,* AASHTO R 30, Washington, D.C. (2010).

Blankenship, P., “Evaluation of Laboratory Performance Tests for Fatigue Cracking of Asphalt Pavements” Presentation, Federal Highway Administration (FHWA) Asphalt Mixture Expert Task Group (ETG) Meeting, Fall River, MA. (April 2005).

Braham, A. F., W. G. Buttlar, T. R. Clyne, M. O. Marasteanu, and M. I. Turos, “The Effect of Long-term Laboratory Aging on Asphalt Concrete Fracture Energy.” *Journal of the Association of Asphalt Paving Technologies*, Vol. 78 (2009).

Das, P. K., N. Kringos, and B. Birgisson. “Microscale Investigation of Thin Film Surface Aging of Bitumen”. *Journal of Microscopy,* Vol. 254(2), (2014), pp. 95-107

Das, P. K., R. Balieu, N. Kringos, and B. Birgisson. “On the Oxidative Aging Mechanism and Its Effect on Asphalt Mixtures Morphology”. *Materials and Structures,* Vol. 48(10) (2015), pp. 3113-3127.

Dickinson, E. J. “The Diffusion Controlled Reaction of Oxygen with Films of Bituminous Binders”. *Australian Road Research,* Vol. 14(3), (1984).

Domke, C. H., M. Liu, R. R. Davison, J. Bullin, and C. J. Glover. “Study of Strategic Highway Research Program Pressure Aging Vessel Procedure Using Long-Term, Low-Temperature Aging Experiments and Asphalt Kinetics”. *Transportation Research Record: Journal of the Transportation Research Board,* No. 1586, Transportation Research Board of the National Academies, Washington D.C., (1997), pp. 10-15.

Dukatz, E. *STH 77 Project Objectives*. FHWA Asphalt Mixture ETG meeting presentation, Fall River, MA, April (2015).

Elwardany, M. D., F. Yousefi Rad, C. Castorena, and Y. R. Kim, “Evaluation of Asphalt Mixture Laboratory Long-Term Ageing Methods for Performance Testing and Prediction.” *Road Materials and Pavement Design*, Vol. 18, No. 1 (2017) pp. 28-61.

Farrar, M. J., J. P. Planche, R. W. Grimes, and Q. Qin, “The Universal Simple Aging Test (USAT): Simulating Short-and Long Term Hot and Warm Mix Oxidative Aging in the Laboratory.” *Asphalt Pavements*, Kim, Y. R., Ed., London: CRC Press, Taylor & Francis Group. (2014) pp. 79-87.

Farrar, M. J., R. W. Grimes, S. Wiseman, and J. P. Planche, *Asphalt Pavement–Micro-sampling and Micro-Extraction Methods,* Fundamental Properties of Asphalts and Modified Asphalts III, Quarterly Technical Report, Federal Highway Administration (FHWA), Contract No. DTFH61-07-D-00005. (2015).

Farrar, M. J., T. F. Turner, J. P. Planche, J. F. Schabron, and P. M. Harnsberger, “Evolution of the Crossover Modulus with Oxidative Aging: Method to Estimate Change in Viscoelastic Properties of Asphalt Binder with Time and Depth on the Road”. Transportation Research Record: Journal of the Transportation Research Board, No. 2370, Transportation Research Board of the National Academies, Washington D.C. (2013), pp. 76-83.

Gibson, N., X. Qi, A. Shenoy, G. Al-Khateeb, M. E. Kutay, A. Andriescu, K. Stuart, J. Youtcheff, and T. Harman. *Performance Testing for Superpave and Structural Validation*. Publication FHWA-HRT-11-045. FHWA, U.S. Department of Transportation, (2012).

Glaser, R., T. F. Turner, J. L. Loveridge, S. L. Salmans, and J. P. Planche, *Fundamental Properties of Asphalts and Modified Asphalts III*, Quarterly Technical Report, Federal Highway Administration (FHWA), Contract No. DTFH61-07-D-00005. (2013).

Glover, C. J., R. Han, X. Jin, N. Prapaitrakul, Y. Cui, A. Rose, J. J. Lawrence, M. Padigala, E. Arambula, E. S. Park, and A. E. Martin. *Evaluation of Binder Aging and Its Influence in Aging of Hot Mix Asphalt Concrete*. Publication FHWA/TX-14/0-6009-2. FHWA, U.S. Department of Transportation, (2014).

Herrington, P. R., J. E. Patrick, and G. F. Ball, "Oxidation of Roading Asphalts." *Industrial and Engineering Chemistry Research*, Vol. 33, No. 11 (1994), pp. 2801-2809.

Morian, N., C. Zhu, and E. Y. Hajj. "Rheological Indexes: Phenomenological Aspects of Asphalt Binder Aging Evaluations". *Transportation Research Record: Journal of the Transportation Research Board*, No. 2505, Transportation Research Board of the National Academies, Washington, D.C., (2015), pp. 32-40.

Morian, N., E. Y. Hajj, and P. Sebaaly. "Significance of Mixture Parameters on Binder Aging in Hot-Mix Asphalt Mixtures". *Transportation Research Record: Journal of the Transportation Research Board*, No. 2370, Transportation Research Board of the National Academies, Washington D.C., (2013), pp. 116-127.

Petersen, J. C., "A Review of the Fundamentals of Asphalt Oxidation: Chemical, Physicochemical, Physical Property, and Durability Relationships." *Transportation Research Board, Transportation Research Circular (E-C140)*, National Research Council, Washington, D.C. (2009).

Petersen, J. C. and P. M. Harnsberger, "Asphalt Aging: Dual Oxidation Mechanism and Its Interrelationships with Asphalt Composition and Oxidative Age Hardening." *Transportation Research Record*, 1638, National Research Council, Washington, D.C. (1998) pp. 47-55.

Petersen, J. C., P. M. Harnsberger, and R. E. Robertson, "Factors Affecting the Kinetics and Mechanisms of Asphalt Oxidation and the Relative Effects of Oxidation Products on Age Hardening" Preprints of Papers, American Chemical Society, Division of Fuel Chemistry, Vol. 41, No. CONF-960807. (1996).

Petersen, J. C. and R. Glaser. "Asphalt Oxidation Mechanisms and the Role of Oxidation Products on Age Hardening Revisited." *Road Materials and Pavement Design*, Vol. 12 (4) (2011), pp. 795-819.

Yousefi Rad, F., M. D. Elwardany, C. Castorena, and Y. R. Kim, "Investigation of Proper Long-Term Laboratory Aging Temperature for Performance Testing of Asphalt Concrete." *Construction and Building Materials*, Vol. *147* (2017), pp. 616-629.

APPENDIX F

Evaluation of Asphalt Mixture Laboratory Long-Term Aging

Introduction

Aging has long been recognized as a major distress mechanism for asphalt concrete and, by extension, asphalt pavements. Aging causes the material to stiffen and embrittle, which leads to a high potential for cracking. The issue of oxidative aging of asphalt binder has been recognized and studied for almost a century. Hubbard and Reeve (1913) published the first results of a study that examined the effects of a year of outdoor weathering on the physical (weight, hardness, etc.) and chemical (solubility) properties of paving grade asphalt cements. Subsequent studies confirmed their basic finding that oxidation, and not volatilization alone, is responsible for changes in asphalt properties that occur due to exposure (Thurston and Knowles 1936, Corbett and Merz 1975). Significant research also has been conducted to investigate the chemical aspects of the aging process, and an excellent review of these studies can be found in Petersen (2009). For some of these studies, researchers conducted sophisticated experiments and proposed conceptual, empirical, and/or analytical models to explain the aging phenomenon of asphalt binder (Liu et al. 1996, Petersen and Harnsberger 1998, Glover et al. 2008). Although a significant amount of effort has been placed on understanding the aging process of asphalt binder, relatively less work has been put forth to develop laboratory aging procedures for producing aged mixture specimens for performance testing. In addition, very little effort has been made to validate the laboratory aging methods with field measurements.

The accurate characterization of asphalt mixture properties in terms of the service life of a pavement is becoming more important as more powerful pavement design and performance prediction methods are implemented. Both an accurate aging model and an optimal laboratory conditioning procedure are required to simulate long-term aging for performance testing and prediction in order to integrate the effects of long-term aging into pavement prediction models and other mechanistic design and analysis methods. This study seeks to evaluate existing laboratory asphalt mixture aging methods to assess their ability to produce oxidation of specimens efficiently and to maintain specimen integrity for performance testing.

Existing Asphalt Mixture Aging Methods

Several asphalt mixture laboratory aging procedures have been utilized in past studies. These procedures can be broadly classified based on the (a) state of the material during aging (compacted specimen vs. loose mix) and (b) pressure level (oven aging vs. pressurized aging). Thus, the discussion of the laboratory aging of asphalt mixtures in this study focuses on these two factors.

Compacted Specimen Aging versus Loose Mixture Aging

The standard method used to assess the long-term aging of asphalt mixtures in the United States is American Association of State Highway and Transportation Officials (AASHTO) R 30 (2001). In this method, compacted asphalt mixture specimens are subjected to short-term aging

at 135°C for four hours. Then, the short-term aged mixtures are compacted. The compacted specimen is cored or sawn to the required dimensions and then placed in a forced draft oven for long-term aging. The long-term aging simulation is performed at 85°C ± 3°C for 120 ± 0.5 hours to represent five to ten years of aging in the field. Additional compacted specimen aging procedures (oven aging at different temperatures with and without pressure) have been tried and are cited in the literature (e.g., Partl et al. 2013, Mollenhauer and Mouillet 2011, Reed 2010, Houston et al. 2005, Hachiya et al. 2003, Korsgaard et al. 1996, Bell et al., 1994a, and Von Quintus et al. 1992). Two specimen integrity issues have been found using compacted specimen aging:

(1) *Distortion:* Changes in air void content and geometry due to compression under self-weight have been reported when using AASHTO R 30 (Reed 2010). To overcome this problem, the National Research Cooperative Highway Research Project (NCHRP) 9-23 protocol recommends wrapping specimens in metal wire mesh secured with three clamps to prevent the samples from geometry distortion (Houston et al. 2005). However, this approach has been reported only to reduce, but not eliminate, specimen distortion during aging (Reed 2010).
(2) *Oxidation gradient:* The NCHRP 9-23 project (2005) demonstrated that the long-term oven aging of compacted specimens leads to both radial and vertical oxidation gradients in mixture specimens, which is a concern for the use of long-term oven aging of compacted specimens in performance testing because properties throughout a specimen differ (Houston et al. 2005).

It is important to take in to consideration that the objective of the laboratory aging method should not be to replicate the field aging gradient. The objective of this study is to select an aging method that yields uniform aging throughout the specimen at the material level. In order to prepare specimens for performance testing and model their behavior in the laboratory, the representative volume element (RVE) requirements should be fulfilled. An aging gradient would lead to multiple |E*| values within the specimen and also variable fatigue performance throughout the specimen.

In addition, the aging gradient in a laboratory-aged specimen does not replicate field aging gradients. In the field, aging is greatest at the surface and reduces with depth. However, in laboratory-aged specimens, aging is greatest at the periphery and reduces towards the center of the specimen. Hence, the direction of aging gradients differ between field cores and compacted specimens prepared in the laboratory (Houston et al. 2005).

Although less common than aging compacted specimens, the laboratory aging of loose (uncompacted) asphalt mixtures also has been tried (e.g., Arega et al. 2013, Partl et al. 2013, Mollenhauer and Mouillet 2011, Van den Bergh 2011, Reed 2010). Several studies recommend aging loose mixtures in the laboratory to simulate the aging of asphalt pavements instead of aging compacted specimens (Mollenhauer and Mouillet 2011, Van den Bergh 2011). It should be noted that some of the laboratory aging studies conducted on loose mixtures were designed to prepare reclaimed asphalt pavement (RAP) materials rather than to investigate compaction and subsequent performance testing (Partl et al. 2013, Mollenhauer and Mouillet 2011, Van den Bergh 2011). Geometry distortion is not a concern with loose mix aging because the specimens are compacted following aging. In addition, aging gradients are not a problem, because the loose mix is aged as a single layer of coated aggregate particles and, thus, oxygen and heat can

circulate easily throughout the mix. Also, the increased surface area of the binder film that is exposed to oxygen is believed to accelerate aging in loose mixtures compared to compacted specimens. However, the compaction of aged loose mix for performance testing can lead to a potential specimen integrity concern, because aged binder is very stiff and thus is expected to be less compactable than unaged material. For example, a study on the loose mix aging of an asphalt rubber friction course (ARFC) indicated that significantly more effort is required to compact long-term aged loose mix than short-term aged loose mix (Reed 2010). However, it is important to note that an ARFC represents an extreme case with rubber-modified asphalt and relatively thick asphalt film. It also has been found that the increased force/effort that is required to reach target air void contents when using compacted aged loose mixtures may cause degradation in the aggregate structure and alter the mixture properties (Gatchalian 2006).

Based on a thorough review of the literature (Arega et al. 2013, Partl et al. 2013, Mollenhauer and Mouillet 2011, Reed 2010, Harrigan 2007, Houston et al. 2005), the advantages and disadvantages of compacted specimen aging and loose mix aging have been compiled and are summarized in Table F-1.

Table F-1. Comparison between loose mix aging and compacted specimens aging methods

Loose Mix	Pros	• Homogenous aging in the mixture • Higher oxidation rate than compacted mix • Maintaining specimen integrity a non-issue
	Cons	• Difficulties associated with compaction of aged loose mix, which limits its use for producing specimens for performance testing • Limited amount of materials can be aged in standard PAV chamber
Compacted Specimen	Pros	• Can produce aged sample for performance tests if slumping is minimized through use of wire mesh
	Cons	• Slower oxidation rate than loose mix • Integrity of the specimens is compromised at high temperatures and pressures due to slump and cracking upon pressure release • Oxidation gradients exist radially and throughout height of the specimen

Oven Aging versus Pressure Aging

Long-term oven aging is the most common method that is used to simulate the oxidative aging of asphalt mixtures in the laboratory. As discussed, the current standard procedure, AASHTO R 30, consists of conditioning compacted asphalt concrete specimens in an oven at 85°C for five days. However, other oven aging procedures have been tried and are cited in the literature. Although these procedures are somewhat similar in terms of methodology, the long-term oven aging procedures differ in terms of temperature and duration (e.g., Bell et al. 1994, Houston et al. 2005, Reed 2010).

The summaries of compacted and loose mixture aging trials (refer to Appendix A) demonstrate that long-term oven aging requires considerable time to produce oxidation levels that correspond to field conditions near the end of a pavement's service life. Hence, researchers have attempted to conduct long-term aging trials using both loose mix and compacted specimens under air pressure to expedite oxidative aging (e.g., Kumar and Goetz 1977, Von Quintus et al. 1988, Bell et al. 1994). Different pressure and temperature combinations were tried in these studies. Generally, these earlier studies suggest that air/oxygen pressure expedites oxidative

aging. However, in the case of aging compacted specimens, the loss of integrity during aging is a concern unless low temperatures are used, which can adversely affect the aging rate.

The standardized pressure aging equipment that is widely used in the asphalt industry is the pressurized aging vessel (PAV). The PAV has been used to age both loose mix and compacted specimens. One of the main shortcomings of PAV aging compared to oven aging is the amount of material that can be aged. Based on previous studies of loose mixture aging, in order to obtain uniform aging, a uniform thin layer of loose mix should be placed in the PAV, which reduces the capacity of the equipment to a very low level (around 1 kilogram) (Partl et al. 2013). Despite this capacity problem, however, it is believed that the air/oxygen pressure in the PAV can expedite aging and reduce the time required to achieve a certain level of aging in an asphalt mixture specimen. Furthermore, if a smaller geometry for asphalt mixture cores is used, more specimens can be aged at once. However, concern remains with respect to maintaining compacted specimen integrity during pressure aging and upon pressure release, which needs to be considered carefully when assessing PAV aging of compacted mix specimens (Bell et al. 1994). Table F-2 presents a brief summary of the pros and cons of conducting oven versus pressurized aging.

Table F-2. Comparison between oven and PAV aging methods

Oven Aging	Pros	• Available and easy to perform and control • Large amount of material can be aged
	Cons	• High variability among ovens, especially in terms of air drafting • More time needed to age materials in the oven than in the PAV • Maintaining compacted specimen integrity is required, especially at high temperatures
Pressure Aging	Pros	• Pressure can expedite the aging process • More reliable than oven aging due to less equipment variability between laboratories
	Cons	• Due to limited capacity of the vessel, less material can be aged in each aging cycle unless new device is developed • Integrity of compacted samples during and after testing is a major concern

Objectives

The objectives of this study are to:

(1) Evaluate aging of loose mix and compacted specimens.
(2) Evaluate laboratory aging with and without the application of pressure
(3) Select the most promising aging method for performance testing and prediction based on efficiency in oxidizing specimen, integrity of the aged specimens for performance testing, cost, and versatility.

Materials and Methods

Aging Methods

Compacted Specimen Aging

To evaluate compacted specimen aging as rigorously as possible, various compacted specimen aging methods were tried in this study. To overcome the specimen integrity issues associated with AASHTO R 30, including distortion and oxidation gradients, two potential remedial approaches were tried:

(1) Application of pressure to increase the diffusion of oxygen and, hence, potentially reduce oxidation gradients.
(2) Use of small specimens, 38 mm in diameter and 100 mm in height, to reduce the diffusion path distances and reduce slump under self-weight.

The compacted specimen aging trials included pressurized and oven aging of both large and small specimens. To prepare the specimens, mixtures were first prepared using component materials and subjected to short-term oven aging. Then, the mixtures were compacted in a Superpave Gyratory Compacter (SGC) to fabricate Ø150-mm × 178-mm specimens. Subsequently, large specimens for aging were obtained through coring to obtain Ø100-mm × 178-mm specimens. The ends of the cored large specimens were not sawn before aging because of the high probability of an aging gradient that could affect the performance test results. To fabricate the small specimens, Ø38-mm cylindrical specimens were cored horizontally from the initial specimens (Ø150 mm × 178 mm).

For the oven aging trials of the large specimens, wire mesh supports were utilized to minimize distortion under self-weight. A single aging temperature, 85°C (as specified by AASHTO R 30), was used for the aging trials. Pressure aging trials were conducted in a standard asphalt binder PAV. A pressure level of 300 kPa was selected for the PAV aging trials because higher pressure levels had been found to damage specimens upon pressure release in the Strategic Highway Research Program (SHRP) (Bell et al. 1994a). In addition, in order to reduce the stress on the large specimens under self-weight in the PAV, a wire mesh hammock-like support was developed to allow the specimen weight to be distributed over a larger area on its sides than if it were positioned vertically, as shown in Figure F-1.

Figure F-1. Simple set-up for holding large specimens during aging in the PAV.

Loose Mix Aging

Long-term aging of loose mix with and without pressure also was tried. Prior to all the long-term aging trials, the loose mix was first subjected to short-term aging. The oven aging of the loose mix was accomplished by separating the mix into several pans such that each pan had a

relatively thin layer of loose mix (approximately equal to the nominal maximum aggregate size (NMAS) of the aged mix), as shown in Figure F-2 (a). The loose mix was agitated several times during oven aging, and the pans in the oven were rotated systematically to minimize any effects of an oven temperature gradient and/or draft on the degree of aging. After long-term aging, the materials were taken out of the oven and mixed together in order to obtain a uniform mixture, and then the mixture was left to cool to room temperature. The loose mixture was then reheated to the compaction temperature for 75 minutes. Specimens were compacted following aging for performance testing. Because the compactability of the aged loose mix was a potential concern, the effect of increasing the compaction temperature on the compactability of the aged loose mix was investigated.

The pressure aging trials for the loose mix utilized the standard binder PAV pressure of 2.1 MPa, because pressure was not anticipated to induce any integrity concerns regarding the loose mixture samples, as compaction follows the aging process. The specimen set-up is shown in Figure F-2 (b) and Figure F-2 (c). The loose mix was dispersed in thin layers, consistent with the process for oven aging. The size of the binder PAV prohibited aging a large quantity of mix efficiently, and thus, any gain in the oxidation rate had to be balanced with the amount of material that could be aged at one time or, conversely, the associated costs in developing a mixture-specific pressure aging device. Due to the capacity constraints of the PAV, the long-term aging trials of the loose mix in the PAV were limited to simply assessing how much pressure would expedite the oxidation of the loose mix. Insufficient quantities of material were aged to produce compacted specimens. However, extracted binder also was tested, which allowed the extent of the oxidation to be determined and, hence, allowed an assessment of the efficiency gains due to pressure in oxidizing the loose mix.

(a) **(b)** **(c)**

Figure F-2. Long-term aging of loose mix: (a) loose mix separated into pans in thin layers for long-term aging in oven, (b) loose mix separated in thin layers in rack developed for long-term aging in PAV, and (c) rack placed in standard binder PAV.

Evaluation of Oxidation Level

Modelling the extent of oxidation in a pavement requires 'tracking' the property with respect to time, which is related directly to the oxidation level in the pavement. Asphalt binder is the component in asphalt mixture that undergoes oxidative aging; hence, the oxidation of a pavement is best tracked using the binder properties. Thus, the extent of oxidation achieved in the asphalt mixture aging trials was evaluated through the extraction and recovery of the binder following a proposed standard AASHTO specification by the Western Research Institute (WRI) (Farrar et al. 2015); the extent of oxidation was evaluated using rheology and chemistry, also. The binder properties that were used to measure the extent of oxidation are referred to herein as the aging index properties (AIPs).

Binder also was extracted from the short-term aged loose mix and tested in order to provide a point of reference to assess the oxidation that was induced during long-term aging. In addition, the AIPs of the binders that were aged using standard rolling thin-film oven (RTFO) aging and RTFO plus PAV aging (i.e., RTFO + PAV) were measured to provide an additional reference, as it is known that the binder PAV is expected to simulate five to ten years of aging in the field.

The chemical and rheological AIPs used to evaluate the oxidation were the C+S absorbance peaks and the binder dynamic shear modulus values (G*) at 64°C and 10 Hz loading frequency. Rheology testing was conducted using a TA ARG2 Dynamic Shear Rheometer (DSR). The DSR tests utilized an 8-mm parallel plate spindle with a strain level of 1 percent. Attenuated total reflectance (ATR) Fourier transform infrared (FTIR) spectroscopy simultaneously collected the absorbance data within a wide spectral range (400 cm^{-1} to 4000 cm^{-1}). Peaks in the spectral data were used to detect the chemical functional groups. Functional groups that contain oxygen include carbonyls and sulfoxides. Hence, changes in the concentration of the carbonyls and sulfoxides could be applied to the AIPs to measure the extent of oxygen uptake in the asphalt binder (Petersen and Glaser 2011, Petersen 1998, Petersen and Harnsberger 1998). Changes in the carbonyl and sulfoxide peaks were tracked at wave numbers 1702 cm^{-1} and 1032 cm^{-1}, respectively. The C+S absorbance peaks was found to be the chemical AIP that was most sensitive to oxidation level. FTIR data presented in this study are based on a minimum of two replicates. Based on a sensitivity investigation (Gundla et al. 2016, Kim 2015), a two percent change in the carbonyl + sulfoxide absorbance and a 15 percent change in the binder dynamic shear modulus both correspond to approximately a 10 percent change in the mixtures' dynamic modulus values. A 10 percent change in the dynamic modulus value is considered a reasonable threshold of significance and, hence, a two percent change in the carbonyl + sulfoxide absorbance peaks and 15 percent change in the dynamic shear modulus values at 64°C and 10 Hz were used as thresholds for detecting significant differences when interpreting the AIP results.

Evaluation of Specimen Integrity

Compacted Specimen Aging

Three criteria were used to evaluate the integrity of the specimens subjected to compacted specimen aging:

(1) *Initial integrity check:* Specimen integrity was evaluated initially by visual inspection, dimension measurements, and air void content comparisons before and after aging to determine if the specimen was damaged during the laboratory aging process. If an aging method was found to disturb specimen integrity, it was eliminated from further consideration.
(2) *Performance testing:* Performance test data were analyzed to detect any integrity issues that were not related to measurable geometry changes (e.g., micro-cracking). Dynamic modulus tests (AASHTO TP 79-12) were conducted to determine the linear viscoelastic characteristics of the asphalt mixtures. The dynamic modulus mastercurve was obtained by fitting a sigmoidal function and the time-temperature shift factors simultaneously using least squares optimization. Additionally, cyclic direct tension fatigue tests following the Simplified Viscoelastic Continuum Damage (S-VECD) procedure (AASHTO TP 107-14) were conducted. The S-VECD model is a rigorous mechanistic model that describes the fatigue behavior of asphalt mixtures under a wide range of loading and environmental conditions. Damage characteristic relationship and pseudo energy-based failure criterion are determined from the fatigue tests. In this study, these properties of the long-term aged mixtures were compared to those from the short-term aged mixtures to determine if specimen integrity was affected during aging.
(3) *Oxidation gradient:* Oxidation gradients in the aged specimens were evaluated through FTIR-ATR and DSR testing of binders extracted and recovered from locations in an aged specimen that varied in terms of distance from the specimen periphery. Differences in the rheology and chemical compositions, along with the distance from the specimen periphery, were used to detect the presence (if any) of an aging gradient.

Loose Mix Aging

Two criteria were used to evaluate the integrity of the specimens that were compacted following loose mix aging:

(1) *Initial integrity check:* The number of gyrations required to meet the target air void content was compared with that for the short-term aged mix in order to assess compactability. Air void content measurements were used to verify that the desired compaction level was met. In addition, digital imaging processing software was used to analyze the internal coarse aggregate structure of the compacted short-term and long-term aged loose mixes to determine if the aggregate structure was degraded by compacting the mixes following long-term aging.
(2) *Performance testing:* Performance tests, including dynamic modulus tests (AASHTO TP 79-12) and cyclic fatigue tests (AASHTO TP 107-14), were conducted on specimens that were compacted following loose mix aging to assess any further potential integrity problems (e.g., dynamic modulus decrease upon aging).

Criteria for Selection of the Most Promising Aging Method

The ultimate outcome of this study is to select the most promising aging method. In order to do so, compacted and loose mix aging methods were compared based on the following criteria:

(1) *Specimen integrity:* Specimen integrity, as related to compacted and loose mix aging, as previously discussed, is important for reliable performance evaluation.
(2) *Efficiency:* The relative rate of oxidation achieved in each method, as evaluated through comparisons of chemical and rheological AIPs, was quantified using FTIR-ATR and DSR temperature-frequency sweep testing, respectively.
(3) *Practicality and versatility:* The relative cost and availability of the required equipment were considered in selecting the most promising aging method. Furthermore, the versatility of the specimen geometries that can be produced for performance testing was an important consideration.

Materials

Phase 1 – Preliminary Evaluation of Aging Methods

In order to evaluate candidate methods, preliminary aging trials were conducted on a typical North Carolina mix with 9.5 mm NMAS and PG 64-22 binder, hereinafter referred to as the 'NC mix'. Loose mixtures were prepared in the laboratory from the original component materials. For the long-term aging of loose mix in the oven using the NC mix at 85°C, specimens were compacted following long-term aging for performance testing at two temperatures, 144°C (consistent with specifications for short-term aged material) and 157°C, to determine if the increased temperature aided the compactability of the mix. The latter temperature is the recommended temperature for compacting less workable mixtures fabricated with high PG binders following the equiviscosity and equiphase angle concepts presented in a study conducted by the National Center for Asphalt Technology (NCAT) (West et al. 2010) that used the SGC to produce 178-mm tall specimens.

Phase 2 – Verification of the Selected Aging Method

Selection of loose mixture aging was the eventual outcome of the Phase 1 aging trials. To verify the findings of Phase 1 using the NC mix, the Federal Highway Administration (FHWA) Accelerated Loading Facility (ALF) styrene-butadiene-styrene (SBS) modified mix, hereinafter referred to as 'FHWA ALF SBS', was used because it is known to be both difficult to compact and highly susceptible to hardening with oxidation (Gibson et al. 2012). Loose mixtures were prepared in the laboratory from the original component materials. Asphalt binder was extracted and recovered from a field core obtained after eight years in service at the FHWA ALF in McLean, VA for comparison to the loose mix aging trial results. Loose mix aging trials were conducted at 70°C, 85°C, and 95°C to determine the time required to match the level of oxidation of the surface layer of the field core at varying depths. To evaluate the integrity of the specimens that were compacted following loose mix aging, two laboratory aging conditions were considered: eight days at 85°C, consistent with Phase 1 of this study, and 21 days at 95°C, which was found to match the level of oxidation of the binder extracted from the surface of the field core. Note that this latter condition is thought to represent an 'extreme' level of oxidation, as oxidation levels dissipate drastically with the depth of the pavement. The conditioning temperature of 95°C was selected because it can expedite aging faster than 85°C but is not expected to lead to volatilization or degradation of the polymers (Petersen 2009).

Experimental Plan

Figure F-3 provides a summary of the experimental plan used to evaluate and select the most promising aging method. The experimental plan was designed to include high temperature conditioning of loose mixtures and compacted specimens with and without pressure. As previously mentioned, the experimental plan was divided to two phases: Phase I – Preliminary evaluation of aging methods, and Phase II – Verification of the selected aging method. For the compacted specimens, two geometries were considered: standard 100 mm diameter specimens and small specimen geometry 38 mm diameter. The small specimen geometry was suggested by the FHWA in its forensic evaluation of ALF pavements (Mbarki et al. 2012). It is important to note that performance assessment in this study was based on dynamic modulus and cyclic direct tension fatigue tests.

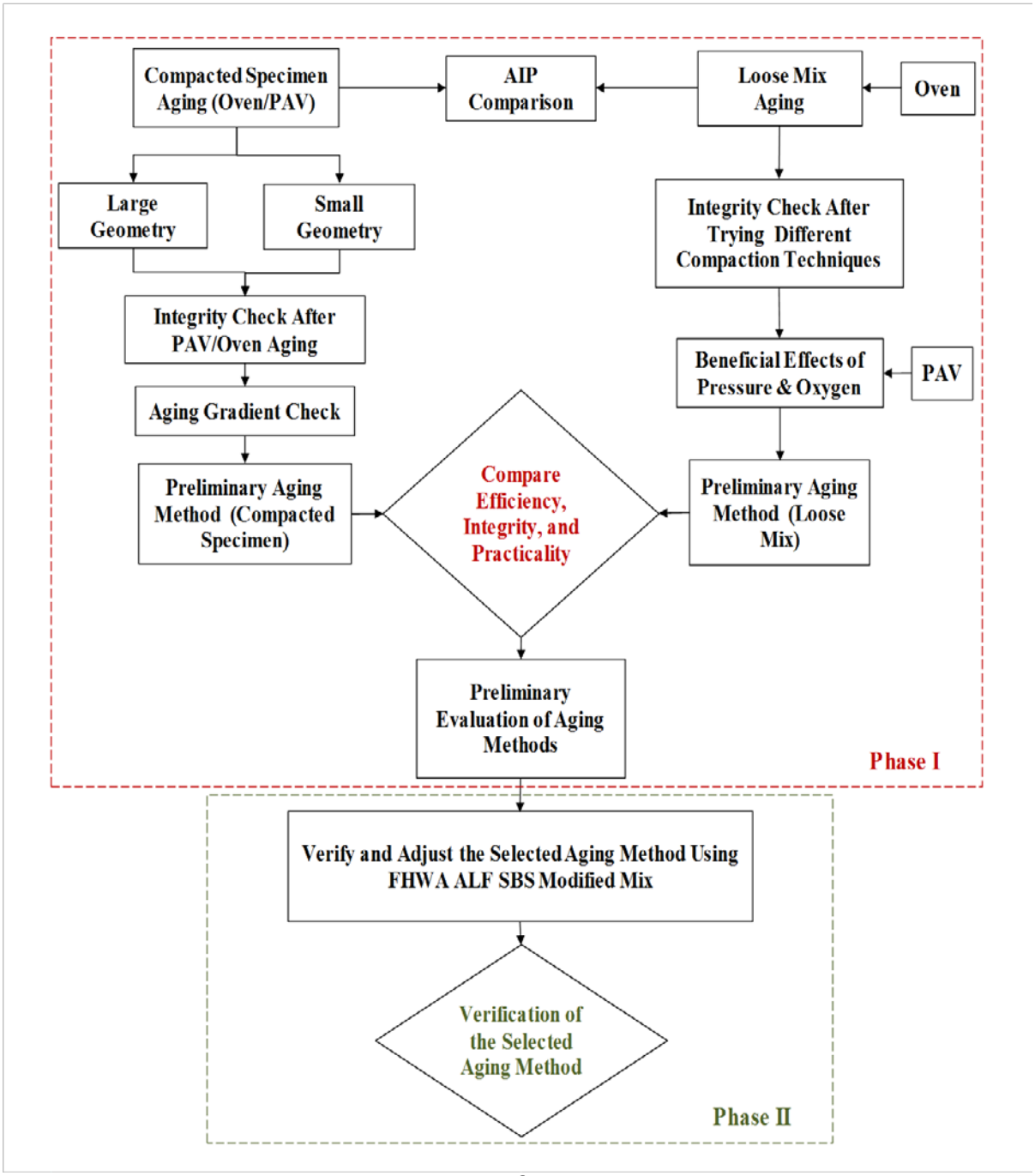

Figure F-3. Summary of the experimental plan.

Table F-3 provides a summary of the experiments conducted in this study. Note that only a subset of the aged materials was subjected to performance testing due to time constraints.

Table F-3. Summary of aging trials and naming scheme description

Mixture	Material		Aging Method	Temp. (°C)	Duration	Air Pressure (kPa)	Sample ID	Performance Testing*
NCS9.5B	Binder		RTFO	163	85 min	-	RTFO-NC	--
			PAV	100	20 hr	2100	PAV-NC	--
	Loose Mix		STA	135	4 hr	-	S-NC	Yes
			Oven	85	8 days, Compacted at 144°C	-	L-O-85-8D-NC-(C144)	Yes
				85	8 days, Compacted at 157°C	-	L-O-85-8D-NC-(C157)	Yes
			PAV	85	2 days	2100	L-P21-85-2D-NC	No
	Compacted Specimen	Small	PAV	85	1 day	300	C-P3-85-1D-NC-S	No
					3 days	300	C-P3-85-3D-NC-S	No
			Oven	85	8 days	-	C-O-85-8D-NC-S	No
		Large	PAV	85	1 day	300	C-P3-85-1D-NC-L	Yes
			Oven	85	8 days	-	C-O-85-8D-NC-L	Yes
FHWA ALF-SBS-LG	Binder		RTFO	163	85 min	-	RTFO-SBS	--
			PAV	100	20 hr	2100	PAV-SBS	--
	Loose Mix		STA	135	4 hr	-	S-SBS	Yes
			Oven	70	35 days	-	L-O-70-35D-SBS	No
				85	8 days	-	L-O-85-8D-SBS	Yes
					10 days	-	L-O-85-10D-SBS	No
				95	21 days	-	L-O-95-21D-SBS	Yes

*Performance testing was conducted only for a select set of aged specimens. Note: STA is short-term aging.

Results of Phase 1

Initial Integrity Check Results

Compacted Specimen Aging

The initial integrity checks of the compacted specimens included visual inspection, air void content, and dimensions of the specimens. In cases where integrity issues were encountered, remedial strategies were developed to eliminate air void content and dimensional integrity problems. These strategies are detailed in Table F-4.

Table F-4. Summary of findings from integrity check of compacted specimen long-term aging

Material State	Temperature	Pressure	Recommendation to Avoid Integrity Problems
Compacted Large Specimen	85°C	-	Wire mesh support used for specimens
Compacted Large Specimen	85°C	0.30 MPa	Specimen placed in a hammock-like support on its side
Compacted Small Specimen	85°C	-	Specimen placed in the oven on its side on a flat surface
Compacted Small Specimen	85°C	0.30 MPa	Controlled air pressure application considered and specimen placed on its side on a flat surface

The comparison of the specimen air void contents before and after aging are shown in Figure F-4 for the aging trials that utilized the strategies detailed in Table F-4. The results indicate that very minor air void changes occurred during the aging of both the small and large specimens with and without pressure. Note that the initial integrity checks for the small specimens aged in the oven at 85°C for eight days indicate that no wire mesh was needed to avoid geometry distortion due to the relatively low weight of the small specimens. In addition to the assessment of air voids, the dimensions of compacted specimens were measured before and after long-term aging to assess integrity. For each specimen, top and bottom diameters, height at three points, and straightness of specimen sides were evaluated. No dimensional changes were observed for the aging trials that utilized the strategies detailed in Table F-4.

However, visual changes were observed for all the specimens that were subjected to oven and PAV aging. A representative example of such visual change is shown in Figure F-5. It can be seen that the exposed aggregate particles appear largely to be coated in asphalt after aging. Although the reason for this visual change is not fully understood, it is thought to be related to the absorption of the binder by the aggregate at the elevated temperatures that were used during aging and/or bleeding of the asphalt binder to the surface of the mix. This visual change also has been reported by other researchers (e.g., Tarbox 2011). The research team speculates that aggregate porosity, binder viscosity, and mixture air void content may influence the visual change observed.

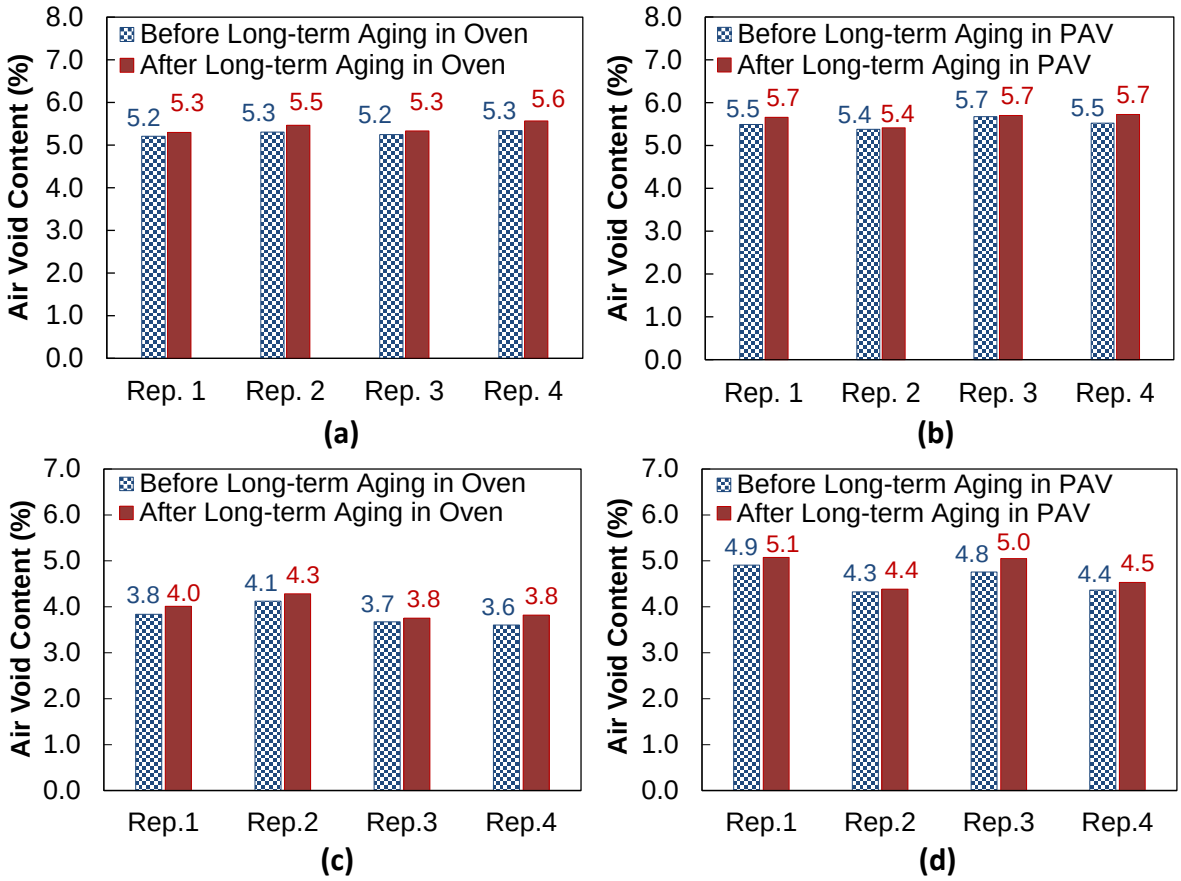

Figure F-4. void measurements for (a) large specimens (100 mm × 178 mm) before and after aging in the oven at 85°C for 8 days, (b) large specimens (100 mm × 178 mm) before and after aging in the PAV at 85°C, 300 kPa air pressure for 24 hours, (c) small specimens (38 mm × 100 mm) before and after aging in the oven at 85°C for 8 days, and (d) small specimens (38 mm × 100 mm) before and after aging in the PAV at 85°C, 300 kPa air pressure for 24 hours.

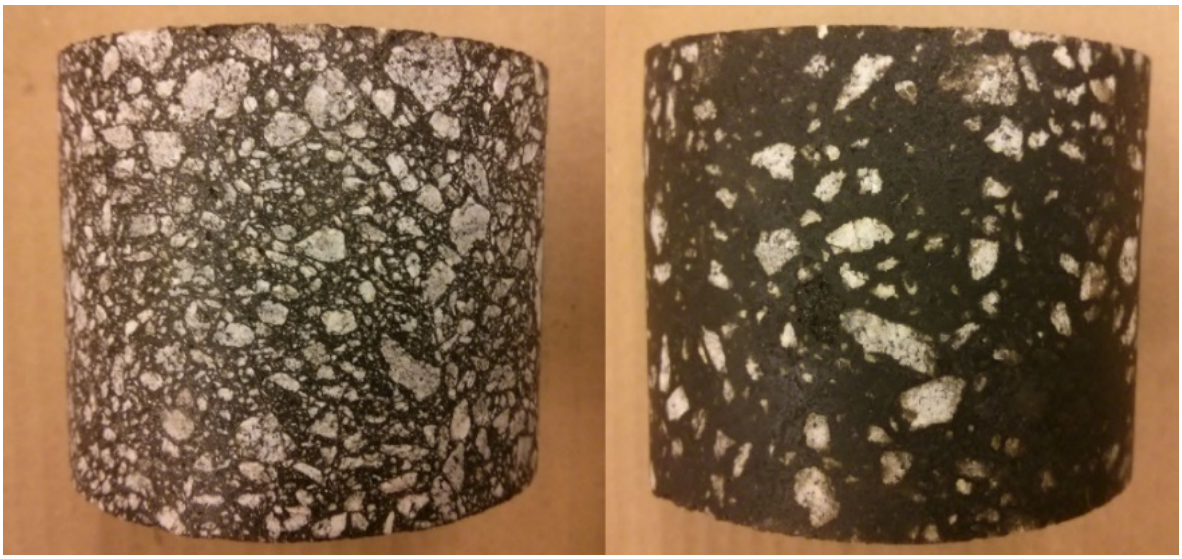

Figure F-5. NC mix specimen before (left) and after (right) long-term aging in the oven.

Loose Mix Aging

The number of gyrations needed to reach the target air void contents and analysis of the coarse aggregate structure were used as initial integrity checks for loose mix aging because the primary integrity concern was the ability to compact aged material for performance testing. Two compaction temperatures were tried: 144°C and 157°C. The numbers of gyrations required to reach the target air void contents for both the short-term and long-term aged materials are shown in Figure F-6. The results indicate no significant difference in the compaction effort required for the short-term and long-term aged materials. The results indicate that it is possible to compact aged loose mix with no adjustment to the compaction temperature.

As an additional check of specimen integrity, the coarse aggregate structures of the specimens that were compacted following the short-term aging and long-term aging (with compaction at 144°C) were analyzed using the image processing software, Image Processing and Analysis System (iPas), developed at the University of Wisconsin-Madison and Michigan State University (Kutay et al. 2010, Coenen et al. 2011, Roohi et al. 2011). To apply iPas, the samples were cut vertically to form four sections, as depicted in Figure F-7 (a). Using a scanner, two-dimensional images of the faces (numbers 2, 3, 4 and 5 shown in Figure F-7 (b)) were obtained and used as inputs for the iPas software. The iPas software outputs several quantities that can be used to quantify an aggregate structure, most notably the number of aggregate particle contacts and the contact length. A contact point is regarded as any point where two aggregate particles are in contact. The contact length is the length between the aggregate particle contacts. The iPas results are shown in Figure F-7 (c) and Figure F-7 (d). The results indicate no reduction in the number of contact points or contact length for the compacted aged material in this study, indicating no integrity problems associated with compacting the aged loose mix.

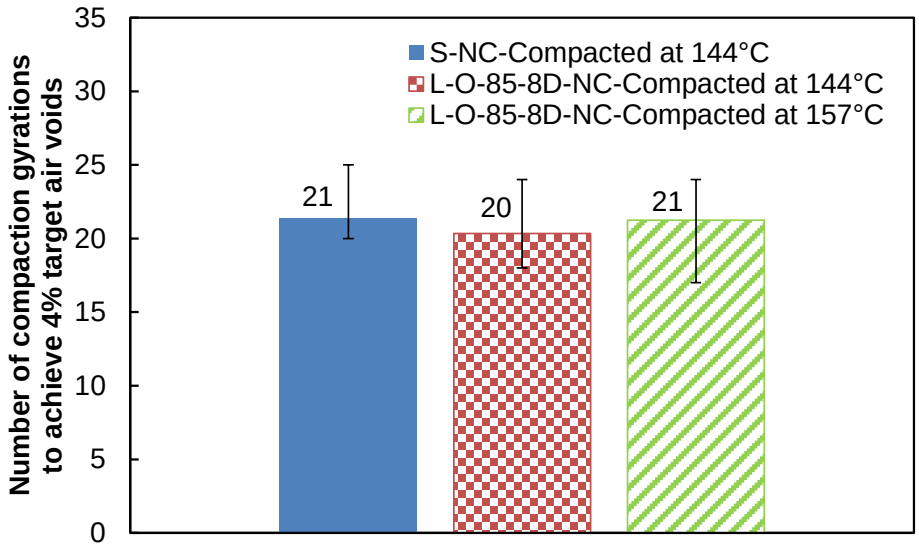

Figure F-6. Number of compaction gyrations required to achieve target air void content.

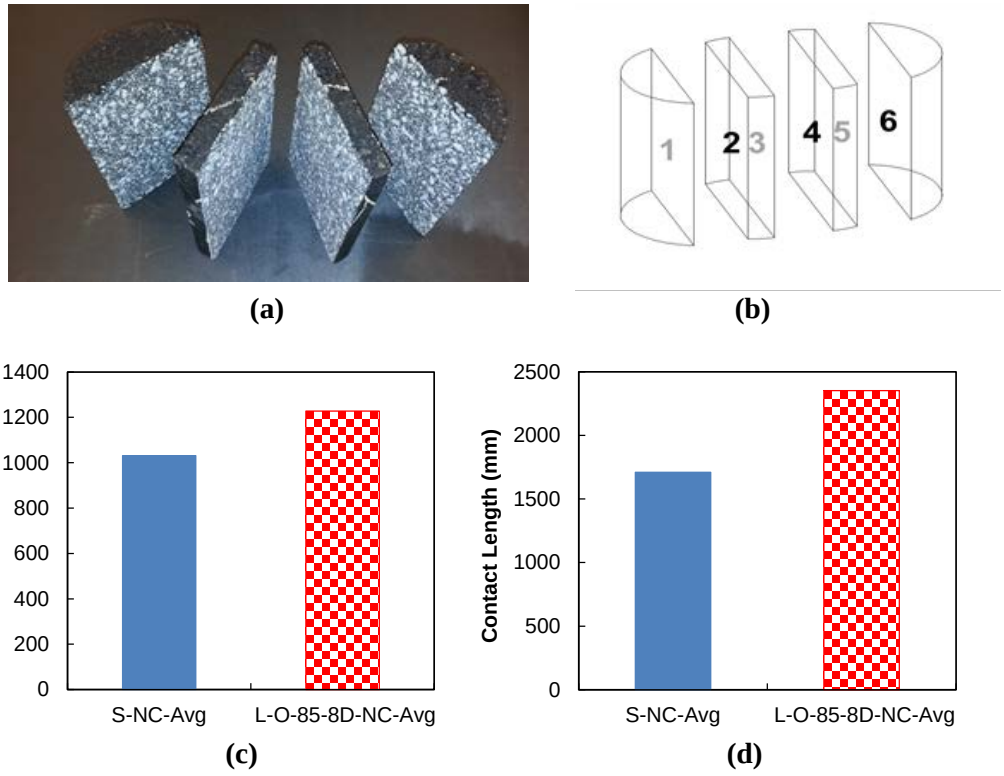

Figure F-7. Course aggregate structure assessment for integrity check of long-term aging trials performed on loose mix (NCS9.5B mix) using iPas software: (a) SGC sample prepared for scanning, (b) schematic shows faces analyzed using iPas (2,3,4, and 5), (c) comparison between the number of contact points of course aggregate structure, and (d) comparison between the total contact length calculated between course aggregates.

Performance Test Results

Following the initial integrity checks, the specimen integrity of the aged mixtures was assessed using performance testing. Only a limited number of aging conditions was selected for performance testing due to the time constraints detailed in Table F-3. For specimens that were aged using compacted specimen aging, the strategies detailed in Table F-4 were utilized to minimize integrity issues.

Dynamic Modulus Results

The dynamic modulus mastercurves are shown in Figure F-8. The results presented in Figure F-8 correspond to the average values of two replicates. No meaningful difference is evident between the dynamic modulus values of the short-term aged and PAV-aged compacted specimens, indicating that either (a) no significant aging occurred or (b) the application of pressure damaged the specimens. The specimens aged using other methods show a significant increase in dynamic modulus values.

Loose mix aging led to slightly higher dynamic modulus values than compacted specimen aging in the oven for the same duration, indicating that aged loose mix can be compacted for performance testing. In addition, these results suggest that higher levels of oxidation can be achieved using loose mix aging compared to compacted specimen aging, given the same temperature and duration of conditioning in an oven. The compaction temperature utilized for the aged loose mixes had little effect on the dynamic modulus values.

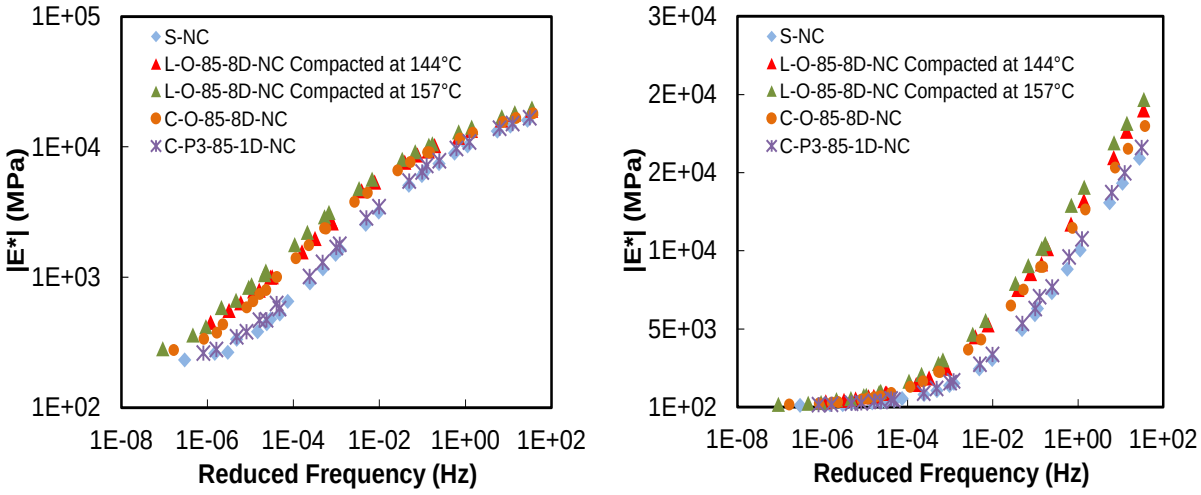

Figure F-8. Dynamic modulus test results: (a) log-log scale and (b) semi-log scale.

Fatigue Performance Testing Results

Figure F-9 presents the damage characteristic curves obtained from the S-VECD model analysis of the cyclic direct tension test results for both the short-term and long-term aged materials. In accordance with AASHTO TP 107-14, each material was tested at three different

cross head displacement amplitudes that are expected to yield to fatigue lives (N_f) that falls in specific ranges as follows: N_f less than 5000 cycles, N_f between 5000 and 25000 cycles, and N_f greater than 25000 cycles. Typically, damage characteristic curves are used to describe the relationship between material integrity and damage and are path-independent (i.e., independent of loading and thermal history). The curves presented in Figure F-9 represent the average of the curves obtained from three different crosshead displacement amplitudes used in the tests. The damage characteristic curves of the stiffer materials usually are higher than the damage characteristic curves of the softer mixtures, as demonstrated also in Hou et al. (2010) and Norouzi et al. (2015). Because aging is expected to increase the stiffness of asphalt mixtures, it is expected that the damage characteristic curves of the long-term aged mixtures would be higher than those of the short-term aged mixtures, unless an integrity problem existed in the specimen. The results demonstrate that all the oven-aged specimens (both aged loose mix and aged compacted specimens) have higher damage characteristic curves than the short-term aged specimens, indicating no integrity issues. In other words, the compaction of aged loose mix does not appear to lead to integrity problems. Furthermore, the results of the long-term aged loose mixture trials show similar damage characteristic curves regardless of the compaction temperature, indicating that specimen integrity can be achieved without elevating the compaction temperature. In addition, the results show that the oven-aged loose mix specimens have slightly higher damage characteristic curves than the oven-aged compacted specimens, which is consistent with the dynamic modulus test results.

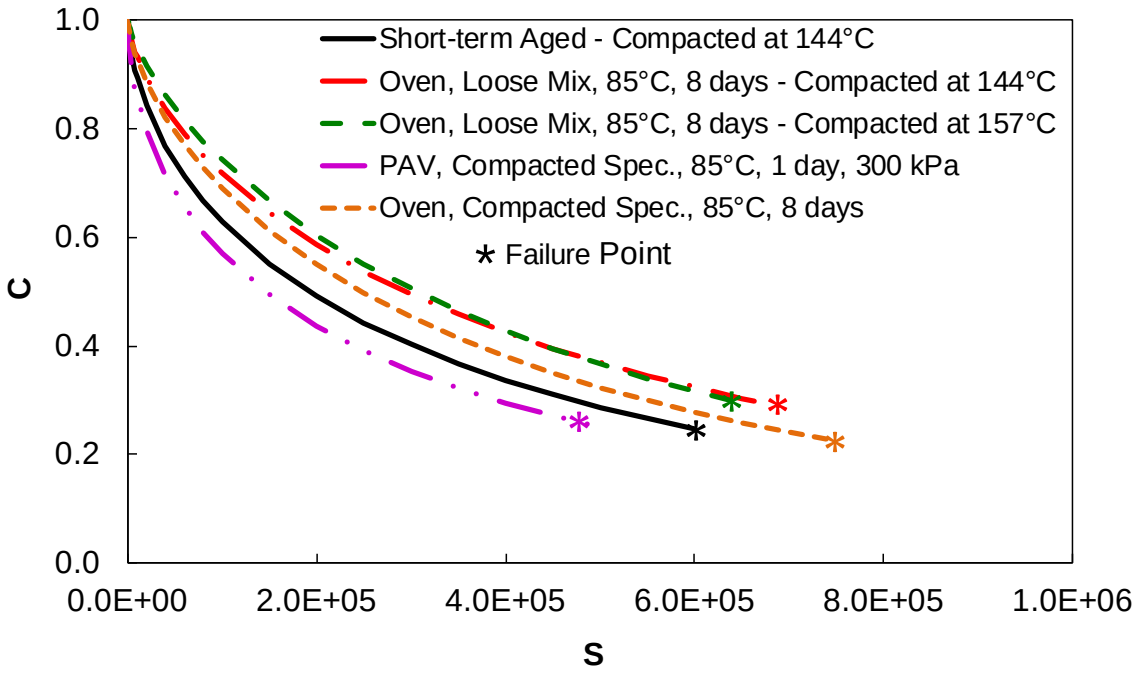

Figure F-9. Comparison of damage characteristic curves from the NC mixtures subjected to different aging conditions.

The research team compared two sets of specimens for the compacted specimens that were subjected to oven aging: aged 178-mm tall specimens, whereby the specimen ends were cut following aging to reduce the height to 130 mm for testing, and 130-mm tall specimens aged in the oven following cutting the ends of the specimens. The damage characteristic curves were

similar for the two sets of samples. However, the specimens that were aged at a height of 130 mm (i.e., ends cut before aging) demonstrated a high propensity for end failure, indicating a higher level of oxidation at the ends of the specimen and, hence, a testing concern. The damage characteristic curves of the PAV-aged compacted specimens lie below those of the short-term aged specimens, indicating that the specimens were damaged by the application and/or release of pressure during aging. Thus, the application of pressure when aging compacted specimens should be avoided.

A new fatigue failure criterion, so-called D^R, (Wang and Kim 2017) was used to evaluate mixtures with different aging levels. The D^R criterion uses the average reduction in pseudo stiffness (i.e., C) up to failure. The D^R value is calculated as the summation of $(1 - C)$, illustrated in Figure F-10, divided by the fatigue life (number of cycles to failure) for individual test replicates. D^R is a material constant that is independent of mode of loading, temperature, and stress/strain amplitude. Note that the calculation of D^R is in arithmetic scale rather than in log-log scale. Consequently, D^R results are not as much affected by test variability as another pseudo energy based failure criterion, so-called G^R, that is calculated in log-log scale (Sabouri and Kim 2014).

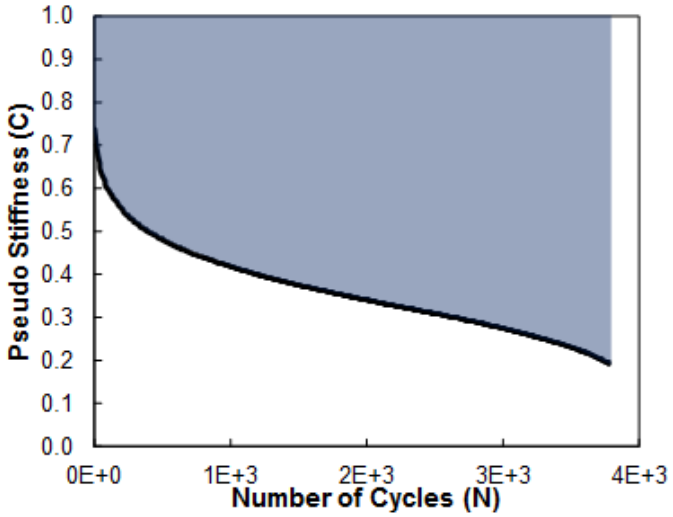

Figure F-10. Illustration of summation of (1-C).

Figure F-11 depicts the D^R energy-based failure criterion plots. Average D^R values for different aging conditions are presented in Table F- 5. For severely aged materials, it is anticipated that the D^R failure criterion lines will fall below those of short-term aged materials due to the loss of fatigue resistance associated with embrittlement imposed by oxidation. Any integrity problem in the specimens is also expected to result in lower D^R values. Thus, the failure criterion results for the PAV-aged compacted specimens indicate a potential integrity problem, as the dynamic moduli values for the PAV-aged compacted specimens were lower than those from the short-term aged mixtures. All the other failure criterion lines fall close to that of the short-term aged materials, which indicates no integrity problems.

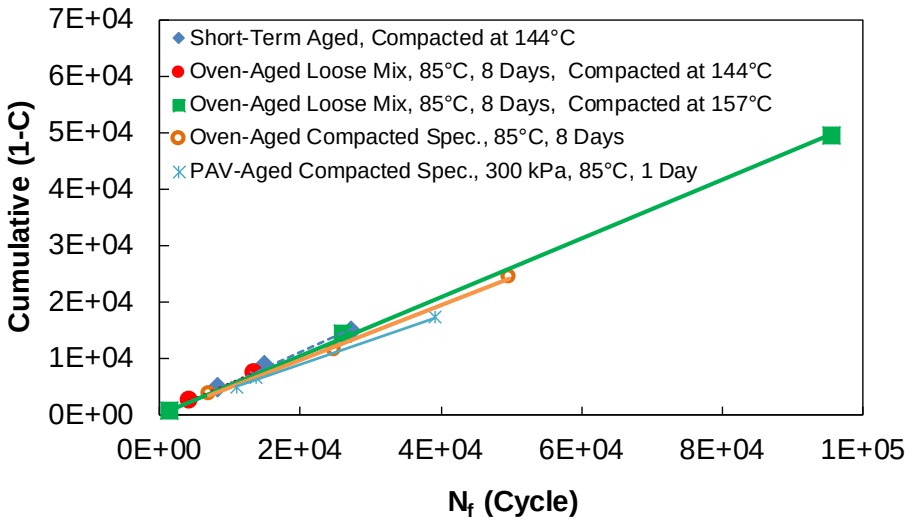

Figure F-11. D^R failure criterion lines of NC mix subjected to different aging conditions.

Table F- 5. Average DR values for NC mix subjected to different aging conditions

Mix ID	Average D^R
Short-Term Aged, Compacted at 144°C	0.574
Oven-Aged Loose Mix, 85°C, 8 Days, Compacted at 144°C	0.541
Oven-Aged Loose Mix, 85°C, 8 Days, Compacted at 157°C	0.535
Oven-Aged Compacted Spec., 85°C, 8 Days	0.494
PAV-Aged Compacted Spec., 300 kPa, 85°C, 1 Day	0.454

Evaluation of Aging Gradient in Compacted Specimen Aging

In compacted specimen aging, the oxygen diffusion from the periphery to the specimen center is impeded by the binder film and aggregate, thus leading to a high possibility of an oxidation gradient within specimens aged in a compacted state. The extraction and recovery of binder from differing distances from the periphery of compacted specimens following long-term aging allows for the assessment of aging gradients. This assessment was accomplished in this study by first coring and cutting the specimens into slices from which the binder was recovered. For the small specimens, the outer segments were obtained by slicing the specimens vertically, as depicted in Figure F-12 (a). The large specimens were cored using a 38-mm core bit and 75-mm core bit to obtain radial slices, as shown in Figure F-12 (b). Binder extraction and recovery was carried out only for the outer layer, middle layer, and core of the oven-aged large specimens.

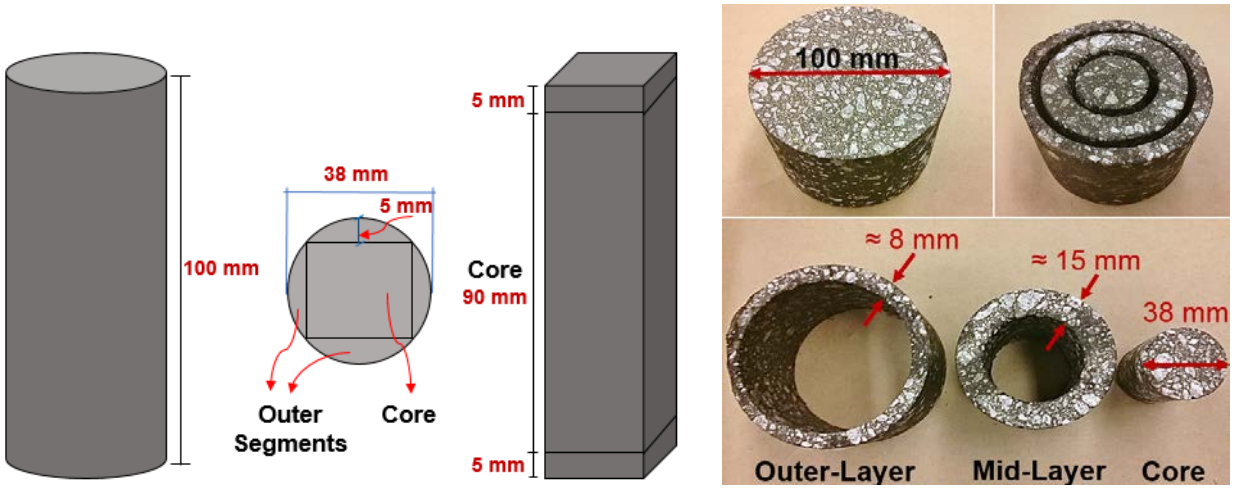

(a) **(b)**

Figure F-12. Schematics of components used to evaluate oxidation gradients: (a) components of small specimen (38 mm × 100 mm) and (b) components of large specimen (100 mm × 150 mm).

The results of the AIP tests of the different specimen components for all the compacted specimen aging trials are shown in Figure F-13 (Note that the logs of the dynamic shear modulus test results are presented to facilitate a comparison to the C+S absorbance peaks results). Considering the two percent threshold for significant changes in carbonyl + sulfoxide absorbance, the results indicate that significant oxidation occurred during all the compacted aging trials, as evident by the increase in the carbonyl + sulfoxide absorbance and dynamic shear modulus values between the long-term and short-term aged materials (uncompacted S-NC-UC); however, the extent of aging that was achieved is slightly less than that between the RTFO aged and PAV aged binder. The AIP measurements for the binders that were extracted and recovered from the different layers of the large specimens that were long-term aged in the oven (8 days at 85°C) reveal significant changes between the cores and outer portions of the specimens in terms of both rheological and chemical AIPs, thereby indicating the existence of an aging gradient within the specimens. The small specimens aged in the oven exhibited levels of oxidation that are similar to those of the large specimens, based on the AIP values. However, the AIP values for the binders extracted and recovered from the outer segments and from the cores of the small specimens that were long-term aged in the oven (8 days at 85°C) indicate no significant aging gradient, thus confirming that shorter diffusion paths can mitigate oxidation gradient concerns. The small specimens aged in the PAV show a higher level of oxidation than the oven-aged specimens, based on the binder dynamic shear modulus values and FTIR spectra, indicating that pressure does expedite the oxidation of the mixtures, as these PAV specimens were aged for only three days at 85°C compared to oven-aged specimens that were conditioned for eight days. However, for the small specimens aged in the PAV (3 days at 85°C and 300 kPa), a significant aging gradient can be observed based on the chemical and rheological AIPs, indicating that pressure does not alleviate the effects of an oxidation gradient.

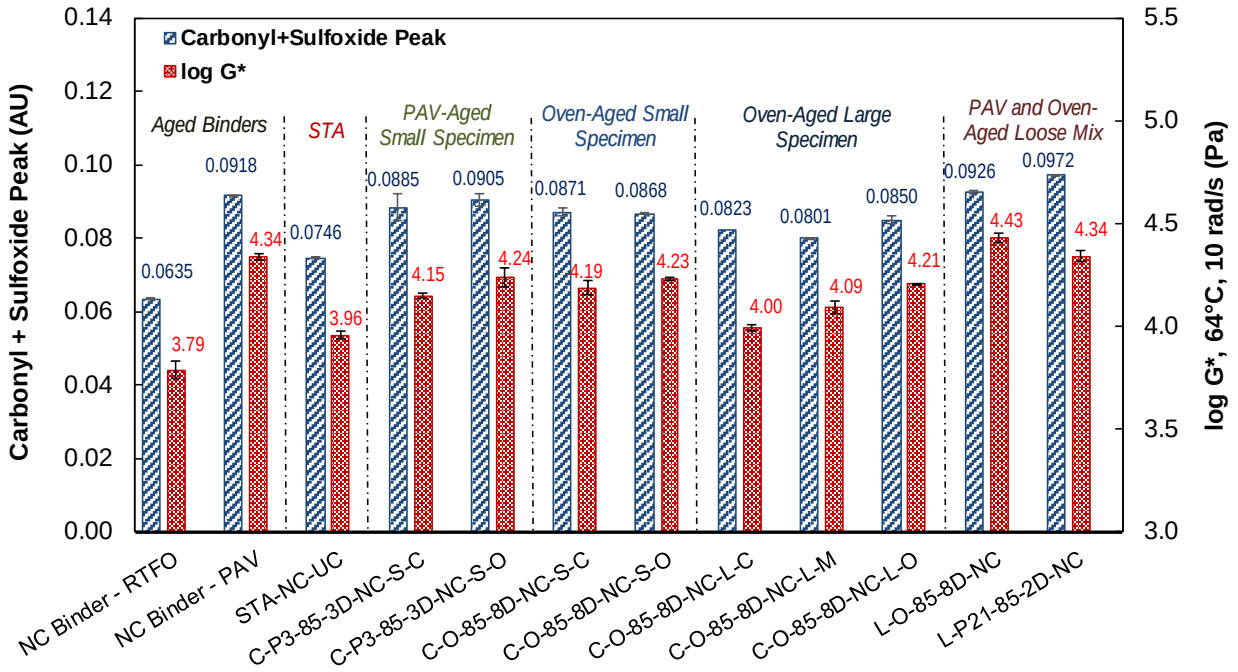

Figure F-13. Comparison between C+S absorbance peaks and log G* at 64°C and 10 rad/s for extracted and recovered binders from different compacted specimen aging processes, loose mix aging trials, and aged binders.

Evaluation of Aging Efficiency of Loose Mix and Compacted Specimen Aging with and without Pressure

In addition to evaluating the aging gradients in the compacted specimens, the AIP measurements of the binders extracted from both the aged loose mix and compacted specimens were used to assess the relative rate at which the different methods oxidized the binder. The AIP results of all the long-term aging trials in addition to those of the short-term aged mix and the asphalt binder aged using standard methods are provided in Figure F- 14. The results demonstrate first that the level of oxidation in the short-term aged mixtures surpasses the level of oxidation produced by the RTFO-aged binder. As discussed, the oven aging of the compacted specimens, both large and small, at 85°C for eight days (i.e., SHRP-A-390 recommendations for long-term aging level 3 (Bell et al. 1994b)) led to oxidation levels that were somewhat lower than those of the PAV aged binder. The application of pressure to the compacted specimens during aging expedited the oxidation process, as discussed, but led to integrity problems in terms of both the aging gradient and the damaging effects that can affect performance test results. The long-term aging of the loose mix in an oven for eight days at 85°C led to a level of oxidation based on chemical and rheological AIPs that exceeded that of the oven aging of the compacted specimens for the same duration and also exceeded the level of RTFO+PAV binder aging. Thus, aging loose mix appears to expedite oxidation significantly compared to aging compacted specimens. The long-term aging of the loose mix in the PAV for two days at 85°C and 2.1 MPa led to a level of oxidation similar to that of the loose mix oven aging for eight days at the same temperature. These results suggest that the addition of pressure can greatly expedite aging almost four times faster than a conventional oven for aging. However, it is important to note that a standard binder PAV does not allow sufficient space for aging sufficient quantities of material

for performance testing in a single trial. Thus, if PAV aging of loose mix were to be adopted for this project, a new (larger) PAV would have to be developed.

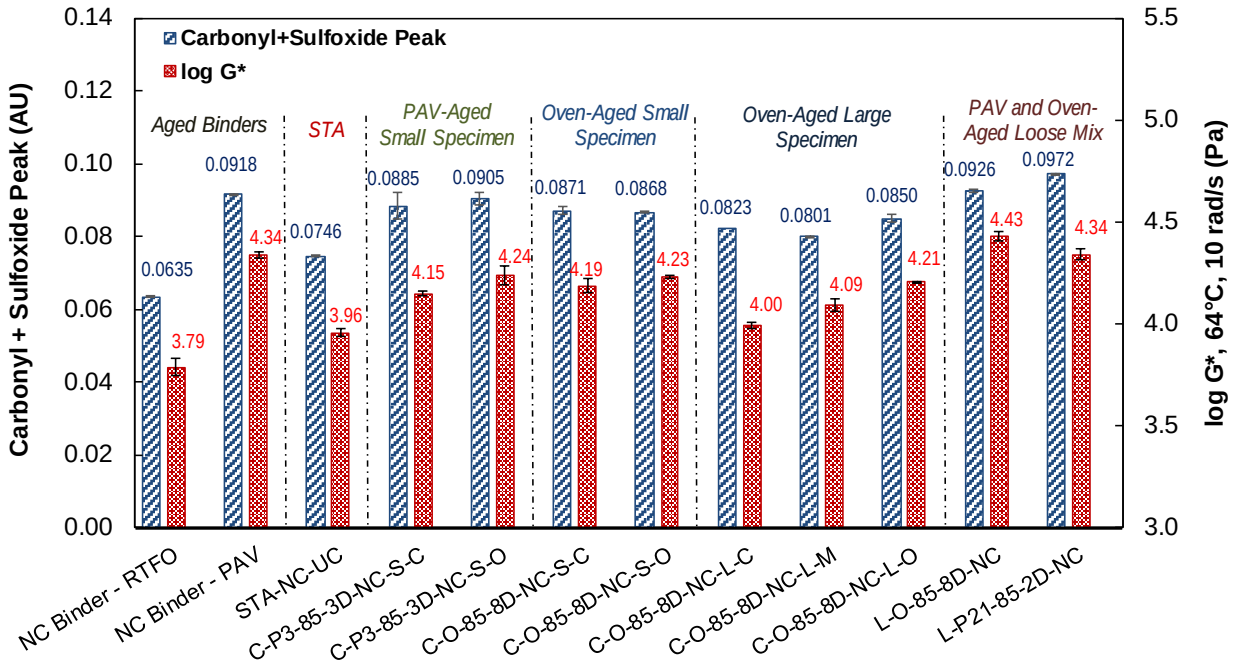

Figure F- 14. Comparison between carbonyl+sulfoxide absorbance peaks and log G* at 64°C and 10 rad/s for extracted and recovered binders from different compacted specimen aging processes, loose mix aging trials, and aged binders.

Figure F-15 presents the correlations between log G* at 64°C and 10 Hz and the C+S absorbance peaks for the binders extracted and recovered from the NC mixes aged in the oven. The results indicate a strong relationship between each rheological AIP and C+S absorbance peaks and thus suggest that both rheology and chemistry can be used as oxidation level indicators.

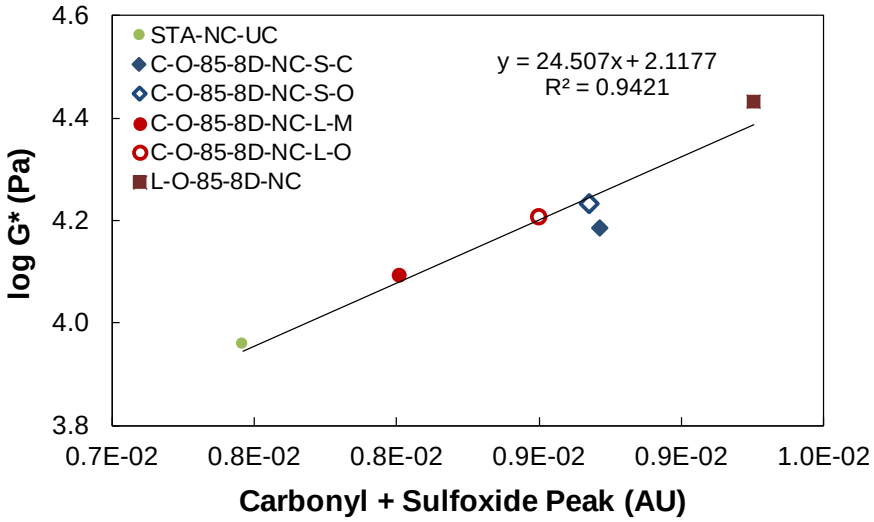

Figure F-15. Correlations between log G* and C+S absorbance peaks for binders extracted and recovered from aged NC mix.

In summary, the Phase 1 results indicate that aging large (100-mm diameter) compacted specimens with and without pressure leads to the development of an aging gradient within the specimen. The lack of uniform properties throughout the specimen is of concern for performance testing. Aging small specimens (38-mm diameter) in an oven shortens the diffusion paths and eliminates the development of oxidation gradients in specimens. However, this aging approach precludes the use of test geometries other than 38-mm diameter cylinders. In addition, the performance test results of the long-term aged compacted specimens in the PAV indicate that the application and/or release of pressure can damage specimens, which thereby precludes their use for performance testing. The compaction of long-term aged loose mix is possible without adjustment to the compaction temperature without negatively impacting performance based on findings of dynamic modulus and S-VECD testing. In addition, aging loose mix is more efficient than aging compacted specimens due to the increased surface area of the binder film that is exposed to oxygen. Also, pressure expedites loose mix aging. However, the current binder PAV does not allow sufficient quantities of mix to be aged for efficient performance testing. Therefore, the oven aging of loose mix is expected to be the most promising method for long-term aging of asphalt specimens for performance testing.

Results of Phase 2

Evaluation of Loose Mix Aging Conditions Required to Match Oxidation Level of Eight-Year-Old Field Core

The eight-year-old field core obtained from the FHWA ALF was cut (sawn) to obtain three half-inch thick slices, as shown in Figure F-16. The asphalt binder was extracted and recovered from the field core slices, and the AIPs were determined. The results were used to evaluate the oxidation level of the field core in terms of depth for comparison to the oxidation levels of the laboratory-aged samples. The C+S absorbance peaks and G* at 64°C and 10 Hz frequency results are shown in Figure F-17. The results demonstrate that a significant oxidation

gradient was found within the field core, with the surface of the field core being oxidized more severely than deeper within the pavement.

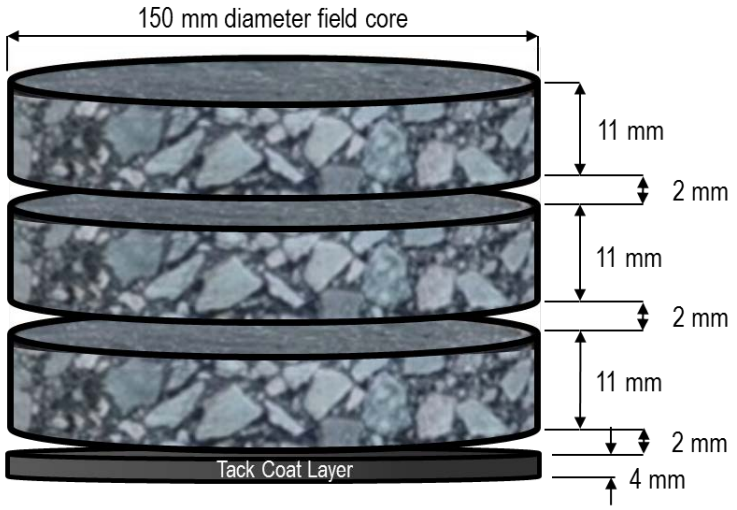

Figure F-16. ALF-SBS field core: top layer slicing details.

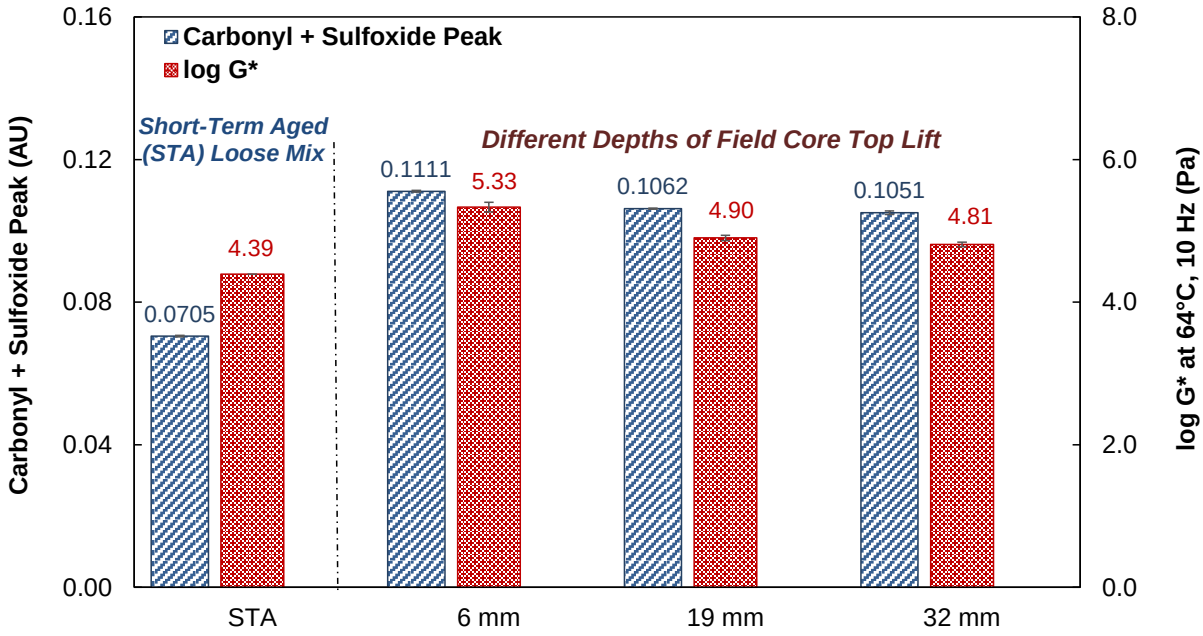

Figure F-17. Chemical and rheological AIP results of field core aging gradient after eight years of service in McLean, VA.

C+S absorbance peaks was used as the AIP to compare the lab- and field-aged materials in order to select the laboratory aging conditions that correspond to those of the field core. Samples that were subjected to extraction and recovery after varying durations of oven conditioning at three different aging temperatures, 70°C, 85°C, and 95°C, were used to establish the laboratory oxidation rates by linear fitting and to determine the oven conditioning time required to match the oxidation level of the field core. The linear fitting was deemed reasonable,

as only data points following the initial oxidation 'spurt' were utilized. The results of the laboratory aging trials are presented in Figure F-18. These results demonstrate that, as the temperature decreased, oxidation occurred at a slower rate, as expected.

Table F-6 shows the aging durations for each temperature that were needed to meet the oxidation level of each field core slice. For example, the results indicate that at the conditioning temperature of 85°C, 41 days of oven conditioning were required to match the level of aging of the surface of the field core. These results, although limited, indicate that the AASHTO R 30 test protocol, which specifies five days of oven conditioning for compacted specimens, greatly underestimates field aging, especially considering the fact that compacted specimen aging leads to substantially lower oxidation rates than loose mix aging. The results at 70°C and 85°C indicate that unreasonable durations of oven conditioning would be required to match the field core conditions. Thus, aging at 95°C appears to be the most reasonable conditioning temperature and is not anticipated to alter the oxidation reactions, lead to volatilization, or degrade the polymers, which can occur if temperatures that exceed 100°C are used (Petersen and Glaser 2011, Petersen 2009, Herrington et al. 1994). However, the performance implications of laboratory aging at temperatures above 100°C merits further investigation.

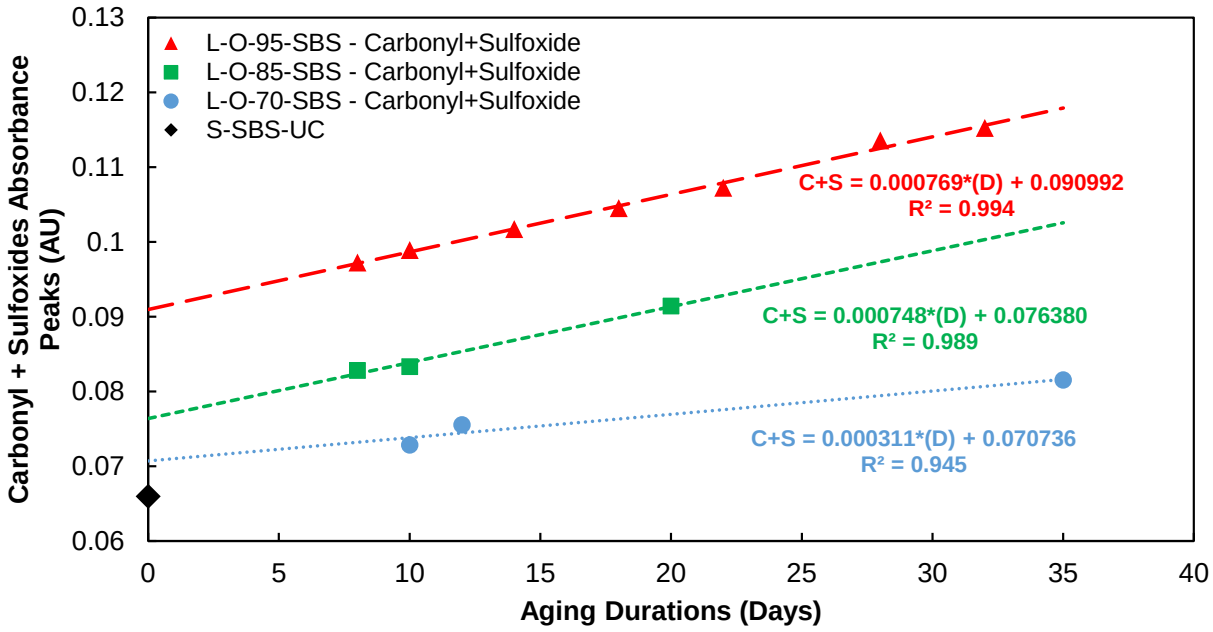

Figure F-18. Constant (slow) rate fitting of loose mix aging at different aging temperatures based on carbonyl + sulfoxides absorbance peaks.

Table F-6. Required aging durations at different temperatures to meet field aging levels at different depths

Field core slice (average depth from surface)	Target C+S Peaks (AU)	Target C+S Peaks before reheating for compaction	Required aging durations to meet field aging level (days)		
			95°C	85°C	70°C
T1 (6 mm)	0.11112	0.10712	21	41	117

T2 (19 mm)	0.10622	0.10222	15	35	101
T3 (32 mm)	0.10512	0.10112	13	33	97

The estimated oxidation levels for loose mix aging at 95°C that would be needed to match the level of oxidation of the field core at different depths are presented graphically in Figure F-19. Even at 95°C, 21 days of oven conditioning would be needed to match the level of oxidation of the surface of the field core. However, it is worth noting that the smallest sample utilized in the performance testing was 38 mm in diameter. Thus, if one considers that in order to extract horizontally a small specimen Ø38 mm × 100 mm for the performance testing of field cores, which would comprise the smallest specimen utilized, the representative aging level for a depth of 38 mm would be close to the oxidation level at a depth of 19 mm. This outcome would indicate that 15 days would be required for loose mix aging to match the age level of an eight-year-old field core in VA. Additionally, for structural modeling and analysis purposes (e.g., using the Layered Viscoelastic Pavement Analysis for Critical Distresses (LVECD) program), typically the averaged properties of each layer are used as inputs. Therefore, for this study, laboratory-prepared samples were aged in order to meet the average level of aging of each layer (in this case, 15 days of aging at 95°C). Based on these results, the oxidation level of the surface is considered to be a severe condition, because oxidation greatly dissipates with depth. Thus, the research team assessed loose mix aged at 95°C for 21 days as an 'extreme' condition for evaluating the compactability and integrity of aged loose mix.

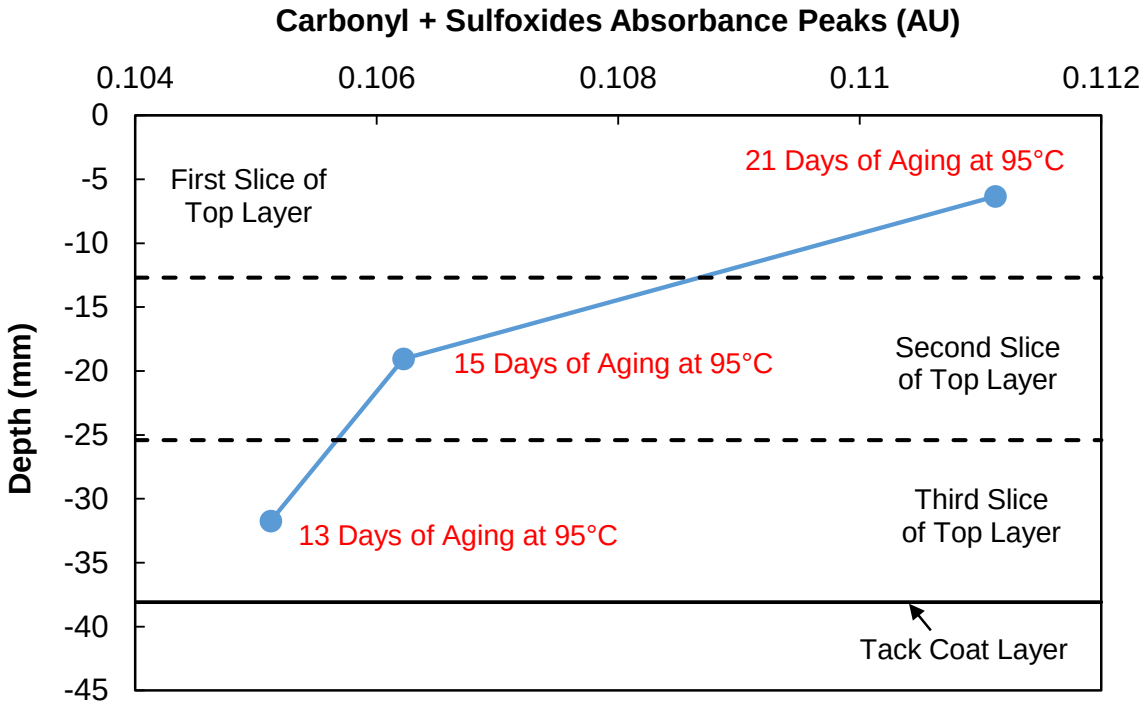

Figure F-19. Comparison between field core aging gradient with respect to depth and long-term aging of loose mix in oven at 95°C.

Figure F-20 presents comparisons of the degree of aging using the C+S absorbance peaks and G* AIPs among the aged loose mix used for the compacted specimen integrity assessment, the short-term aged mix, and binders aged in the RTFO and PAV. The results demonstrate that 21 days of loose mix conditioning at 95°C greatly exceeds the oxidation level of the binder PAV, which is comparable to eight days of loose mix aging at 85°C.

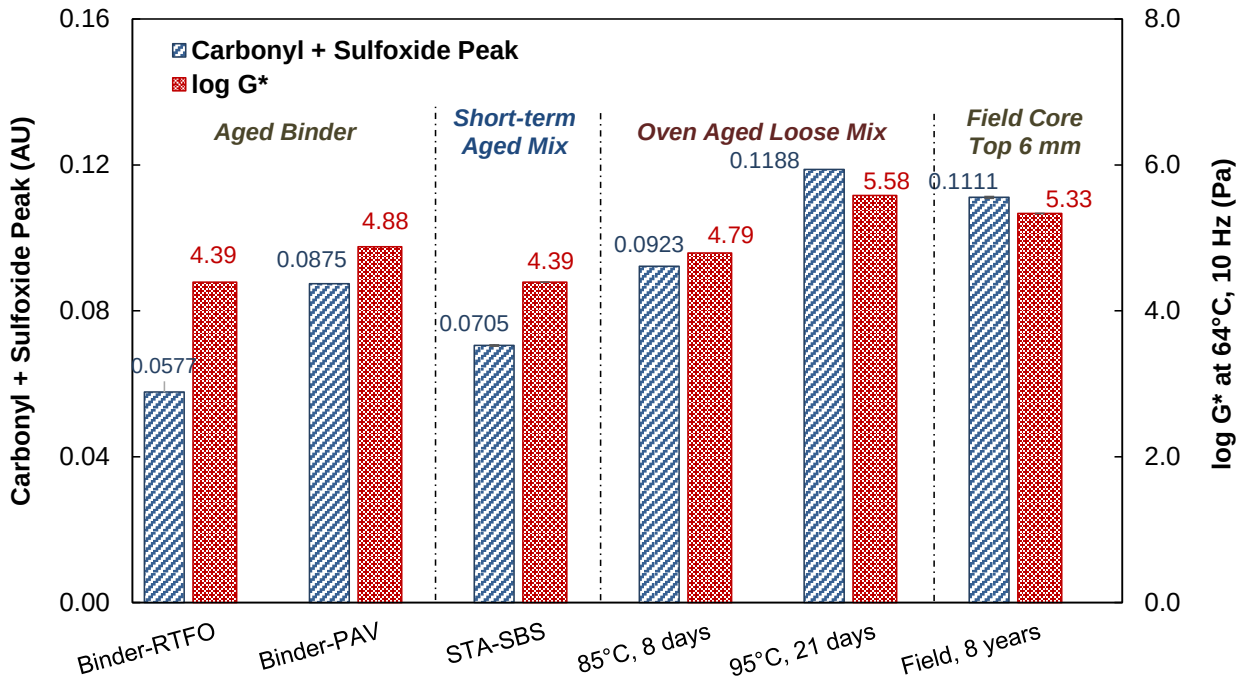

Figure F-20. Comparisons between C+S absorbance peaks and log G* at 64°C and 10 Hz for extracted and recovered binders from different loose mix aging trials, field core top layer surface slices, and aged binders (SBS-modified mixture).

Figure F-21 shows the correlation between log G* at 64°C and 10 Hz and C+S absorbance peaks, for the binders extracted and recovered from the ALF-SBS-LG mix field core and from the loose mix aging trials in the oven at two different temperatures. Based on the limited results presented in Figure F-21, the dynamic shear modulus values show a strong aging temperature-independent relationship with the C+S absorbance peaks, with the field core extracted data points falling relatively close to the laboratory aging trial data points.

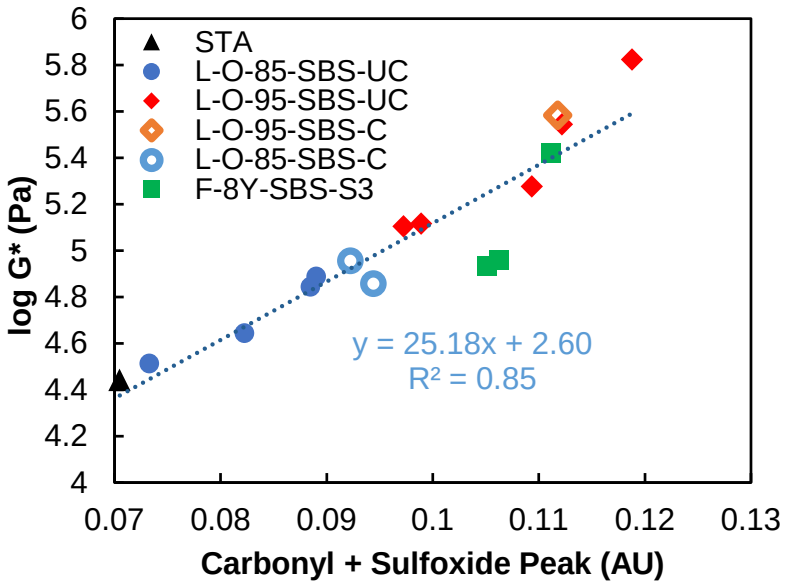

Figure F-21. Correlation between log G* and C+S absorbance peaks for binders extracted and recovered from aged ALF-SBS-LG mix.

Initial Integrity Check

The compactability of the long-term aged FHWA ALF SBS mix was evaluated as an initial specimen integrity check by comparing the number of gyrations needed to reach the target air void content to the number needed for the short-term aged materials. The results are shown in Figure F- 22. The number of gyrations needed to reach the target air void contents is similar for both the short-term aged mix and the two levels of long-term aged loose mixture (8 days at 85°C and 21 days at 95°C) with no adjustment of the compaction temperature. Thus, the compaction of the long-term aged loose mix was not problematic.

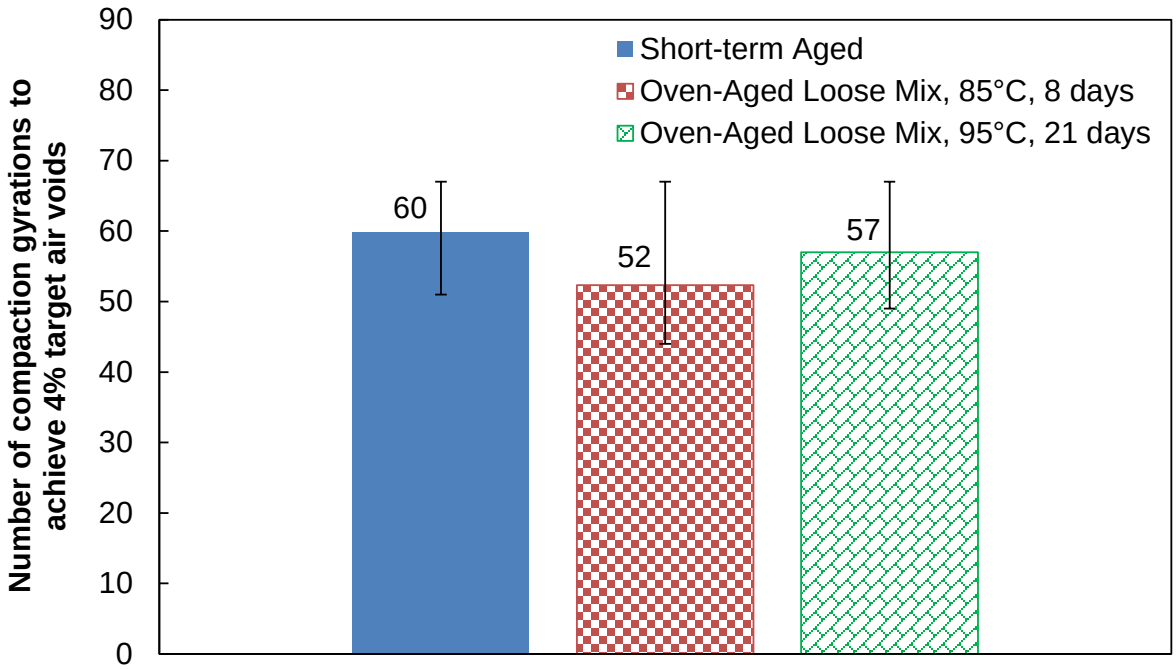

Figure F- 22. Number of compaction gyrations required to achieve the target air void content.

Performance Test Results

Performance testing was utilized as an additional means to evaluate the integrity of the FHWA ALF SBS specimens that were compacted following long-term loose mix aging. Comparisons between the dynamic modulus and S-VECD model damage characteristic curves of the short-term aged material and the long-term aged material were used to evaluate the specimen integrity of the compacted long-term aged material based on adherence to expected trends with increased aging.

Dynamic modulus test results

The dynamic modulus mastercurves are shown in Figure F-23. The mastercurves represent the averaged values of two replicates. The results indicate that the oven-aged loose mix specimens have higher dynamic modulus values than the short-term aged specimens. Furthermore, the results suggest that the specimens that were compacted after 21 days of oven aging at 95°C have significantly higher dynamic modulus values than the specimens compacted after eight days of oven aging at 85°C, as was expected based on the AIPs. If severe integrity problems had been present in the long-term aged specimens, then the dynamic modulus values would not be significantly higher than those of the short-term aged specimens, regardless of the aging level (because damage in the specimen reduces the dynamic modulus value), and thus, no integrity problems were detected in the dynamic modulus test results.

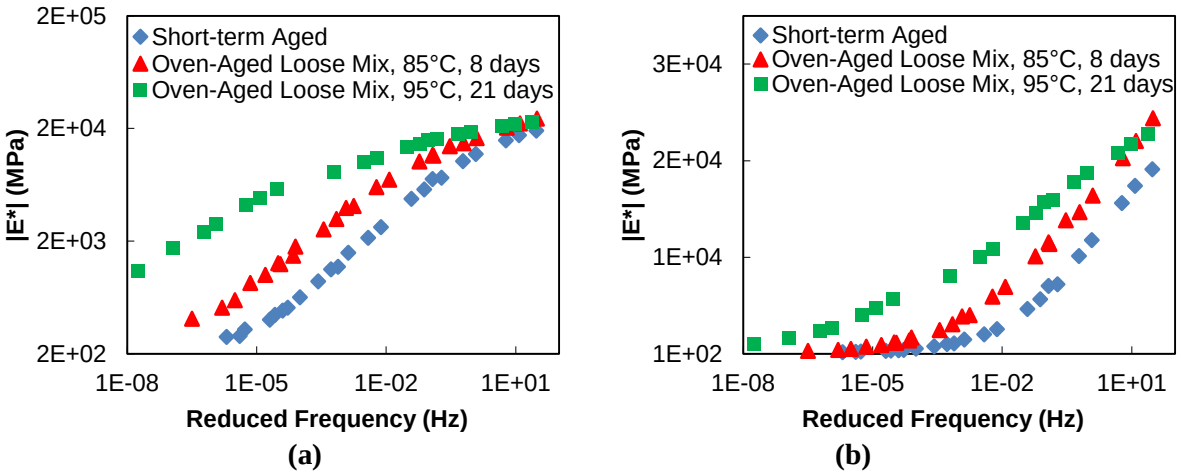

Figure F-23. Dynamic modulus test results: (a) log-log scale and (b) semi-log scale.

In order to evaluating the integrity of the specimens that were compacted following long-term loose mix aging, binder samples were extracted and recovered from the tested specimens, and the dynamic shear modulus values of these binder samples were input into existing asphalt concrete dynamic modulus prediction models to determine, as an additional means of integrity assessment, if the measured mixture dynamic modulus values were in the expected range based on the asphalt binder dynamic shear modulus values. The modified Witczak model (Bari et al. 2006), Hirsch model (Christensen et al. 2003), and the North Carolina State University Artificial Neural Network (NCSU ANN) model (Sakhaei Far 2011) were used to accomplish this task. Figure F-24 presents the comparisons between the model predictions and the measured dynamic modulus values at 20°C and 10 Hz. The results demonstrate that the measured dynamic modulus values of the long-term aged material are within the range of the model predictions based on the binder properties, thereby indicating that the results are reasonable. The research team surmises that if the long-term aged specimens had had an integrity problem, the measured dynamic modulus values of these specimens would have been lower than the expected values commonly used in the predictive models.

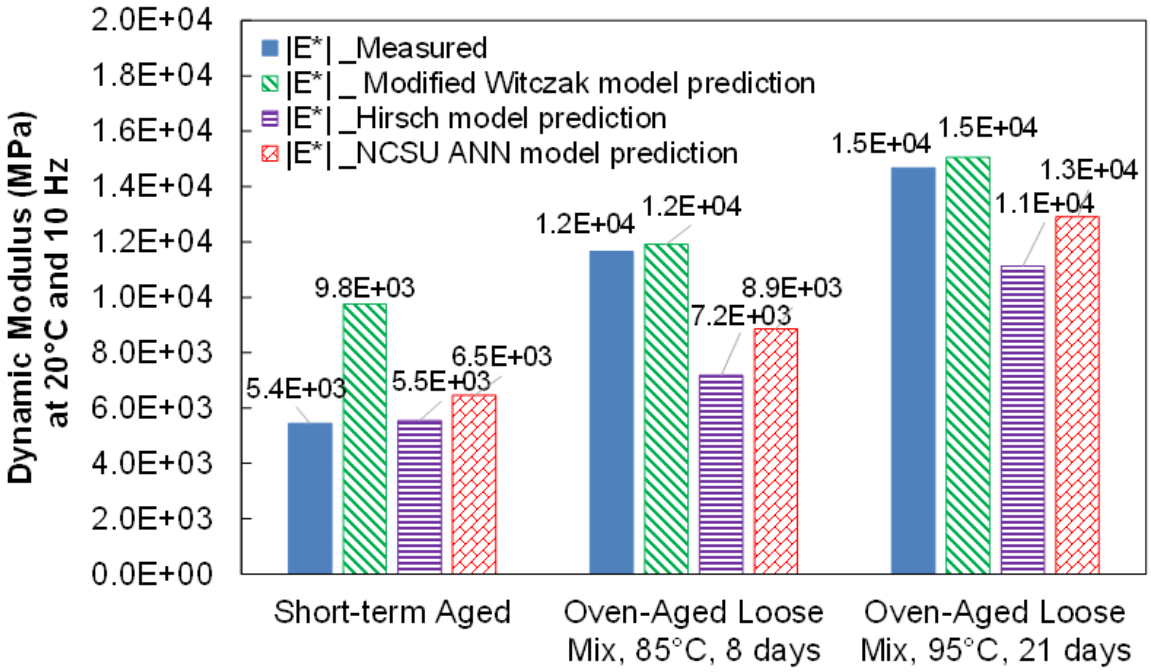

Figure F-24. Comparison of predictive model results and measured data.

Cyclic Fatigue Performance Testing Results

Figure F-25 presents the cyclic fatigue characteristic curves for the short- and long-term aged materials. These curves define how damage grows in a material and represent the averaged results of three tests that were conducted using various cross-head displacement amplitudes. The long-term aged specimens have higher damage characteristic curves than the short-term aged specimen, which follows expected trends. Thus, the performance test results indicate that no integrity issues are associated with the compaction of the aged loose mix.

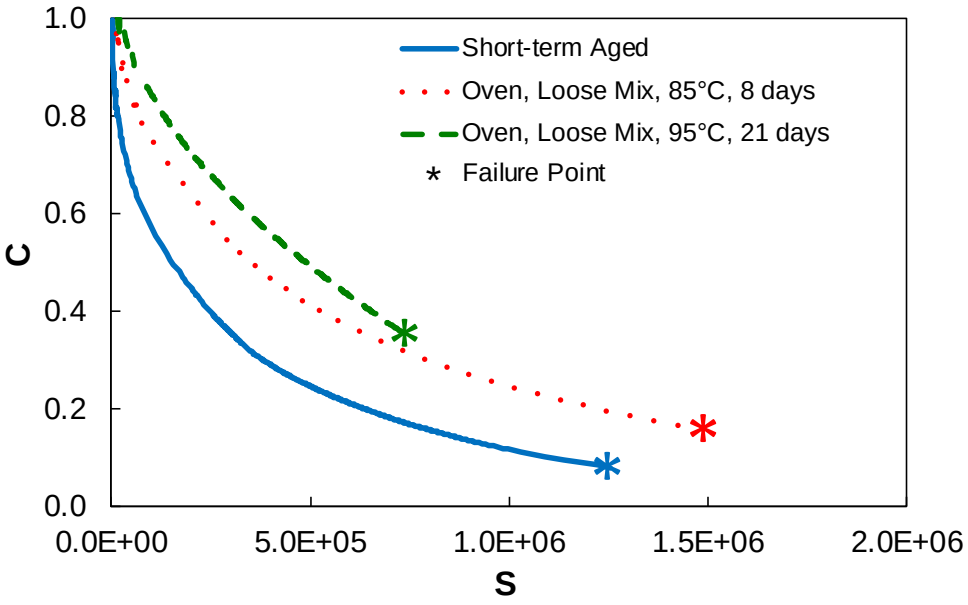

Figure F-25. Comparison of damage characteristic curves from FHWA ALF SBS mixtures subjected to different aging conditions.

Figure F-26 shows the D^R energy-based failure criterion results for the SBS-modified mix. The failure criterion line for the specimens that were compacted following long-term aging for 21 days at 95°C falls significantly lower than the failure criterion lines of the short-term aged specimens and the specimens aged for eight days at 85°C. This outcome suggests that the severe level of aging led to embrittlement and consequently degraded the resistance to fatigue and, hence, suggests no integrity problems.

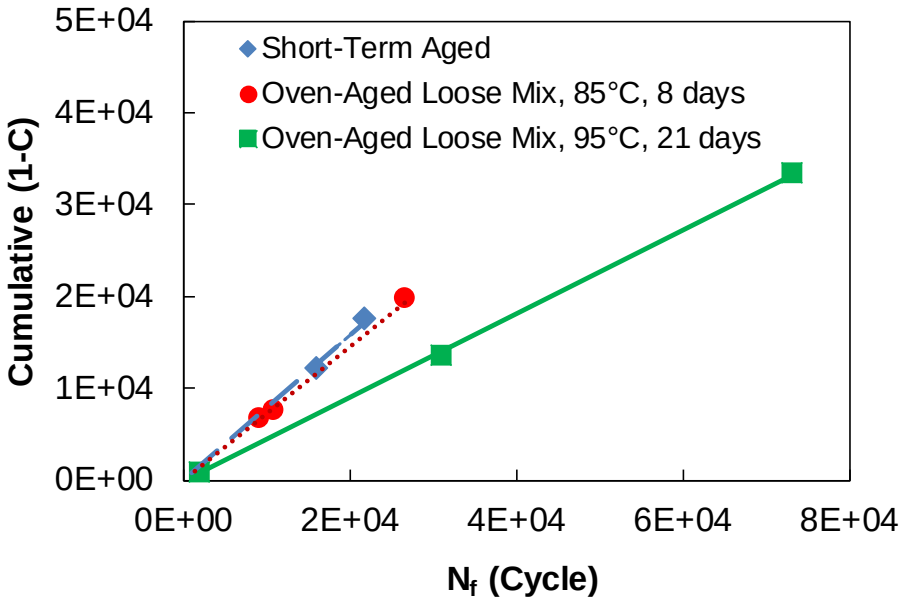

Figure F-26. Comparison of DR failure criterion lines for SBS-modified mixtures.

It can be concluded that the compaction of long-term aged loose mix is possible with no adjustment to the compaction temperature, based on both the number of compaction gyrations required to reach the target air void contents and the performance test results. The long-term aged loose mix that was aged at 95°C for 21 days had an oxidation level that was equivalent to that of the surface of an eight-year-old field core obtained from the FHWA ALF in McLean, VA. This level is assumed to represent an extreme oxidation level that nonetheless allows for compaction of the mix. Additional details on the selection of the aging procedure is included in the Appendix F and elsewhere (Elwardany et al. 2017b).

Summary

Compacted Specimen Aging

Although no integrity issues in terms of changes in air void content or specimen dimensions were encountered with the AASHTO R 30 test protocol, the aging of large (100-mm diameter) compacted specimens with wire mesh support in an oven at 85°C led to the development of an aging gradient within the specimens. This lack of uniform properties throughout the specimen is of concern for performance testing and was observed directly through a high rate of end failure at the end locations where oxidation was most significant in the cyclic direct tension fatigue tests. However, the high rate of end failure could be overcome by aging specimens 178 mm in height and then trimming the ends to produce 130-mm tall specimens for testing. The aging gradient observed in the large compacted specimens subjected to oven aging was eliminated by using small specimens (38-mm diameter with 100-mm height) due to their shorter diffusion paths.

The application of pressure in compacted specimen aging was found to expedite aging. However, oxidation gradients were observed in the pressure-aged specimens. In addition, although no changes in air void content or specimen dimensions were induced by pressurized aging, the performance test results indicate that the application and/or release of pressure can damage specimens. Therefore, the results indicate that the most promising method for aging compacted specimens is to age small specimens in an oven without pressure.

Loose Mix Aging

The primary concern associated with loose mixture aging is the ability to compact the material after long-term aging. However, in this study, the compaction of the NC mix after eight days of oven conditioning at 85°C was possible with no adjustment to the compaction temperature. Similar numbers of compaction gyrations were required for both the short-term aged and long-term aged loose mixes. The image analysis of the aggregate structure also indicated comparable compaction of both the short- and long-term aged loose materials. Furthermore, the performance test results indicated a significant increase in the dynamic modulus values of the long-term aged material compared to those of the short-term aged material, and the fatigue performance test results indicated no integrity concerns. In addition, loose mix aging exposes a large surface area of the binder to oxygen, and hence, a faster rate of oxidation was observed in the loose mix oven aging compared to compacted specimen aging based on the measured asphalt binder chemical and rheological aging indices. The application of pressure also was found to expedite the oxidation of the loose mix. However, only 500 g of loose mix could be aged at one time in the binder PAV. One SGC specimen requires the preparation of

7,000 g to 8,000 g of loose mix. Thus, the binder PAV would need to be run approximately 15 times to generate enough loose mix to prepare a compacted specimen for performance testing, which is inefficient and therefore was deemed impractical. Otherwise, a larger PAV would need to be developed, which would be costly. Thus, given that aging loose mix can be accomplished relatively quickly in an oven using multiple pans, this method is considered a more practical approach. Currently, the research team is using a conventional oven with inner chamber dimensions of 36 inches × 24 inches × 19 inches (W × H × D). Using only six shelves, 18 pans can fit inside the oven. Loose mix spread in four pans is sufficient for the preparation of one SGC-compacted specimen that is 150 mm in diameter and 178 mm in height.

The findings for the loose mixture aging tests using the FHWA ALF SBS mix were consistent with those for the NC mix. The compaction of the long-term aged loose mix was possible with no adjustment to the compaction temperature, based on both the number of compaction gyrations required to reach the target air void content and the performance test results. The long-term aged loose mix that was aged at 95°C for 21 days had an oxidation level that was equivalent to that of the surface of an eight-year-old field core in McLean, VA. This level is assumed to represent an extreme oxidation level that nonetheless allows compaction of the mix. The results indicate that loose mix aging at 95°C is the most promising condition for the long-term aging of asphalt concrete for performance testing. Aging at lower temperatures precludes long-term oxidation within a reasonable time-frame. Aging at temperatures exceeding 95ºC would be beneficial in terms of efficiency. However, past research indicates that Aging at temperatures above 100°C may alter oxidation mechanisms. The performance implications of laboratory aging at temperatures exceeding 100°C merits further investigation.

Conclusions

The conclusions are summarized as follows:

- The current standard procedure for the long-term aging of asphalt mixtures (AASHTO R 30), which consists of conditioning large 100-mm diameter compacted specimens in an oven at 85°C, leads to the development of an oxidation gradient from the specimen center to the periphery. The lack of uniform properties throughout the specimen is of concern for performance testing, which was observed directly through a high rate of end failure at specimen locations where oxidation was most significant in cyclic direct tension fatigue tests.
- The application of pressure in the compacted specimen aging process expedites oxidation. However, the performance test results indicate that the application and/or release of pressure damages specimens.
- The aging gradient observed in the large compacted specimens that were subjected to oven aging was eliminated by the use of small specimens (38-mm diameter with 100-mm height) due to the latter's shorter diffusion paths. Therefore, oven aging of small compacted specimens is the most promising compacted specimen aging method, as no integrity issues were observed. This specimen geometry allows for only dynamic modulus and direct tension testing. Other tests (e.g., permanent deformation tests) would not be possible under this scenario.
- Aging asphalt mixtures in a loose mix state expedites oxidation compared to compacted specimen aging under the same conditions.

- The compactive effort required to compact long-term aged loose mixes is comparable to that required for short-term aged mixes, with no adjustment to the compaction temperature based on the results for two mixtures, PG 64-22 and PG 70-28 SBS-modified, the latter of which is known to be difficult to compact.
- Dynamic modulus and cyclic, direct tension performance test results indicate no problems with loose mixtures compacted after long-term aging.
- Pressure expedites the aging of loose mix. However, the size of the standard binder PAV prohibits the generation of enough aged material for performance testing. If the pressure aging of loose mix were to be selected to age asphalt specimens for performance testing, a larger PAV would need to be developed.
- Based on the aforementioned conclusions, loose mix aging in an oven is the most promising aging method to produce mixture specimens for performance testing in terms of efficiency and integrity without the need to develop costly new equipment. In addition, any specimen geometry (e.g., slabs and beams) can be produced using aged loose mix, which also makes this method the most versatile option.
- The results indicate that loose mix aging at 95°C is the most promising method for the long-term aging of asphalt concrete for performance testing. Aging at lower temperatures precludes reaching field levels of oxidation within a reasonable time-frame. Aging at temperatures exceeding 95ºC would be beneficial in terms of efficiency. However, past research indicates that Aging at temperatures above 100°C may alter oxidation mechanisms. The performance implications of laboratory aging at temperatures exceeding 100°C merits further investigation.

References

American Association of State Highway and Transportation Officials, “Standard Practice for Mixture Conditioning of Hot Mix Asphalt”, AASHTO R 30, Washington, D.C., 2012.

American Association of State Highway and Transportation Officials, “Standard Method of Test for Determining the Dynamic Modulus and Flow Number for Hot Mix Asphalt (HMA) using Asphalt Mixture Performance Tester (AMPT)”, AASHTO TP 79, Washington, D.C., 2012.

American Association of State Highway and Transportation Officials, “Determining the Damage Characteristic Curve of Asphalt Concrete from Direct Tension Cyclic Fatigue Tests”, AASHTO TP 107, Washington, D.C., 2014.

Arega, Z. A., Bhasin, A., and De Kesel, T. “Influence of extended aging on the properties of asphalt composites produced using hot and warm mix methods”, *Construction and Building Materials*, Vol. 44, 2013, pp. 168-174.

Bari, J. and Witczak, M. W. “Development of a New Revised Version of the Witczak E* Predictive Model for Hot Mix Asphalt”, *Journal of the Association of Asphalt Paving Technologists*, Vol. 75, 2006, pp. 381-423.

Bell, C. A., AbWahab, Y., Cristi, R. E., and Sognovske, D. “Selection of Laboratory Aging”, SHRP-A-384, Strategic Highway Research, Washington, D.C., 1994.

Bell, C. A., Wieder, A. J., and Fellin, M. J. “Laboratory Aging of Asphalt-Aggregate Mixtures: Field Validation. SHRP-A-390, Strategic Highway Research Program. National Research Council, Washington, D. C., 1994.

Christensen, Jr., D. W., Pellinen, T. K., and Bonaquist, R. F. “Hirsch Model for Estimating the Modulus of Asphalt Concrete”, *Journal of the Association of Asphalt Paving Technologists*, Vol. 72, 2003, pp. 97-121.

Coenen, A., Kutay, M., and Bahia H. “Aggregate Structure Characterization of Asphalt Mixtures Using 2-Dimentional Image Analysis. *Road Materials and Pavement Design”*, Vol. 13(3), 2011, pp. 433-454.

Corbett, L. W., and Merz, R. E. “Asphalt Binder Hardening in the Michigan Test Road after 18 Years of Service”, *Transportation research record*, 1975, pp. 27-34.

Farrar, M. J., Grimes, R. W., Wiseman, S., and Planche, J. P. “Asphalt Pavement–Micro-sampling and Micro-extraction Methods", 2015.

Gatchalian, D., Masad, E., Chowdhury, A., and Little, D. “Characterization of Aggregate Resistance to Degradation in Stone Matrix Asphalt Mixtures”, *Transportation research record,* 2006, pp. 55-63.

Gibson, N., Qi, X., Andriescu, A., and Copeland, A. “Recommended Asphalt Binder Fatigue Performance Specification from Full-scale Accelerated Pavement Tests Considering Aging Effects”, *Advances in Pavement Design through Full-scale Accelerated Pavement Testing*, 2012, pp. 433.

Glover, C. J., Martin, A. E., Chowdhury, A., Han, R., Prapaitrakul, N., Jin, X., and Lawrence, J. “Evaluation of Binder Aging and its Influence in Aging of Hot Mix Asphalt Concrete: Literature Review and Experimental Design”, Texas: Report 0-6009-1, 2008.

Gundla, A., Gudipudi, P.P., and Underwood, B.S. “Evaluation of the Sensitivity of Asphalt Concrete Modulus to Binder Oxidation with a Multiple Length Scale Study”, *95th Annual Meeting of the Transportation Research Board*, Washington D.C., 2016.Hachiya, Y., Nomura, K., and Chen, J. “Accelerated Aging Test for Asphalt Concretes”, *Zurich: 6th RILEM Symposium PTEBM*, 2003.

Harrigan, E. T. “Simulating the Effects of Mot Mix Asphalt Aging for Performance Testing and Pavement Structural Design”, Report, National Cooperative Highway Research Program, Research Results Digest 324, National Research Council, Washington, D.C., 2007.

Herrington, P. R., Patrick, J. E., and Ball, G. F. “Oxidation of roading asphalts”. *Industrial and engineering chemistry research*, V. 33(11), 1994, pp. 2801-2809.

Hou, T., Underwood, B. S., and Kim, Y. R. "Fatigue Performance Prediction of North Carolina Mixtures Using Simplified Viscoelastic Continuum Damage Model", *Journal of the Association of Asphalt Paving Technologists*, Vol. 79, 2010, pp. 35-80.

Houston, W. M., Mirza, M. W., Zapata, C. E., and Raghavendra, S. "Environmental Effects in Pavement Mix and Structural Design Systems", Report, National Cooperative Highway Research Program, No. Project 9-23, National Research Council, Washington, D.C., 2005.

Hubbard, P., and Reeve, C. S. "The Effect of Exposure on Bitumens", *Journal of Industrial and Engineering Chemistry*, Vol. 5(1), 1913, pp. 15-18.

Kim, Y. R. "Long-Term Aging of Asphalt Mixtures for Performance Testing and Prediction", Quarterly Report (April - June, 2015), National Cooperative Highway Research Program, No. Project 9-54, National Research Council, Washington, D.C., 2015.

Korsgaard, H. C., Blumensen, J., Sundahl, J., and Gonzales, C. "Accelerated Ageing of Asphalt in Pressure Ageing Vessel", *Eurasphalt and Eurobitume Congress. Strasbourg*, Vol. 1, 1996, pp. 4.048.

Kutay, M., Arambula, E., Gibson, N., and Youtcheff, J. "Three-Dimensional Image Processing Methods to Identify and Characterize Aggregates in Compacted Asphalt Mixtures", *International Journal of Pavement Engineering*, Vol. 11, Issue 6, 2010, pp. 511-528.

Liu, M., Lunsford, K. M., Davison, R. R., Glover, C., and Bullin, J. A. "The Kinetics of Carbonyl Formation in Asphalt", *American Institute of Chemical Engineers Journal*, Vol. 42(4), 1996, pp. 1069-1076.

Mbarki, R., Kutay, M. E., Gibson, N., and Abbas, A.R. "Comparison between Fatigue Performance of Horizontal Cores from Different Asphalt Pavement Depths and Laboratory Specimen", *Road Materials and Pavement Design*, Vol. 13(3), 2012, pp. 422-432.

Mollenhauer, K., and Mouillet, V. "Re-road – End of Life Strategies of Asphalt Pavements", European Commission DG Research, 2011.

Norouzi, A., and Kim, Y. R. "Mechanistic Evaluation of the Fatigue Cracking in Asphalt Pavements", *International Journal of Pavement Engineering*, 2015.

Partl, M. N., Bahia, H. U., Canestrari, F., De la Roche, C., Di Benedetto, H., Piber, H., and Sybilski, D. "Advances in Interlaboratory Testing and Evaluation of Bituminous Materials", *The International Union of Laboratories and Experts in Construction Materials, Systems and Structures (RILEM),* 2013.

Petersen, J. C. "A Dual, Sequential Mechanism for the Oxidation of Petroleum Asphalts", *Petroleum Science and Technology*, Vol. 16(9-10), 1998, pp. 1023-1059.

Petersen, J. C. “A Review of the Fundamentals of Asphalt Oxidation: Chemical, Physicochemical, Physical Property, and Durability Relationships”, *Transportation Research E-Circular* (E-C140), 2009.

Petersen, J. C., and Glaser, R. “Asphalt Oxidation Mechanisms and the Role of Oxidation Products on Age Hardening Revisited”, *Road Materials and Pavement Design*, Vol. 12(4), 2011, pp. 795-819.

Petersen, J. C., and Harnsberger, P. M. “Asphalt Aging: Dual Oxidation Mechanism and Its Interrelationships with Asphalt Composition and Oxidative Age Hardening”, *Transportation Research Record: Journal of Transportation Research Board*, 1998, pp. 47-55.

Reed, J. “Evaluation of the Effects of Aging on Asphalt Rubber Pavements”, Ph.D. Dissertation, Arizona State University, Phoenix, Arizona, 2010.

Roohi Sefidmazgi, N., Tashman, L., and Bahia, H. “Internal Structure Characterization of Asphalt Mixtures for Rutting Performance Using Imaging Analysis”, *Association of Asphalt Pavement Technologies*, Vol. 13, 2011, pp. 21-37.

Sabouri, M., and Kim, Y. R. “Development of Failure Criterion for Asphalt Mixtures under Different Modes of Fatigue Loading”, *Transportation Research Record: Journal of Transportation Research Board*, 2014.

Sakhaei Far, M. S. “Development of New Dynamic Modulus (|E*|) Predictive Models for Hot Mix Asphalt Mixtures”, Ph.D. Dissertation, North Carolina State University, Raleigh, North Carolina, 2011.

Tarbox, S. J. “Effect of Long Term Oven Aging on RAP Mixtures”, Master’s Thesis, University of New Hampshire, Durham, New Hampshire, 2011.

Thurston, R., and Knowles, E. “Oxygen Absorption Tests on Asphalt Constituents”, *Journal of Industrial and Engineering Chemistry*, V. 28(1), 1936, pp 88-91.

Von Quintas, H., Scherocman, J., Kennedy, T., and Hughes, C. “Asphalt Aggregate Mixture Analysis System (AAMAS)”, Report, National Research Cooperative Highway Research Program, No. Project 9-6, National Research Council, Washington, D.C., 1992.

West, R., Watson, D., Turner, P., and Casola, J. “Mixing and Compaction Temperatures of Asphalt Binders in Hot-Mix Asphalt”, Report, National Cooperative Highway Research Program, No. Project 9-39, National Research Council, Washington, D.C., 2010

APPENDIX G

Investigation of Proper Long-Term Aging Temperature

Introduction

The accurate characterization of asphalt mixture properties in terms of the service life of asphalt pavement is becoming more important as more powerful pavement design and performance prediction methods are implemented. Both an accurate aging model and an optimal laboratory conditioning procedure are required to simulate long-term aging for performance testing and prediction in order to integrate the effects of long-term aging into pavement prediction models and other mechanistic design and analysis methods. The standard method that is used to assess the long-term aging of asphalt mixtures in the United States is American Association of State Highway and Transportation Officials (AASHTO) R 30 (2001). In this method, compacted asphalt mixture specimens are conditioned at 85°C ± 3°C for 120 ± 0.5 hours to represent five to ten years of aging in the field. However, the long-term oven aging of compacted specimens leads to both radial and vertical oxidation gradients, which is a concern for performance testing because the properties throughout the specimen can vary (Elwardany et al. 2016). As an alternative, the long-term oven aging of loose (uncompacted) asphalt mixture has been gaining attention in recent years because it eliminates the oxidation gradient by promoting oxygen exposure to the mixture (e.g., Arega et al. 2013, Partl et al. 2013, Mollenhauer and Mouillet 2011, Van den Bergh 2011, Reed 2010, Braham et al. 2009, Dukatz 2015, Elwardany et al. 2016). In addition, aging loose asphalt mixture is more efficient than aging compacted specimens at a given temperature (Elwardany et al. 2016). Elwardany et al. (2016) demonstrated that long-term aged loose mixture can be compacted for performance testing and prediction.

The rate of oxidation increases as the temperature increases, and thus, laboratory aging at a higher temperature is more efficient than at a lower temperature (Elwardany et al. 2016). This phenomenon has led several recent studies to propose loose mixture long-term aging at 135°C as an efficient alternative to the aging procedure recommended in AASHTO R 30 (Braham et al. 2009, Blankenship 2015, Dukatz 2015). Although increasing the aging temperature increases the rate of oxidation, which is a desirable attribute, it can also disrupt polar molecular associations and lead to the thermal decomposition of sulfoxides in asphalt binders. Thus, accelerated aging of asphalt binder at significantly high temperatures may lead to a fundamentally different aged asphalt binder than asphalt aged in the field (at a lower temperature) (Branthaver et al. 1993). The literature indicates that the disruption of polar molecular associations and subsequent sulfoxide decomposition become critical at temperatures that exceed 100°C (Petersen et al. 1981, Herrington et al. 1994, Petersen 2009, Petersen and Glaser 2011, Glaser et al. 2013). However, past research efforts have not evaluated the implications of these chemical changes with regard to asphalt mixture performance. In addition, aging at temperatures above 100°C can lead to asphalt mastic drain-down from the loose mix because asphalt binder has low viscosity values at elevated temperatures (Braham et al. 2009). This study seeks to evaluate the performance implications of long-term laboratory aging of loose mixture at 135°C.

Objectives

The objective of this study is to evaluate the performance implications of laboratory long-term aging temperature.

Materials and Methods

For this study, comparative tests between loose mixtures aged at 95°C and 135°C were conducted to evaluate the implications of loose mix aging at 135°C with regard to asphalt mixture performance using three mixtures, all prepared with the same Federal Highway Administration Accelerated Load Facility (FHWA ALF) aggregate, but with different binders: ALF styrene-butadiene-styrene (SBS), SHRP AAD, and SHRP AAG. The SHRP AAD and SHRP AAG binders were selected due to their known differences in chemistry. SHRP AAD has high sulfur content (6.9%) and is highly structured (incompatible). Thus, SHRP AAD was expected to be especially susceptible to changes in oxidation kinetics and mechanics at 135°C. SHRP AAG has low sulfur content (1.3%) and is less structured (more compatible) than SHRP AAD. Thus, SHRP AAG was expected to be less susceptible to changes in oxidation kinetics and mechanisms when the temperature for loose mixture aging was increased from 95°C to 135°C. The FHWA ALF SBS mixture was selected in order to include a common asphalt-modified asphalt binder in the study and because field core data were available for it. Figure G-1 presents a summary of the experimental plan implemented for each mixture to evaluate the implications of loose mixture aging at 135°C.

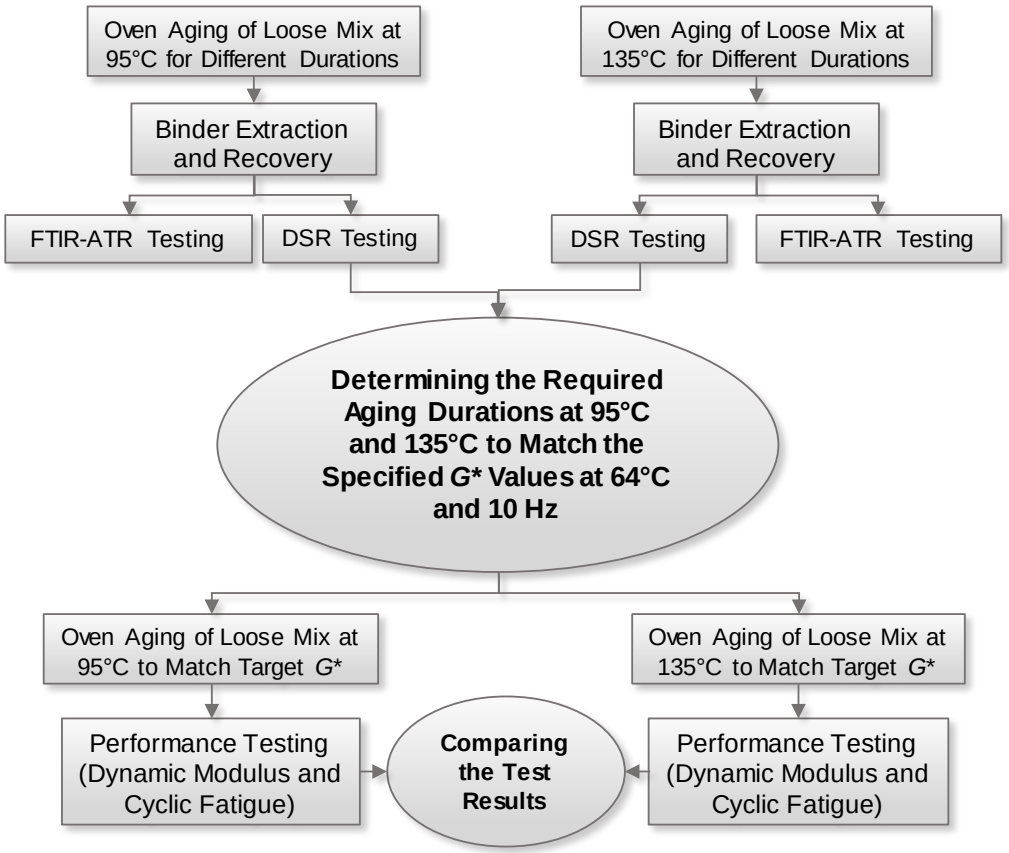

Figure G-1. Summary of experimental plan.

Table G-1 presents the naming scheme for the samples subjected to different aging procedures. Loose mix aging at 70°C and 85°C was included to evaluate the comparison between effect of aging temperatures on the physiochemical properties of asphalt mixture, regarding the properties of the extracted and recovered asphalt binders. More details on this matter will be provided later in this paper. The designation of 'UC' (uncompacted) at the end of a sample's identification indicates that the sample was extracted from the loose mix sample prior to reheating and compaction. The designation of 'C' (compacted) indicates that the sample was extracted from a specimen compacted after long-term loose mixture aging.

Table G-1. Naming Scheme Used for Samples Subjected to Different Aging Conditions

Mixture	Sample Identification	Aging Condition		
		Field/ Oven	Temp. (°C)	Duration
FHWA ALF-SBS	Short-term, UC	Oven	135	4 Hours
	Loose Mix, 70°C, UC	Oven	70	-
	Loose Mix, 85°C, UC	Oven	85	-
	Loose Mix, 95°C, UC	Oven	95	-
	Loose Mix, 135°C, UC	Oven	135	-
	Field, 8 Years	Field		8 Years
	Short-term, C	Oven	135	4 Hours
	Loose Mix, 95°C, 21 Days, C	Oven	95	21 Days
	Loose Mix, 135°C, 52 Hr, C	Oven	135	52 Hours
SHRP AAD	Short-term, UC	Oven	135	4 Hours
	Loose Mix, 70°C, UC	Oven	70	-
	Loose Mix, 95°C, UC	Oven	95	-
	Loose Mix, 135°C, UC	Oven	135	-
	Short-term, C	Oven	135	4 Hours
	Loose Mix, 95°C, 8.9 Days, C	Oven	95	8.9 Days
	Loose Mix, 135°C, 16.8 Hr, C	Oven	135	16.8 Hours
SHRP AAG	Short-term, UC	Oven	135	4 Hours
	Loose Mix, 70°C, UC	Oven	70	-
	Loose Mix, 95°C, UC	Oven	95	-
	Loose Mix, 135°C, UC	Oven	135	-
	Short-term, C	Oven	135	4 Hours
	Loose Mix, 95°C, 8.9 Days, C	Oven	95	19 Days
	Loose Mix, 135°C, 16.8 Hr, C	Oven	135	37.6 Hours

First, two batches of loose mix were aged separately at 95°C and 135°C for a prolonged duration. The loose mixtures were prepared using component materials in the laboratory and then subjected to short-term aging (4 hours at 135°C) in accordance with AASHTO R 30. These short-term aged loose mixtures then were spread in a single layer in aluminum pans and placed in a forced draft oven with lateral air-flow for long-term aging. Figure G-2 shows pans

containing loose mix undergoing long-term aging in the oven. The pans were shifted frequently to compensate for air flow and temperature differences inside the oven.

Figure G-2. Loose mix prepared for long-term aging.

Small samples of the loose mixture were taken from the pans at periodic intervals to assess the changes in the asphalt binder oxidation level versus the aging duration. These loose mixture samples were subjected to binder extraction and recovery in a rotary evaporator. Asphalt binder is the asphalt concrete constituent that undergoes oxidative aging. Therefore, the oxidation of pavements is best characterized using asphalt binder chemical and rheological properties, referred to as 'aging index properties' (AIPs) herein. The extracted and recovered binder samples were tested using a dynamic shear rheometer (DSR) and an attenuated total reflectance Fourier transform infrared (ATR-FTIR) spectrometer to determine the chemical and rheological AIPs, respectively. The DSR tests included temperature and frequency sweeps, with temperatures ranging from 5°C to 64°C and frequencies ranging from 0.1 Hz to 30 Hz.

The primary oxidation products in asphalt binders are ketones and sulfoxides, detected by carbonyl and sulfoxide infrared absorption peaks. Ketone formation changes the polarity of the associated aromatic ring components, leading to an increase in the asphaltenes, which in turn increases viscosity (Petersen and Glaser 2011, Petersen 2009). Sulfoxides are polar and, hence, serve to increase asphalt binder viscosity (Petersen and Glaser 2011). The specific ketone and sulfoxides that are formed, combined with the physico-chemical interactions among the asphalt binder constituents, affect the binder rheology (Petersen 2009). Therefore, the relationship between chemical and rheological AIPs can be used to detect changes in oxidation reaction mechanisms. The relationship between chemical and rheological AIPs is unique to a binder, given that the oxidation reaction mechanism is consistent. However, if the chemical oxidation products change, the relationship between the chemical and rheological AIPs will change. Herein, the G* value at 64°C and 10 Hz frequency is used as the rheological AIP. The carbonyl plus sulfoxide (C+S) absorbance peak is used as the primary chemical AIP. However, trends in carbonyl absorbance area (CA) are also evaluated.

Figure G-3 shows the relationship between the G* value at 64°C and 10 Hz frequency and the C+S absorbance peaks for the binder samples extracted and recovered from FHWA ALF SBS loose mixes aged at 95°C and 135°C for different durations. Figure G-3 indicates that the binders aged at the two different temperatures have different C+S absorbance peaks for the same G* value, indicating that a change in the oxidation reaction mechanism occurred when the aging temperature was increased from 95°C to 135°C. An analogous trend was observed for the SHRP

AAD mixture and, to a lesser extent, the SHRP AAG mixture. The G* value was selected as the aging index to match the degree of aging between the two aging temperatures because binder rheology is speculated to be related to asphalt mixture performance more directly than binder chemistry. Also, the selection of G* as the primary aging index allows the effects of different C+S absorbance peaks on mixture performance to be evaluated, because the same G* value for mixtures aged at two different temperatures will result in two different C+S absorbance peaks.

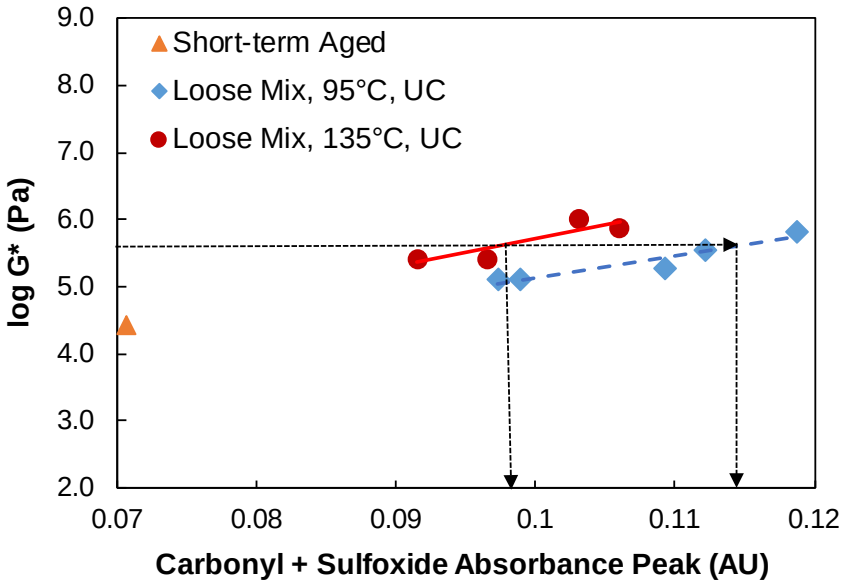

Figure G-3. FHWA ALF SBS loose mix prepared for long-term aging.

The next step in the experimental plan was to determine the aging durations for the samples tested at 95°C and 135°C that would yield the same G* value. For the 95°C aging, 21 days of conditioning was determined for the FHWA ALF SBS mixture. Note that 21 days of conditioning at 95°C led to an equivalent oxidation level for the top 6 mm of an eight-year-old field core obtained from McLean, VA (the location of the FHWA ALF). The G* value for 21 days of conditioning at 95°C was determined to be approximately four times the value of G* for pressurized aging vessel (PAV) -aged asphalt binder. Field cores that corresponded to the SHRP AAD and SHRP AAG mixtures were not available. Therefore, based on the finding for FHWA ALF SBS, four times the G* values of the PAV-aged binders was used as the target G* values that would reflect reasonable field aging levels of the pavement surface after a prolonged in-service period. Thus, the required aging durations at 95°C and 135°C to achieve G* values equal to four times that of PAV-aged binder were determined and used to evaluate the implications of aging at 135°C for both the SHRP AAD and SHRP AAG mixtures.

Figure G-4, Figure G-5, and Figure G-6 show the procedures that were used to match the aging levels between the loose mixtures aged at 95°C and 135°C for the FHWA ALF SBS, SHRP AAD, and SHRP AAG materials, respectively. To match the aging levels between the loose mixtures aged at 95°C and 135°C, first the relationship between the log G* and aging duration was obtained for each aging temperature. Then, in the case of the FHWA ALF SBS material, the G* value that corresponded to 95°C before compaction was determined. Based on the relationship between log G* and time that corresponded to the loose mix aged at 135°C, the required duration of aging at 135°C to match this G* value was then determined via

interpolation. For the SHRP AAD and SHRP AAG materials, the aging durations required to match the predetermined G* values, which corresponded to four times the value of G* for the binder after PAV aging (the target G*), at both 95°C and 135°C were determined. Note that the results presented in Figure G-5 and Figure G-6 demonstrate that SHRP AAD requires shorter aging times at both 95°C and 135°C to achieve the requisite G* values than SHRP AAG. This finding matches expectations regarding the binders' microstructures. SHRP AAD is incompatible and therefore was expected to have a high hardening susceptibility with oxidation level compared to SHRP AAG, which is compatible and therefore less structured.

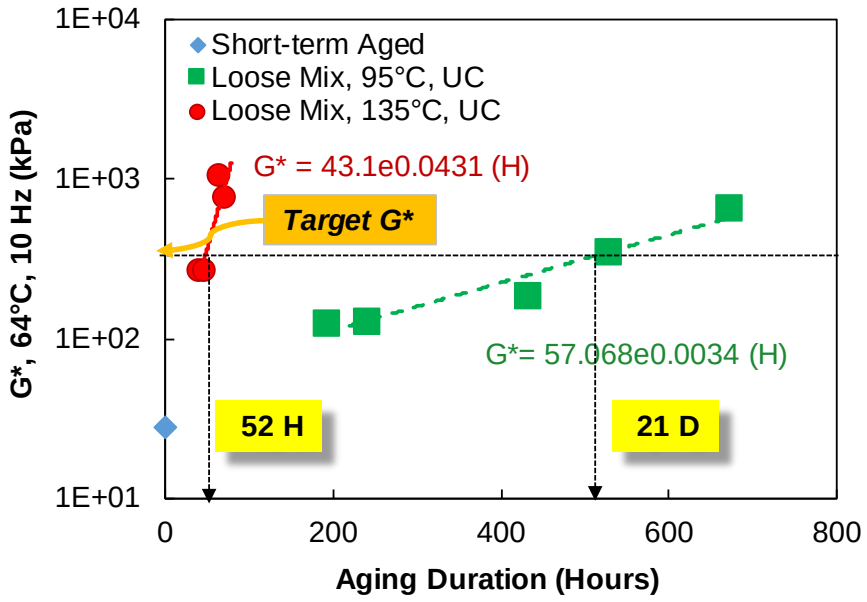

Figure G-4. Determination of FHWA ALF SBS aging durations.

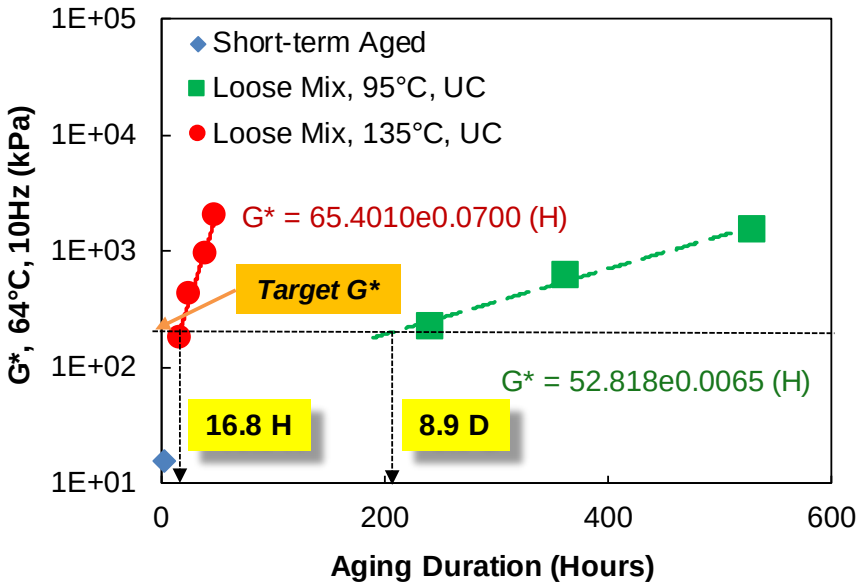

Figure G-5. Determination of SHRP AAD aging durations.

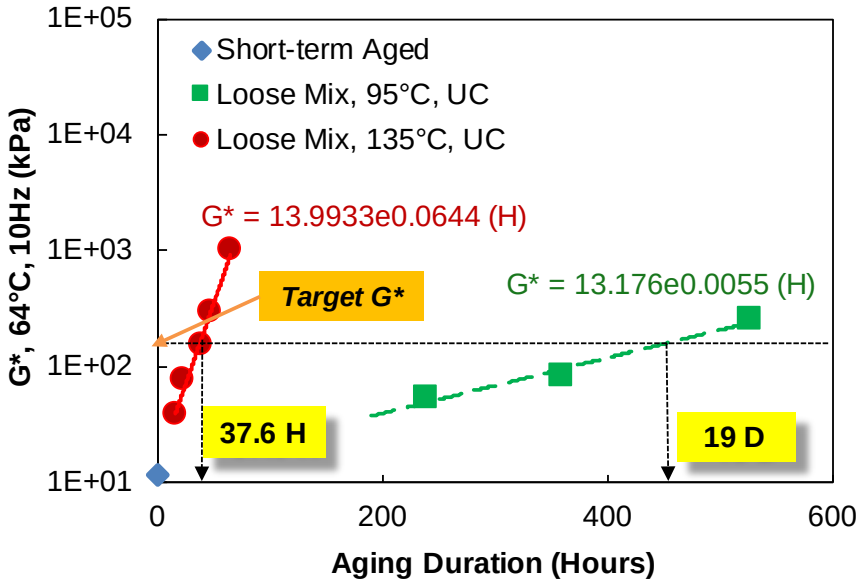

Figure G-6. Determination of SHRP AAG aging durations.

Once the required aging durations were determined, sufficient amounts of loose mix for the production of gyratory-compacted specimens for performance testing were prepared and conditioned in an oven for the predetermined durations. These specimens were compacted following long-term aging. The compacted specimens were then cut, cored, and subjected to dynamic modulus and direct tension cyclic fatigue testing (AASHTO TP 107). Comparisons of the performance of the mixtures prepared by aging at 95°C and 135°C (with equivalent binder G* values) were used to assess the performance implications of the aging temperatures. Note that to build dynamic modulus mastercurves, frequency sweep tests were conducted at multiple temperatures. Dynamic modulus testing of all specimens was conducted in accordance with AASHTO T 342. For the first set of FHWA ALF SBS specimens, five temperatures (-10°C, 5°C, 20°C, 40°C, and 54°C) were used to build dynamic modulus mastercurves. However, the dynamic modulus test results from the first set of specimens revealed insufficient overlap between the dynamic modulus values at the different test temperatures. This lack of overlap in the dynamic modulus values precluded an accurate application of time-temperature superposition in order to build mastercurves. Therefore, to enable the construction of dynamic modulus mastercurves, additional dynamic modulus tests were conducted at -10°C, 5°C, 15°C, 27°C, 40°C, and 54°C for the FHWA ALF SBS mixture. For the SHRP AAD and SHRP AAG mixtures, the -10°C test temperature was excluded because the effect of aging on the dynamic modulus is most pronounced at high temperatures. Therefore, the test temperatures used to construct the dynamic modulus mastercurves for the SHRP AAD and SHRP AAG mixtures were 5°C, 15°C, 27°C, 40°C, and 54°C.

In addition to applying the conventional criterion (e.g., 10% difference threshold for dynamic modulus values), statistical analysis was conducted to determine any meaningful differences in the dynamic modulus test results and the fatigue test results between different aging conditions. The t-test paired two-sample statistical analysis method was used to evaluate the differences between pairs of aging treatments for each material tested. A level of confidence of 95 percent was used for the statistical analysis. Therefore, for any pair of aging treatments, if the t-test results showed a p-value of less than 0.05, the difference was considered significant.

In addition to material testing, the effects of the aging temperature on fatigue performance were evaluated at the pavement level. The pavement performance was predicted using FlexPAVE™, a software program that was developed under the FHWA-sponsored Hot Mix Asphalt Performance-Related Specifications project (Kim et al. 2017). The FlexPAVE™ program computes pavement responses and predicts performance under moving loads using three-dimensional viscoelastic analysis, taking into account the pavement's structure and material properties. The FlexPAVE™ program calculates the long-term fatigue damage and rut depths of asphalt pavements under changing environmental and loading conditions, and the resulting distress information can be plotted in various ways. In this research, the dynamic modulus test results and the cyclic fatigue test results were used within the FlexPAVE™ program to predict the fatigue performance of pavements.

Note that loose mixture aging at 70°C and 85°C also was evaluated. Although performance tests were not conducted using mixtures aged at 70°C or 85°C in this study, the extracted and recovered binder test results are incorporated into some of the analysis results presented herein.

Discussion of Results

Binder Test Results

Chemistry versus Rheology

In order to evaluate the implications of the aging temperatures with regard to the resultant asphalt binders, first a comparison study between the chemical and rheological AIPs was conducted. The chemical AIPs include the C+S absorbance peak and the CA determined via ATR-FTIR spectrometry. Based on the literature review, sulfoxide decomposition may take place. Therefore, the C+S AIP may be affected significantly by sulfoxide decomposition whereas the CA AIP may be affected only marginally by the aging temperature. The rheological AIP used in this study was the G* value at 64°C and 10 Hz frequency.

Figure G-7 presents comparisons between the rheological and chemical AIPs for all the laboratory aging trials and field cores that correspond to the FHWA ALF SBS mixture. The results demonstrate that the relationship between the chemical and rheological AIPs is independent of laboratory aging temperatures of 70°C, 85°C, and 95°C. However, a clear shift in the relationship between the chemical and rheological AIPs is evident at 135°C, with a smaller shift when the CA, as opposed to the C+S peaks, was used as the chemical AIP. Note that the field core test results fall much closer to the results that correspond to an aging temperature at or below 95°C. Thus, it is evident that aging at 135°C affects the kinetics of the oxidation reaction and the reaction products. However, it remains to be resolved whether or not this difference affects performance. Mixture performance is tied more closely to the rheological properties of the asphalt binder than to its chemistry. Therefore, further investigation into the rheological properties of asphalt binders extracted from loose mixtures aged at different temperatures and field cores was conducted.

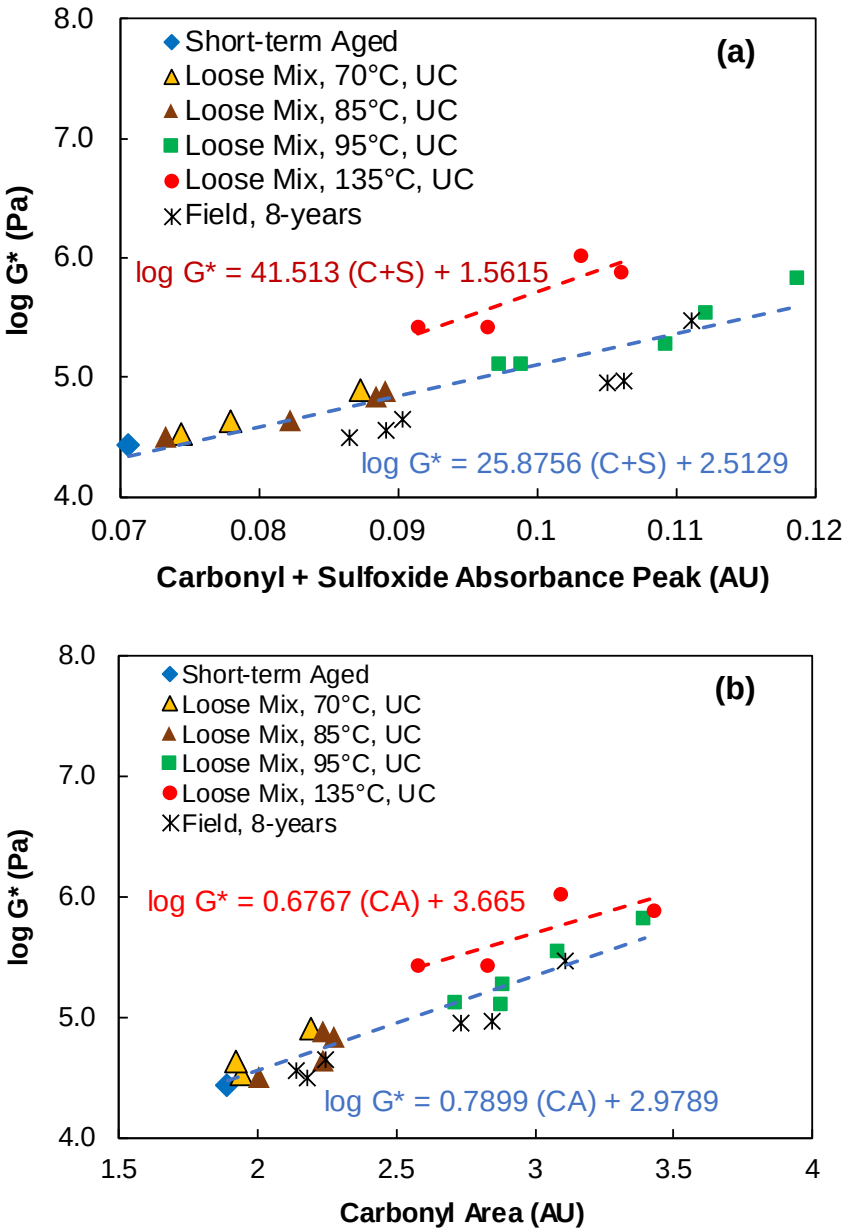

Figure G-7. Relationships between chemical and rheological indices for asphalt binders extracted and recovered from ALF SBS loose mix aged at different temperatures and binders extracted and recovered from different depths of asphalt pavement after 8 years of aging in the field: (a) log G* versus carbonyl + sulfoxide absorbance peaks and (b) log G* versus carbonyl area.

Figure G-8 presents comparisons between the rheological and chemical AIPs for all the laboratory aging trials that correspond to the SHRP AAD mixture. The results demonstrate that the relationship between the chemical and rheological AIPs is independent of the laboratory aging temperatures of 70°C and 95°C. A clear shift in the relationship between the C+S absorbance peaks and log G* is evident at 135°C. Comparatively, a relatively small change in the relationship between CA and log G* at 135°C is observed. These results suggest that

sulfoxide decomposition is significant when SHRP AAD is aged at 135°C. Recall, SHRP AAD has high sulfur content and thus high potential for sulfoxide decomposition. In short, the observed trends match expectations.

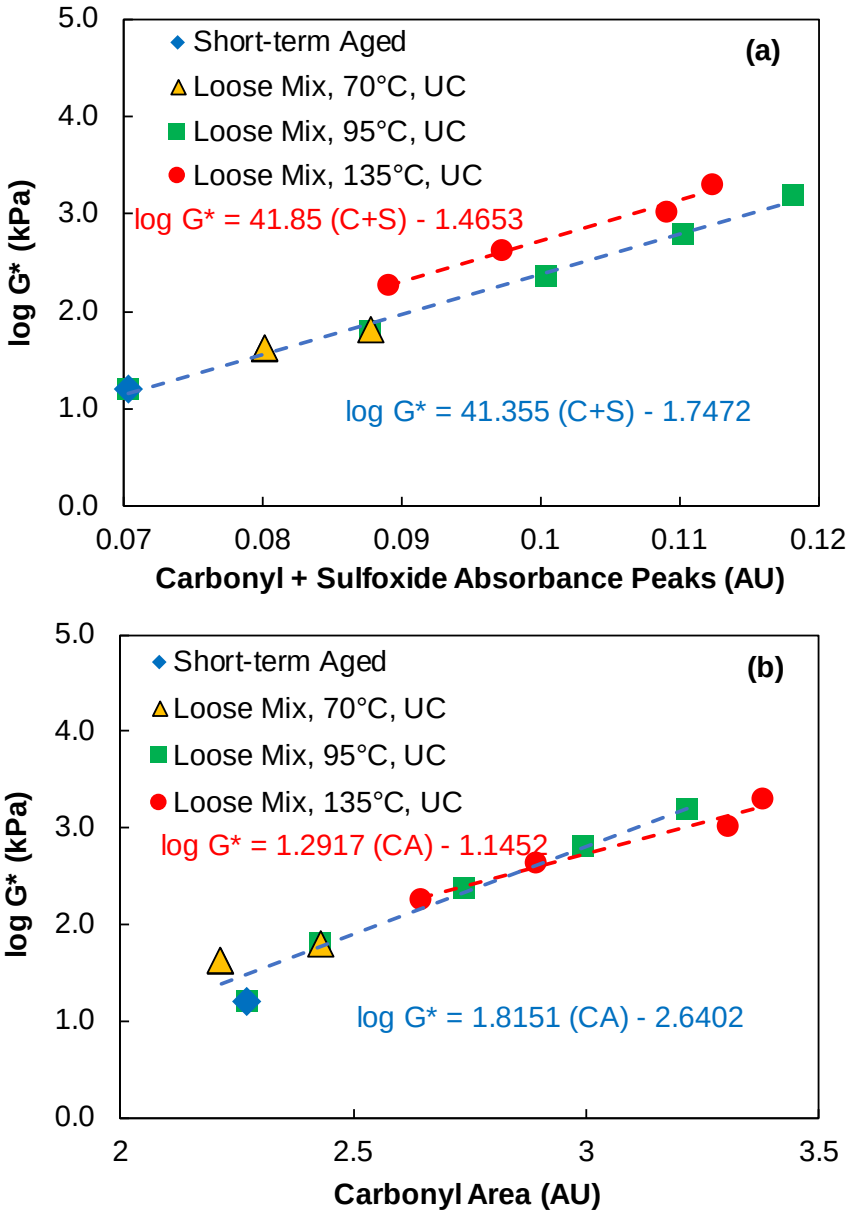

Figure G-8. Relationships between chemical and rheological indices for asphalt binders extracted and recovered from SHRP AAD loose mix aged at different temperatures: (a) log G* versus carbonyl + sulfoxide absorbance peaks and (b) log G* versus carbonyl area.

Figure G-9 presents comparisons between the rheological and chemical AIPs for all the laboratory aging trials that correspond to the SHRP AAG mixture. The results demonstrate that the relationship between the chemical and rheological AIPs is independent of laboratory aging temperatures of 70°C and 95°C, with only a minor shift in the relationship between the C+S absorbance peaks and log G* at 135°C. The relationship between CA and log G* is not

significantly affected by aging at 135°C. Recall, SHRP AAG is a compatible binder with relatively low sulfur content. Thus, it is expected that SHRP AAG would experience less change in chemistry when the aging temperature was increased from 95°C to 135°C than SHRP AAD. The results confirm this expectation.

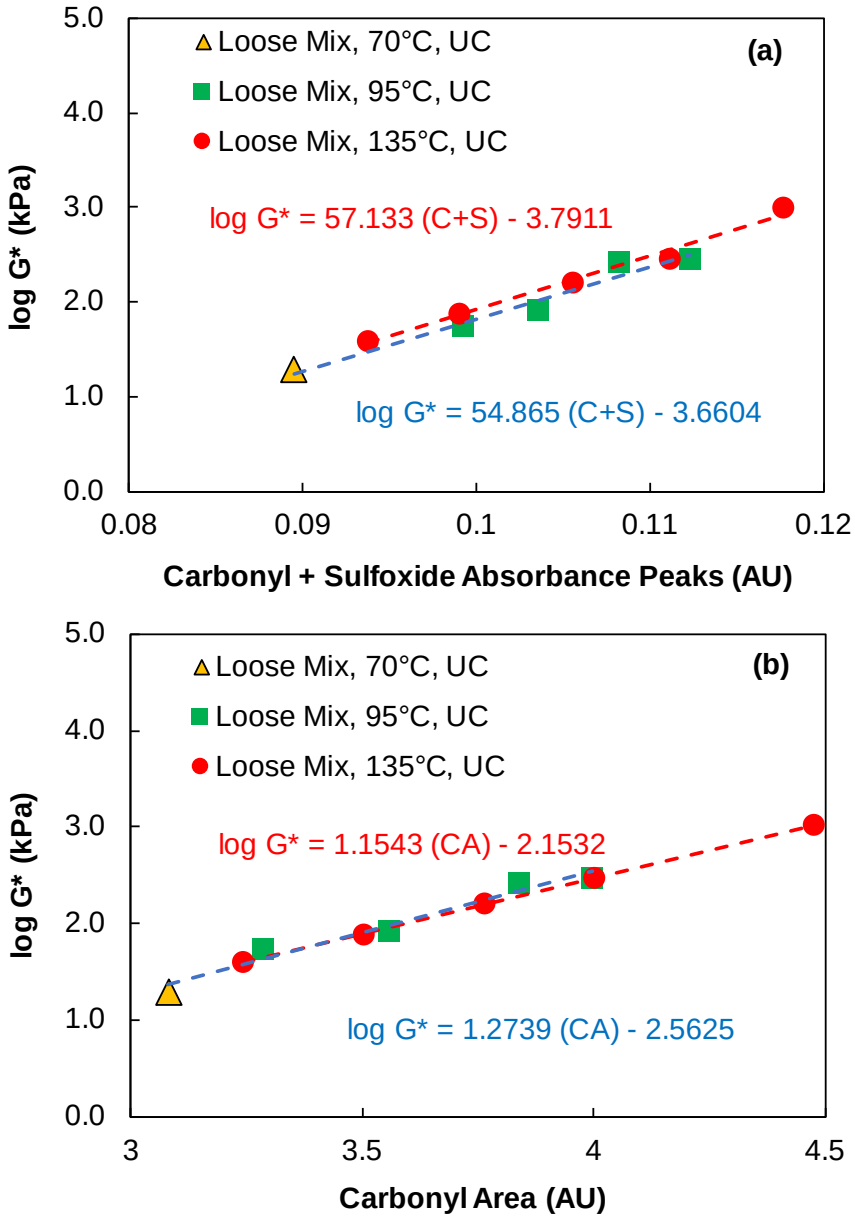

Figure G-9. Relationships between chemical and rheological indices for asphalt binders extracted and recovered from SHRP AAG loose mix aged at different temperatures: (a) log G* versus carbonyl + sulfoxide absorbance peaks and (b) log G* versus carbonyl area.

Binder Rheology

As discussed, the G* values at 64°C and 10 Hz loading frequency were used as the basis for selecting long-term aging durations at 135°C and 95°C. However, further investigation into the rheology of the binders aged at these two conditions was carried out, because 64°C and 10 Hz frequency constitute only a single point condition. Also, matching the G* values was undertaken on the basis of uncompacted material, and hence, binder extracted and recovered from compacted specimens was needed because additional aging had occurred. Figures 10, 11, and 12 present the analysis results for the binders extracted and recovered from compacted specimens and include, respectively, comparisons of (a) dynamic modulus mastercurves, (b) phase angle mastercurves, and (c) black space plots (i.e., G* versus phase angle plots).

Figure G-10 presents the rheological binder test results for the binders extracted and recovered from the FHWA ALF SBS mixtures. The FHWA ALF SBS results that correspond to the binder extracted after loose mixture aging at 95°C for 21 days and after loose mixture aging for 52 hours at 135°C are very similar, indicating that the binder's rheology was not impacted by the chemical changes that were induced by aging at 135°C as opposed to 95°C.

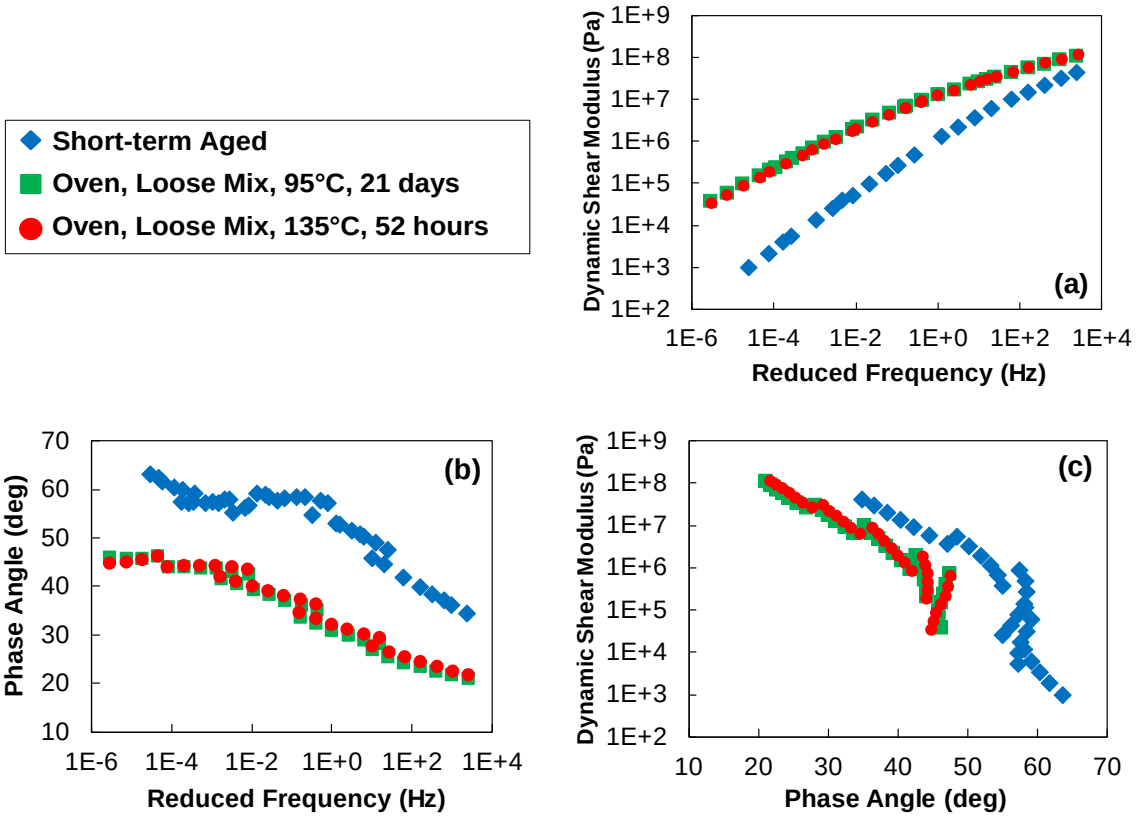

Figure G-10. FHWA ALF SBS DSR test results: (a) dynamic shear modulus mastercurves, (b) phase angle mastercurves, and (c) black space plot.

Figure G-11 presents the binder rheological test results of the binders extracted and recovered from the SHRP AAD mixture. Similar to the FHWA ALF SBS findings, the SHRP AAD results that correspond to the binders extracted after loose mixture aging at 95°C for 8.9

days and after loose mixture aging for 16.8 hours at 135°C are very similar, indicating that rheology was not impacted by the sulfoxide decomposition induced by aging at 135°C as opposed to 95°C.

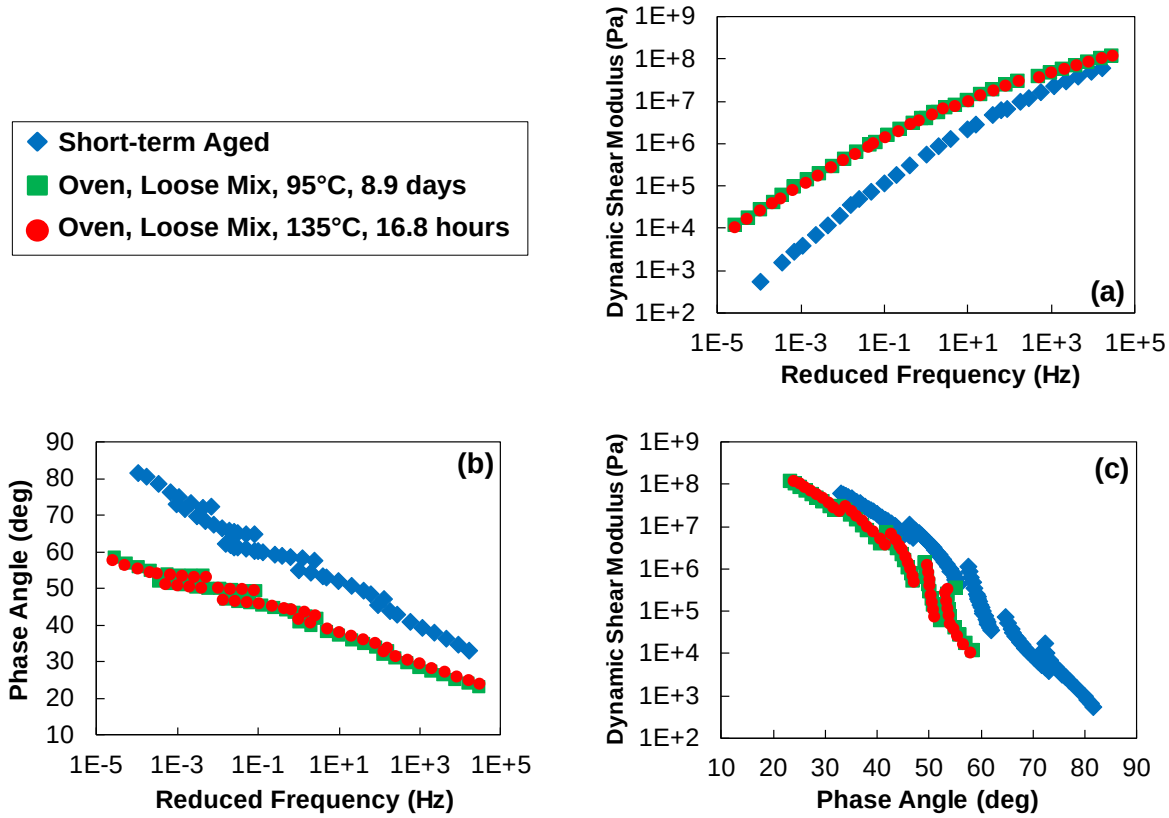

Figure G-11. SHRP AAD DSR test results: (a) dynamic shear modulus mastercurves, (b) phase angle mastercurves, and (c) black space plot.

Figure G-12 presents the binder rheological test results of the binders extracted and recovered from the SHRP AAG mixture. The results demonstrate that the binders extracted from specimens aged at 135°C for 37.6 hours have similar modulus values and phase angle values to those of the binders extracted from specimens aged at 95°C for 19 days, with slightly greater differences than the FHWA ALF SBS and SHRP AAD binders. In general, the SHRP AAG binder rheology testing data show higher variability compared to the FHWA ALF SBS and SHRP AAD binder test data. Also, note that only minor changes in the relationship between chemistry and rheology are evident when the laboratory aging temperature was increased from 95°C to 135°C.

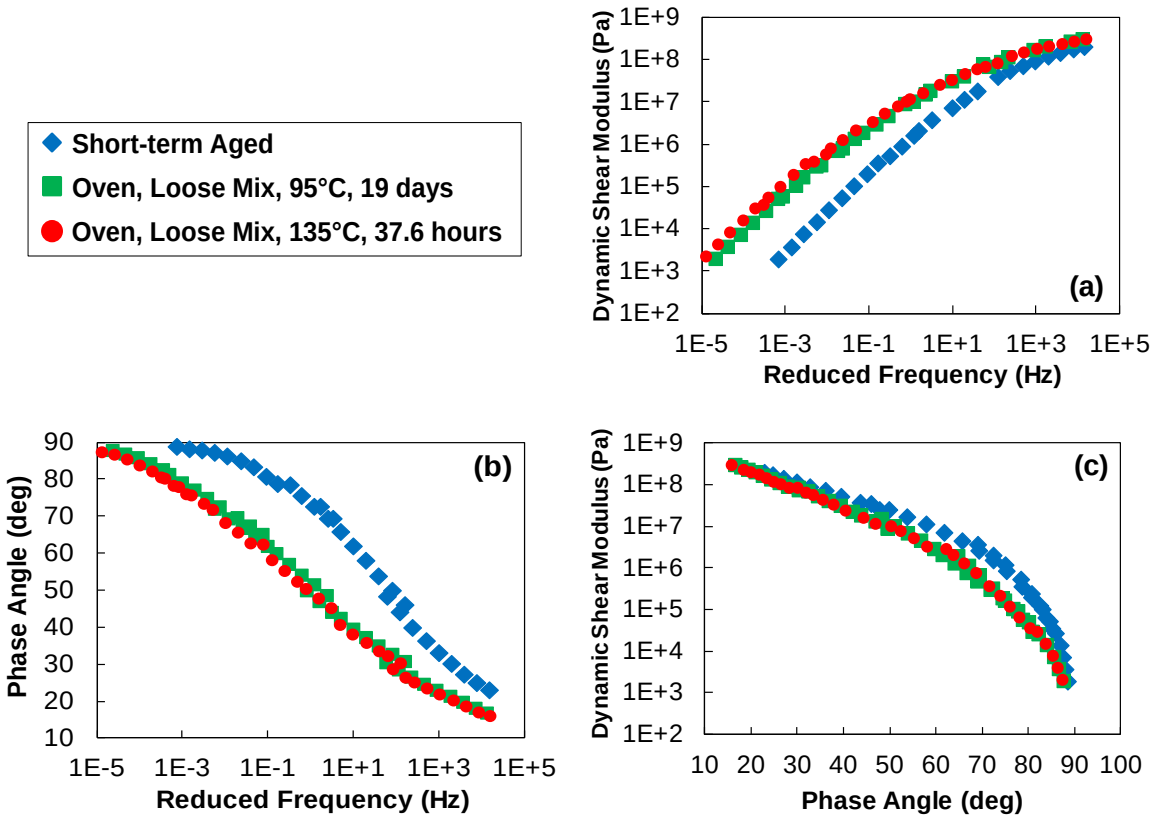

Figure G-12. SHRP AAG DSR test results: (a) dynamic shear modulus mastercurves, (b) phase angle mastercurves, and (c) black space plot.

Mixture Performance

FHWA ALF SBS

Figure G-13 presents the mixture performance test results for the FHWA ALF SBS mixture. Figure G-13 (a) presents the FHWA ALF SBS mixture dynamic modulus mastercurves that correspond to the specimens fabricated after aging at 95°C for 21 days and 135°C for 52 hours. The dynamic modulus test results for the specimens fabricated after short-term aging only also are provided for reference. The results indicate a significant increase in dynamic modulus values with long-term aging. The results also indicate very little difference in the dynamic modulus mastercurves that correspond to mixtures aged at 95°C for 21 days and 135°C for 52 hours, suggesting that the chemical changes, represented by the C+S absorbance peaks, induced by aging at 135°C do not have a significant effect on the mixture dynamic modulus of the FHWA ALF SBS mixture. Differences in the time-temperature shift factors between the short-term and long-term aged materials led to the differences in the reduced frequency range observed in the corresponding mastercurves. It can be seen that the data obtained from testing long-term aged specimens cover a larger reduced frequency domain than the short-term aged data, whereas the specimens that correspond to both conditions were tested over the same range of temperatures.

Direct tension cyclic tests were performed on the FHWA ALF SBS mixture specimens that are aged at 95°C for 21 days and at 135°C for 52 hours to assess the implications of aging

temperature with regard to fatigue cracking performance. The fatigue tests were conducted using three cross-head displacement levels (low, intermediate, and high) that were selected based on the displacement of the test machine's actuator, thus resulting in different on-specimen strain levels. Figure G-13 (b) presents the C versus S curves. The results show similar C versus S curves for the two long-term aging conditions, whereas the short-term aging C versus S curves are considerably lower, which is attributable to the short-term aged mixtures' lower stiffness values (age level) compared to those of the long-term aged material. These results indicate no significant effect of aging temperature on the fatigue performance of the FHWA ALF SBS mixture.

In addition to the C versus S curves, the D^R failure criterion that corresponds to the average reduction in pseudo stiffness (i.e., C) up to failure was evaluated in this study (Wang and Kim 2017). Figure G-13 (c) presents the failure criterion results for the FHWA ALF SBS mixture, showing that the failure criterion lines for the long-term aged materials fall below the line for the short-term aged material, which is indicative of the lower fatigue resistance of long-term aged materials as a result of the brittleness caused by oxidative aging in the asphalt binder. However, the results indicate very similar failure criterion lines for the specimens prepared with loose mixture aged at 95°C for 21 days and at 135°C for 52 hours.

These results suggest that the chemical changes induced by aging at 135°C do not significantly affect the performance of the FHWA ALF SBS mixture. The FHWA ALF SBS mixture contains SBS modification, which may mask the effects of microstructural changes induced by aging at 135°C. Hence, the evaluation of asphalt mixtures that contain unmodified asphalt binders (i.e., SHRP AAD and SHRP AAG) is also important.

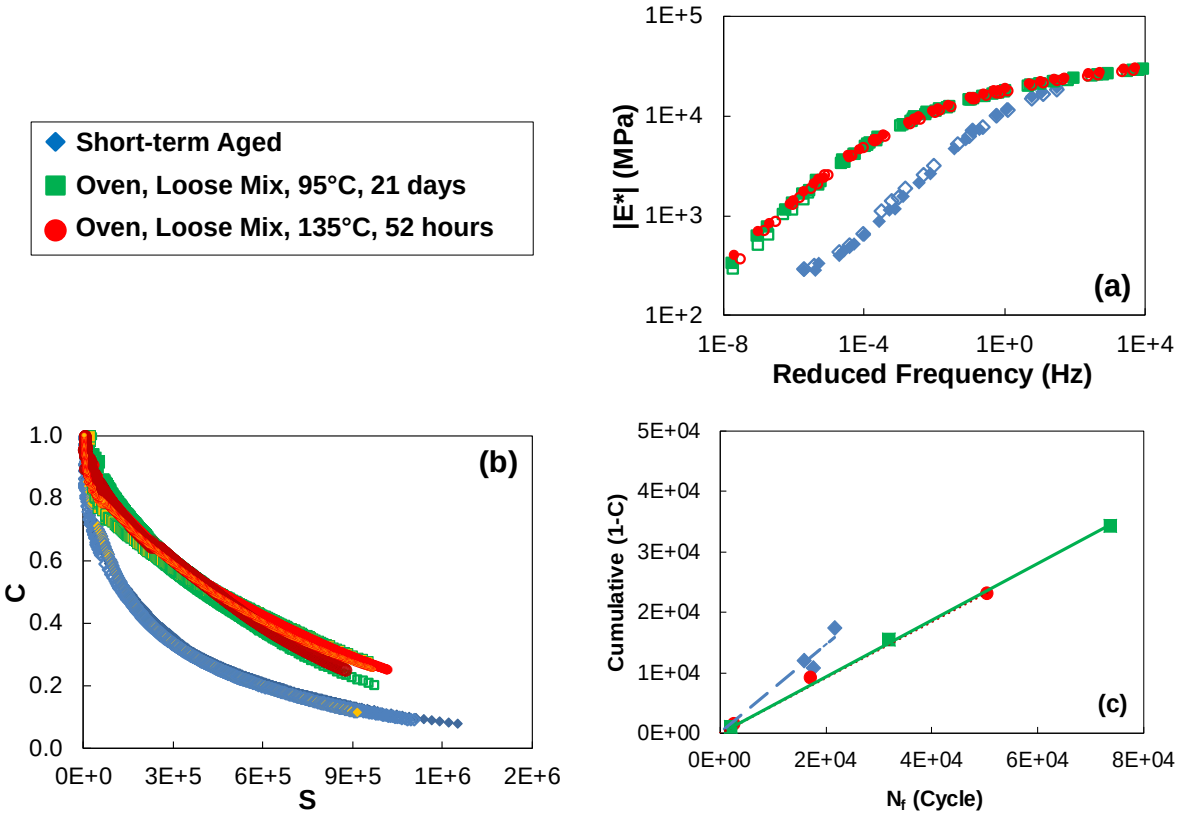

Figure G-13. FHWA ALF SBS mixture performance test results: (a) dynamic modulus curves, (b) C versus S curves, and (c) DR failure criterion lines.

Table G-2 presents the statistical t-test analysis outcomes for the dynamic modulus and fatigue test results that correspond to the FHWA ALF SBS materials with different aging conditions. For each pair of compared samples, the data points that correspond to the selected reduced frequencies or S values were used for the analysis. The selection of the reduced frequencies and S values was based on the ranges of both the dynamic modulus mastercurves and C versus S curves. Very high reduced frequencies were avoided due the fact that the aging effect on the dynamic modulus is more pronounced at low frequencies or high temperatures. Also, very low S values were not considered because the properties of asphalt mixture specimens are more distinguishable at higher S values (or smaller C values) when different materials are compared with each other.

The data points for two dynamic modulus test replicates and three fatigue test replicates were used for the statistical analysis. As mentioned earlier, a confidence level of 95 percent was employed to evaluate the difference between the pairs of aging treatments.

The pairs with significant differences ($p < 0.05$) are highlighted in Table G-2. The statistical analysis results suggest a significant difference between the dynamic modulus test results for the short-term aged and long-term aged materials. However, as inferred from the comparison of the mastercurves, no significant difference is seen between the ALF SBS materials aged at 95°C and at 135°C. The p-values for the C versus S curves indicate a similar conclusion.

Table G-2. Statistical t-Test Analysis Outcomes for Dynamic Modulus and Cyclic Fatigue Test Results for FHWA ALF SBS Materials

	Sample	**Reduced Frequency**			
		2.0E-06	1.0E-04	1.0E-03	1.0E-01
		p-value			
Dynamic Modulus	Short-term, C Loose Mix, 95°C, 21 Days, C	**0.0263**	**0.0014**	**0.0037**	**0.0201**
	Short-term, C Loose Mix, 135°C, 52 Hr, C	**0.0061**	**0.0028**	**0.0051**	**0.0150**
	Loose Mix, 95°C, 21 Days, C Loose Mix, 135°C, 52 Hr, C	0.3529	0.1453	0.0591	0.3346
		S			
Cyclic Fatigue	Sample	1.0E+05	3.0E+05	5.0E+05	7.0E+05
		p-value			
	Short-term, C Loose Mix, 95°C, 21 Days, C	**0.0005**	**0.0001**	**0.0006**	**0.0025**
	Short-term, C Loose Mix, 135°C, 52 Hr, C	**0.0078**	**0.0004**	**0.0004**	**0.0029**
	Loose Mix, 95°C, 21 Days, C Loose Mix, 135°C, 52 Hr, C	0.3599	0.0918	0.1230	0.4560

The FlexPAVE™ program was executed using the dynamic modulus and fatigue test results for each set of specimens in order to evaluate the fatigue performance of the aged materials in a typical pavement. Considering the different positions of the failure criterion lines between short-term aged and long-term aged conditions, very different field performance predictions were anticipated between these two conditions.

A simple pavement structure was considered: a 10-cm asphalt concrete layer over a 20-cm aggregate base and 380-mm subgrade. For each binder type, based on the reported performance grade, different Enhanced Integrated Climatic Model (EICM) data were selected for use in the performance predictions. EICM data for Washington, DC were used for the ALF SBS material, and climatic data for Ann Arbor, MI and San Luis Obispo, CA were used for the SHRP AAD and SHRP AAG materials, respectively. The traffic input was 3,500 daily equivalent single-axle loads (ESALs). The analysis was performed for a 20-year service life.

Figure G-14 shows the distribution of damage within a cross-section of the asphalt concrete layer of the pavement for different aging treatments predicted using the FlexPAVE™ program. This figure suggests no significant differences between the distribution of damage predicted for asphalt loose mixture aged at 95°C compared to at 135°C. However, as expected, the short-term aged material performed better than the long-term aged material. It is also noted that the long-term aging of the SBS mixture increases the top-down cracking propensity of the study pavement greatly. Although this observation is based on the unrealistic aging condition (i.e., constant aging through the thickness of asphalt layer), it signifies the importance of including accurate aging condition in long-term pavement performance prediction.

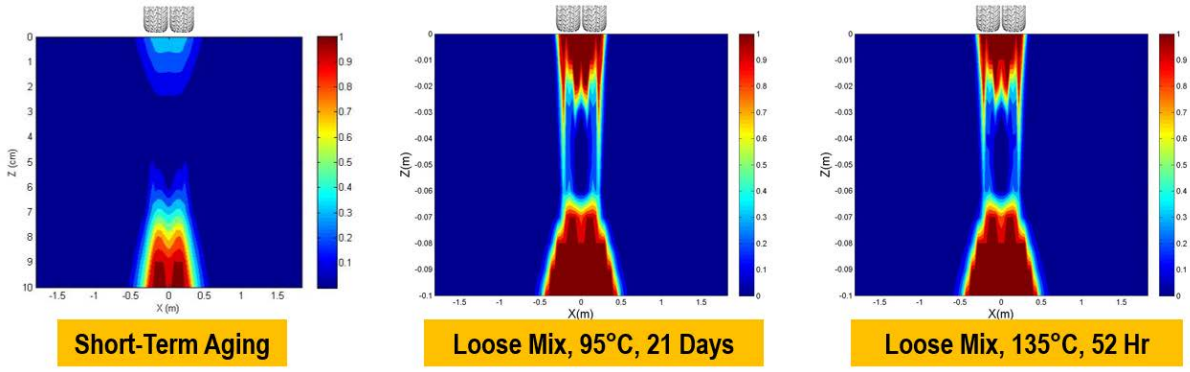

Figure G-14. Damage contours for FHWA ALF-SBS mixture aged at different conditions.

FlexPAVE™ program output data were used to calculate the fatigue damage area as a function of traffic load repetition. Figure G-15 presents the fatigue damage area versus the service life for the three aging treatments. A significant difference can be observed between the fatigue performance of the short-term and long-term aged materials, whereas the results for the two long-term aging treatments at 95°C and 135°C do not indicate any significant differences. These observations are in agreement with the fatigue performance data.

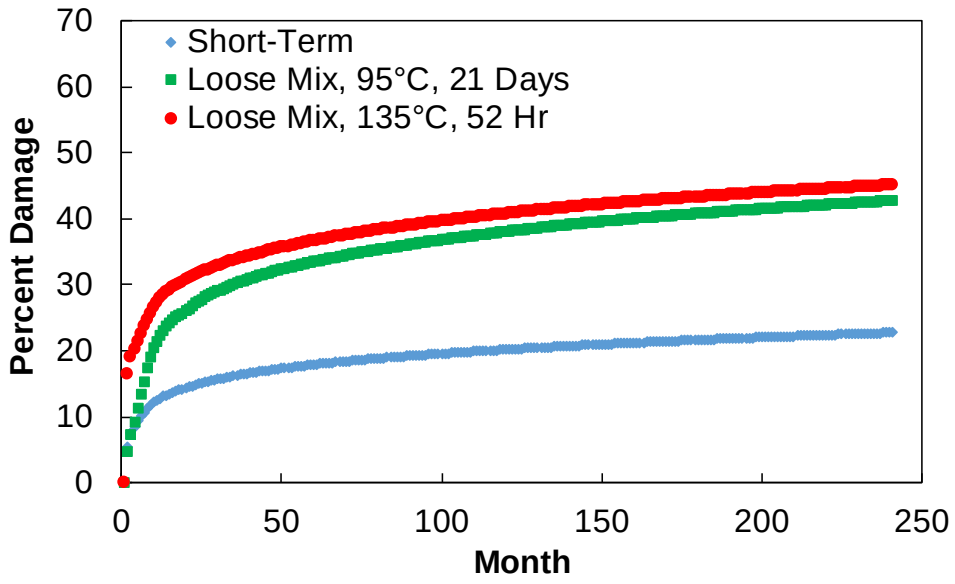

Figure G-15. Comparison of fatigue damage area versus service life for FHWA ALF SBS mixture aged at different conditions.

SHRP AAD

Figure G-16 presents the mixture performance test results for the SHRP AAD mixture. Figure G-16 (a) presents the SHRP AAD mixture dynamic modulus mastercurves that correspond to the specimens fabricated after aging at 95°C and 135°C for 8.9 days and 16.8 hours, respectively. The dynamic modulus test results of the specimens fabricated after short-term aging only also are provided for reference. The results indicate a significant increase in the dynamic modulus value with long-term aging. The results also indicate a significant difference in the dynamic modulus mastercurves that correspond to the mixtures aged at 95°C for 8.9 days and 135°C for 16.8 hours, despite the mixtures' equivalent binder rheology. A 10 percent threshold was used to determine the significance of difference between the dynamic modulus test results at the intermediate and high temperatures. The mixture aged at 135°C exhibits a reduction in modulus value compared to the material aged at 95°C. These results suggest that the chemical changes and/or other effects (e.g., absorption, drain-down) induced by aging at 135°C have a significant effect on the performance of the SHRP AAD mixture. Note that the SHRP AAD binder has high sulfur content and is highly structured, indicating high potential for changes between the oxidation products of laboratory aging at 135°C versus 95°C. Figure G-16 (b) presents the C versus S fatigue damage characteristic replicate curves for the SHRP AAD mixture. The results show that the C versus S curves for the two long-term aging conditions are both higher than the short-term aging C versus S curve, which is attributable to the short-term aged mixture's lower stiffness value (age level) compared to that of the long-term aged materials.

Figure G-16 (b) shows individual replicate C versus S curves that were used to investigate further the significance of the differences between the two long-term aging temperatures. The results demonstrate that the C versus S curves for the mixture aged at 135°C are consistently lower than the curves for the mixture aged at 95°C, which is consistent with the dynamic modulus test results that indicate that the mixture aged at 135°C is less stiff than the

mixture aged at 95°C. Moreover, the C value at failure, indicated by the end point of the C versus S curve, is considerably higher for the mixture aged at 135°C than at 95°C. The average C value at failure is 0.18 for the short-term aged material. The average C values at failure are 0.37 and 0.21 for the long-term aged material conditioned at 95°C and 135°C, respectively. The observed difference in the C values at failure for the long-term aged materials indicates that the mixture aged at 135°C is more brittle than the mixture aged at 95°C.

Figure G-16 (c) presents the failure criterion results for the SHRP AAD mixture, showing that the failure criterion line for the mixture long-term aged at 95°C is similar to that for the short-term aged mixture. However, the failure criterion line for the mixture long-term aged at 135°C is considerably lower than that for the short-term aged mixture, which is indicative of lower fatigue resistance. Note that the x-axis is in logarithmic scale and any difference between the failure criterion lines results in a significant difference in the number of cycles to failure. These results suggest that long-term aging at 135°C leads to degradation of fatigue resistance.

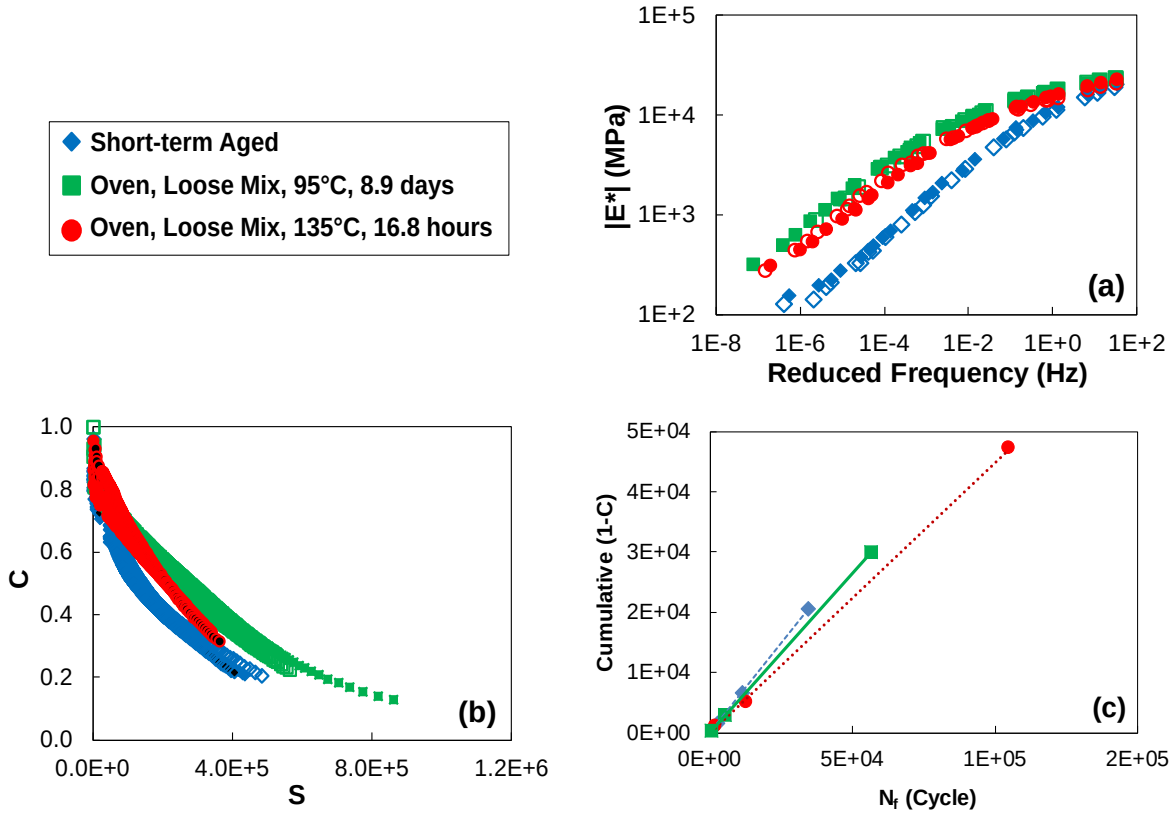

Figure G-16. SHRP AAD mixture performance test results: (a) dynamic modulus curves, (b) C versus S curves, and (c) DR failure criterion lines.

The results presented suggest that long-term aging at 135°C should be avoided due to negative performance implications. In addition to the trends noted in the performance test results, visual observations of fractured specimens also indicate changes between the SHRP AAD mixtures aged at 95°C and 135°C. Figure G-17 presents photos of specimens following fatigue testing. The long-term aged specimens exhibit a higher degree of adhesive failure compared to the short-term aged specimen. Furthermore, the photos indicate that the degree of adhesion loss

is greater in the mixture specimen aged at 135°C than at 95°C, thus supporting observations that aging at 135°C degrades fatigue resistance.

Table G-3 presents the statistical analysis outcomes for the SHRP AAD mixture performance test results. Both long-term aging conditions have a significant effect on the dynamic modulus values and fatigue performance for the SHRP AAD mixture. In spite of the matched binder rheology at the 95°C and 135°C aging temperatures, the significant difference is observed in the dynamic modulus and fatigue performance test data between the 95°C and 135°C aging treatment. Note that, due to the very brittle nature of the SHRP AAD materials aged at 135°C, the comparison is limited to low S values. As suggested by the t-test results, 95°C and 135°C have different effects on the SHRP AAD materials.

Table G-3. Statistical t-Test Analysis Outcomes for Dynamic Modulus and Cyclic Fatigue Test Results for SHRP AAD Materials

	Sample	**Reduced Frequency**			
		1.0E-05	1.0E-04	1.0E-03	1.0E-02
		p-value			
Dynamic Modulus	Short-term, C Loose Mix, 95°C, 8.9 Days, C	**0.0055**	**0.0002**	**0.0058**	**0.0063**
	Short-term, C Loose Mix, 135°C, 16.8 Hr, C	**0.0264**	**0.0213**	**0.0188**	**0.0072**
	Loose Mix, 95°C, 8.9 Days, C Loose Mix, 135°C, 16.8 Hr, C	0.0537	**0.0338**	**0.0218**	**0.0043**
	Sample	**S**			
		1.0E+05	2.0E+05	2.5E+05	3.0E+05
		p-value			
Cyclic Fatigue	Short-term, C Loose Mix, 95°C, 8.9 Days, C	**0.0337**	**0.0062**	**0.0002**	**0.0006**
	Short-term, C Loose Mix, 135°C, 16.8 Hr, C	**0.0093**	**0.0036**	**0.0037**	**0.0044**
	Loose Mix, 95°C, 8.9 Days, C Loose Mix, 135°C, 16.8 Hr, C	0.4232	0.1304	**0.0176**	**0.0134**

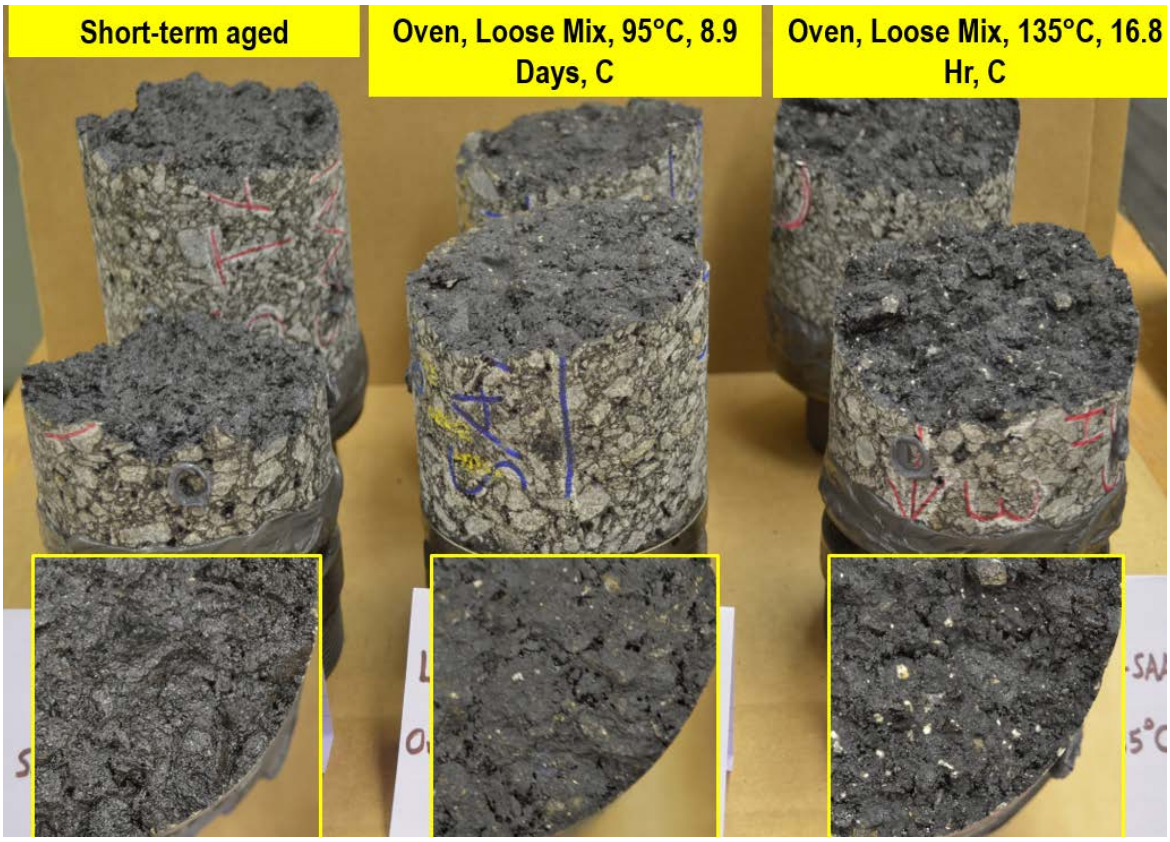

Figure G-17. SHRP AAD specimens following fatigue tests.

Figure G-18 presents the damage contours for the SHRP AAD mixture with different aging treatments. The short-term aged material shows considerably better performance than the long-term aged asphalt materials. Notably, based on the damage contours, the asphalt mixture aged at 95°C shows better performance than the material aged at 135°C; the same conclusion was drawn from the fatigue performance data as well.

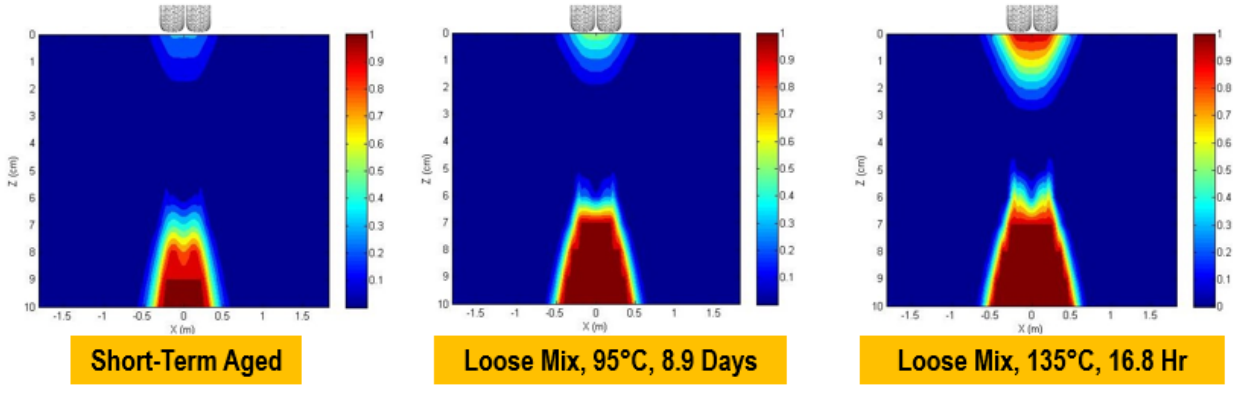

Figure G-18. Damage contours for SHRP AAD mix aged at different conditions.

Figure G-19 presents the fatigue damage area versus service life (month) for the SHRP AAD mixture with different aging treatments. A significant difference between the fatigue performance of the asphalt mixture aged at 95°C and at 135°C is evident.

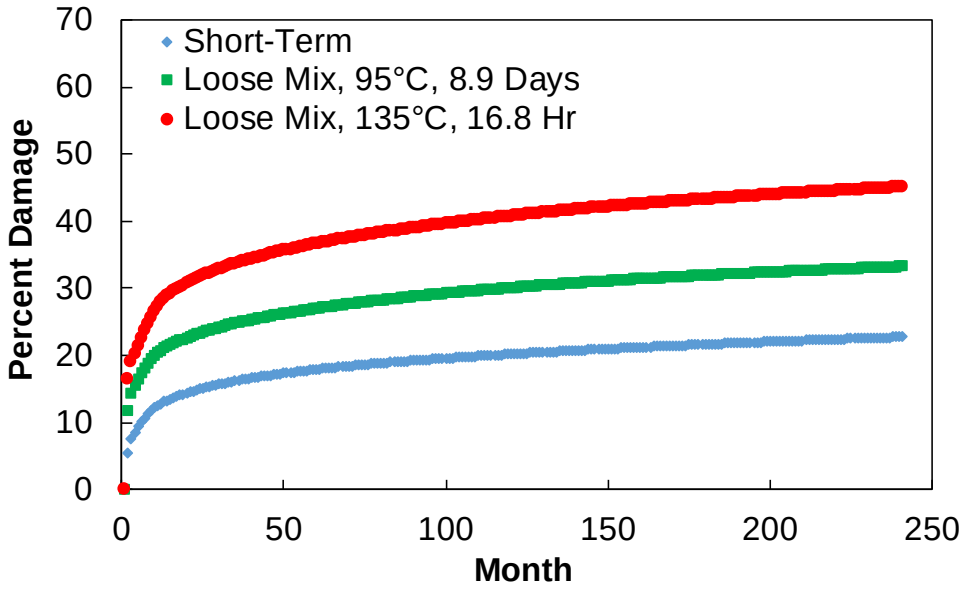

Figure G-19. Comparison of fatigue damage area versus service life for SHRP AAD mixture aged at different conditions.

In order to investigate further the observations made from Figure G-16, asphalt bond strength (ABS) tests (AASHTO TP 91) were conducted using binder extracted and recovered from the SHRP AAD mixture. ABS tests consist of measuring the bond strength between a binder sample and a granite substrate by applying a pneumatic tensile load to an affixed metal pull-out stub. Both the bond strength and failure mechanism can be determined using the ABS test. Figure G-20 presents the ABS test results. These results indicate insignificant differences between the bond strength of binder extracted from short-term aged mixture, binder extracted from mixture long-term aged at 135°C, and binder extracted from mixture long-term aged at 95°C. However, the failure mechanisms clearly differ, as indicated by photos overlaid on the asphalt bond strength (ABS) test results shown in Figure G-20. The binder extracted from mixture aged at 135°C exhibits complete adhesive failure, whereas the binder extracted from mixture aged at 95°C exhibits a greater tendency towards cohesive failure.

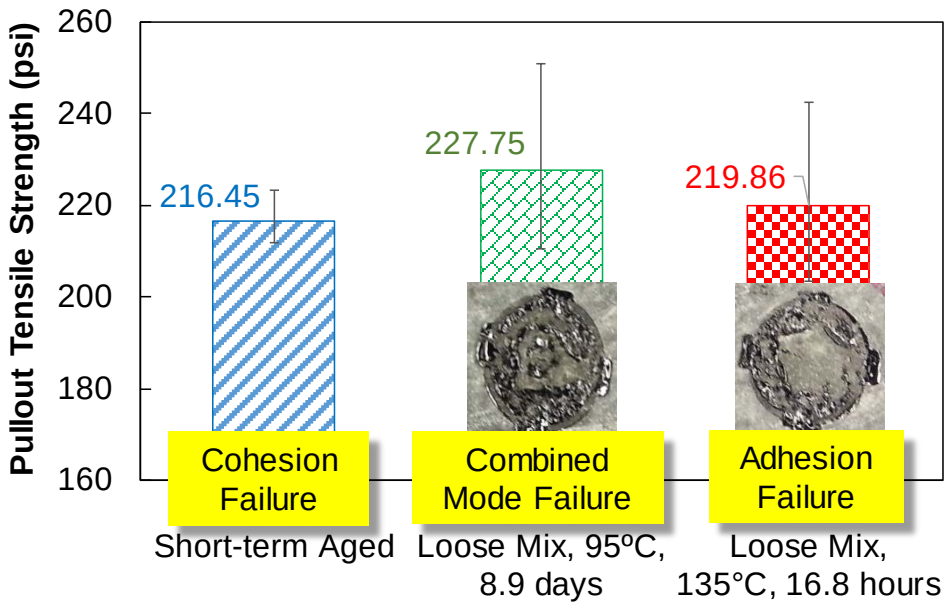

Figure G-20. Asphalt bond strength test results of extracted SHRP AAD binder.

SHRP AAG

Figure G-21 shows the mixture performance test results for the SHRP AAG mixture. Figure G-21 (a) presents the SHRP AAG mixture dynamic modulus mastercurves that correspond to the specimens fabricated after aging at 95°C and 135°C for 19 days and 37.6 hours, respectively. The dynamic modulus test results of specimens fabricated after short-term aging only also are provided for reference. The results indicate a significant increase in the dynamic modulus value with long-term aging. The results also suggest similar dynamic modulus mastercurves that correspond to mixtures aged at 95°C for 19 days and 135°C for 37.6 hours, with slightly higher dynamic modulus values for the mixture aged at 135°C compared to 95°C. However, the binder rheology test results shown in Figure G-12 suggest that the binder contained within the mixture aged at 135°C is slightly stiffer than the binder contained within the mixture aged at 95°C. Thus, it is difficult to ascertain whether or not the results suggest a change in mixture performance as a result of laboratory aging at 135°C as opposed to 95°C. The results presented in Figure G-12 suggest that little chemical change is induced by aging SHRP AAG at 135°C. Hence, any difference noted in performance that results from aging at 135°C as opposed to 95°C is speculated to reflect changes other than chemistry (e.g., absorption, drain-down). Figure G-21 (b) presents the C versus S fatigue damage characteristic curves that correspond to the SHRP AAG mixture. The results show somewhat different trends in the C versus S curves for the two long-term aging conditions, with the short-term aging C versus S curve falling considerably lower than the long-term aged condition curves. Figure G-21 (c) presents the failure criterion results for the SHRP AAG mixture, showing that the failure criterion line for the mixture long-term aged at 95°C is similar to that of the short-term aged mixture, but that the failure criterion line for the mixture long-term aged at 135°C falls somewhat lower, which is indicative of less fatigue resistance.

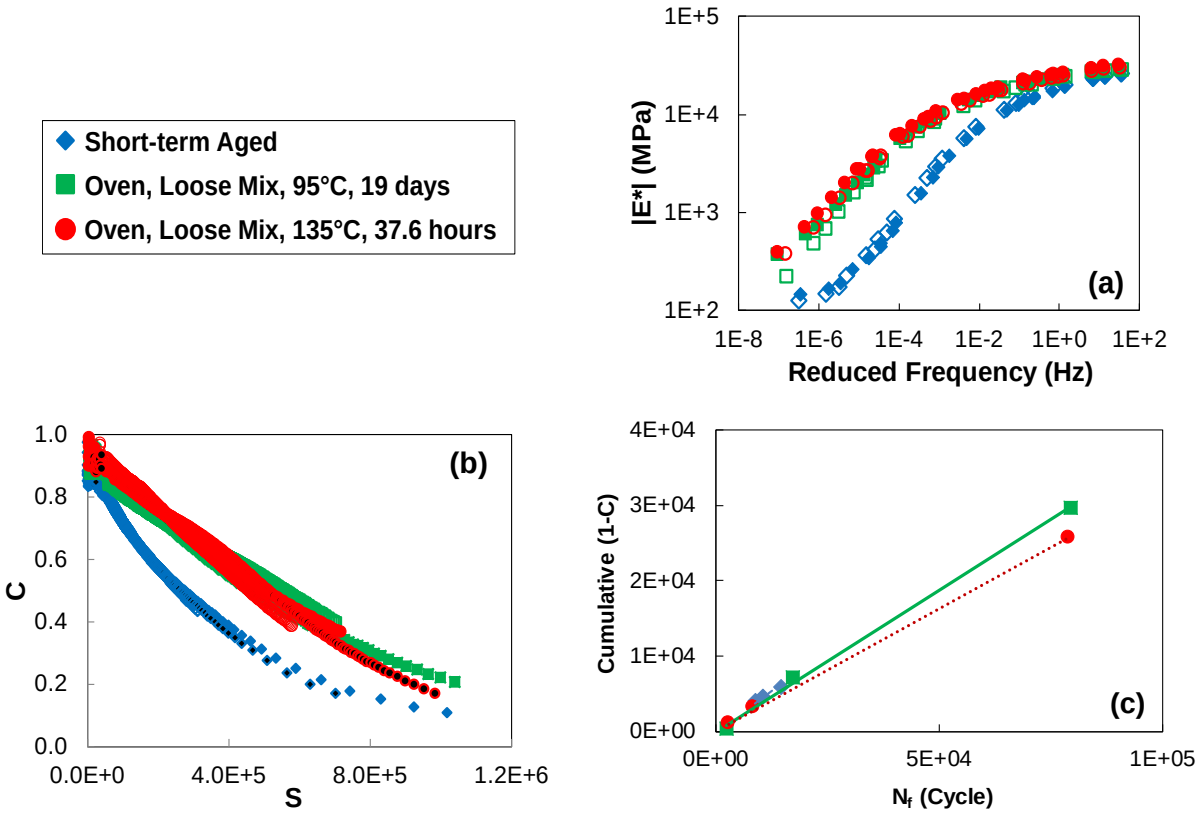

Figure G-21. SHRP AAG mixture performance test results: (a) dynamic modulus curves, (b) C versus S curves, and (c) DR failure criterion lines.

Table G-4 presents the statistical analysis results for each pair of aging treatments. The p-values indicate a significant difference between the performance of the short-term aged and long-term aged SHRP AAG materials. However, although no significant difference can be observed between the dynamic modulus values of the material aged at 95°C and at 135°C, a significant difference between the fatigue test results for these two temperatures is evident. This observation suggests that the 135°C aging temperature induces more brittle behavior than the 95°C aging temperature.

Table G-4. Statistical t-Test Analysis Outcomes for Dynamic Modulus and Cyclic Fatigue Test Results for SHRP AAG Materials

	Sample	Reduced Frequency			
		2.0E-06	1.0E-04	1.0E-03	1.0E-01
		p-value			
Dynamic Modulus	Short-term, C Loose Mix, 95°C, 8.9 Days, C	**0.0102**	**0.0084**	**0.0044**	**0.0109**
	Short-term, C Loose Mix, 135°C, 16.8 Hr, C	**0.0296**	**0.0120**	**0.0023**	**0.0049**
	Loose Mix, 95°C, 8.9 Days, C Loose Mix, 135°C, 16.8 Hr, C	0.0928	0.1169	0.3271	0.2768
	Sample	**S**			
		1.0E+05	2.0E+05	3.0E+05	5.0E+05
		p-value			
Cyclic Fatigue	Short-term, C Loose Mix, 95°C, 8.9 Days, C	**0.0082**	**0.0020**	**0.0001**	**0.0314**
	Short-term, C Loose Mix, 135°C, 16.8 Hr, C	**0.0062**	**0.0001**	**0.0004**	**0.0235**
	Loose Mix, 95°C, 8.9 Days, C Loose Mix, 135°C, 16.8 Hr, C	**0.0161**	**0.0289**	**0.0415**	0.0940

The FlexPAVE™ program results also suggest less fatigue resistance of material aged at 135°C compared to at 95°C. The damage contours presented in Figure G-22 indicate that more severe fatigue cracking is associated with long-term aging at 135°C than at 95°C. Figure G-23 also suggests a significant decrease in fatigue cracking resistance when the 135°C long-term aging treatment is applied.

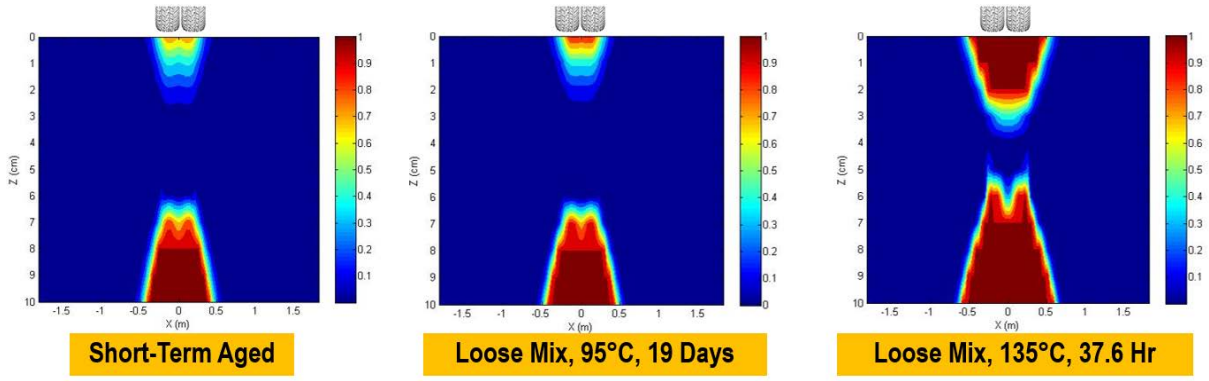

Figure G-22. Damage contours for SHRP AAG mixture aged at different conditions.

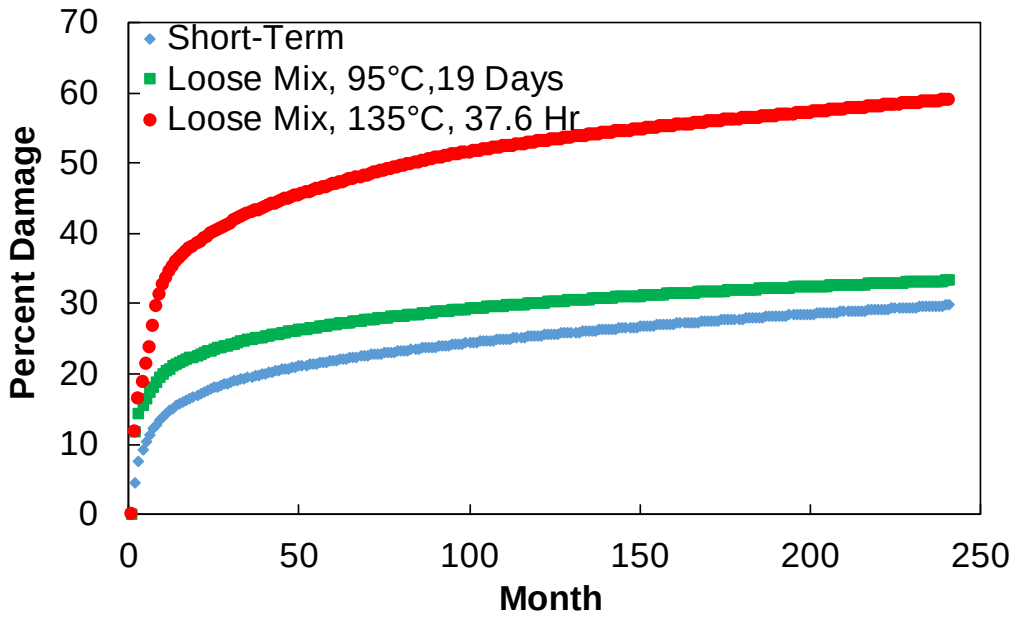

Figure G-23. Comparison of fatigue damage area versus service life for SHRP AAG mixture aged at different conditions.

Conclusions

The primary findings of this study are as follows:

- A significant change in the relationship between binder rheology and chemistry occurs when the aging temperature is increased from 95°C to 135°C. This change implies corresponding changes in the kinetics and mechanisms of the oxidation reactions that are associated with an increase in temperature from 95°C to 135°C, which is consistent with findings described in the literature.
- Asphalt mixture performance can be negatively impacted by long-term aging at 135°C. Despite matching rheology, decreases in both dynamic modulus values and fatigue resistance were observed in two of the three mixtures evaluated in this study. Therefore, it is recommended that aging at 135°C for performance assessment and prediction should be avoided.
- When the loose mix laboratory aging temperature is at or below 95°C, the relationship between binder chemistry and rheology is unaffected by the aging temperature, based on all three mixtures evaluated, indicating that the aging temperature does not affect the oxidation reaction mechanism. The rate of oxidation increases with an increase in temperature, and thus, the results suggest that the optimal loose mixture laboratory aging temperature is 95°C.

References

AASHTO (2012). AASHTO R 30, *Standard Practice for Mixture Conditioning of Hot Mix Asphalt*.AASHTO, Washington, D.C.

AASHTO (2011). AASHTO 342-11, *Standard Method of Test for Determining Dynamic Modulus of Hot Mix Asphalt (HMA)*. AASHTO, Washington, D.C.

AASHTO (2014). AASHTO TP 107, *Determining the Damage Characteristic Curve of Asphalt Concrete from Direct Tension Cyclic Fatigue Tests*. AASHTO, Washington, D.C.

Arega, Z. A., A. Bhasin, and T. De Kesel (2013). Influence of Extended Aging on the Properties of Asphalt Composites Produced Using Hot and Warm Mix Methods. *Construction and Building Materials*, Vol. 44, pp. 168-174.

Blankenship, P. (2015). *Evaluation of Laboratory Performance Tests for Fatigue Cracking of Asphalt Pavements.* Presentation, Federal Highway Administration (FHWA) Asphalt Mixture Expert Task Group (ETG) Meeting, April 2015, Fall River, MA.

Braham, A. F., W. G. Buttlar, T. R. Clyne, M. O. Marasteanu, and M. I. Turos (2009). The Effect of Long-term Laboratory Aging on Asphalt Concrete Fracture Energy. *Journal of the Association of Asphalt Paving Technologies*, Vol. 78.

Branthaver, J. F., J. C. Petersen, et al. (1993). *Binder Characterization and Evaluation – Vol. 2: Chemistry*. Strategic Highway Research Program (SHRP) Report No. SHRP-A-368, National Research Council, Washington, D.C.

Dukatz, E. (2015). *STH 77 Project Objectives*. Presentation, Federal Highway Administration (FHWA) Asphalt Mixture Expert Task Group (ETG) Meeting, April 2015, Fall River, MA.

Elwardany, M. D., F. Yousefi Rad, C. Castorena, and Y. R. Kim (2015). Evaluation of Asphalt Mixture Laboratory Long-Term Aging Methods for Performance Testing and Prediction. *Road Materials and Pavement Design*. Submitted.

Glaser, R., J. Schabron, T. Turner, J. P. Planche, S. Salmans, and J. Loveridge (2013). Low-Temperature Oxidation Kinetics of Asphalt Binders. *Transportation Research Record: Journal of the Transportation Research Board* 2370, pp. 63-68.

Herrington, P. R., J. E. Patrick, and G. F. Ball (1994). Oxidation of Roading Asphalts. *Industrial and Engineering Chemistry Research*, 33(11), pp. 2801-2809.

Kim, Y.R., M.N. Guddati, Y.T. Choi, D. Kim, A. Norouzi, Y. Wang, B. Keshavarzi, M. Ashouri, and A.D. Wargo (2017). Development of Asphalt Mixture Performance-Related Specifications. Final report, Contract No. DTFH61-08-H-00005, North Carolina State University, Raleigh, NC.

Mollenhauer, K. and V. Mouillet (2011). *Re-road – End of Life Strategies of Asphalt Pavements*. European Commission DG Research.

Partl, M. N., H. U. Bahia, F. Canestrari, C. De la Roche, H. Di Benedetto, H. Piber, and D. Sybilski (2013). Advances in Interlaboratory Testing and Evaluation of Bituminous

Materials. The International Union of Laboratories and Experts in Construction Materials, Systems and Structures (RILEM).

Petersen, J. C. (1984). Chemical Composition of Asphalt as Related to Asphalt Durability: State of the Art. *Transportation Research Record* 999, pp. 13-30.

Petersen, J. C. (2009). A Review of the Fundamentals of Asphalt Oxidation: Chemical, Physicochemical, Physical Property, and Durability Relationships. *Transportation Research E-Circular* (E-C140).

Petersen, J. C., S. M. Dorrence, M. Nazir, H. Plancher, and F. A. Barbour (1981). *Oxidation of Sulfur Compounds in Petroleum Residues: Reactivity-Structural Relationships*. American Chemical Society, Division of Petroleum Chemistry, Preprints (United States) 26, No. CONF-810813 (Vol. 2).

Petersen, J. C. and R. Glaser (2011). Asphalt Oxidation Mechanisms and the Role of Oxidation Products on Age Hardening Revisited. *Road Materials and Pavement Design*, 12(4), pp. 795-819.

Petersen, J. C. and P. Harnsberger (1998). Asphalt Aging: Dual Oxidation Mechanism and Its Interrelationships with Asphalt Composition and Oxidative Age Hardening. *Transportation Research Record: Journal of the Transportation Research Board* 1638, pp. 47-55.

Reed, J. (2010). *Evaluation of the Effects of Aging on Asphalt Rubber Pavements*. Ph.D. Dissertation, Arizona State University, Phoenix, AZ.

Sabouri, M. and Y. Kim (2014). Development of A Failure Criterion for Asphalt Mixtures Under Different Modes of Fatigue Loading. *Transportation Research Record: Journal of the Transportation Research Board* 2447, Transportation Research Board of the National Academies, Washington, D.C., pp. 117-125.

Van den Bergh, W. (2011). *The Effect of Aging on Fatigue and Healing Properties of Bituminous Mortars.* Ph.D. Thesis, Delft University of Technology, Delft University.

Wang, Y. and Y. R. Kim. (2017). Development of an Energy-Based Fatigue Failure Criterion for Asphalt Mixtures Based on Viscoelastic Continuum Damage Theory. Submitted to *Construction and Building Materials*.

APPENDIX H

Climatic Aging Index

The current standard method used to assess the long-term aging of asphalt mixtures in the United States is AASHTO R 30 (2010). In this method, asphalt mixtures in the loose state are subjected to short-term aging at 135°C for four hours. Then, the short-term aged mixtures are compacted. The compacted specimen is cored or sawn to the required dimensions and then placed in a forced draft oven for long-term aging. The long-term aging simulation is performed at 85°C ± 3°C for 120 ± 0.5 hours to represent five to ten years of aging in the field. One of the major drawbacks of the current standard long-term aging procedure is that it recommends a single aging duration at 85°C to match field aging at any given location, regardless of the temperature history and climatic region of the pavement of interest. Moreover, the current standard aims to match the average field aging of the top 1.5 to 2 inches of the pavement without addressing the significant aging gradient observed in the field within the top 2 inches of the pavement. In other words, matching the top 0.5 inch from the pavement surface is expected to require longer aging than matching field aging at lower layers, which is not addressed in the current standard AASHTO R 30 standard (Harrigan 2007).

Several climatic indices have been used in different studies to quantify the effect of field temperature history on aging. The Global Aging System (GAS) model (Mirza and Witczak 1995) uses the mean annual air temperature (MAAT) to predict the field aging level, represented as the binder shear modulus (G^*) as a function of time and depth in Pavement ME Design. The cumulative degree days (CDD) index, defined as the sum of the daily high temperatures above freezing, was proposed as a potential means to link laboratory aging duration to an equivalent pavement temperature history in the NCHRP 09-49 and NCHRP 09-52 projects (Newcomb et al. 2015, Martin et al. 2014).

In this study, a climatic aging index (CAI) was derived using a simplification of a rigorous oxidation kinetics model. This CAI was developed to relate the pavement temperature history to the required laboratory aging duration. The main advantage of the CAI over other available climatic indices is the fact that it is based on pavement temperature (not air temperature) and thus can be applied to different pavement depths. It can be used to determine the required laboratory aging duration to match the field aging at any location of interest and depth of interest using pavement temperature hourly data obtained from the Enhanced Integrated Climatic Model (EICM).

Loose mix aging at 95°C was selected in this study as the most promising aging method for the long-term aging of asphalt mixtures. This procedure was applied to some selected component materials for a prolonged duration. Samples were removed periodically and subjected to extraction and recovery after which the binder aging index properties (AIPs) were measured. In addition, binders were extracted and recovered from varying depths of a selected group of field cores obtained from in-service pavements. The AIPs of the field-aged binders were measured and compared to the laboratory-aged oxidation rates to determine the laboratory aging durations that are required to match the target field AIPs for specific projects.

In addition to the CAI, a depth correction factor was developed based on the comparisons between the AIPs measured from the field cores and the AIPs predicted from the kinetics model at different depths and durations. Finally, CAI analysis has been used in this study to generate

maps of the United States that allow the visual determination of the required laboratory aging durations for the field age of interest and depth of interest.

In the following sections, the research efforts undertaken in this study to identify a promising climatic index among different indices are discussed. The overarching approach is described as follows. The laboratory aging duration that is needed to match the age-level field aging was first determined experimentally using the materials and sections presented in Table H-1. Loose mixture aging was conducted using the materials presented in Table H-1 at 95°C, and binders were extracted and recovered at periodic intervals and from corresponding field cores at various depths. The laboratory aging duration that is required to match the age level of the field cores was determined subsequently based on matching the G^* values at 64°C and 10 rad/s. The measured laboratory aging durations to match the field aging durations were compared against the different climatic indices in order to compare them and evaluate their applicability to relate long-term aging duration to different climatic regions and temperature histories in the field.

Table H-1. Selected test sections for evaluating different climatic indices and calibrating the climatic aging index (CAI)

Site ID	Location	Binder/Modification	Date Built	Date Core Extracted
FHWA ALF	Virginia	Control, SBS-LG	2001	2013
LTPP[a] SPS-8	New Mexico	Asphalt Cement AC-20	1996	2006, 2014
	South Dakota	Asphalt Cement 120-150 pen	1993	2014
	Texas	Asphalt Cement AC-20	1996	2014
	Wisconsin, SR-29	-	1997	2005, 2014
WesTrack Fine Sections (1, 2, 3, 4, 14, 17, 18)	Dayton, Nevada	PG 64-22	1995	1995, 1999, 2014
WesTrack Coarse Sections (36, 39)	Dayton, Nevada	PG 64-22	1997	1997, 1999

[a] LTPP stands for Long-Term Pavement Performance.

Grouping Sections Based on Climatic High Temperature Performance Grade (PG)

One simple method that can be used to specify long-term aging durations based on climatic region is to use the climatic high temperature PG as an index value to group different geographic areas based on their climate. The climatic high temperature PG is determined using a model that is based on a depth of 20 mm, yearly degree days above 10°C, and the assumed threshold for the allowable rut depth of 12.7 mm (Mohseni et al. 2005). These values can be obtained from LTPPBind v3.1 software and are presented in Figure H-1.

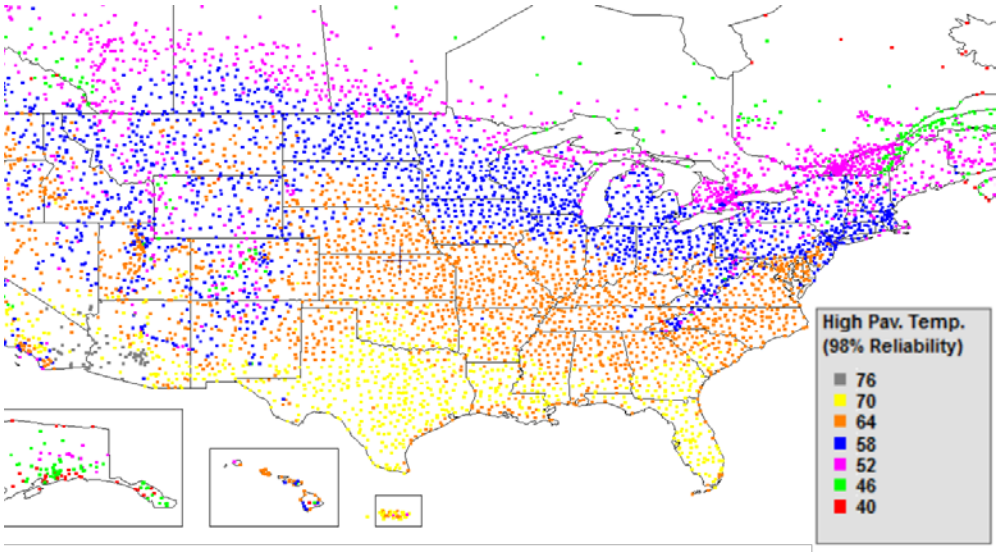

Figure H-1. Climatic high temperature performance grades.

The climatic high temperature PG (°C) is multiplied by the field age (years) and used as a climatic index value to represent the pavement climatic history and pavement age using a single number. Figure H-2 shows the correlation between the climatic high temperature PG × field age and the laboratory aging duration at 95°C to match the field aging at a depth of 20 mm.

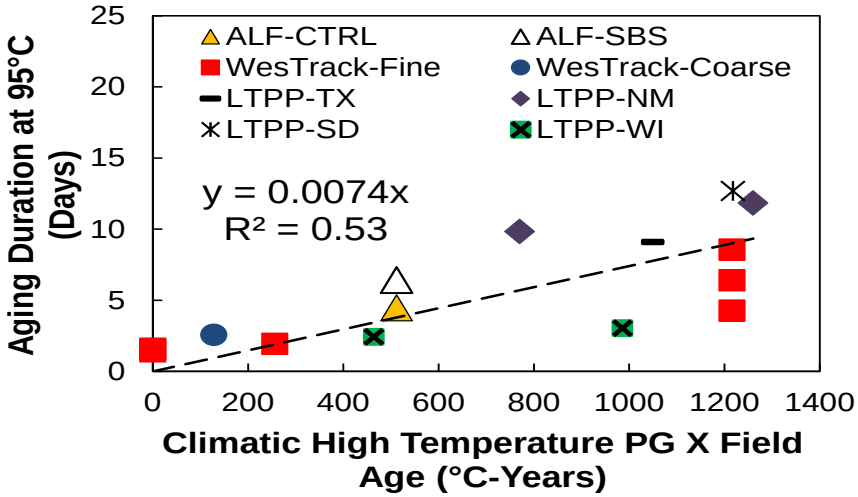

Figure H-2. Correlation between climatic high temperature PG × field age (°C-years) and measured aging durations at 95°C to match field aging at 20-mm depth.

Mean Annual Air Temperature (MAAT)

The GAS model (Mirza and Witczak 1995) is an empirical model that allows for the prediction of the change in binder viscosity as a function of age, given the MAAT as a climatic index value. The GAS model also considers the aging gradient with pavement depth. The model assumes a hyperbolic aging function that predicts a decreasing rate of viscosity increase with an increase in age, under the assumption that most age hardening occurs within the first ten years of

a pavement's service life. The GAS model is summarized in Equations H-1 and H-2. Figure H-3 shows the correlation between the MAAT multiplied by age and the laboratory aging duration at 95°C to match field aging at 20-mm depth.

$$\log\log(\eta_{aged}) = \frac{\log\log(\eta_{t=0}) + At}{1 + Bt} F_v \quad \text{(H-1)}$$

$$\log\log(\eta_{aged,z}) = \frac{\eta_{aged}(4+E) - E \times \eta_{t=0}(1-4z)}{4(1+E \times z)} F_v \quad \text{(H-2)}$$

where

η_{aged} = aged viscosity (centipoise),
$\eta_{t=0}$ = viscosity at mix/laydown (centipoise),
A and B = functions of the temperature and MAAT for the location of interest and $\eta_{t=0}$,
F_v = optional air void content adjustment factor,
t = time in months,
z = depth, and
E = function of MAAT.

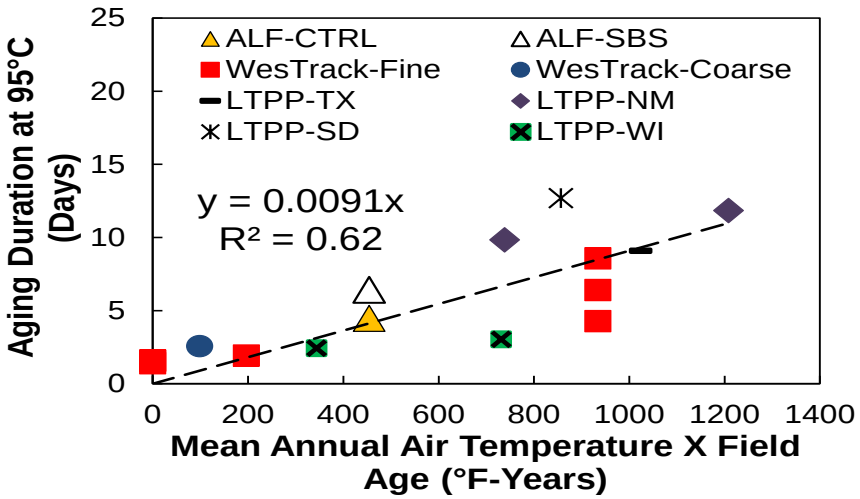

Figure H-3. Correlation between mean annual air temperature × field age (°F-years) and measured aging duration at 95°C to match field aging at 20-mm depth.

Cumulative Degree Days (CDD)

The CDD index has been proposed in the NCHRP 09-49 and NCHRP 09-52 projects (Newcomb et al. 2015, Martin et al. 2014) as a field metric that accounts for both in-service temperature and time and is defined as the sum of the daily high temperatures above freezing. The CDD index was proposed as a potential means to link laboratory aging durations to an equivalent pavement temperature history. Thus, mixtures placed in two different climatic regions, for example, New Mexico and Wisconsin, could be considered to age differently over the same period (Newcomb et al. 2015). The CDD index can be calculated using Equation H-3.

Figure H-4 shows the correlation between the CDD index values and the laboratory aging durations at 95°C to match field aging at 20-mm depth.

$$CDD = \sum (T_{d\max} - 32) \quad \text{(H-3)}$$

where

$T_{d\ max}$ = daily maximum temperature, °F.

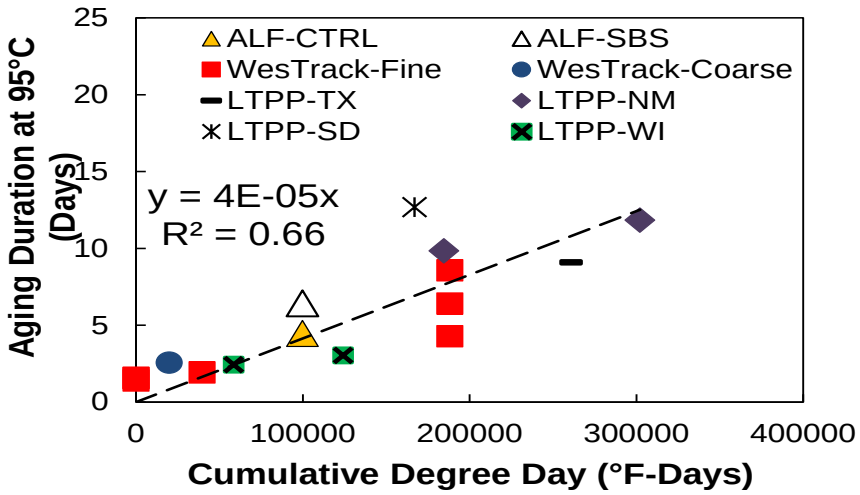

Figure H-4. Correlation between cumulative degree days (°F-Days) and the measured aging duration at 95°C to match field aging at 20-mm depth.

Development of Climatic Aging Index (CAI)

The CAI is the climatic index developed in this study using the *G**-based kinetics model shown in Equation H-4. First, it was verified that loose mix aging is a kinetics-controlled reaction mechanism, which is a requirement for applying kinetics models without considering diffusion. (This verification work is presented in the *Evaluation of the Loose Mixture Aging Reaction Mechanism* section of the main report on page 57.) Then, a kinetics model for loose mixture aging was developed and then validated using log *G** at 64°C and 10 rad/s frequency as the AIP within Glaser et al.'s (2013) kinetics model framework that was developed initially for binder aging. (Details regarding the *G**-based kinetics model development and verification are presented in the *Kinetics Modeling of Loose Mixtures under Isothermal Aging* section and *Kinetics Modeling of Non-Isothermal Aging* section on pages 57-61 of the main report.) Equation H-4 shows the developed kinetics model. Additionally, the kinetics model was calibrated using AIP measurements obtained from isothermal aging at a single temperature. Furthermore, it was proven, theoretically and experimentally using both laboratory and field data, that the laboratory oven aging duration that is required to match field aging for a given mixture is *independent* of the mixture-specific kinetics model parameters (*G** of the short-term aged material and *M*), as shown in Equation H-5. (This work is presented in the *Kinetics Derivation of Laboratory Aging Duration* section on pages 62-64 of the main report).

The use of Equation H-5 to determine laboratory aging durations as a function of pavement temperature history is computationally expensive. Furthermore, the kinetics model

expressed in Equation H-5 does not consider the diffusion that affects oxidation levels within pavements. Therefore, the application of Equation H-5 to determine laboratory loose mixture aging durations would likely be inaccurate without either the inclusion of a diffusion model or calibration against the field data. To overcome these challenges, the kinetics model was simplified and calibrated against field data that correspond to a wide range of climatic conditions and depths in order to develop a CAI that can prescribe laboratory aging durations using pavement temperature history.

Equation H-6 shows the kinetics model for the prediction of log G^* as a function of pavement temperature and pressure history. The required inputs of this model are the pavement temperature and pressure history, reaction orders for fast and constant reactions (m and n, respectively), and the mixture-specific kinetics parameters, M and log G^*_o, where G^*_o is the G^* that corresponds to the short-term aged condition. Although the effect of the oxidation spurt is clearly evident in laboratory aging that is conducted at an elevated temperature, e.g., 85°C and 95°C, the log G^* and aging duration relationship is almost linear at 70°C. Therefore, the effect of the oxidation spurt on aging of pavements in service is relatively small because pavement temperatures do not go as high as 85°C and 95°C. Therefore, when Equation H-6 is used to predict log G^* as a function of time using pavement temperature history data, the effect of the fast-rate oxidation spurt is negligible, which allows Equation H-6 to be simplified to the form given in Equation H-7.

To further support the simplification of Equation H-6 to Equation H-7, k_c and k_f are shown as functions of temperature in Figure H-5. Figure H-5 shows that, at temperatures below 15°C, k_f is very small, which gives the exponential term in Equation H-6 a value that is close to one. Consequently, at temperatures below 15°C, the second term in the red portion of Equation H-6 tends towards zero. At temperatures between 15°C and 60°C, k_c/k_f is relatively close to one, which causes the first parenthesis in the red term in Equation H-6 to be close to zero. Hence, at typical pavement temperatures, the red term in Equation H-6 tends to be zero and thus Equation H-6 can be simplified to Equation H-7.

Equation H-5 demonstrates that the determination of laboratory aging durations at 95°C is independent of the mixture-specific parameters, M and G^*_o. Thus, with regard to the duration of laboratory aging, the pertinent parameters in Equation H-7 are k (rate of reaction) and P^n (oxygen pressure term). The P^n parameter is affected by altitude and pavement depth. Because all the sections shown in Table H-1 that were used in the climatic index study are not in locations with high altitudes, the P^n parameter is affected mostly by pavement depth. Therefore, the P^n parameter is replaced by the D term (representing the depth correction factor) in Equation H-8 to define the CAI. The CAI in Equation H-8 is now defined by the rate of reaction, reaction time, and pavement depth.

The slow reaction rate term k in Equation H-8 can be represented using Arrhenius equation parameters, as shown in Equation H-9, where the units of time are days. In order to consider hourly temperature data, a summation of the CAI values is applied based on the hourly temperature history, as shown in Equation H-10.

$$\log G^*_{lab} = \log G^*_{o,lab} + M\left[\left(1-\frac{k_c}{k_f}\right)(1-\exp(-k_f t)) + k_c t\right]_{lab} \qquad \text{(H-4)}$$

$$\left[\left(1-\frac{k_c}{k_f}\right)(1-\exp(-k_f t))+k_c t\right]_{field} = \left[\left(1-\frac{k_c}{k_f}\right)(1-\exp(-k_f t))+k_c t\right]_{lab} \quad \text{(H-5)}$$

$$\log G^*_{field} = \log G^*_{o,\text{field}} + M\left[\left(1-\frac{k_c.P^n}{k_f.P^m}\right)(1-\exp(-k_f P^m t)) + k_c P^n t\right]_{field} \quad \text{(H-6)}$$

$$\log G^*_{field} = \log G^*_{o,\text{field}} + MkP^n t \quad \text{(H-7)}$$

$$CAI = Dkt \quad \text{(H-8)}$$

$$CAI = D\times(A\times\exp(-E_a / RT))\times t \quad \text{(H-9)}$$

$$CAI = \sum DA\exp(-E_a / RT)/24 \quad \text{(H-10)}$$

where

k = rate of reaction,
k_f = rate of fast reaction,
k_c = rate of constant reaction,
t = reaction time (days),
P = absolute oxygen pressure,
m = reaction order of fast reaction,
n = reaction order of constant reaction,
D = depth correction factor,
M = fitting parameter related to fast reaction reactive material, and
CAI = climatic aging index.

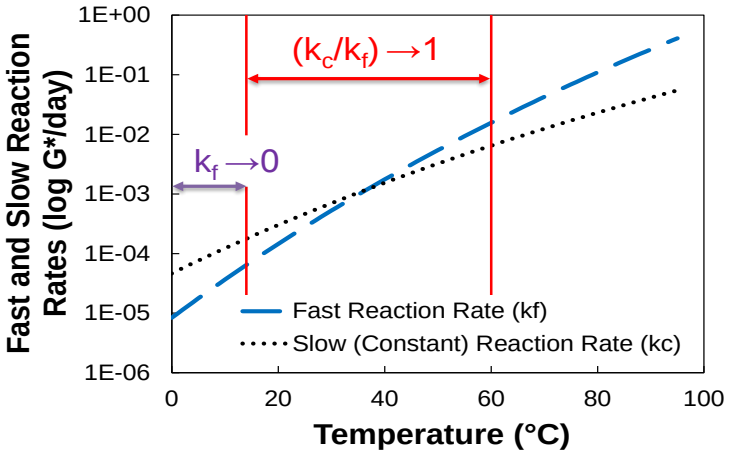

Figure H-5. Fast and slow reaction rates at different temperatures.

The CAI can be applied to determine the loose mixture aging duration at 95°C to match a given pavement temperature history at any depth of interest. However, a comparison of different climatic indices requires their index values to be determined at the same depth. Because the high-

temperature PG is determined at a depth of 20 mm from the surface, all other climatic indices, including the CAI, are determined at that depth.

In order to calculate CAI values at a depth of 20 mm, the pavement temperature histories acquired from EICM data for the sections presented in Table H-1 were input into Equation H-10. Then, parameters E_a and A in Equation H-10 were regressed to provide the best fit between the CAI values and measured laboratory aging durations using a D value of 0.4565. The data and discussion behind the determination of the depth correction factor (D = 0.4565) at the 20-mm depth are presented later in this appendix. Figure H-6 shows the correlation between the CAI values and the measured aging durations at 95°C to match field aging at 20-mm depth.

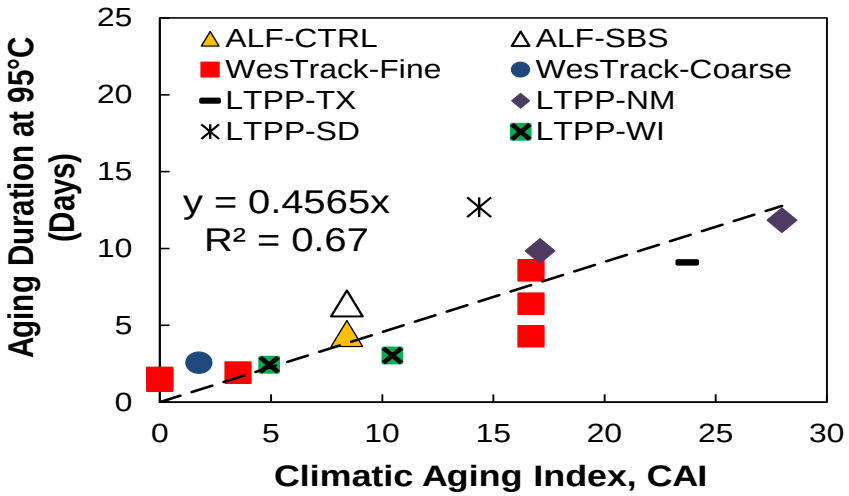

Figure H-6. Correlation between climatic aging index values at 20-mm depth and measured aging durations at 95°C to match field aging at 20-mm depth.

Comparison among Different Climatic Indices

Figure H-7 shows the correlations between the different climatic indices and the laboratory aging durations at 95°C to match field aging at 20-mm depth. Figures H-2, H-3, H-4, and H-6 are duplicated in Figure H-7 in order to aid the comparison among different indices. Based on these comparisons, the CDD index and CAI showed good correlations with the measured laboratory aging durations (R^2 values greater than 0.65); however, of these two indices, the CAI was selected as the better of the two as it is based on pavement temperature (not air temperature) and thus can be applied to different pavement depths. That is, the CAI accounts for the effect of the temperature gradient throughout the pavement depth using the rigorous G^*-based oxidation kinetics model. Although an additional depth correction factor was needed to account for the diffusion of oxygen throughout the depth of the pavement, detailed modeling of the temperature effect on aging throughout the pavement depth in the CAI is deemed to be a significant enhancement over the CDD index.

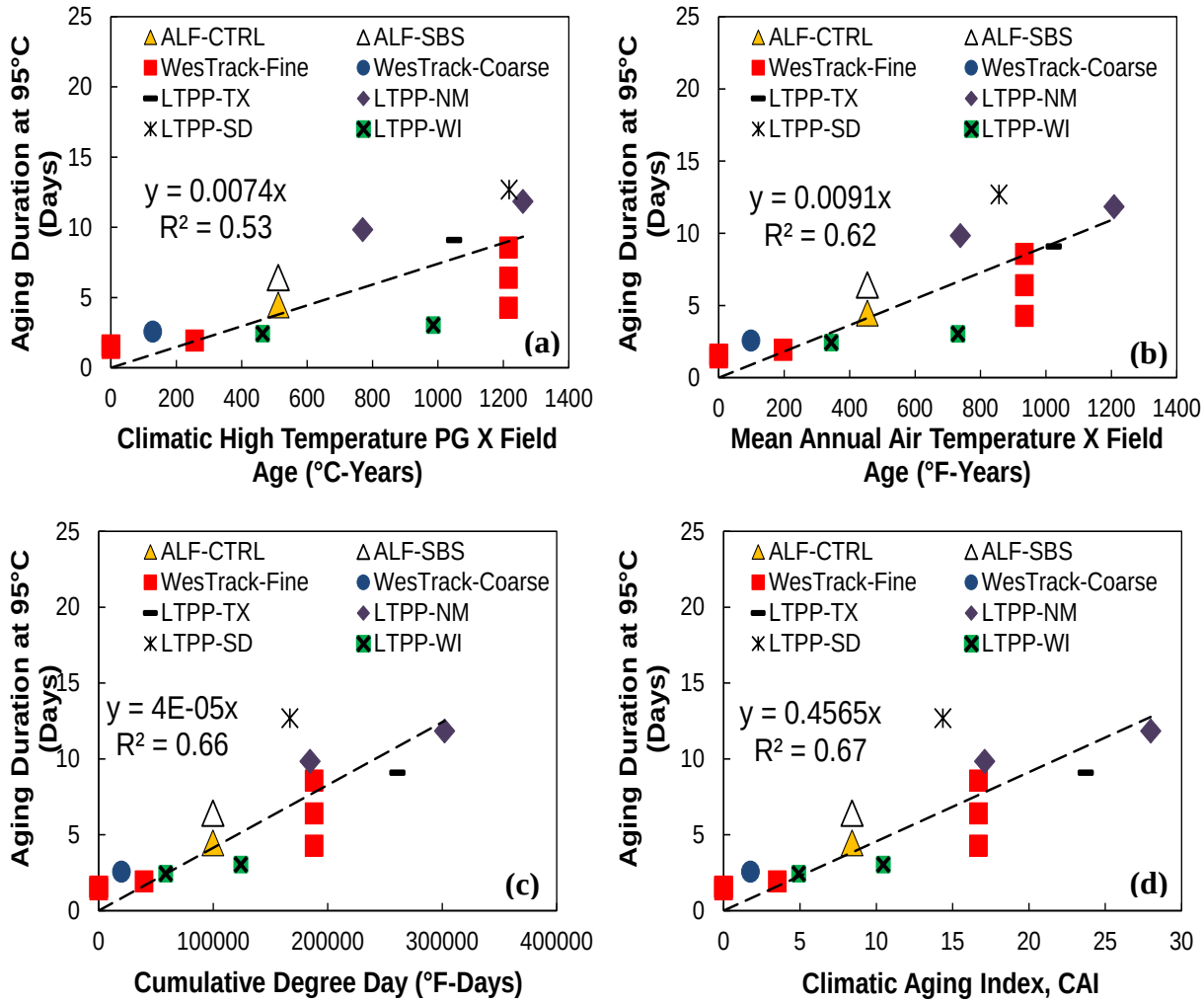

Figure H-7. Correlations between measured aging durations at 95°C to match field aging at 20-mm depth and different climatic indices: (a) climatic high temperature performance grade (PG) × field age (°C-years), (b) mean annual air temperature (MAAT) × field age (°F-years), (c) cumulative degree days (CDD) (°F-days), and (d) climatic aging index (CAI).

Climatic Aging Index (CAI) at Different Pavement Depths

Figure H-8 (a) shows the relationship between the CAI values and measured laboratory durations at 95°C without applying the depth correction factor *D* in Equations H-10. The figure shows significant scatter in the data and an overall low R^2 value. Figure H-8 (b) presents the CAI calibrations separately for three depths: the near-surface layer 6 mm from the surface, 20 mm from the surface, and deeper layers below 20 mm. Figure H-8 (b) also shows that separating the data according to depth improves the relationship between the CAI values and laboratory aging durations significantly, thereby highlighting the need for the depth correction. Thus, the E_a and *A* parameters were first calibrated using the data that correspond to a depth of 6 mm to provide a CAI value that is equivalent to the required laboratory aging duration at 95°C to match the pavement temperature history. Then, the *D* values were calibrated using the data that correspond to depths of 20 mm and deeper. It is worth mentioning that the depth correction factor *D* is

affected not only by diffusion mechanisms but also by photo-oxidation effects at the pavement surface. Figure H-8 (c) shows the relationship between the laboratory aging durations and CAI values after applying the depth correction factors shown in Table H-2. The results demonstrate a strong one-to-one relationship between the CAI values and measured laboratory aging durations. Thus, the CAI value can be regarded as the required laboratory aging duration at 95°C to match a given pavement temperature history and depth.

Table H-2. Climatic aging index fitting coefficients

MIX ID	Depth Correction Factor (*D*)	Arrhenius Equation, Pre-exponential Factor (*A*)	Arrhenius Equation, Activation Energy E_a
Surface Layer (6 mm)	1.0000	1.40962	13.3121
20-mm depth	0.4565	1.40962	13.3121
Deeper Layers (below 20 mm)	0.2967	1.40962	13.3121

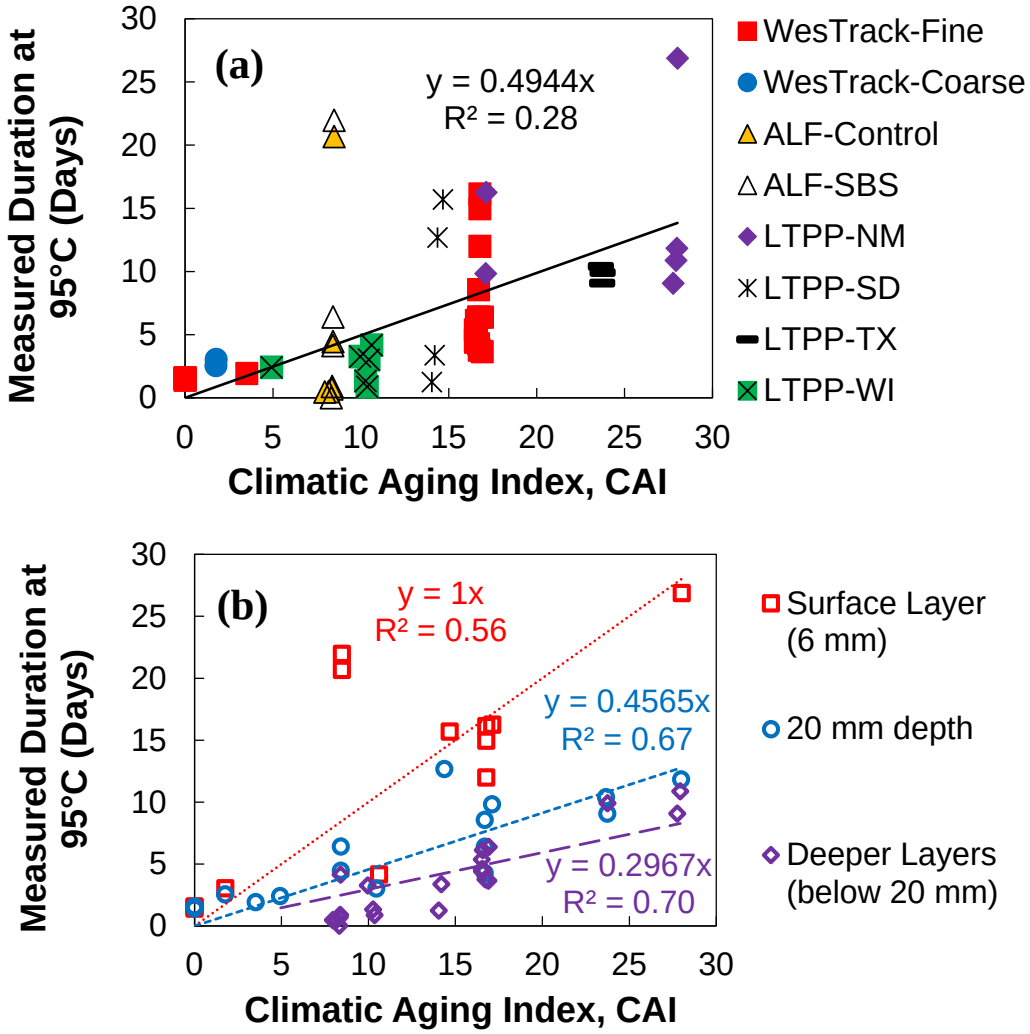
(a)
y = 0.4944x
R² = 0.28
Measured Duration at 95°C (Days)
Climatic Aging Index, CAI
0
5
10
15
20
25
30
WesTrack-Fine
WesTrack-Coarse
ALF-Control
ALF-SBS
LTPP-NM
LTPP-SD
LTPP-TX
LTPP-WI
(b)
y = 1x
R² = 0.56
y = 0.4565x
R² = 0.67
y = 0.2967x
R² = 0.70
Measured Duration at 95°C (Days)
Climatic Aging Index, CAI
Surface Layer (6 mm)
20 mm depth
Deeper Layers (below 20 mm)

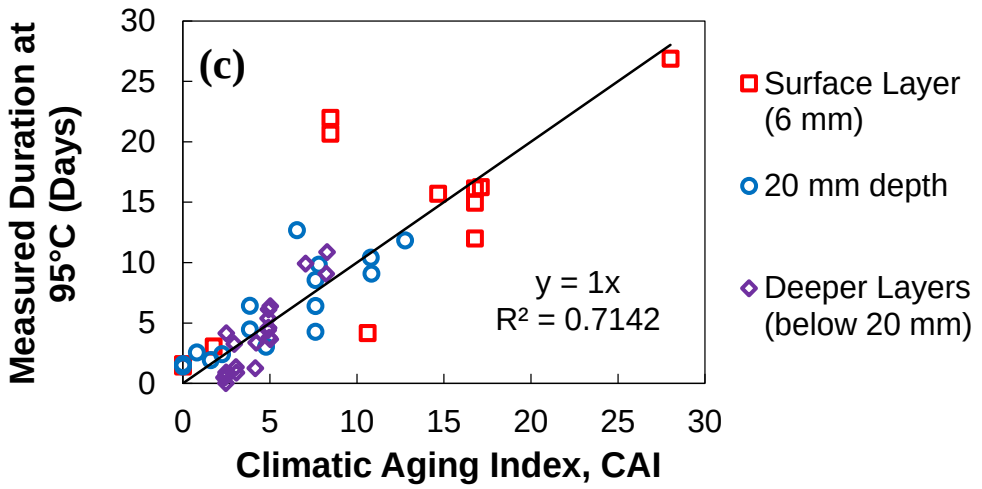

Figure H-8. Climatic aging index (CAI) predictions: (a) overall CAI fitting without depth correction factor *D*, (b) CAI fitting based on layer depth without depth correction factor *D*, and (c) overall CAI fitting after applying depth correction factor *D*.

Application

CAI values for various locations in the United States can be calculated using hourly pavement temperature history data obtained from the EICM to provide an overview of the proposed laboratory aging durations for various climates, field aging durations, and depths. As shown in Figure H-8 (c), the CAI values and measured durations that are needed to match field aging correlate linearly in a one-to-one relationship. Thus, the CAI values represent the required durations at 95°C that are needed to match the field aging for a given pavement temperature history and depth. For instance, Figure H-9 shows the CAI-determined loose mixture aging durations at 95°C that are required to match eight years of field aging at a depth of 20 mm from the pavement surface. (Similar maps for different field ages and pavement depths are presented in the *Laboratory Aging Duration Maps* section on pages 69-75 of the main report).

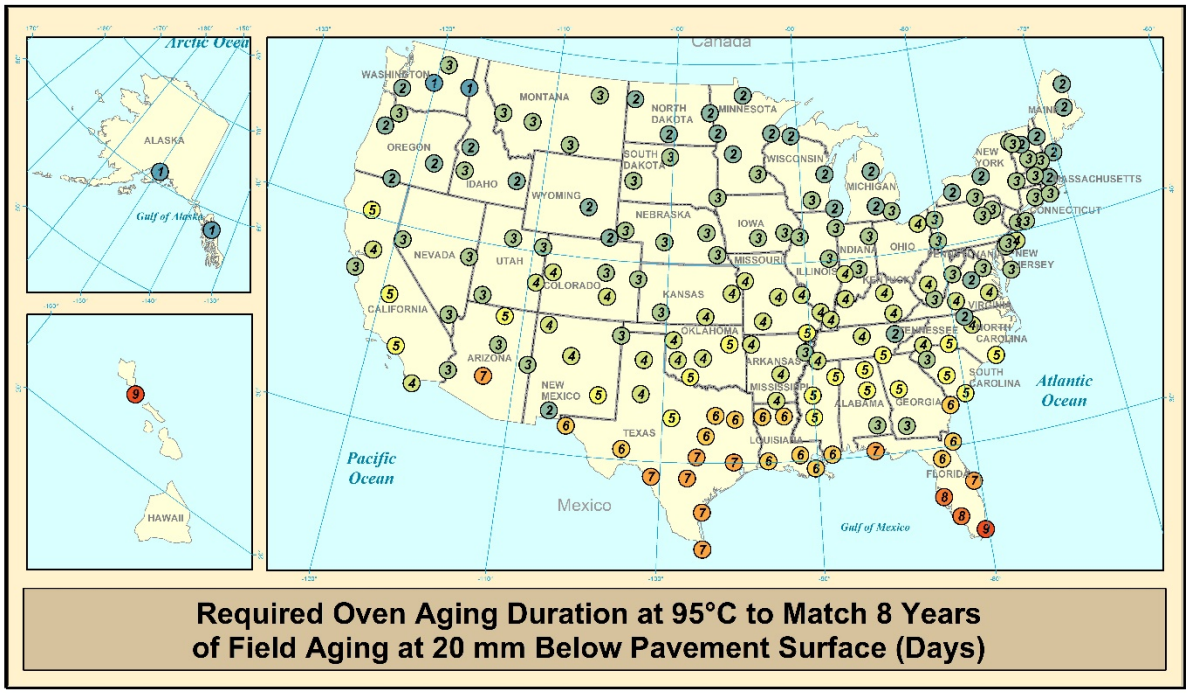

Figure H-9. Example of an aging duration map showing the required oven aging durations at 95°C to match level of field aging 20 mm below pavement surface for eight years of field aging.

Conclusions

The following conclusions pertain to the comparisons between different climatic indices and the development of the CAI.

- CDD and CAI climatic indices showed good correlations with measured aging durations at 95°C to match field aging at 20-mm depth.
- The CAI is advantageous over alternative aging indices for several reasons:

  (1) The CAI is based on pavement temperature rather than air temperature.
  (2) The CAI can be applied at different depths and uses a depth correction factor (*D*) and variations in pavement temperature with depth.
  (3) The CAI considers the exponential relationship between aging rate and temperature.
  (4) The CAI captures hourly pavement temperatures.

- Depth correction factor *D* significantly improved CAI correlations with measured aging durations at 95°C to match field aging at various pavement depths. The R^2 values for CAI correlations with measured laboratory durations to match field aging

increased from 0.28 before applying the depth correction factor to 0.71 after applying the depth correction factor.

References

American Association of State Highway and Transportation Officials (AASHTO), *Standard Practice for Mixture Conditioning of Hot Mix Asphalt*, AASHTO R 30, Washington, D.C. (2010).

Glaser, R., J. Schabron, T. Turner, J. P. Planche, S. Salmans, and J. Loveridge, "Low-Temperature Oxidation Kinetics of Asphalt Binders." *Transportation Research Record: Journal of the Transportation Research Board*, No. 2370 (2013) pp. 63-68.

Harrigan, E. T. *Research Results Digest 324 - Simulating the Effects of Hot Mix Asphalt Aging for Performance Testing and Pavement Structural Design.* National Cooperative Highway Research Program (2007).

Martin, A. E., E. Arambula, F. Yin, L. G. Cucalon, A. Chowdhury, R. Lytton, J. Epps, C. Estakhri, and E. S. Park, *Evaluation of the Moisture Susceptibility of WMA Technologies*, Final Report, National Cooperative Highway Research Program, No. Project 09-49, NCHRP Report 763, National Research Council, Washington, D.C. (2014).

Mirza, M. W. and M. W. Witczak, "Development of Global Aging System for Short and Long Term Aging of Asphalt Cements." *Journal of the Association of Asphalt Paving Technologists*, Vol. 64 (1995) pp. 393-430.

Mohseni, A., S. H. Carpenter, and J. D'Angelo. "Development of Superpave High-Temperature Performance Grade (PG) Based on Rutting Damage (with Discussion and Closure)." *Journal of the Association of Asphalt Paving Technologists*, Vol. 74, No. 1 (2005), pp. 197-254.

Newcomb, D., A. E. Martin, F. Yin, E. Arambula, E. S. Park, A. Chowdhury, R. Brown, C. Rodezno, N. Tran, E. Coleri, and D. Jones, *Short-Term Laboratory Conditioning of Asphalt Mixtures*, Final Report, National Cooperative Highway Research Program, No. Project 09-52, NCHRP Report 815, National Research Council, Washington, D.C. (2015).

APPENDIX I

Performance Testing of Field Cores

Introduction

Because the goal of this project is to develop a long-term aging protocol for performance testing and analysis, it is important to compare the performance characteristics of laboratory-aged materials and field cores that both have been aged for the same level of oxidation. However, the performance properties of laboratory-aged specimens and those of field cores may not match, even though they have the same oxidation level, due to the presence of moisture and thermal cycling in the field. With this situation in mind, the NC State University research team tested field cores extracted from several Long-Term Pavement Performance (LTPP) sections. The initial goal of the performance testing of these field cores was to inform the development of calibration functions to account for differences in the performance of laboratory-aged and field-aged materials, other than differences caused by oxidation. However, the variability in the air void contents and uncertainty in the traffic loading (uncertainty that is due to the fact that the load level depends on the location of the pavement from which the core is extracted) precluded development of such calibration functions. The performance analysis of the field cores is presented in the following sections.

Field Sample Testing Method

The research team acquired field cores from four LTPP sections. Small specimens (38-mm diameter by 110-mm tall) were extracted horizontally from the top lift of the field cores for dynamic modulus and cyclic fatigue testing. Figure I-1 (a) shows small specimens extracted from a 6-inch field core from a LTPP Wisconsin section at three depths. The team also performed dynamic modulus testing in compression mode using a MTS servo-hydraulic test system according to AASHTO PP 342. Four temperatures (4°C, 15°C, 27°C, and 40°C) and six loading frequencies (25, 10, 5, 1, 0.5, and 0.1 Hz) were used for the dynamic modulus tests. Figure I-1 (b) shows a 38-mm specimen prepared for dynamic modulus testing.

Figure I-1. LTPP Wisconsin field core: (a) small specimens extracted from a 6-inch field core and (b) small specimen prepared for dynamic modulus testing.

The research team performed the cyclic fatigue tests using a MTS servo-hydraulic test system according to AASHTO TP 107. Also in accordance with AASHTO TP 107, the team selected the cyclic fatigue test temperature based on the local binder performance grade. The team conducted the cyclic fatigue tests at three cross-head displacement amplitudes and then combined the results with the dynamic modulus test results to determine the Simplified Viscoelastic Continuum Damage (S-VECD) model parameters. Table I-1 summarizes the information that pertains to the evaluated LTPP sections. Note that the field cores were acquired at two levels of field aging for all sections evaluated.

Table I-1. Summary of LTPP field sections considered for performance testing

Project ID	Location	Section ID	Construction Date	Date Core Extracted (Core Age)		Climatic Zone
LTPP SPS-8	NM	LTPP SPS-8 New Mexico	1996	2006	2014	Dry/Non-Freeze
	WA	LTPP SPS-8 Washington	1995	2006	2014	Dry/Freeze
	WI	LTPP SPS-8 Wisconsin, SR-29	1997	2005	2014	Wet/Freeze
	SD	LTPP SPS-8 South Dakota	1993	2006	2014	Dry/Freeze

The dynamic modulus and cyclic fatigue test results were used within the FlexPAVE™ program to predict the cracking performance within a pavement structure under realistic traffic and climate conditions. Typical pavement structures (10-cm asphalt concrete layer, 20-cm aggregate base, and 380-cm subgrade) and traffic levels (3500 daily ESALs) were used in the FlexPAVE™ simulations. Climatic data for each of the locations listed in Table I-1 were obtained from the Enhanced Integrated Climatic Model (EICM) and used in the simulations.

Test Results and Discussion

LTPP South Dakota

Figure I-2 presents the air void contents and performance test results for the LTPP South Dakota field cores. Figure I-2 (a) shows the average air void contents and standard errors for six measurements of Ø38-mm samples extracted from field cores. The average air void content for both aging levels is about two percent. A much greater variability in air void content can be observed for the 21-year-old field specimens compared to the 14-year-old specimens. Specimens were prepared for performance testing for use in at least two repeatable dynamic modulus tests and three cyclic fatigue tests. The dynamic modulus mastercurves presented in Figure I-2 (b) show that the 21-year-old field cores were significantly stiffer than the 14-year-old field cores.

Figure I-2 (c) and (d) are the results from the cyclic fatigue test. The damage characteristic curve (i.e., *C* versus *S* curve) in Figure I-2 (c) describes the damage evolution within the material and is independent of temperature, stress/strain level, and mode of loading. Figure I-2 (d) presents the failure criterion based on D^R, which is defined as the average reduction in pseudo stiffness up to failure. Wang and Kim (2017) found that cumulative (1-*C*)

values up to failure and the number of cycles to failure, N_f, have a linear relationship which passes through the origin. The slope of this linear relationship is the material property that defines the failure of the material. This slope is denoted as D^R. Therefore, the 14-year-old cores have the D^R value of 0.4123 whereas the D^R value of the 21-year-old cores is 0.4984 as can be seen in Figure I-2 (d). In general, a higher D^R value represents better cracking resistance. Wang and Kim (2017) also concluded that the 90% confidence level can be obtained by using data from three fatigue tests if ±0.04 is used for the D^R value as a tolerance to the variation. Based on this observation, the D^R values shown in Figure I-2 (d) are significantly different.

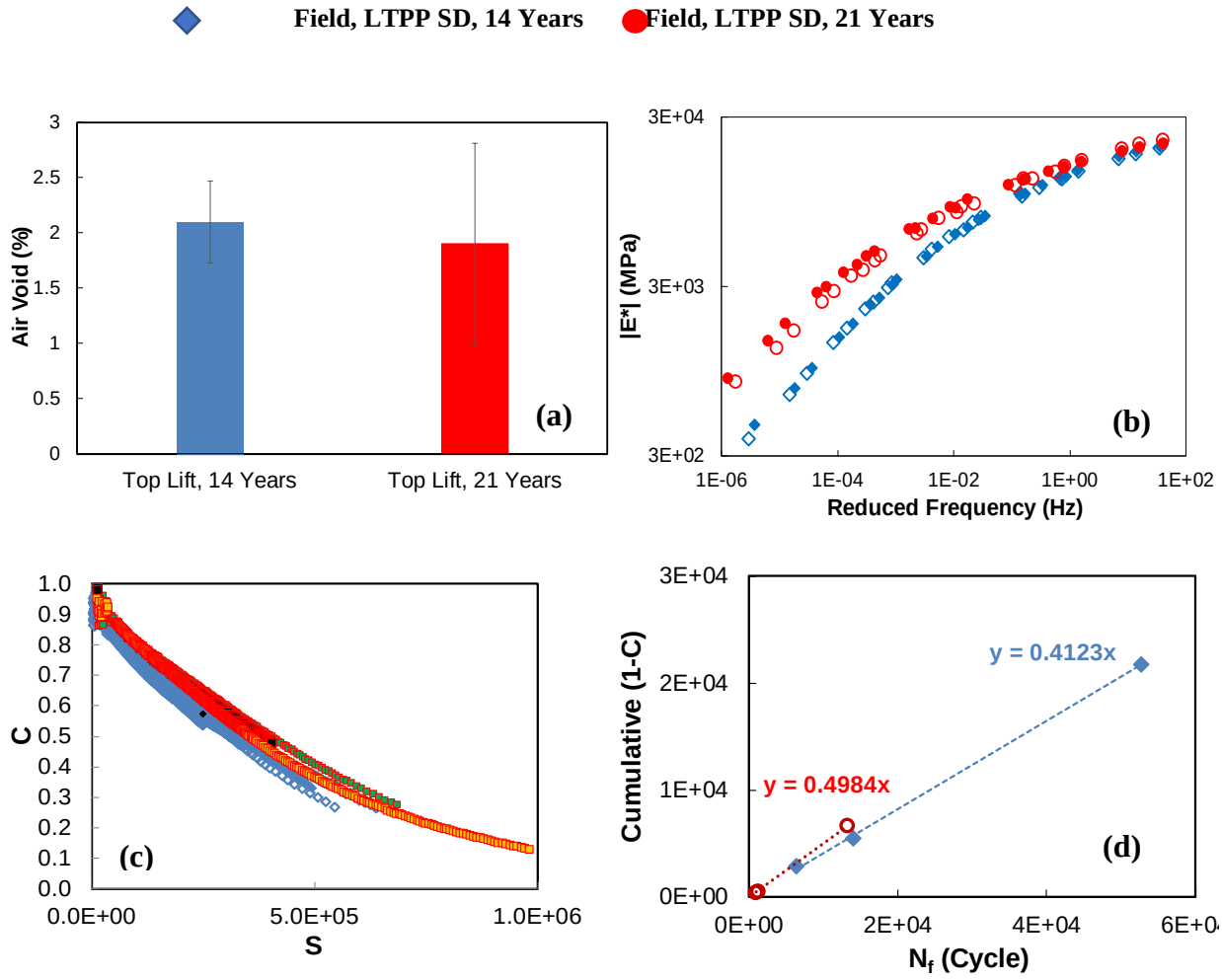

Figure I-2. LTPP South Dakota section cores after 14 and 21 years of aging in the field: (a) air void measurements with standard error bars, (b) dynamic modulus mastercurves, (c) damage characteristic curves, and (d) D^R values for failure criterion.

The material properties shown in Figure I-2 were input to FlexPAVE™ for cracking performance prediction of the study pavement. Figure I-3 shows the FlexPAVE™ predicted distribution of damage within a cross-section of the asphalt pavement layer after 20 years of traffic loading. The wheel path is directly above the region of damage localization. To compare the results of the fatigue cracking predictions, the percent damage was computed as a function of

time for each case. The percentage of damage (referred to as 'percent damage') is defined as the ratio of the sum of the damage factors within the reference cross-section area to the reference cross-section area, as shown in Equation I-1.

$$Percent\ Damage = \left. \sum_{i=1}^{M} \left(\frac{N}{N_f}\right)_i \times A_i \right/ \sum_{i=1}^{M} A_i \qquad \text{(I-1)}$$

where

i = nodal point number in finite element mesh,
M = total number of nodal points in finite element mesh,
N/N_f = damage factor,
N = number of load applications,
N_f = number of load applications to failure,
A_i = area represented by nodal point i in finite element mesh, and
$\sum A_i$ = reference area.

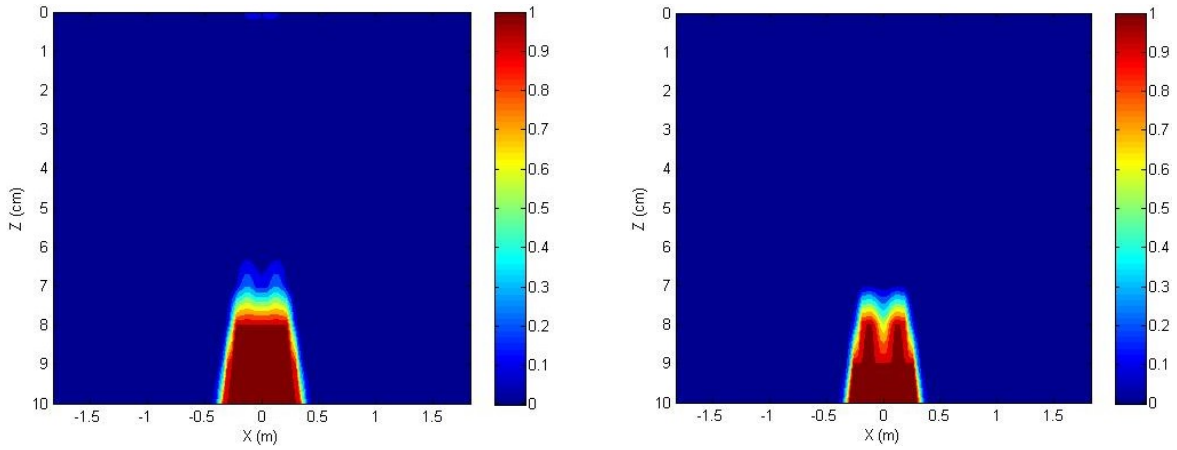

(a) **(b)**

Figure I-3. Damage contours for LTPP South Dakota section: (a) 14-year-old and (b) 21-year-old specimens.

FlexPAVE™ uses two overlapping triangles to form the reference cross-section area within which the damage evolution can be considered (Kim et al. 2017). The top inverted triangle has a 170-cm wide base that is located at the top of the surface layer and a vertex that is located at the bottom of the bottom asphalt layer. The 12-cm wide base of the second triangle is located at the bottom of the bottom asphalt layer and its vertex is positioned at the surface layer. Figure I-4 presents the final shape of these overlapping triangles.

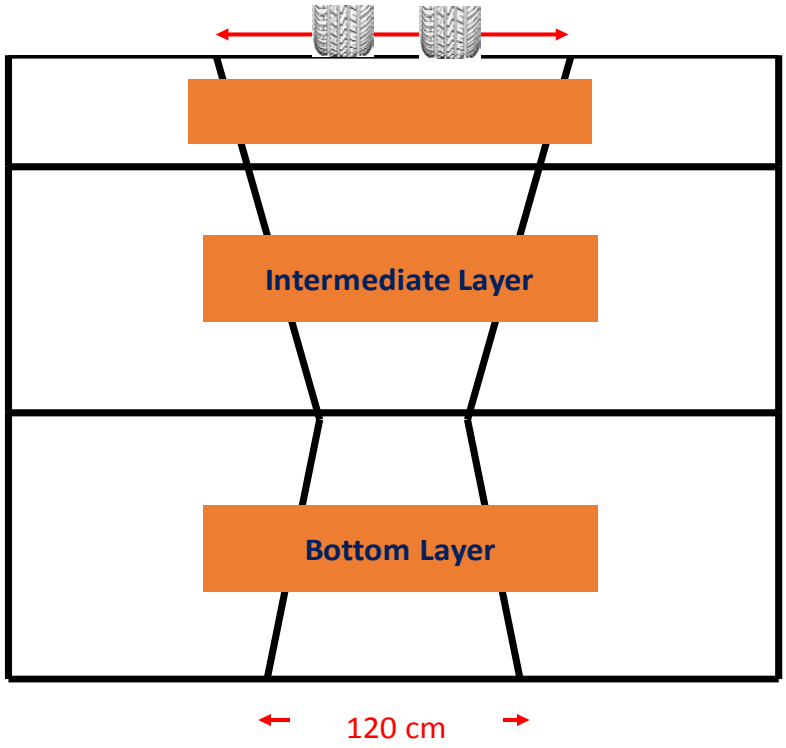

Figure I-4. Area for 'percent damage' definition.

Figure I-5 shows the percent damage growth as a function of service life in months for the 14-year-old and 21-year-old materials. The FlexPAVE™ results indicate that the 14-year-old material shows slightly better performance than the 21-year-old material. This reverse trend is probably due to the large sample-to-sample variability found in the field cores, including the variability in air void contents.

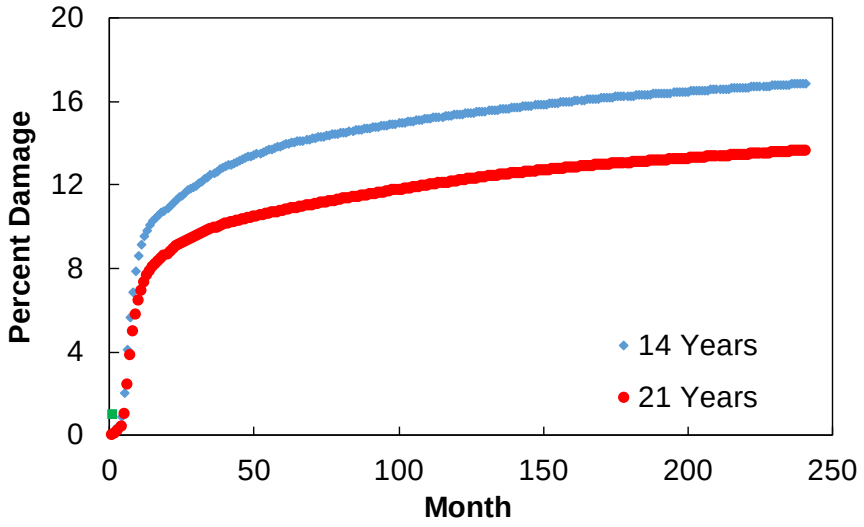

Figure I-5. Comparison of percent damage versus service life (months) for LTPP South Dakota section at two different aging levels.

LTPP Wisconsin

Figure I-6 presents the G^* measurements for extracted and recovered binders, air void contents, and performance test results for the LTPP Wisconsin field cores. Figure I-6 (a) shows the G^* measurements for binders extracted and recovered from a field core at a depth of 19 mm and at the aging levels of 8 years and 17 years. The 17-year-old field core contains stiffer binder than the 8-year-old field core. A significant change in the air void content was observed between the two field age levels, as shown in Figure I-6 (b). This change in air void content with aging may have been caused by densification under traffic loading and/or construction variability. Although the 17-year-old cores show a significantly lower air void content than the 8-year-old cores, the dynamic modulus mastercurves of the two age levels are similar, as shown in Figure I-6 (c), with the 17-year-old cores showing slightly higher dynamic modulus values than the 8-year-old cores. Figure I-6 (d) and (e) present the cyclic fatigue test results. Generally, the stiffer materials exhibit higher C versus S curves than the less stiff materials, which may explain the trend shown in Figure I-6 (d). The D^R values for the two age levels are comparable, as shown in Figure I-6 (e).

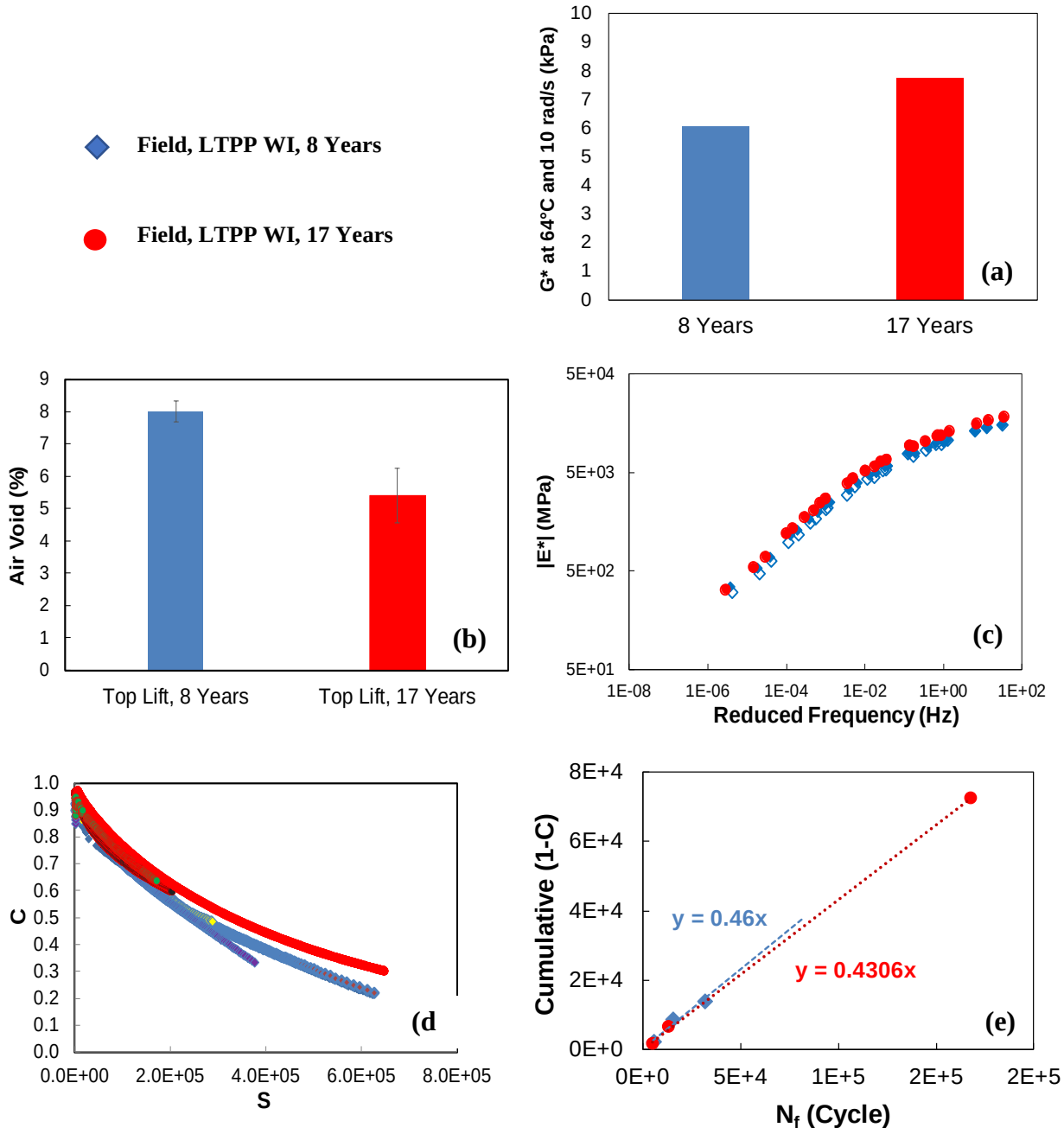

Figure I-6. LTPP Wisconsin section cores after 8 and 17 years of aging in the field: (a) *G of extracted and recovered binders at 64°C and 10 rad/s, (b) air void measurements, (c) dynamic modulus curves, (d) damage characteristic curves, and (e) D^R values for failure criterion.**

Figure I-7 shows the FlexPAVE™ predicted distribution of damage within a cross-section of the LTPP Wisconsin asphalt pavement layer after 20 years of traffic loading. Figure I-8 presents the percent damage as a function of time. The data obtained from the 17-year-old field cores indicate greater fatigue cracking susceptibility than the data obtained from the 8-year-old

field cores. The lower air void content in the 17-year-old field cores would result in better fatigue cracking resistance compared to the 8-year-old field cores. That is, if the air void contents were about the same, the data obtained from the 17-year-old field cores would indicate worse fatigue cracking resistance than the 8-year-old field core data, which would make the difference in percent damage between the data obtained from the 8-year-old and 17-year-old cores even greater than the difference shown in Figure I-8.

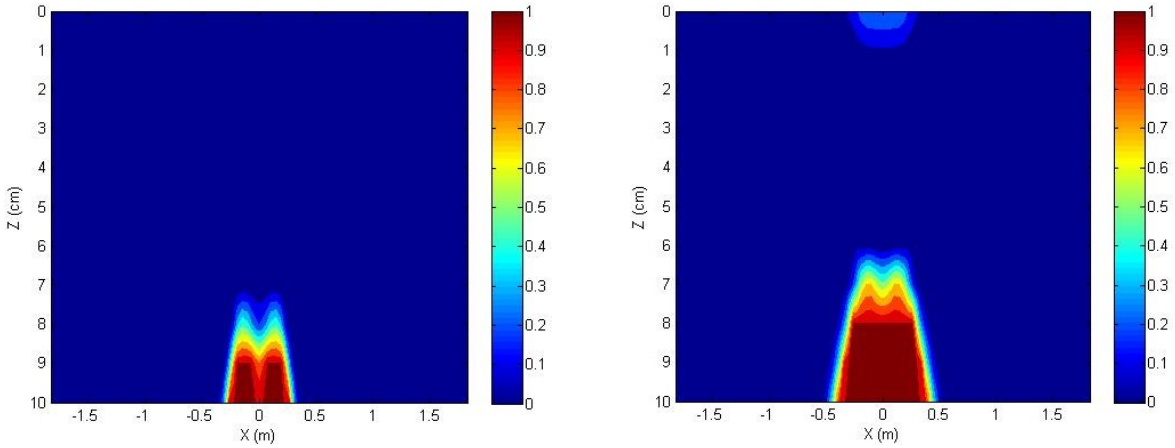

(a) **(b)**

Figure I-7. Damage contours for LTPP Wisconsin section: (a) 8-year-old and (b) 17-year-old specimens.

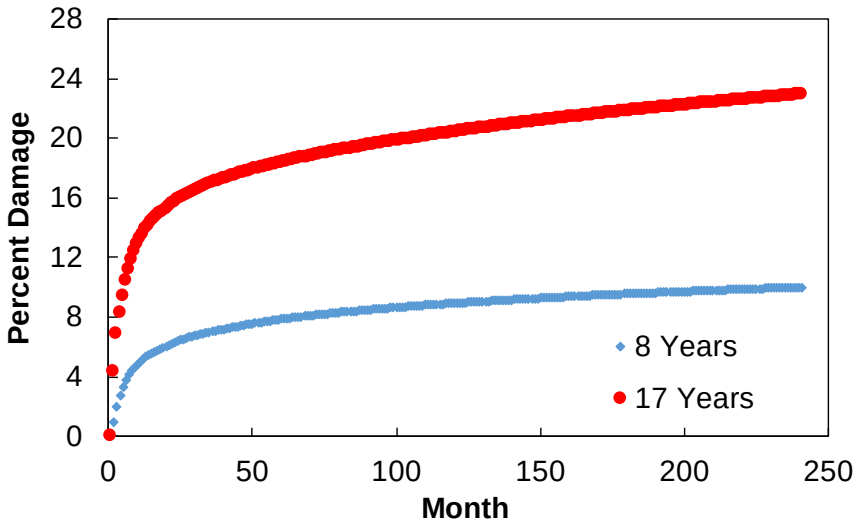

Figure I-8. Comparison of percent damage versus service life (months) for LTPP Wisconsin section at two different aging levels.

LTPP New Mexico

Figure I-9 presents the *G** measurements for extracted and recovered binders, air void contents, and performance test results for the LTPP New Mexico field cores. Figure I-9 (a) presents the *G** measurements for binders extracted and recovered from a field core at a depth of

19 mm and at the two aging levels of 10 years and 18 years. The binder results suggest greater stiffness for the 18-years old core than for the 10-years old field core. A significant change in the air void content can be observed between the two field age levels, as shown in Figure I-9 (b). The change in air void content with age level may have been caused by densification under traffic loading and/or construction variability. The 18-year-old field cores show higher dynamic modulus values and higher damage characteristic curves than the 10-year-old field cores in Figure I-9 (c) and Figure I-9 (c), respectively, although the damage characteristic curves show relatively large scatter. D^R value is slightly higher for the 10-year-old field cores compared to the 18-year-old field cores as presented in Figure I-9 (e).

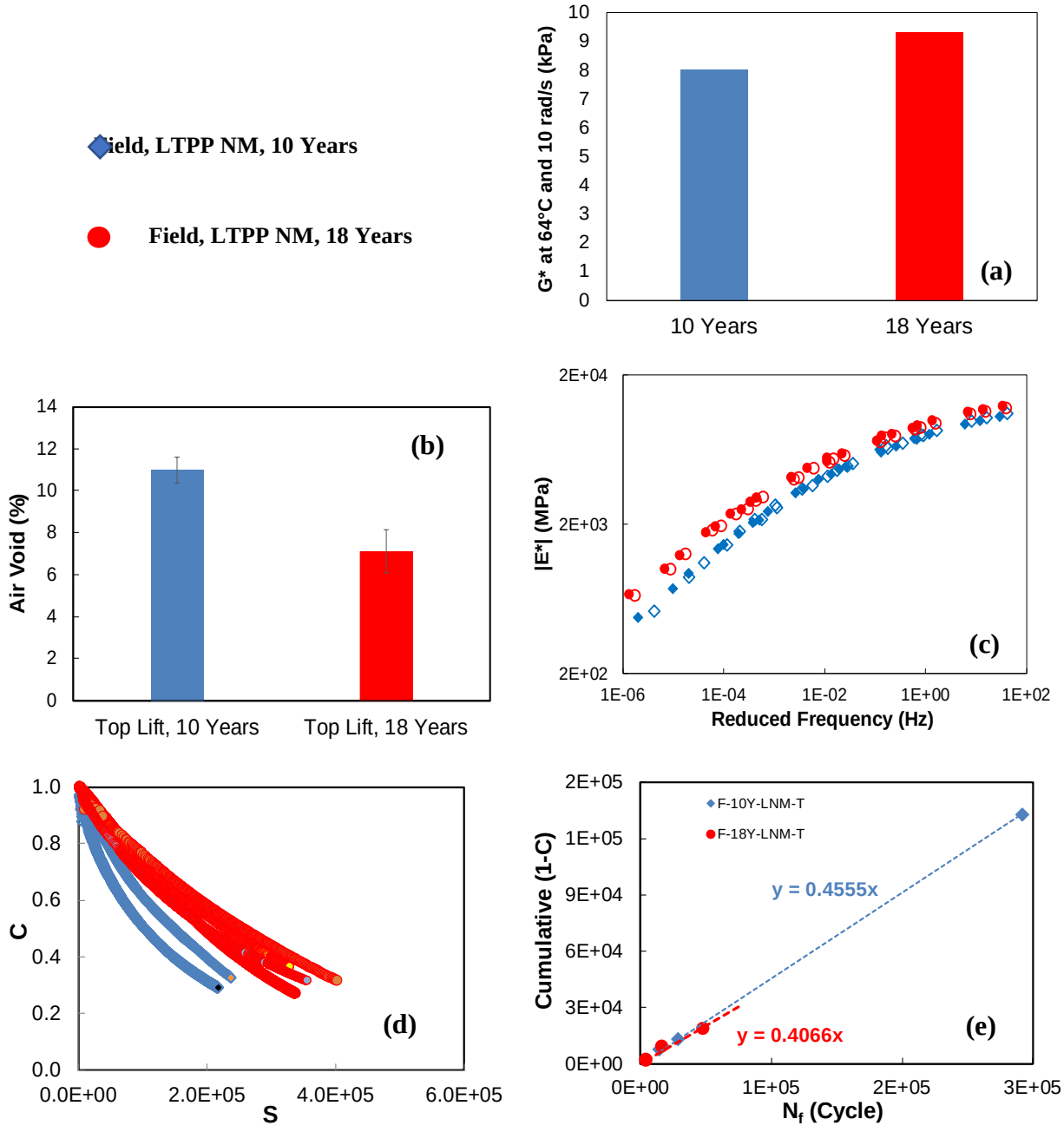

Figure I-9. LTPP New Mexico section cores after 10 and 18 years of aging in the field: (a) *G of extracted and recovered binders at 64°C and 10 rad/s, (b) air void measurements, (c) dynamic modulus curves, (d) damage characteristic curves, and (e) D^R values for failure criterion.**

Figure I-10 shows the FlexPAVE™ predicted distribution of damage within a cross-section of the asphalt pavement layer after 20 years of traffic loading. Figure I-11 presents the fatigue damage area as a function of time. The 10-year-old field cores exhibit greater cracking susceptibility than the 18-year-old field cores. This reverse trend may be due to the difference in air void contents between the cores at the two age levels. That is, the positive effect of the low air void content in the 18-year-old cores on fatigue resistance may be greater than the negative effect of additional aging of the 18-year-old cores, resulting in better fatigue cracking resistance of the 18-year-old cores.

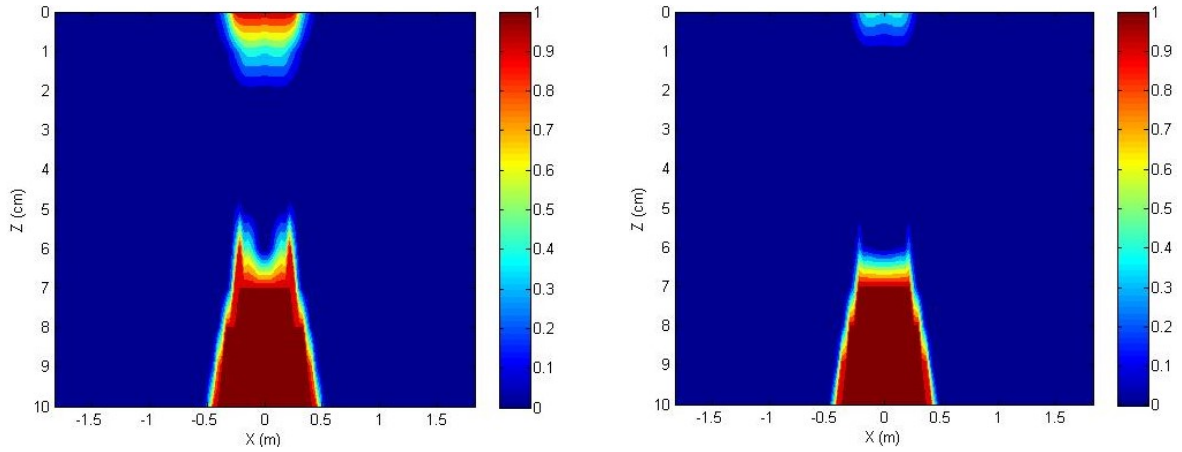

(a) **(b)**

Figure I-10. Damage contours for LTPP New Mexico section: (a) 10-year-old and (b) 18-year-old specimens.

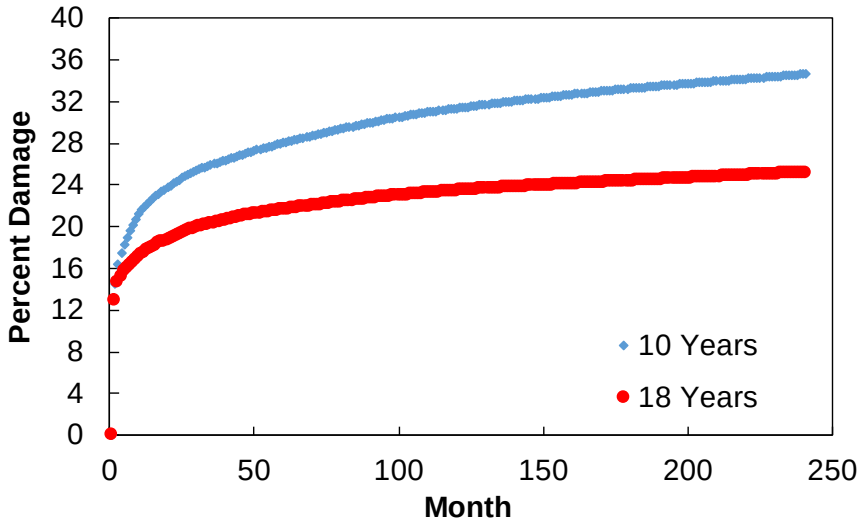

Figure I-11. Comparison of percent damage versus service life (months) for LTPP New Mexico section at two different aging levels.

LTPP Washington

Figure I-12 presents the air void contents and performance test results for the LTPP Washington field cores. A significant change in the air void content can be observed between the two field age levels, as shown in Figure I-12 (a). The change in air void content with age level may have been caused by densification under traffic loading and/or construction variability. The dynamic modulus test results for the two aging levels are similar, as shown in Figure I-12 (b). The damage characteristic curves in Figure I-12 (c) suggest greater cracking susceptibility of the 13-year-old pavement material than the 21-year-old material due to its lower position. However, much larger D^R values for the 13-year-old cores compared to those for the 21-year-old cores in Figure I-12 (d) indicate greater cracking resistance of the 13-year-old cores.

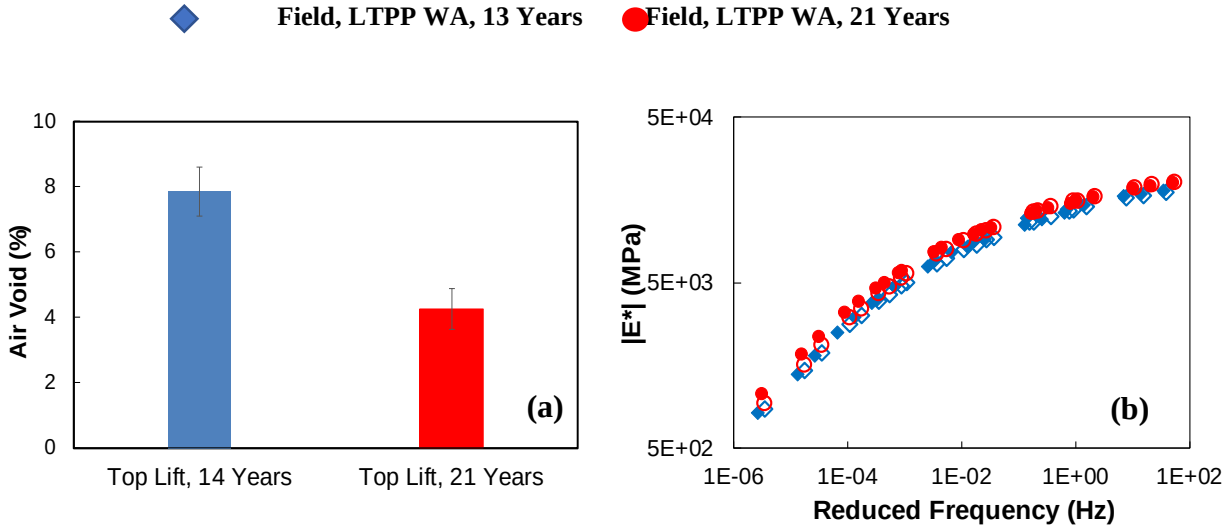

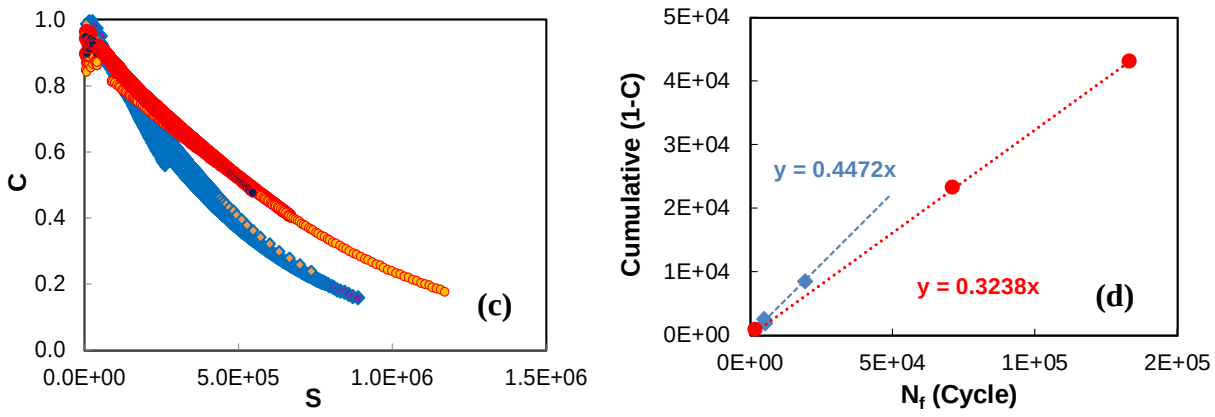

Figure I-12. LTPP Washington section cores after 13 and 21 years of aging in the field: (a) air void measurements, (b) dynamic modulus curves, (c) damage characteristic curves, and (d) D^R values for failure criterion.

The material properties presented in Figure I-12 were input to FlexPAVE™ to predict the damage within a cross-section of the asphalt pavement after 20 years of traffic loading. Figure I-13 and Figure I-14 show the damage contour results and the percent damage as a function of time, respectively. The results suggest that the fatigue damage susceptibility of the 21-year-old field cores is significantly greater than that of the 13-year-old field cores, indicating that the lower D^R value of the 21-year-old cores has a greater effect on fatigue cracking resistance than the higher position of the damage characteristic curve and lower air void content observed from the 21-year-old cores.

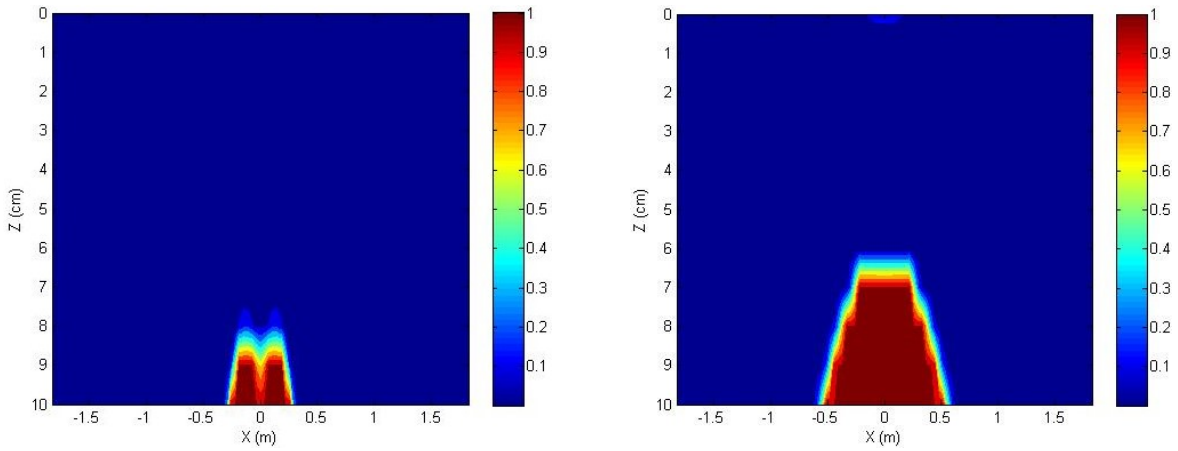

Figure I-13. Damage contours for LTPP Wisconsin section: (a) 13-year-old and (b) 21-year-old specimens.

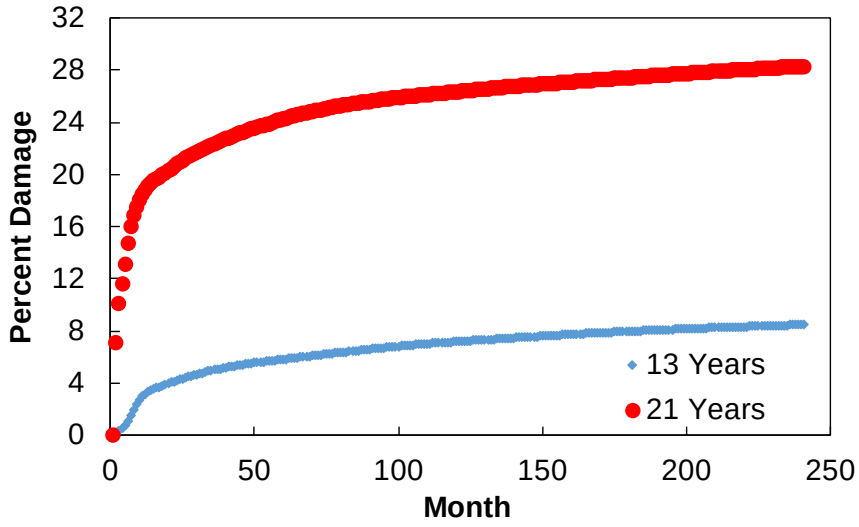

Figure I-14. Comparison of percent damage versus service life (months) for LTPP Washington section at two different aging levels.

Summary of Findings

Based on the test results obtained for the four test sections investigated in this study, the following observations were made:

- In general, the dynamic modulus values of field cores with higher aging levels (longer in-service durations in the field) are higher than those of field cores with lower aging levels.
- In general, much greater variability is found from the cyclic fatigue material properties (i.e., damage characteristic curve and D^R value) of the field cores than the variability that has been observed from laboratory-fabricated specimens in other research projects at NC State University.
- A fair comparison of the fatigue cracking performance between field cores at two age levels was masked by the differences in the air void contents of the field cores at two age levels. It is recommended that future performance testing efforts should use laboratory-fabricated specimens with the same air void contents but different aging levels to investigate further the effect of oxidation aging on fatigue cracking performance.

References

Kim, Y. R., M. N. Guddati, Y. T. Choi, D. Kim, A. Norouzi, Y. Wang, B. Keshavarzi, M. Ashouri, and A. D. Wargo (2017). *Development of Asphalt Mixture Performance-Related Specifications*. Final report, Contract No. DTFH61-08-H-00005, North Carolina State University, Raleigh, NC.

Wang, Y. and Y. R. Kim (2017). Development of an Energy-Based Fatigue Failure Criterion for Asphalt Mixtures Based on Viscoelastic Continuum Damage Theory. Submitted to *Construction and Building Materials*.